



Universidad de Valladolid

**FACULTAD DE CIENCIAS/ I. U. CINQUIMA
DEPARTAMENTO DE QUÍMICA FÍSICA Y QUÍMICA
INORGÁNICA**

TESIS DOCTORAL

**KINETIC AND THERMODYNAMIC STUDIES
ON TRANSMETALATION REACTIONS**

Presentada por **Desiré Carrasco Fernández**
para optar al grado de Doctor por la Universidad
de Valladolid

Dirigida por
Prof. Dr. Juan A. Casares González
Prof. Dr. Pablo Espinet Rubio

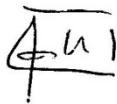
Valladolid, 2016

AUTORIZACIÓN DE LOS DIRECTORES DE TESIS

D. Pablo Espinet Rubio, con D.N.I. nº 17176361F y D. Juan Ángel Casares González, con D.N.I. nº 09740156R, Catedráticos de Universidad del Departamento de Química Física y Química Inorgánica de la Facultad de Ciencias, como Directores de la Tesis Doctoral Kinetic and Thermodynamic studies on transmetalation reactions, presentada por Desiré Carrasco Fernández dentro del programa: “Doctorado en Química: Química de síntesis, métodos de separación, catálisis y materiales avanzados” impartido por el Instituto Universitario CINQUIMA, autorizan la presentación de la misma, considerando que cumple todos los requisitos para ello.

Valladolid,

Los Directores de la Tesis



Fdo. Pablo Espinet Rubio



Fdo. Juan Al Casares González



Consolider Ingenio 2010
CSD2006-0003

Diseño de Catalizadores
para una Química Sostenible:
una Aproximación Integrada



La Tesis Doctoral Kinetic and Thermodynamic studies on transmetalation reactions, ha sido realizada gracias al apoyo económico del Ministerio de Educación y Ciencia (contrato predoctoral de Formación de Personal Investigador), de la Dirección General de Investigación del MICINN (proyectos INTECAT Consolider Ingenio 2010 CSD2006-0003, CTQ2010-18901/BQU, CTQ2013-48406-P), y la Junta de Castilla y León (proyecto VA302U13 y GR169).

Se agradece la colaboración del Dr. Max García Melchor y de la Prof. Rosana Álvarez, por la realización del trabajo computacional en los capítulos I y II y su contribución a la discusión de los mismos y de Juan del Pozo cuyos resultados catalíticos en la reacción de Stille han sido utilizados para la discusión del capítulo I.

At the time of completion of this memory, the results described in it have led to the following publications:

- *Stille Coupling Involving Bulky Groups Feasible with Gold Cocatalyst.* delPozo, J.; **Carrasco, D.**; Pérez-Temprano, M. H.; García-Melchor, M.; Álvarez, R.; Casares, J. A.; Espinet, P. *Angew. Chem. Int. Ed.* **2013**, *52*, 2189–2193.
- *Cross Alkyl-Aryl versus Homo Aryl-Aryl Coupling in Palladium-Catalyzed Coupling of Alkyl-Gold(I) and Aryl-Halide.* **Carrasco, D.**; Pérez-Temprano, M. H.; Casares, J. A.; Espinet, P. *Organometallics.* **2014**, *33*, 3540–3545.
- *Dramatic Mechanistic Switch in Sn/Au^I Group Exchanges.* **Carrasco, D.**; García-Melchor, M.; Casares, J. A.; Espinet, P. *Chem. Commun.* **2016**, *52*, 4305–4308.

CONTENTS	PAGE
PRESENTATION	17
GENERAL INTRODUCTION	23
CHAPTER I: <i>Thermodynamic study of Sn/Au transmetalation equilibria and consequences for the Gold Cocatalyzed Stille Coupling</i>	43
1.1 INTRODUCTION	45
1.2 RESULTS AND DISCUSSION	45
1.2.1 <i>Thermodynamics of the Au/Sn transmetalation equilibria</i>	45
1.2.2 <i>Consequences for the catalytic implementation of the process</i>	48
1.3 EXPERIMENTAL SECTION	49
CHAPTER II: <i>Mechanistic study of Sn/Au^I Group Exchanges</i>	57
2.1 INTRODUCTION	59
2.2 RESULTS AND DISCUSSION	59
2.2.1 <i>Thermodynamics of the transmetalation reaction</i>	59
2.2.2 <i>Kinetics of the reaction</i>	60
2.2.3 <i>Discussion of the results</i>	66
2.3 EXPERIMENTAL SECTION	70

CHAPTER III: Cross Alkyl-Aryl vs. Homo Aryl-Aryl Coupling in Pd Catalyzed Reactions	83
3.1 INTRODUCTION	85
3.2 RESULTS AND DISCUSSION	86
3.2.1 Mechanism of the reaction	87
3.2.2 Analysis of the kinetic data	94
3.3 EXPERIMENTAL SECTION	98
CHAPTER IV: Similarities between gold and zinc in the Aryl by Alkyl exchange reaction with palladium dimers	111
4.1 INTRODUCTION	113
4.2 RESULTS AND DISCUSSION	116
4.2.1 Reactions between $\text{trans-[Pd}_2(\mu\text{-X})_2\text{Rf}_2\text{L}_2]$ and $[\text{AuMeL}]$	116
4.2.2 Reactions between $\text{trans-[Pd}_2(\mu\text{-X})_2\text{Rf}_2\text{L}_2]$ and ZnMe_2	127
4.3 EXPERIMENTAL SECTION	133
CHAPTER V: Study of the Zn-Pd transmetalation in the Negishi cross-coupling reaction	149
5.1 INTRODUCTION	151
5.2 RESULTS AND DISCUSSION	157
5.2.1 Kinetics of transmetalation reaction between $\text{trans-[PdRfCl(PPh}_3)_2]$ and ZnMeCl	157

5.2.2	<i>Kinetics of transmetalation reaction between trans-[PdRfCl(PPh₃)₂] with [ZnMeCl₂]⁻ and [ZnMeCl₃]²⁻</i>	166
5.3	EXPERIMENTAL SECTION	170
CHAPTER VI:	<i>Development of new palladium catalysts for amination of aryl halides with ammonia</i>	185
6.1	INTRODUCTION	187
6.2	RESULTS AND DISCUSSION	192
6.2.1	<i>Condensation reaction for the synthesis of the imine</i>	193
6.2.2	<i>Lithiation reaction and hydrolysis</i>	194
6.2.3	<i>Synthesis of the amine</i>	194
6.2.4	<i>Condensation reaction to generate the new imine</i>	194
6.2.5	<i>Formation of the phosphonium salt</i>	195
6.2.6	<i>Synthesis of the palladium complex</i>	195
6.3	EXPERIMENTAL SECTION	195
	RESUMEN	201
	CONCLUSIONES GENERALES	211
	ÍNDICE	217

Abbreviations and acronyms

Ar	Aryl
Bu	Butyl
Bz	Benzyl
CAAC	Cyclic(alkyl)amino carbene
COD	1,5-cyclooctadiene
Cy	Cyclohexyl
DCM	Dichloromethane
dba	Dibenzylideneacetone
DFT	Density Functional Theory
DMF	N,N-dimethylformamide
DPCb	Diphosphinocarborane
dppf	1,1'-Bis-(diphenylphosphino)ferrocene
EDG	Electro donating group
Et	Ethyl
EWG	Electro withdrawing group
GS	Ground state
HOMO	Highest Occupied Molecular Orbital
IPr	Isopropyl
KHMDS	Potassium bis(trimethylsilyl) amide
L	ligand
LUMO	Lowest Unoccupied Molecular Orbital
Me	Methyl

NBO	Natural Bond Orbital
NHC	N-heterocyclic carbene
NTf ₂	(trifluoromethanesulfonyl)imide
Nu	Nucleophile
OTf	Trifluoromethanesulfonate (CF ₃ SO ₃) ⁻
<i>o</i> -tol	Ortho-tolyl
Pf	Pentafluorophenyl (C ₆ F ₅)
Ph	Phenyl
Rf	3,5-dichlorotrifluorophenyl (2,5-C ₆ Cl ₂ F ₃)
RT	Room temperature
THF	Tetrahydrofuran
tht	Tetrahydrothiophene
TMP	2,2,6,6-tetramethylpiperidyl
TS	Transition State
X	Halogen
ΔH^\ddagger	Gibbs free enthalpy
ΔG^\ddagger	Gibbs free energy
ΔS^\ddagger	Gibbs free entropy

NMR abbreviations and symbols

s	singlet
bs	broad singlet
d	doublet

t	triplet
m	multiplet
dd	doublet of doublets
dt	doublet of triplets
dm	doublet of multiplets
ppm	parts per million
δ	chemical shift
<i>J</i>	spin-spin coupling constant

PRESENTATION

This memory contains the results of the research that I have developed in the Institute CINQUIMA and the Department of Inorganic Chemistry at the University of Valladolid during my thesis work. It is a contribution to the understanding of the transmetalation reactions and other mechanistic studies on Sn/Au, Au/Pd and Zn/Pd systems. Some of the results obtained are already published in scientific journals and part of the contents and figures may be coincident.

This thesis memory is organized in different parts with a preliminary introduction and six independent chapters. The purpose of the introduction is to establish the general context and significance of the study of transmetalation reactions in gold and palladium systems. All chapters of this thesis are organized in the same way: introduction, results and discussion, experimental part and references. The bibliographical references have been included at the end of every chapter. Footnotes are used to provide relevant comments when appropriate.

In **Chapter I** we focus on the study of the Au/Sn transmetalation equilibria for different organotin and gold derivatives. From the study of the transmetalation reactions, cross-coupling catalytic reactions have been developed in which the system Sn/Au/Pd is used for the coupling of bulky aryls that are inert under the classic conditions of the Stille reaction. This was developed in a collaborative project in which the catalytic cross-coupling experiments were carried out by Dr. Juan del Pozo as part of his Ph.D. project.¹ The results of these catalytic experiments are shortly discussed here to allow the reader to understand the relevance of transmetalation equilibria.

In **Chapter II** we collect kinetic and thermodynamic studies on the exchange Ph/X reactions between the complexes [AuPhL] (L: PPh₃, PMe₃, PCy₃) and SnBu₃X (X = Cl, OTf and vinyl). This work has been completed with DFT studies in collaboration with Dr. Max Garcia-Melchor. These studies reveal a dramatic mechanistic change in the reaction, which explains unexpected differences in transmetalation rates: When X = Cl and OTf a usual

concerted mechanism is produced whereas for X = vinyl an unexpected oxidative addition/reductive elimination mechanism via an Au^{III} intermediate is produced.

Chapter III is about the study of Au/Pd systems. Aryl/methyl exchange reactions between the complexes *trans*-[PdRfClL₂] (Rf = C₆Cl₂F₃, L = PPh₃) with [AuMeL] have been studied. NMR ³¹P and ¹⁹F studies support a mechanistic proposal based on these studies. The Pd catalyzed Me-Ar coupling of AuMe and ArI is also studied in this chapter.

During our studies we found similarities between the gold transmetalation reactions with transmetalation reactions between organozinc and palladium compounds. For this reason **Chapter IV** compares the reactivity between [AuMeL] and ZnMe₂ with palladium dimers [Pd₂(μ-Cl)₂Rf₂L₂] (L = PPh₃, PCy₃ and PMe₃). The Me/Rf exchange is always the fastest reaction produced in these systems. Mechanistic studies have also been carried out.

Chapter V deals with Zn/Pd transmetalation. It is a mechanistic study of the transmetalation and retrotransmetalation step between Zn and Pd in the Negishi cross-coupling reaction. The study is focused on reactions of *cis*- and *trans*-[PdRfMe(PPh₃)₂] with ZnCl₂, and on reactions of *trans*-[PdRfCl(PPh₃)₂] with ZnMeCl, [ZnMeCl₂]⁻ and [ZnMeCl₃]²⁻.

The content of **Chapter VI** is the activity of my 3 months stay at UCSD (University of California, San Diego, USA) under the supervision of professor Guy Bertrand. During this time I was involved in a project focused on the development of new palladium catalysts for amination of aryl halides with ammonia, and my contribution was the synthesis of new carbene ligands and their palladium complexes.

This memory is presented to obtain the International Ph.D. In order to fulfill the requirements for the International Doctor Mention, this memory is written in English, and includes a summary of the results, as well as the general

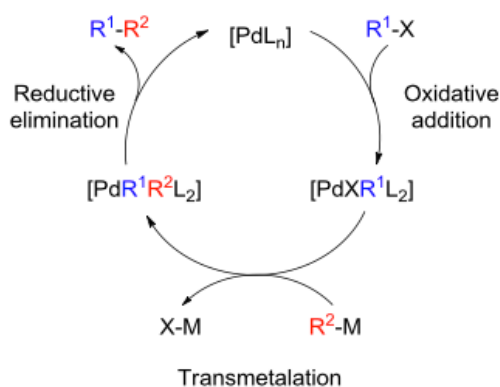
conclusions, in Spanish.

¹ Juan delPozo Doctoral Thesis. University of Valladolid, January 2016.

GENERAL INTRODUCTION

Palladium-catalyzed cross-coupling reactions are one of the most powerful synthetic methods for the formation of C-C bonds. These reactions proceed through mechanisms involving three main steps (Scheme 1):

- **Oxidative addition** of the organic electrophile to the metal center.
- **Transmetalation** in which an organic fragment is transferred from a main group nucleophilic reagent to the metal catalysts.
- **Reductive elimination** affording the C-C bonded reaction product.



Scheme 1. Simplified mechanistic cycle of Pd-catalyzed cross-coupling reactions.

The oxidative addition and reductive elimination steps are common to the different catalytic cross-coupling processes, while the transmetalation step depends on the nucleophile used, defines the type (name) of reaction (Scheme 2), and follows mechanisms somehow different in their details. The nature of the nucleophile changes aspects such as the transmetalation rate, the addition of additives, the tolerance to different groups and the reaction conditions.



M = B (Suzuki-Miyaura)
 Sn (Stille)
 Si (Hiyama)
 Zn (Negishi)
 Mg (Kumada) ...

Scheme 2. General scheme for the transmetalation step in cross-coupling reactions.

The term *retrotransmetalation reaction* is used throughout this memory to refer to the inverse reaction to the transmetalation (Scheme 2).

The thermodynamics of the transmetalation equilibria is an important aspect to be taken into account. Considering the general transmetalation reaction represented in Scheme 2, Pd-X and M-R² bonds are broken while Pd-R² and M-X bonds are formed. The knowledge of the bond energy values, allows us to deduce to which side is the equilibrium displaced for each individual case.

In order to better understand the importance of the study of the thermodynamic aspects of the transmetalation steps, a more detailed analysis for each Pd-catalyzed cross-coupling reaction is now described.

The Suzuki-Miyaura reaction is one of the most used synthetic methods for the construction of biaryls and substituted aromatic moieties and it is produced between an organic halide (or triflate) and a boronic acid R-B(OH)₂, in presence of a base.¹ Two main roles are proposed for the addition of the base: in the first one the base binds first to the boronic acid to form the organoboronate species, whereas in the second one the base substitutes first the leaving group X in the coordination sphere of the catalyst. These two pathways have been evaluated theoretically,² finally concluding that both are feasible. However, a higher energetic barrier was found in absence of the base, which explains why the reaction does not proceed without base. In addition to this relevant kinetic influence, it is even more important and not always stated that the base is necessary to displace the transmetalation equilibrium toward the reaction products.

In the Hiyama reaction an organosilicon compound acts as aryl source towards organic electrophiles. Often the presence of a nucleophile activator is required, due to the very low polarity of the C-Si bond. The activator used is a fluoride F⁻ in most cases, although also oxygen donor groups (from alcoxides or silanols) can be used.³

The silane becomes pentavalent in the transition state. This is the key reason why fluoride makes the transmetalation kinetically feasible. The formation of a very strong Si–F bond stabilizes the hypervalent Si center of the TS. The expansion of the coordination of the Si is only possible when stabilized by highly electronegative groups. From a thermodynamic point of view, the addition of F⁻ acts as the thermodynamic driving force of the transmetalation step, displacing the equilibrium toward the breaking of the Si-C bond by formation of a very strong Si-F bond.

In 2006 the fluoride-free Hiyama reaction was postulated by the research group of Denmark.⁴

The Stille reaction is one of the C-C cross-coupling reactions more deeply studied. The reaction takes place between an organic halide (or triflate) and an aryl or vinyl stannane. No addition of base is required. All aspects of the transmetalation step in this reaction have been studied in our research group and analyzed in several reviews.^{5,6} For the transmetalation process involved in this reaction two mechanisms, cyclic and open, have been proposed. Kinetic studies have demonstrated that the open mechanism takes place when the two ancillary ligands (usually phosphines or arsines) remain attached to palladium in the TS, while the cyclic mechanism requires that one ligand is released during the process. The open mechanism is favored in presence of good leaving groups such as triflate, and by polar solvents.

Talking about the thermodynamics of the reaction, the products Pd-C and Sn-X are not clearly favored in the energetic balance. The transmetalation step depends on the halide used and is more favored for Cl than for I.⁷ Also F⁻ and OH⁻ are commonly used as promoters of the Stille reaction because they form stable bonds with tin, displacing the transmetalation reaction to the right. The irreversible reductive elimination step acts as a thermodynamic driving force of the catalytic cycle.

Finally, the Negishi reaction involves the use of an aryl or vinyl halide or triflate and an organozinc compound as nucleophile. This reaction can be

applied to all kinds of carbon substrates (sp , sp^2 and sp^3) and tolerates many functional groups. Two types of neutral organometallic reagents are used, $ZnRX$ and ZnR_2 , in addition to zincates.

The main issue about the mechanism of this reaction has been the identification of the active organozinc species that undergoes transmetalation and the role of the experimentally observed palladium intermediates.

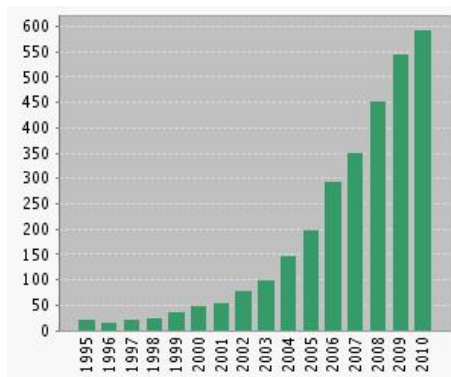
The first experimental studies on the mechanism of the transmetalation step in the Negishi coupling were carried out by our research group, in the coupling of an alkylzinc reagent with $[PdRXL_2]$.⁸ An unexpected observation was found in the reaction with $ZnMe_2$ or $ZnMeCl$ using *trans*- $[PdRfCl(PPh_3)_2]$: each methylating agent afforded preferently a different isomer (*cis*- or *trans*-) of the coupling intermediate $[PdRfMe(PPh_3)_2]$. Also $ZnRfMe$ and $ZnRfCl$, respectively, were detected. Soon, an experimental mechanistic study of the reaction between *trans*- $[PdMeCl(PMePh_2)_2]$ and $ZnMeCl$ was reported, affording the first experimental determination of thermodynamic parameters of the Negishi transmetalation.⁹ In 2011 our group studied the reaction between *trans*- $[PdMeCl(PMePh_2)_2]$ and $ZnMe_2$ in presence and in absence of free ligand, discovering that the reaction course can involve cationic intermediates.¹⁰ Very recently, our group also reported an experimental study onto the *cis* to *trans* isomerization reaction of $[PdMeAr(PR_3)_2]$ ($Ar = C_6F_5, C_6Cl_2F_3$) catalyzed by $ZnMe_2$, involving methyl exchange between Pd and Zn.¹¹ Other studies about the mechanism of the Negishi reaction have been carried out by the research group of A. Lei using *in situ* IR,¹² and by the group of M. Organ in complexes containing N-heterocyclic-carbene ligands.¹³

Due to the high nucleophilicity of the organometallic zinc complexes, they are very active transmetalating agents. Being the C-Zn and C-Pd bond energies quite similar, the use of a large excess of the organometallic zinc compound makes the transmetalation step favorable, and no additive is needed. The activation energy for the transmetalation is usually low, leading to fast exchange of organic groups between both metals. These reactions can result in

the formation of undesired products, as exemplified by the formation of ZnRfMe in the reaction between ZnMe_2 and *trans*- $[\text{PdRfCl}(\text{PPh}_3)_2]$. The formation of C-C bonds in the irreversible step of the reductive elimination has also a decisive role that displaces the transmetalation equilibrium to the products.

Many other metals, from zirconium to indium or bismuth,¹⁴ can provide useful arylating reagents toward palladium, but group 11 metals are particularly important because they have led to the development of useful bimetallic catalytic systems. In this work, we chose to study mainly transmetalation reactions that involve the participation of gold, due to its relevance as catalyst. This opens the possibility of combine catalytic processes in which gold and palladium play different roles.

The first notable example of a homogeneous gold-catalyzed reaction was reported in 1986 by the group of Hayasi.¹⁵ They showed that a combination of a gold(I) complex with a ferrocenyl diphosphine ligand catalyzed the asymmetric addition of an isocyanate to aldehydes to produce oxazolines. Since then, the interest in processes that imply the participation of gold compounds has been continuously growing, and numerous reviews on gold catalysis have been published (Scheme 3).¹⁶



Scheme 3. Graphic of the number of gold-catalyzed reactions from 1995 to 2010. Source: ISI Web of Knowledge.

The electronic configuration of gold is $[\text{Xe}] 4f^{14} 5d^{10} 6s^1$ and it belongs, along with copper and silver, to group 11 of the periodic table of the elements. While various oxidation states are accessible for gold, ranging from -1 to $+5$, the chemistry of gold is mainly based on gold(0), gold(I) and gold(III) species. Most of the chemistry that has been developed with Au^{I} catalyst is based on its Lewis acid properties. It is important to note that gold(I) compounds, with d^{10} electronic configuration, as copper(I) and palladium(0), are linear molecules as often is copper(I) but palladium(0) complexes are tetrahedral.

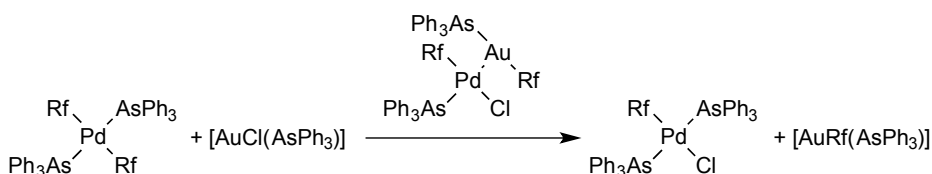
The cationic gold(I) complexes are very electrophilic species that have the ability of activate π -systems such as alkynes, allenes and alkenes toward the addition of a nucleophile. In particular, gold(I) catalysts have found application in cyclization reactions of unsaturated molecules, where gold firstly activates the π -system for a further nucleophilic attack.¹⁷ One recent example of one of the gold cyclization reactions is the sequential cyclization/rearrangement reaction of O-allyl hydroxamates, an atom economical synthesis of 3-hydroxyisoxazoles.¹⁸

Comparatively other gold catalyzed processes such as cross-coupling reactions, activations of carbonyl groups and alcohols, hydrogenation or oxidation reactions,¹⁹ have been much less developed. Most of the elementary organometallic reactions are already known in gold complexes such as: oxidative additions,²⁰ transmetalations,²¹ and reductive eliminations.²² However, in contrast to palladium or rhodium chemistry for which those steps have been profusely described and studied, the studies of these reactions in gold complexes are scarce, and only recently one review about elementary organometallic reactions that involve the participation of gold has been published.²³ Since our work deals with transmetalation reactions, in the next pages we will focus on this particular step.

Transmetalations involving gold complexes.

Transmetalations between organogold and zirconium,²⁴ iron and ruthenium,²⁵ rhodium,²⁶ nickel,²⁷ boron²⁸ and palladium,²⁹ have been already documented. Also transmetalation reactions between gold and zinc, lithium, or magnesium are known because are used for the synthesis of gold complexes. However, only a few mechanisms of these transmetalations have been studied in detail.

Our research group studied the mechanism of the Au/Pd aryl transmetalation, showing that the formation of *trans*-[PdRf₂(AsPh₃)₂] from *trans*-[PdRfCl(AsPh₃)₂] (Rf = C₆Cl₂F₃) and [AuRf(AsPh₃)] is an endergonic process that takes place via intermediates and transition states stabilized by Au-Pd methalophilic interactions (Scheme 4).³⁰



Scheme 4. Reaction on the Au/Pd aryl transmetalation.

In DFT calculations the Au-Cl bond displaces a ligand from Pd, forming a Pd-Au strong bond interaction in the intermediates and the transition states (Figure 1). In the intermediates, the Pd coordination is almost square planar and there is a Pd-Au covalent bond.

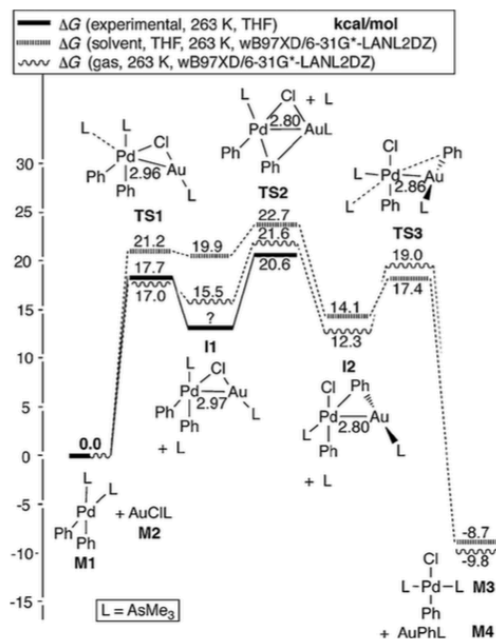
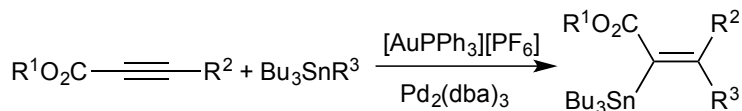


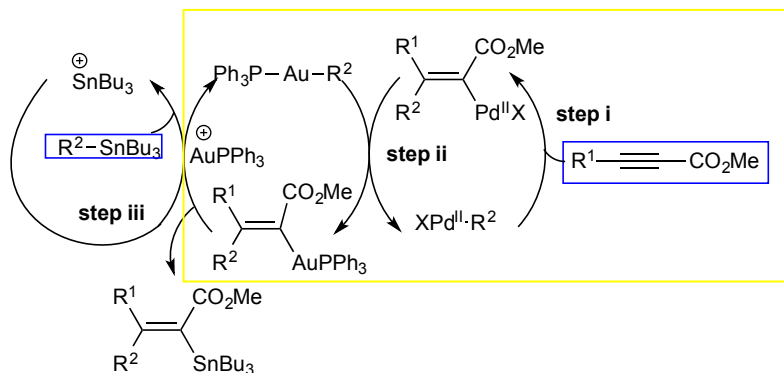
Figure 1. Profile of the exchange reaction $M1 + M2$ to give $M3 + M4$, showing the experimental value for TS1 and TS2 in THF at $-10\text{ }^{\circ}\text{C}$ and the calculated values (Ref. 30).

Gold complexes can also undergo transmetalation reactions with Group 14 compounds. Blum *et al.* studied the vinyl exchange between Au and Sn in the co-catalyzed carbostannylation of alkynes (Scheme 5).³¹ The treatment of the alkynes with stannanes in the presence of Pd and Au as co-catalysis, affords the olefin carbostannylation products with excellent regio and stereoselectivity.



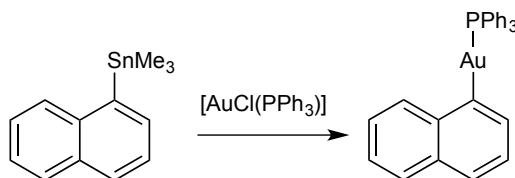
Scheme 5. Pd/Au co-catalyzed carbostannylation of alkynes.

The proposed mechanism occurs in three different cycles: i) migratory insertion of alkyne into organopalladium intermediate; ii) transmetalation to gold affording a vinylgold intermediate; iii) transmetalation to Sn to generate the final vinyltin product (Scheme 6).



Scheme 6. Mechanism for the Au/Pd Dual-Catalyzed Carbostannylation of Alkynes^a.

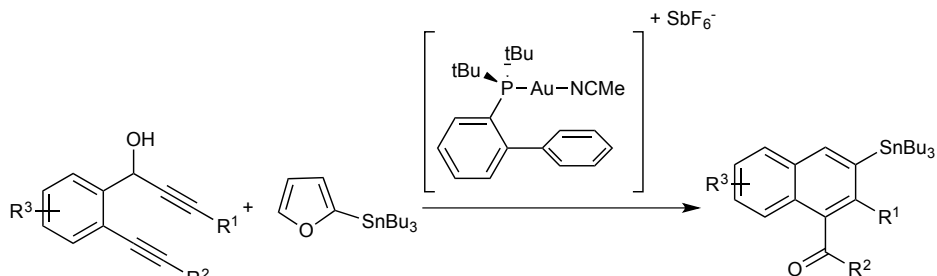
The group of F. Mohr studied the transmetalation reaction on the transfer of organic groups using organotin compounds.³² SnMe_3R ($\text{R} = \text{Ph}$, naphthalene, 8-iodonaphthalene) react with $[\text{AuClL}]$ ($\text{L} = \text{AsPh}_3, \text{PPh}_3$) producing $[\text{AuRL}]$ and SnMe_3Cl (Scheme 7).



Scheme 7. Example of the transmetalation reaction between tin and gold reported by Mohr.

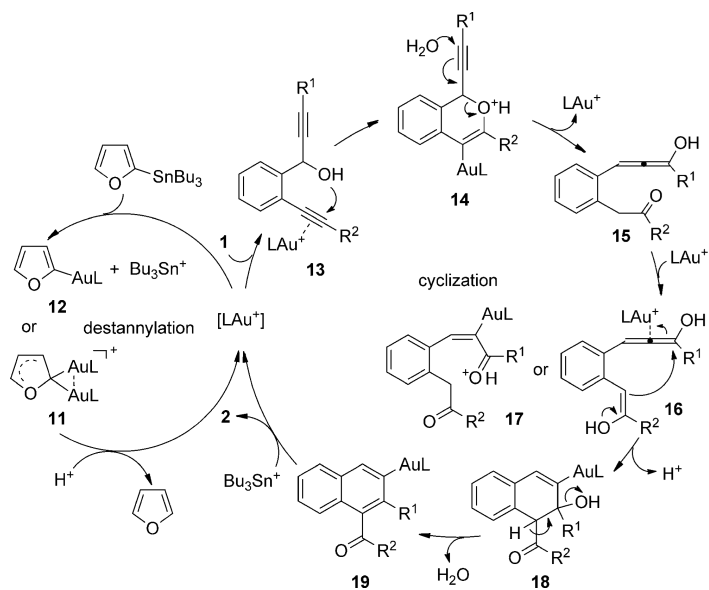
Chen *et al.* reported the gold-catalyzed cycloisomerization/stannylation cascade reaction of 1,6-diyne-4-en-3-ols using $\text{Sn}(n\text{-Bu})_2\text{-}(furyl)$ leading to stannyl naphthalenes (Scheme 8).³³

^a Generation of the active catalysts is omitted for clarity. Starting materials are highlighted in blue boxes. The yellow box highlights a palladium-catalyzed carbocoupling reaction that operates as a subcycle within the broader carbostannylation cycle.



Scheme 8. Gold catalyzed cyclization/stannylation/transfer reactions.

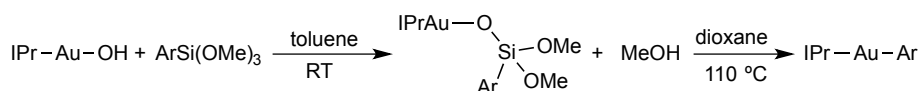
They propose the following mechanism for this cascade reaction. The reaction is initiated by a nucleophilic attack of the hydroxy group onto the gold-coordinated alkyne to give an oxacyclic species, which undergoes C-O bond cleavage to give an allenol. The formed allenol compound can be activated by gold to form species that after a cyclization reaction would afford a 2-naphthyl gold intermediate. In an auxiliary catalytic cycle, the gold complex could catalyze the destannylation of 2-tributylstannylfuran through transmetalation and protodemetalation (Scheme 9). A gold to tin transmetalation reaction and a gold-catalyzed destannylation reaction are involved in this domino process.



Scheme 9. Proposed reaction mechanism taken as published in reference 32.

In the year 2013, Canovese *et al.* published a kinetic study on the transmetalation between [AuCIL] (L = DIC, PPh₃, NHCs) and tributylphenylethynylstannane to give the derivatives [AuCCPhL].³⁴ The study was carried out in CHCl₃ and CH₃CN by UV-Vis technique, and an associative pathway was proposed for the mechanism.

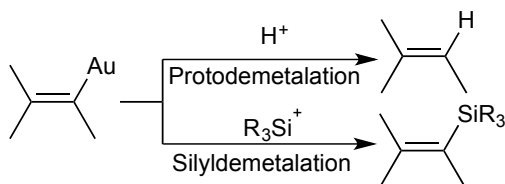
In 2012, Nolan and co-workers reported a fluoride-free OH based transmetalation of organosilanes to gold.³⁵ [Au(OH)(IPr)] complexes react with ArSi(OMe)₃ to give [AuAr(IPr)] (Scheme 10).



Scheme 10. Si to Au transmetalation for the synthesis of arylgold complexes.

Bourissou communicated the transmetalation from vinylgold complexes to SnBu₃(OTf) in presence of PPh₃.³⁶ In this work; the resulting organotin compound was used in a Stille cross-coupling reaction.

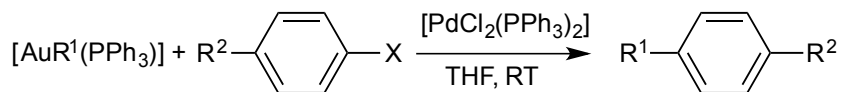
For a large number of gold- catalyzed reactions, trapping the vinylgold intermediate with a proton completes the catalytic cycle. This step is called protodemetalation. It has been discovered that such intermediates can also be captured by carbon electrophiles and by silicon or tin electrophiles (Scheme 11).³⁷



Scheme 11. Capture of the Vinyl-Gold intermediate by proton and silicon electrophiles.

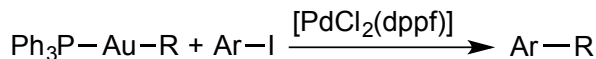
Organogold nucleophiles in palladium catalyzed reactions.

Several transmetalation reactions between gold and palladium have been reported in cross-coupling reactions. An early example was reported by the group of Sarandeses in the palladium-catalyzed cross-coupling reaction of organogold(I) reagents (R = alkyl, alkenyl, aryl and alkynyl, benzoyl chloride) with organic electrophiles (R' = aryl and alkenyl halides, aryl triflates and benzyl bromide) (Scheme 12).³⁸



Scheme 12. Pd catalyzed cross-coupling of organogold(I) reagents with aryl halides and triflates.

Analogously, by using $[\text{PdCl}_2(\text{dppf})]$ as catalyst, aryl iodides were coupled with organogold compounds to form Ar-C(sp²), Ar-C(sp) and Ar-Ar C-C bonds in good yields (Scheme 13).³⁹



Ar = Ph, (H. EWG, EDG), Py

R = Ar, alkyne, alkene

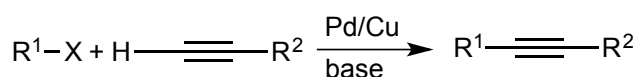
Scheme 13. Pd catalyzed cross-coupling of organogold(I) reagents with aryl iodides.

Unlike organometallic compounds of transition metals, alkylgold(I) compounds are not likely to produce β -elimination hydrogen reactions, what makes them particularly useful for alkyl coupling reactions.^{38,40}

Bimetallic catalysis.

Our research group has been interested in bimetallic catalysis, involving one transition metal and one Group 11 element.⁴¹ The principal aim of this type of catalysis is to take advantage of the specific behavior of each catalyst. Frequently, a third metal may participate in the reaction.

The most common process in bimetallic catalysis is the C-C bond formation. Most of the bimetallic processes include the participation of Pd combined with a second metal, often Cu or Au. The most famous example is the Sonogashira reaction that uses the bimetallic system Pd/Cu.⁴² In this process Cu acts as a catalyst in the transfer of an alkynyl group from the alkyne to Pd in the presence of a base (Scheme 14). In this line, the palladium-catalyzed Stille reaction is sometimes co-catalyzed by the addition of Cu salts. Cu acts as aryl transfer from organotin to palladium.⁴³

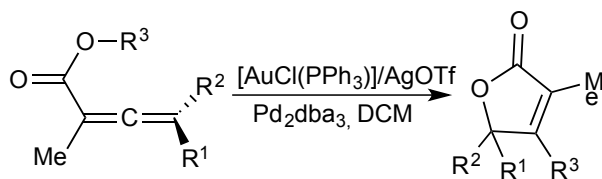


Scheme 14. Sonogashira cross-coupling.

Gold catalysis is by itself a very important catalytic area and palladium is the transition metal most frequently used in catalysis, but only recently has the benefit of the combination of the two metals, which does not require the isolation and purification of reaction intermediates, has been discovered.

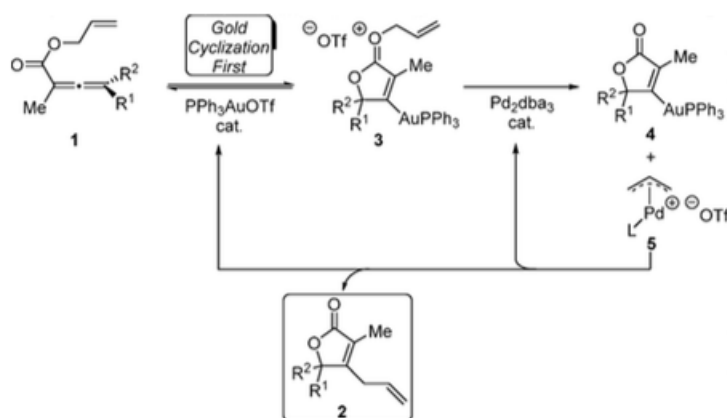
Blum and co-workers have reported the Pd-catalyzed carboauration of alkynes with vinylgold triphenylphosphine to produce *syn*alkenyl gold complexes.⁴⁴

Regarding this idea, the research group of Blum published a mechanistic study on the gold and palladium cooperative catalytic cyclization/cross-coupling reaction (Scheme 15).^{29a}



Scheme 15. Au/Pd catalyze cyclization/cross coupling reaction.

They conclude that the mechanism is consistent with a “gold-cyclization first” hypothesis (Scheme 16).



Scheme 16. Gold Cyclization First Mechanism for Au/Pd Dual-Catalytic Synthesis of Butenolides.

In 2011, the group of Hashmi reported the rhodium-catalyzed carboauration of alkynes, involving a transmetalation step between rhodium and gold complexes.⁴⁵

Finally, it is also worth mentioning the need of a judicious election of ligands in bimetallic catalysis, since ligand metathesis reactions can take place. Our research group has studied the ligand metathesis in the Stille co-catalyzed Au/Pd coupling of bulky substrates ArX with SnBu₃R.⁴⁶ A good ligand election can become decisive for the success of the reaction when different ligands and metals are involved in a bimetallic catalytic system.

¹ a) Miyaura, N. and Suzuki, A. *Chem. Rev.* **1995**, *95*, 2457–2483; b) Phan, N.; V. D. Sluys, M. and Jones, C. W. *Adv. Synth. Catal.* **2006**, *348*, 609–679; c) Maluenda, I. and Navarro, O. *Molecules*, **2015**, *20*(5), 7528–7557.

² García–Melchor, M.; Braga, A.; Lledós, A.; Ujaque, G.; Maseras, F. *Acc. Chem. Res.* **2013**, *46*, 2626–2634.

³ a) Hiyama, J. *J. Organomet. Chem.* **2002**, *653*, 58–61; b) Nakao, I. and Hiyama, T. *Chem. Soc. Rev.* **2011**, *40*, 4893–4901; c) Sore, H. F.; Galloway, W. and Spring, D. R. *Chem. Soc. Rev.* **2012**, *41*, 1845–1866.

⁴ Denmark, S. E. and Baird, J. D. *Chem. Eur. J.* **2006**, *12*, 4954–4963.

⁵ Espinet, P. and Echavarren, A. M. *Angew. Chem. Int. Ed.* **2004**, *43*, 4704–4734.

⁶ Cordovilla, C.; Bartolomé, C.; Martínez–Ilarduya, J. M. and Espinet, P. *ACS Catal.* **2015**, *5*, 3040–3053.

⁷ Casado, A. L.; Gallego, A. M. and Espinet, P. *J. Am. Chem. Soc.* **2000**, *122*, 11771–11782.

⁸ Casares, J. A.; Espinet, P.; Fuentes, B. and Salas, G. *J. Am. Chem. Soc.* **2007**, *129*, 3508–3509.

⁹ Fuentes, B.; García–Melchor, M.; Lledós, A.; Maseras, F.; Casares, J. A.; Ujaque, G. and Espinet, P. *Chem. Eur. J.* **2010**, *16*, 8596–8599.

¹⁰ Garcia–Melchor, M.; Fuentes, B.; Lledos, A.; Casares, J. A.; Ujaque, G. and Espinet, P. *J. Am. Chem. Soc.* **2011**, *133*, 13519–13526.

¹¹ delPozo, J.; Gioria, E.; Casares, J. A.; Álvarez, R. and Espinet, P. *Organometallics*, **2015**, *34*, 3120–3128.

¹² a) Jin, L.; Zhang, H.; Li, P.; Sowa, J. R. and Lei, A. *J. Am. Chem. Soc.*, **2009**, *131*, 9892–9893; b) Jin, L.; Xin, J.; Huang, Z.; He, J. and Lei, A. *J. Am. Chem. Soc.*, **2010**, *132*, 9607–9609; c) Xin, J.; Zhang, G.; Deng, Y.; Zhang, H. and Lei, A. *Dalton Trans.* **2015**, *44*, 19777–19781.

¹³ a) Avola, S.; Dubovyk, I.; Hadei, N.; Kantchev, E. A. B.; O’Brien, C. J. Valente, C.; and Organ, M. G. *Chem. Eur. J.* **2006**, *12*, 4749–4755; b) Achonduh, G. T.; Hadei, N.; Valente, C.; Avola, S.; O’Brien, C. J. and Organ, M. G. *Chem. Commun.* **2010**, *46*, 4109–4111; c) Hunter, H. N.; Hadei, N.; Blagojevic, V.; Patschinski, P.; Achonduh, G. T.; Avola, S.; Bohme, D. K. and Organ, M. G. *Chem. Eur. J.* **2011**, *17*, 7845–7851; d) McCann, L. C. and Organ, M. G. *Angew. Chem. Int. Ed.* **2014**, *53*, 4386–4389.

¹⁴ a) Ryabov, A. N.; Izmer, V. V.; Tzarev, A. A.; Uborsky, D. V.; Asachenko, A. F.; Nikulin, M. V.; Canich, J. A. M. and Voskoboinikov, A. Z. *Organometallics*, **2009**, *28*, 3614–3617; b) Cleghorn, L. A.; Grigg, R.; Savic, V. and Simic, M. *Tetrahedron*, **2008**, *64*(37), 8731–8737; c) Grigg, R.; Blacker, J.; Kilner, C.;

McCaffrey, S.; Savic, and Sridharan, V. *Tetrahedron*, **2008**, *64*(35), 8177–8181; d) Jagenbrein, M.; Monakhov, K. and Braunstein, P. *J. Organomet. Chem.* **2015**, *796*, 11–16; e) Pérez–Temprano, M. H.; Casares, J. A. and Espinet, P. *Chem. Eur. J.* **2012**, *18*, 1864–1884.

¹⁵ Hayashi, I.; Yamamoto, A.; Hagihara, T. and Ito, Y. *Tetrahedron Lett.* **1986**, *27*, 191–194.

¹⁶ For Reviews on gold catalysis, see: a) Hashmi, A. S. K. and Hutchings, G. J. *Angew. Chem. Int. Ed.* **2006**, *45*, 7896–7936; *Angew. Chem.* **2006**, *118*, 8064–8105; b) Hashmi, A. S. K. *Chem. Rev.* **2007**, *107*, 3180–3211; c) Fürstner, A. and Davies, P. W. *Angew. Chem. Int. Ed.* **2007**, *46*, 3410–3449; *Angew. Chem.* **2007**, *119*, 3478–3519; d) Arcadi, A. *Chem. Rev.* **2008**, *108*, 3266–3325; e) Jiménez-Núñez, E. and Echavarren, A. M. *Chem. Rev.* **2008**, *108*, 3326–3350; f) Gorin, D. J.; Sherry, B. D. and Toste, F. D. *Chem. Rev.* **2008**, *108*, 3351–3378; g) Fürstner, A. *Chem. Soc. Rev.* **2009**, *38*, 3208–3221; h) Corma, A.; Leyva-Perez, A. and Sabater, M. J. *Chem. Rev.* **2011**, *111*, 1657–1712; i) N. Krause, C. Winter, *Chem. Rev.* **2011**, *111*, 1994–2009; j) Rudolph, M. and Hashmi, A. S. K. *Chem. Soc. Rev.* **2012**, *41*, 2448–2462; k) I. Braun, A. M. Asiri, A. S. K. Hashmi, *ACS Catal.* **2013**, *3*, 1902–1907; l) C. M. Friend, A. S. K. Hashmi, *Acc. Chem. Res.* **2014**, *47*, 729–730.

¹⁷ a) Fürstner, A. and Davies, P. W. *Angew. Chem. Int. Ed.* **2007**, *46*, 3410–3449; b) Hashmi, A. S. K.; Lothschutz, C.; Dopp, R.; Ackermann, M.; De Buck Becker, J.; Rudolph, M.; Scholz, C. and Rominger, F. *Adv. Synth. Catal.* **2012**, *354*, 133–147; c) Hashmi, A. S. K.; *Acc. Chem. Res.* **2014**, *47*, 864–876; d) Dorel, R. and Echavarren, A. M. *Chem. Rev.* **2015**, *115*(17), 9028–9072.

¹⁸ Sugita, S.; Ueda, M.; Doi, N.; Takeda, N. and Miyata, O. *Tetrahedron*, **2016**, *57*, 1786–1789.

¹⁹ Hashmi, A. S. K. *Chem. Rev.* **2007**, *107*, 3180–3211.

²⁰ a) Blaya, M.; Bautista, D.; Gil–Rubio, J. and Vicente, J. *Organometallics*, **2014**, *33*, 6358–6368; b) Wu, C. Y.; Jacobsen, C. B. and Toste, F.D. *Nat. Chem.* **2015**, *517*, 449–454; c) Teles, J. H. *Angew. Chem. Int. Ed.* **2015**, *54*, 5556–5558.

²¹ a) Wolf, W. J.; Winston, M. S. and Toste, F. D. *Nat. Chem.* **2014**, *6*, 159–164; b) Cornell, T. P.; Shi and Y.; Blum, S. A. *Organometallics*, **2012**, *31*, 5990–5993; c) Molinari, L. and Hashmi, A. S. K. *Organometallics*, **2011**, *30*, 3457–3460; d) Shi, Y. and Blum, S. A. *Organometallics*, **2011**, *30*, 1776–1779; e) Hansmann, M. M.; Hashmi, A. S. K. and Lautens, M. *Org. Lett.* **2013**, *15*, 3226–3229; f) Peña–López, M.; Sarandeses, L. A. and Sestelo, J. P. *Eur. J. Org. Chem.* **2013**, 2545–2554; g) Larsen, M. H. and Nielsen, M. B. *Organometallics* **2015**, *34*, 3678–3685; h) Hirner, J. J. and Blum, S. A. *Organometallics*, **2011**, *30*, 1299–1302; i) Partyka, D. V.; Zeller, M.; Hunter, A. D. and Gray, T. G. *Inorg. Chem.* **2012**, *51*, 8394–8401 and j) Hirner, J. H. and Blum, S. A. *Tetrahedron*, **2015**, *71*, 4445–4449.

²² a) Joost, M.; Estévez, L.; Miqueu, K.; Amgoune, A. and Borissou, D. *Angew. Chem. Int. Ed.* **2015**, *54*, 5236–5240; b) Mankad, N. P. and Toste, F. D. *Chem. Sci.*,

2012, *3*, 72–76 and c) Blaya, M.; Bautista, D.; Gil–Rubio, J. and Vicente, J. *Organometallics*, **2014**, *33*, 6358–6368.

²³ Joost, M.; Amgoune, A. and Borissou, D. *Angew. Chem. Int. Ed.* **2015**, *54*, 2–26.

²⁴ Cornell, T. P.; Shi and Y.; Blum, S. A. *Organometallics*, **2012**, *31*, 5990–5993.

²⁵ Molinari, L. and Hashmi, A. S. K. *Organometallics*, **2011**, *30*, 3457– 3460.

²⁶ a) Shi, Y. and Blum, S. A. *Organometallics*, **2011**, *30*, 1776–1779; b) Hansmann, M. M.; Hashmi, A. S. K. and Lautens, M. *Org. Lett.* **2013**, *15*, 3226–3229; c) Peña–López, M.; Sarandeses, L. A and Sestelo, J. P. *Eur. J. Org. Chem.* **2013**, 2545–2554; d) Larsen, M. H. and Nielsen, M. B. *Organometallics* **2015**, *34*, 3678– 3685.

²⁷ Hirner, J. J. and Blum, S. A. *Organometallics*, **2011**, *30*, 1299–1302.

²⁸ a) Partyka, D. V.; Zeller, M.; Hunter, A. D. and Gray, T. G. *Inorg. Chem.* **2012**, *51*, 8394–8401; b) Hirner, J. H. and Blum, S. A. *Tetrahedron*, **2015**, *71*, 4445–4449.

²⁹ a) Al–Amin, M.; Roth, K. E. and Blum, S. A. *ACS Catal.* **2014**, *4*, 622–629; b) Hansmann, M. M.; Pernpointner, M.; Doop, R. and Hashmi, A. S. K. *Chem. Eur. J.* **2013**, *19*, 15290–15303.

³⁰ Pérez–Temprano, M. H.; Casares, J. A.; deLera, A. R.; Alvarez, R. and Espinet, P. *Angew. Chem. Int. Ed.* **2012**, *20*, 4917–4920.

³¹ Shi, Y.; Peterson, S. M.; Haberaecker, W. W. and Blum, S. A. *J. Am. Chem. Soc.* **2008**, *130*, 2168–2169.

³² Meyer, N.; Sivanathan, S. and Mohr, F. *J. Organomet. Chem.* **2011**, *696*, 1244–1247.

³³ Chen, Y.; Chen, M. and Liu, Y. *Angew. Chem. Int. Ed.* **2012**, *51*, 6181–6186.

³⁴ Canovese, L.; Levi, C.; Visentin, F.; Santo, C. and Bertolasi, V. *Inorg. Chim. Acta.* **2013**, *404*, 105–112.

³⁵ Dupuy, S.; Slawin, A. M. Z. and Nolan, S. P. *Chem. Eur. J.* **2012**, *18*, 14923–14928.

³⁶ Joost, M.; Gualco, P.; Mallet-Ladeira, S.; Amgoune, A. and Bourissou, D. *Angew. Chem. Int. Ed.* **2013**, *52*, 7160–7163.

³⁷ Namakura, I.; Sato, T.; Terada, M. and Yamamoto, Y. *Org. Lett.* **2007**, *9*, 4081–4083.

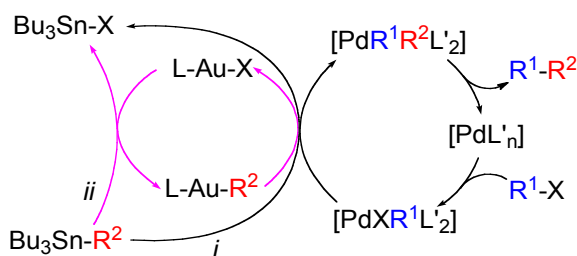
- ³⁸ Peña-López, M.; Ayán-Varela, M.; Sarandeses, L. A. and Sestelo, J. P. *Chem. Eur. J.* **2010**, *16*, 9905–9909.
- ³⁹ Hashmi, A. S. K.; Lothschütz, C.; Dopp, R.; Rudolph, M.; Ramamurthi, T. D. and Rominger, F. *Angew. Chem. Int. Ed.* **2009**, *48*, 8243–8246.
- ⁴⁰ Hansmann, M. M.; Pernpointner, M.; Döpp, R.; Hashmi, A. S. K. *Chem. Eur. J.* **2013**, *19*, 15290–15303.
- ⁴¹ Recent reviews on bimetallic catalysis: a) Pérez-Temprano, M. H.; Casares, J. A. and Espinet, P. *Chem. Eur. J.* **2012**, *18*, 1864–1884; b) Blum, S. A.; Hirner, J. J. and Shi, Y. *Acc. Chem. Res.* **2011**, *44*, 603–613; c) cita 3.
- ⁴² Chinchilla, R. and Najera, C. *Chem. Soc. Rev.* **2011**, *40* (10), 5084–5121.
- ⁴³ a) Marino, J. P. and Long, J. F. *J. Am. Chem. Soc.* **1988**, *110*, 7916–7917; b) Liebeskind, L. S.; Fengl, R. W. *J. Org. Chem.* **1990**, *55*, 5359–5364; c) Liebeskind, L. S. and Wand, J. *Tetrahedron Lett.* **1990**, *31*, 4293–4296; d) Liebeskind, L. S.; Yu, M. S.; Yu, R. H.; Wang, J. and Hagen, K. S. *J. Am. Chem. Soc.* **1993**, *115*, 9048–9055; e) Han, X.; Stoltz, B. M. and Corey, E. J. *J. Am. Chem. Soc.* **1999**, *121*, 7600–7605; f) Casado, A. L. and Espinet, P. *Organometallics*, **2003**, *22*, 1305–1309; g) Flçistrup, E.; Goede, P.; Strçmberg, R. and Malm, J. *Tetrahedron Lett.* **2011**, *52*, 209–211.
- ⁴⁴ Y. Shi, S. D. Ramgren, S. A. Blum, *Organometallics*, **2009**, *28*, 1275–1277.
- ⁴⁵ A. S. K. Hashmi, L. Molinari, *Organometallics*, **2011**, *30*, 3457–3460.
- ⁴⁶ delPozo, J.; Casares, J. and Espinet, P. *Chem. Commun.* **2013**, *49*, 7246–7248.

CHAPTER I

Thermodynamic study of Sn/Au transmetalation equilibria and consequences for the Gold Cocatalyzed Stille Coupling

1.1 INTRODUCTION

The classic Pd-catalyzed Stille reaction is a well-known efficient catalytic process for which every step has been deeply studied. The reaction is sometimes accelerated by addition of CuX salts. The so-called “copper effect” is frequently thought to be due to copper(I) mediating aryl transfer from organotin to palladium, although it has been shown also that in some cases the kinetic effect is simply due to the ability of the copper(I) to sequester the excess of ligand in the solution.^{1,2} We thought that using [AuXL] complexes as the transmetalating co-catalyst to [PdR¹XL₂] intermediates, instead of CuX salts, we would skip the L sequestering “copper effect” occurring in a Stille reaction with CuX, and would observe only the catalytic effect of Au on transmetalation in a Stille co-catalyzed reaction, in this case with gold(I) instead of copper(I) (Scheme I-1).



Scheme I-1. i) Classic Stille reaction; ii) Au co-catalyzed Stille reaction.

This reaction might be a good model to check the compatibility of palladium and gold as co-catalysts, and to explore the thermodynamic and kinetic parameters controlling this bimetallic system.

1.2 RESULTS AND DISCUSSION

1.2.1 Thermodynamics of the Au/Sn transmetalation equilibria

Due to the importance of the thermodynamics of the Au/Sn transmetalation equilibria in the system we decided to study it separately. We studied the equilibrium for different combinations of reagents ($X = Cl, I$; $R =$

vinyl, aryl, alkynyl) and ligands ($L = \text{PPh}_3, \text{AsPh}_3$), and the K_{eq} values are shown in Table 1. For $L = \text{PPh}_3$ and PMe_3 the equilibria were measured in THF, whereas for $L = \text{AsPh}_3$ the equilibria were measured in MeCN (the complexes are not soluble in THF) in the presence of added L ($L/\text{Au} = 2:1$) to stabilize the gold complexes. Most equilibria were achieved within 5 minutes (for $L = \text{AsPh}_3$) or 24 hours (for $L = \text{PPh}_3$) at room temperature. More time was needed for systems with bulky aryl groups. Numerical values were obtained for a few cases by integration of the peaks for the two gold complexes at equilibrium as observed in the ^{31}P NMR spectrum. For the rest, only reagents or only products were observed, thus restricting us to fix a minimum or maximum value for K_{eq} , assuming that 1% (for ^{31}P) or 0.1% (for ^1H and ^{19}F) concentration or higher should be observable by NMR spectroscopy. Since the relaxation times for gold compounds are almost identical (see experimental section), the integration of the ^{31}P NMR spectra is a reliable measurement of the relative concentration of the compounds in solution.

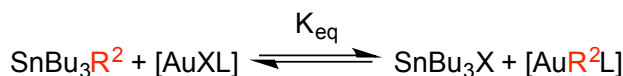


Table I-1. K_{eq} for Sn/Au transmetalation ($L^1 = \text{PPh}_3$; $L^2 = \text{AsPh}_3$; $L^3 = \text{PMe}_3$). The same results shown for $p\text{-CF}_3\text{C}_6\text{H}_4$ are obtained for $p\text{-MeOC}_6\text{H}_4$ and L^1 .

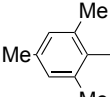
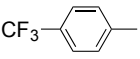
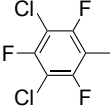
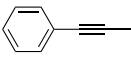
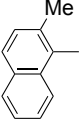
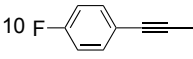
Entry	R ²	$K_{\text{eq}}(\text{X} = \text{I})$	$K_{\text{eq}}(\text{X} = \text{Cl})$	Entry	R ²	$K_{\text{eq}}(\text{X} = \text{I})$	$K_{\text{eq}}(\text{X} = \text{Cl})$
1	Vinyl	$< 10^{-5} (L^1)$ $< 10^{-5} (L^3)$	$< 10^{-5} (L^1)$ $0.2 (L^3)$	6		$0.02 (L^1)$ $> 10^6 (L^2)$	$0.30 (L^1)$ $> 10^6 (L^2)$
2		$< 10^{-5} (L^1)$ $< 10^{-5} (L^3)$	$< 10^{-5} (L^1)$ $0.9 (L^3)$	7		$5 (L^3)$	$10^{+6} (L^3)$
3		$< 10^{-5} (L^1)$ $< 10^{-4} (L^2)$	$< 10^{-5} (L^1)$ $2 \times 10^{-2} (L^2)$	8		$< 10^{-5} (L^1)$ $> 1.4 (L^3)$	$< 10^{-5} (L^1)$ $> 232 (L^3)$
4		$< 10^{-5} (L^1)$ $< 10^{-4} (L^2)$	$2 \times 10^4 (L^1)$ $> 10^6 (L^2)$	9		$0.12 (L^1)$	$0.50 (L^1)$
5		$< 10^{-5} (L^1)$ $< 10^{-4} (L^2)$ $0.04 (L^3)$	$39 (L^1)$ $> 10^6 (L^2)$ $454 (L^3)$	10		$0.15 (L^1)$	$0.20 (L^1)$

Table I-1 shows that for $X = I$ all the equilibria studied are shifted to the left, that is, the desired transmetalation from tin to gold is counter-thermodynamic. This shift is very pronounced for vinyl and most aryl groups (entries 1-5), and less so for alkynyl groups (entries 9 and 10) and for mesityl (entry 6). For $R = C_6Cl_2F_3$ and C_6F_5 (entries 7 and 8) and $X = I$, the equilibria are shifted to the right due to the stronger Au-C bond for perhaloaryl groups compared to non-halogenated aryls. Importantly, electronic and steric factors can modify this observed trend. Thus, all the equilibria are less shifted to the left for $L = AsPh_3$ than for $L = PPh_3$, probably because the better donor PPh_3 (compared to $AsPh_3$) stabilizes better gold(I) complexes with electronegative ligands $[AuXL]$. The halide is very influential, and these equilibria shift more to the right for $X = Cl$. This effect is more clearly observed in entries 4-6, and is mostly a result of the energetic contribution of the markedly different Sn-X bond energies ($Sn-Cl = 350 \text{ kJ mol}^{-1}$; $Sn-I = 235 \text{ kJ mol}^{-1}$) compared to the similar Au-X bond energies ($Au-Cl = 280 \text{ kJ mol}^{-1}$; $Au-I = 276 \text{ kJ mol}^{-1}$).³ Steric features of the transmetalated group are also influential: for bulky R^2 groups (entries 5 and 6) the equilibrium is more shifted to the right than for electronically similar but smaller R^2 groups. This trend results from some steric constraint at the tetrahedral tin center that is released upon transmetalation of the bulky group to the linear gold(I) complex.

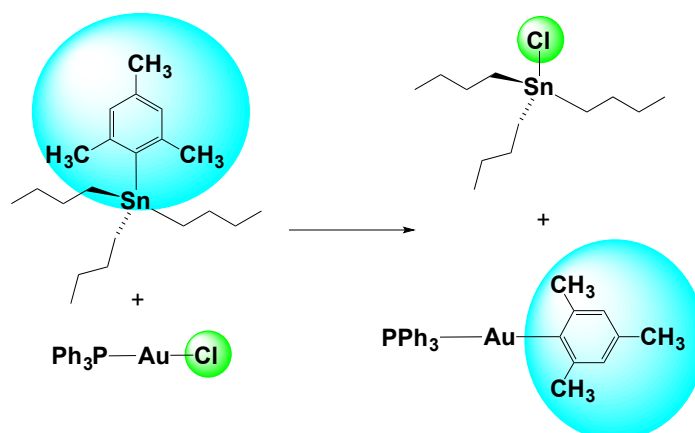
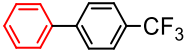
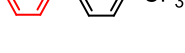
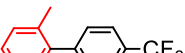
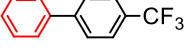
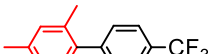
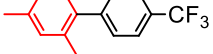
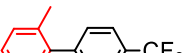
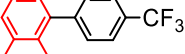
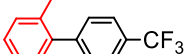


Figure I-1. Representation of the steric constraint at the tetrahedral tin center that is released upon transmetalation of the bulky mesityl group to a linear gold(I) complex.

1.2.2 Consequences for the catalytic implementation of the process

Our thermodynamic results suggest that, as far as the reaction rate depends on a higher concentration of the organogold intermediate, the reactions should be favored for $X = \text{Cl}$, according to the effect of X on the equilibria. Thus, starting with $[\text{AuClL}]$ should favor thermodynamically the transmetalation of R^2 to gold, increasing the available concentration of $[\text{AuR}^2\text{L}]$ for the subsequent transmetalation to $[\text{PdR}^1\text{XL}_2]$. However, the aryl halide used for the catalysis must be, with conventional ligands, an iodide ArI . Consequently the Pd intermediate formed is $[\text{PdR}^1\text{IL}_2]$ and the solution becomes progressively enriched in iodide, so in $[\text{AuIL}]$. In order to favor the predominance of $[\text{AuClL}]$, addition of a large excess of a soluble chloride salt should be used to regenerate $[\text{AuClL}]$ from $[\text{AuIL}]$. This was the protocol used for the catalytic coupling $p\text{-CF}_3\text{C}_6\text{H}_4\text{I}$ and aryl stannanes of different bulk. In fact the catalytic conditions included the use of added LiCl , and $[\text{AuCl}(\text{AsPh}_3)]$ and $[\text{PdCl}_2(\text{AsPh}_3)_2]$ as catalysts. This part of the study was carried out by another person of our research group, J. del Pozo, as a part of his thesis.⁴ Table I-2 summarizes the catalytic results and is included with the purpose of information of the results when applying the conditions deduced from our thermodynamic study. The percentage of untransformed **1**, and of the main side products $p\text{-CF}_3\text{C}_6\text{H}_4\text{-C}_6\text{H}_4\text{CF}_3\text{-}p$ (**2**) and $p\text{-CF}_3\text{C}_6\text{H}_5$ (**3**) are given in the column “other products”.

Table I-2. Pd-catalyzed cross-coupling of *p*-CF₃C₆H₄I (**1**) with several aryltributyltin compounds using AsPh₃ and added LiCl in absence and presence of gold co-catalysis.^a

Entry	Au Co-cat	ArC ₆ H ₄ CF ₃ product	Time (h)	Yield (%)	Other products (%)
1	Yes		5	83	2(7), 3(10)
2	No		5	68	1(22), 2(5), 3(5)
3	Yes		6	89	2(8), 3(3)
4	No		6	4	1(80), 2(3), 3(12)
5	Yes		24	84	1(<1), 2(8), 3(6)
6	No		24	<1	1(85), 2(3), 3(10)
7	Yes		24	90	2(4), 3(6)
8	No		24	0	1(81), 2(5), 3(11)
9	Yes		48	64	1(1), 2(19), 3(1)
10	No		48	0	1(19), 2(38), 3(29)

1.3 EXPERIMENTAL SECTION

General methods. All reactions were carried out under N₂ or Ar, in THF dried using a Solvent Purification System (SPS). NMR spectra were recorded on a Bruker AV 400 instrument equipped with a VT-100 variable-temperature probe, or a Varian 400-MR. Chemical shifts are reported in ppm from tetramethylsilane (¹H), CCl₃F (¹⁹F), or 85% H₃PO₄ (³¹P), with positive

^a Reactions conditions: MeCN, 80 °C, [*p*-CF₃C₆H₄I] = 0.10 M, [ArSn-(*n*Bu)₃] = 0.11 M, [AsPh₃] = 4.07x10⁻³ M, [LiCl] = saturated solution. Pd catalyst: [PdCl₂(AsPh₃)₂] = 2.0x10⁻³ M, Au catalyst: [AuCl(AsPh₃)] = 2.0x10⁻³ M. The reactions were monitored until total conversion of the starting *p*-CF₃C₆H₄I was observed, or for the time indicated. Yields were determined by peak integration of the ¹⁹F NMR spectra, and are average of two runs.

shifts downfield, at ambient probe temperature unless otherwise stated. The temperature for the NMR probe was calibrated using ethylene glycol ($T > 300\text{K}$) and methanol ($T < 300\text{K}$) as temperature standards. In the ^{19}F and ^{31}P spectra measured in non-deuterated solvents, a coaxial tube containing acetone- d_6 was used for the lock ^1H signal. The Gas Chromatography-Mass analyses were performed in a Thermo-Scientific DSQ II GC/MS Fows GL. Combustion CHN analyses were made on a Perkin-Elmer 2400 CHN microanalyzer. Unless specified, all the compounds were used from commercial sources and used without further purification. The compounds $[\text{AuCl}(\text{tht})]$,⁵ $[\text{AuCl}(\text{PPh}_3)]$,⁶ $[\text{AuCl}(\text{AsPh}_3)]$,⁷ $[\text{AuI}(\text{PPh}_3)]$,⁸ $[\text{AuMe}(\text{PPh}_3)]$,⁹ $[\text{Au}(\text{vinyl})(\text{PPh}_3)_2]$,¹⁰ $[\text{Au}(\text{C}_6\text{H}_4\text{C}\equiv\text{C})(\text{PPh}_3)]$, $[\text{Au}(\text{C}_6\text{H}_5)(\text{PPh}_3)]$,¹¹ $[\text{Au}(p\text{-CF}_3\text{C}_6\text{H}_4)(\text{PPh}_3)]$,¹² $[\text{Au}(2\text{-MeC}_{10}\text{H}_6)(\text{PPh}_3)]$, 2-methyl-1-iodonaphthalene,¹³ mesityltributyltin,¹⁴ and 2-methyl-1-naphyltributyltin,¹⁵ were prepared by literature methods. $[\text{AuRf}(\text{PPh}_3)]$, and $[\text{Au}(o\text{-MeC}_6\text{H}_4)(\text{PPh}_3)]$ were obtained by an alternative more convenient procedure.¹⁶

1.3.1 Synthesis of the complexes

$[\text{Au}(\text{C}_6\text{Cl}_2\text{F}_3)(\text{PPh}_3)]$ PPh_3 (446 mg, 1.70 mmol) was added to a stirred solution of $[\text{AuRf}(\text{tht})]$ (750 mg, 1.55 mmol) in DCM (25 mL) at room temperature. After 1 h the solution was filtered through silica, and the solvent was evaporated affording a white solid, which was washed with hexanes and re-crystallized from dichloromethane/ethanol. Yield: 657 mg. (64 %). ^1H NMR (acetone- d_6): δ 7.72–7.57 (m, 15H). ^{19}F NMR (CDCl_3): δ -90.12 (s, 2F); δ -116.17 (s, 1F). ^{31}P NMR (CDCl_3): δ 42.71 (s). Cald. for $\text{C}_{24}\text{H}_{15}\text{AuCl}_2\text{F}_3\text{P}$: C, 43.73; H, 2.51. Found: C, 43.56; H, 2.29.

$[\text{Au}(p\text{-FC}_6\text{H}_4\text{C}\equiv\text{C})(\text{PPh}_3)]$ A two-necked flask was charged with 74 μL of $p\text{-FC}_6\text{H}_4\text{C}\equiv\text{CH}$ (1.212 mmol) and 50 mL of THF. The mixture was cooled to -78°C and 0.75 mL (1.2 mmol) of a 1.6 M solution of Li^iBu in hexanes were added dropwise. The reaction was stirred for 1h, and then 500 mg of $[\text{AuCl}(\text{PPh}_3)]$ (1.01 mmol) were added. The mixture was heated to 23°C and

stirred for 1 h, and three drops of methanol were added to hydrolyze the unreacted organolithium. The solution was filtered and the solvents were evaporated. The residue was extracted with 2 x 10 mL of toluene, the toluene solution was filtered and the toluene was evaporated giving a white solid, which was re-crystallized from hexane/EtOH. Yield 175 mg (30 %). ^1H NMR (acetone- d_6 , 293 K): δ 7.55–7.45 (m, 15H), 7.3–7.2 (m, 2H), 6.95–6.85 (m, 2H). ^{31}P NMR (acetone- d_6 , 293 K): δ 42.02 (s, 1P). ^{19}F NMR (acetone- d_6 , 293 K): δ 115.75 (s, 1F). Anal. Calcd for $\text{C}_{26}\text{H}_{19}\text{AuFP}$: C, 53.99; H, 3.31. Found: C, 53.37; H, 3.01.

[Au(*p*- $\text{CF}_3\text{C}_6\text{H}_4$)(AsPh $_3$)] A two-necked flask was charged with 143 μL (1.02 mmol) of *p*- $\text{CF}_3\text{C}_6\text{H}_4\text{Br}$ and 50 mL of THF. The mixture was cooled to -78 $^\circ\text{C}$ and 0.64 mL (1.02 mmol) of a 1.6 M solution of LiBu in hexanes were added dropwise. The reaction was stirred for 1h, and then 65 mg of AsPh $_3$ (0.21 mmol) and 500 mg of [AuCl(AsPh $_3$)] (0.929 mmol) were added. The mixture was heated to 0 $^\circ\text{C}$ and stirred for further 15 minutes. The solution was concentrated to 10 mL and 20 mL of EtOH were added. Partial evaporation of the solution gave a white solid that decomposes during its isolation, rendering a purple solid. The solid was dissolved in the minimum amount of DCM (5 mL), treated with graphite powder and filtered to a flask containing cold *n*-hexane in an ice bath. The white solid obtained was filtered and vacuum dried. Yield 275 mg (40 %). ^1H NMR (acetonitrile- d_3 , 293 K): δ 7.50–7.25 (m, 19H). ^{19}F NMR (acetonitrile- d_3 , 293 K): δ -62.72 (s, 1F). Anal. Calcd for $\text{C}_{25}\text{H}_{19}\text{AsAuF}_3$: C, 46.32; H, 2.95. Found: C, 46.09; H, 2.78.

[Au(2,4,6-Me $_3$ C $_6$ H $_2$)(AsPh $_3$)] The same procedure as for [Au(*p*- $\text{CF}_3\text{C}_6\text{H}_4$)(AsPh $_3$)] but using 2-bromomesitylene (156 μL , 1.02 mmol) instead of *p*- $\text{CF}_3\text{C}_6\text{H}_4\text{Br}$. Yield 370 mg (58 %). ^1H NMR (acetonitrile- d_3 , 293 K): δ 7.65–7.50 (m, 15H), 2.26–2.22 (s, 3H), 2.12–2.05 (s, 6H). Anal. Calcd for $\text{C}_{27}\text{H}_{26}\text{AsAu}$: C, 52.10; H, 4.21. Found: C, 51.92; H, 4.11.

[Au(*o*-MeC₆H₄)(AsPh₃)] The same procedure as for [Au(*p*-CF₃C₆H₄)(AsPh₃)] but using 2-bromotoluene (246 μ L, 2.04 mmol) instead of *p*-CF₃C₆H₄Br and 1.28 mL (2.04 mmol) of a 1.6 M solution of LiBu (an excess of organolithium was used because using the stoichiometric amount the yield was very low. Yield 360 mg (59 %). ¹H NMR (acetonitrile-*d*₃, 293 K): δ 7.65–7.55 (m, 15H), 2.13–2.10 (s, 3H). Anal. Calcd for C₂₅H₂₂AsAu: C, 50.52; H, 3.73. Found: C, 50.34; H, 3.51.

[Au(2-MeC₁₀H₆)(AsPh₃)] The same procedure as for [Au(*p*-CF₃C₆H₄)(AsPh₃)] but using 160 μ L of 1-bromo-2-methylnaphthalene (1.02 mmol) instead of *p*-CF₃C₆H₄Br. Yield 363 mg (55 %). ¹H NMR (acetonitrile-*d*₃, 293 K): δ 8.55–8.47 (d, 1H), 7.77–7.72 (d, 1H), 7.71–7.64 (m, 6H), 7.6–7.51 (m, 10H), 7.1–7.64 (m, 2H), 7.34–7.27 (m, 1H). Anal. Calcd for C₂₉H₂₄AsAu: C, 54.05; H, 3.75. Found: C, 53.93; H, 3.49.

[Au(*o*-MeC₆H₄)(PPh₃)] A two-necked flask was charged with 447 μ L (3.72 mmol) of 2-bromotoluene and 50 mL of THF. The mixture was cooled to –78 °C and 2.32 mL (3.72 mmol) of a 1.6 M solution of LiBu in hexanes were added dropwise. The solution was stirred for 1h, 1000 mg (1.86 mmol) of [AuCl(AsPh₃)] were added, and the reaction was placed in an ice bath. After one hour at 0 °C, 975 mg (3.72 mmol) of PPh₃ were added and the solution was concentrated to 5 mL. A white crystalline product was obtained by the addition of 20 mL of EtOH and further concentration to 15 mL. The solid was filtered, washed with EtOH and hexane and vacuum dried. Yield 950 mg (88 %). ¹H NMR (CDCl₃, 293 K): δ 7.65–7.55 (m, 6H), 7.55–7.40 (m, 10H), 7.25–7.20 (d, 1H), 7.15–7.10 (t, 1H), 7.10–7.00 (t, 1H), 2.65–2.60 (s, 3H). ³¹P NMR (CDCl₃, 293 K): δ 44.40 (s, 1P). Anal. Calcd for C₂₅H₂₂AuP: C, 54.56; H, 4.03. Found: C, 54.36; H, 4.11.

2,6-Diisopropylphenyl-tributyltin A two-necked flask was charged with 2,6-diisopropyl-1-bromo-benzene (1.078 g, 4.47 mmol) and 20 mL of

Et₂O. The mixture was cooled to -78 °C and a 1.5 M solution of Li^tBu in hexanes (3.3 mL, 4.92 mmol) was added dropwise. The solution was stirred for one hour at this temperature, then for 15 minutes more at room temperature. The solution was cooled again to -78 °C and ISnBu₃ (1.42 mL, 4.47 mmol) was added dropwise. The solution was allowed to warm to room temperature overnight, and then it was quenched with a saturated aqueous solution of NH₄Cl (30 mL). The aqueous layer was decanted and extracted with Et₂O (3x30 mL). All the organic layers were combined, washed with brine (3x60 mL) and dried over MgSO₄. The solvent was removed under reduced pressure. The product was purified by chromatography in silica, with hexane as eluent, to give a colorless liquid, identified as a mixture of 2,6-diisopropylphenyl-tributyltin and 1,3-diisopropylbenzene. The final product was obtained by distilling off the 1,3-diisopropylbenzene at 160 °C under reduced pressure. A colorless liquid was obtained (yield: 665 mg, 34 %). ¹H NMR (500 MHz, CDCl₃) δ 7.33 (t, $J = 7.6$ Hz, 1H), 7.19 (d, $J = 7.6$ Hz, 2H), 2.94 (m, $J = 6.98$ Hz, 2H), 1.64–1.52 (m, 6H), 1.40 (m, $J = 14.6, 7.3$ Hz, 6H), 1.29 (d, $J = 6.8$ Hz, 12H), 1.21–1.04 (m, 6H), 0.95 (m, 9H). ¹³C NMR (126 MHz, CDCl₃) δ 156.14 (s), 141.23 (s), 128.73 (s), 122.64 (s), 36.87 (s), 29.26 (s), 27.48 (s), 25.25 (s), 13.66 (s), 13.13 (s). ¹¹⁹Sn NMR (186 MHz, CDCl₃) δ -61.22 (s). GC–MS: MS (EI⁺, 70 eV): m/z (%): 395 (100) [M–Bu]⁺, 339 (20), 281 (45) [M–Bu₃]⁺.

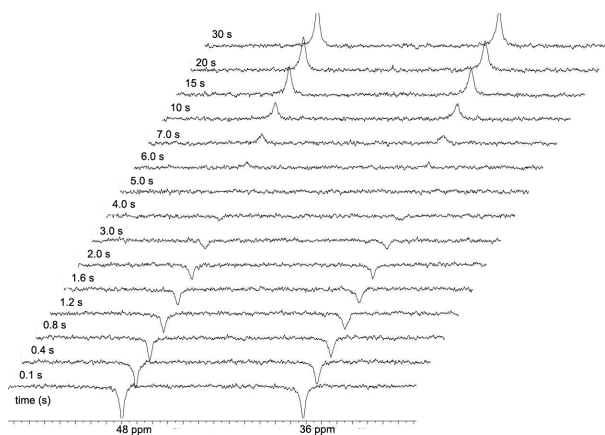
***p*-Fluorophenylacetylene-tributyltin** A solution of *p*-FC₆H₄CCH (0.64 mL, 5.24 mmol) in THF (50 mL) was cooled to -78 °C and 3.28 mL of *n*-BuLi 1.6 M in hexane (5.25 mmol) were added. The reaction was stirred for one hour, and then SnClBu₃ (1.36 mL, 5.0 mmol) was added. The solution was taken to room temperature and stirred for one hour. After this time three drops of EtOH were added to quench the remaining organolithium and the solvent was evaporated to dryness. The residue was dissolved in hexane, the solution filtered with silica, and the hexane was evaporated affording the compound as colorless oil. Yield 1.6 g, (79 %). ¹H NMR (acetone-*d*₆, 293 K): δ 7.50–7.43 (m, 2H), 7.15–7.08 (t, 2H), 1.8–1.56 (m, 6H), 1.45–1.34 (m, 6H), 1.19–1.00 (m,

6H), 0.97–0.87 (t, 9H). ^{119}Sn NMR (acetone- d_6 , 293 K): δ –65.41 (s). ^{19}F NMR (acetone- d_6 , 293 K): δ –113.47–113.19 (m, 1F). Anal. Calcd for $\text{C}_{20}\text{H}_{31}\text{FSn}$: C, 58.71; H, 7.64. Found: C, 58.57; H 7.75. GC–MS: MS (EI $^+$, 70 eV): m/z (%): 353 (65) $[\text{M–Bu}]^+$, 297 (40) $[\text{M–Bu}_2]^+$, 239 (100) $[\text{M–Bu}_3]^+$.

1.3.2 General procedure of the reactions between organotin compounds with gold(I) complexes

Calibrated NMR tubes (5mm) were charged with the corresponding gold complex $[\text{AuXL}]$ or $[\text{AuRL}]$ (in the case of $\text{L} = \text{AsPh}_3$, 2 equivalents of AsPh_3 respect to the gold complex were added to prevent their decomposition), dissolved in *ca.* 0.4 mL of deoxygenated CD_3CN . The desired amount of SnBu_3X or SnBu_3R^2 , and then further solvent to reach a total volume of 0.6 mL were added. The samples were left at room temperature and were checked periodically by ^1H NMR until the equilibrium had been established (typically a few minutes to one hour) and then checked again after 24 hours to verify that the concentration values kept constant. The equilibrium constants (K_{eq}) were calculated from the integrated values of the ^1H NMR signals in equilibrium. An acetone- d_6 capillary was added for NMR look. The equilibrium constants of reactions involving complexes with PPh_3 and PMe_3 were measured analogously using THF as solvent, since they are not soluble in CD_3CN at 25 °C. No added free ligand was used because they are stable enough in solution. The K_{eq} values were obtained from the ^{31}P NMR integrated signals.

1.3.3 ^{31}P NMR T_1 Inversion Recovery Experiment of a mixture of PhAuPPh_3 and ClAuPPh_3



$T_1 = 7.2$ s for both complexes. Since the relaxation times are almost identical for both complexes, the integration of the ^{31}P NMR spectra is a reliable measurement of the relative concentration of the compounds in solution.

- ¹ a) Marino, J. P. and Long, J. F. *J. Am. Chem. Soc.* **1988**, *110*, 7916–7917; b) Liebeskind, L. S. and Fengl, R. W. *J. Org. Chem.* **1990**, *55*, 5359–5364; c) Liebeskind, L. S. and Wand, J. *Tetrahedron Lett.* **1990**, *31*, 4293–4296; d) Liebeskind, L. S.; Yu, M. S.; Yu, R. H.; Wang, J. and Hagen, K. S. *J. Am. Chem. Soc.* **1993**, *115*, 9048–9055; e) Liebeskind, L. S. and Riesinger, S. W. *J. Org. Chem.* **1993**, *58*, 408–413; f) Allred, G. D. and Liebeskind, L. S. *J. Am. Chem. Soc.* **1996**, *118*, 2748–2749; g) Mazzola, R.D.; Giese, S.; Benson, C. L. and West, F.G. *J. Org. Chem.* **2004**, *69*, 220–223; h) Flöistrup, E.; Goede, P.; Strömberg, R. and Malm, J. *Tetrahedron Lett.* **2011**, *52*, 209–211.
- ² a) Casado, A. L. and Espinet, P. *Organometallics*, **2003**, *6*, 1305–1309; b) Farina, V.; Kapadia, S.; Krishnan, B.; Wang, C. and Liebeskind, L. S. *J. Org. Chem.* **1994**, *59*, 5905–5911.
- ³ CRC Handbook of Chemistry and Physics, Internet Version 2005 (Ed. D. R. Lide), CRC, Boca Raton, FL, 2005; <http://www.hbcpnetbase.com>.
- ⁴ Juan delPozo Doctoral Thesis. University of Valladolid, January 2016.
- ⁵ Usón, R. and Laguna, M. *Inorg. Synth.* **1989**, *26*, 85–91.
- ⁶ Sinha, P.; Wilson, A. K. and Omary, M. A. *J. Am. Chem. Soc.* **2005**, *127* (36), 12488–12489.
- ⁷ Nieto–Oberhuber, C.; López, S. and Echavarren, A. M. *J. Am. Chem. Soc.* **2005**, *127*, 6178–6179.
- ⁸ Schuster, O. and Schmidbaur, H. *Inorg. Chim. Acta.* **2006**, *359* (11), 3769–3775.
- ⁹ Mizushima, E.; Cui, D–M.; Chandra, D.; Nath, D.; Hayashi, T. and Tanaka, M. *Org. Synth.* **2006**, *83*, 55–60.
- ¹⁰ Mohr, F.; Falvello, L. R. and Laguna, M. *Eur. J. Inorg. Chem.* **2006**, 833–838.
- ¹¹ Peña–López, M.; Ayán–Varela, M.; Sarandeses, L. A. and Sestelo, J. *Chem. Eur. J.* **2010**, *16*, 9905–9909.
- ¹² Shi, Y.; Ramgren, S. D. and Blum, S. A. *Organometallics*, **2009**, *28*(5), 1275–1277.
- ¹³ Cammidge, A. N. and Crépy, K. V. L. *Tetrahedron*, **2004**, *60* (20), 4377–4386.
- ¹⁴ Littke, A. F.; Schwarz, L. and Fu, G. C. *J. Am. Chem. Soc.* **2002**, *124*, 6343–6348.
- ¹⁵ Weisemann, C.; Schmidtberg, G. and Brune, H. J. *Organomet. Chem.*, **1988**, *361*, 299–307.
- ¹⁶ Partyka, D. V.; Zeller, M.; Hunter, A. D. and Gray, T. G. *Angew. Chem. Int. Ed.* **2006**, *45*, 8188–8191.

CHAPTER II

Mechanistic study of Sn/Au^I Group Exchanges

2.1 INTRODUCTION

Whereas organic group/halide exchanges in cross-coupling catalysis have been deeply studied,¹ transmetalations exchanging two carbon groups between metals, often involved in bimetallic catalysis and in formation of homocoupling products, are very little studied. Only recently, transmetalations between gold complexes and organotin derivatives have been studied due to its appearance in multimetallic catalytic processes.

In this chapter kinetic and thermodynamics studies on the Sn/Au transmetalation reactions involving different organostannanes and gold(I) complexes have been done. We examine the thermodynamic and kinetic behavior of the transmetalation reactions in which an organic group ($R = C_6H_5$) is exchanged by: i) Cl; ii) trifluoromethylsulfonate ($CF_3SO_3^-$) and iii) vinyl. The work has been completed with DFT studies that have been carried out by Dr. Max García-Melchor, uncovering a dramatic mechanistic switch in the reaction mechanism for the vinyl group compared to the halogen and the triflate that explains the marked kinetic differences observed in our experimental study. When $X = Cl$ or triflate a concerted mechanism is produced whereas an oxidative addition/reductive elimination pathway through an Au^{III} intermediate is produced when $X = vinyl$.

2.2 RESULTS AND DISCUSSION

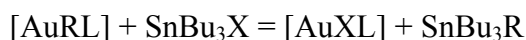
2.2.1 Thermodynamics of the transmetalation reaction

The thermodynamics of X for R exchange between Au(I) and Sn was discussed in the Chapter I (pages 47-49). As discussed before, for $X = I$, the equilibria are strongly shifted to the left, except for $R = C_6Cl_2F_3$ and C_6F_5 that are shifted to the right; this is due to the stronger Au-C bond for perhaloaryl groups compared to non-halogenated aryls. For $X = Cl$ the equilibria are more balanced because of the high energy of the Sn-Cl bond. For $X = vinyl$, the

aryl/vinyl exchange is too slow at 303 K and the equilibrium is only reached in a reasonable time at 323 K, showing that it is slightly displaced to the left.

2.2.2 Kinetics of the reaction

2.2.2.1 Reactions between [AuPhL] (L = PCy₃, PMe₃, and PPh₃) and SnBu₃Cl



The reaction rates, from left to right of the previous equation, for Ph/Cl exchanges at 303 K with L = PCy₃, PMe₃, and PPh₃ were measured.

Table II-1. Values for the rate constants of transmetalation reactions between [AuPhL] and SnBu₃Cl in THF at 303 K.

Gold compound	[AuPhL] / mol L ⁻¹	Rate constant / L mol ⁻¹ s ⁻¹
[AuPh(PMe ₃)]	0.039	5.08(±3) x10 ⁻⁴
[AuPh(PPh ₃)]	0.027	9.4(±2) x10 ⁻⁵
[AuPh(PCy ₃)]	0.026	3.453(±8) x10 ⁻⁴

The modest dependence on the phosphine ligand suggests that phosphine dissociation during the Ar/X exchange reaction does not occur and the variations are only due to the electronic differences of the phosphines as coordinating ligands.

2.2.2.2 Reactions between [AuPh(PMe₃)] with SnBu₃Cl and SnBu₃I in THF and acetonitrile

The effect of the leaving group in the tin atom has also been tested. The reactions between [AuPh(PMe₃)] with SnBu₃Cl and SnBu₃I were monitored in THF and acetonitrile at -20 °C.

Experiments in THF. The experimental value for the reaction rate in the reaction between [AuPh(PMe₃)] and SnBu₃Cl is 1.95 (±3) x10⁻⁴ L mol⁻¹ s⁻¹ and

for the reaction with SnBu₃I the experimental value is $1.81 (\pm 2) \times 10^{-3} \text{ L mol}^{-1} \text{ s}^{-1}$.



a) X = Cl

b) X = I

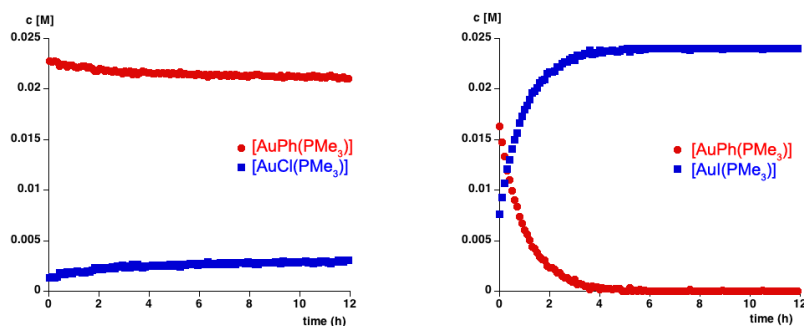


Figure II-1. Observed concentrations of $[\text{AuPh}(\text{PMe}_3)]$ and $[\text{AuX}(\text{PMe}_3)]$ ($X = \text{Cl}, \text{I}$) as a function of time. Starting concentrations: $[\text{SnBu}_3\text{X}]_0 = 0.24 \text{ mol L}^{-1}$ and $[\text{AuPh}(\text{PMe}_3)] = 0.024 \text{ mol L}^{-1}$ at 253 K in THF.

Experiments in acetonitrile. In this solvent the reactions go faster than in THF. For the reaction between $[\text{AuPh}(\text{PMe}_3)]$ and SnBu₃Cl the experimental value for the reaction rate is $2.39 (\pm 5) \times 10^{-3} \text{ L mol}^{-1} \text{ s}^{-1}$ at 253 K. The reaction between $[\text{AuPh}(\text{PMe}_3)]$ and I-SnBu₃ or SnBu₃OTf is so fast that at -20°C in the first spectra of ^{31}P there is only the final product $[\text{AuX}(\text{PMe}_3)]$.

With these previous data in hand, we chose for detailed study the exchanges between $[\text{AuPh}(\text{PMe}_3)]$ and SnBu₃X with $X = \text{Cl}, \text{OTf}$ and vinyl, in view of the remarkable rate difference observed for them. These reactions were monitored in THF and in toluene solutions, using ^{31}P NMR.

2.2.2.3 Reaction between $[\text{AuPh}(\text{PMe}_3)]$ and SnBu₃Cl

The solutions of SnBu₃Cl and $[\text{AuPh}(\text{PMe}_3)]$ in THF are non-conducting, supporting that the Cl ligand is coordinated to one metal center, throughout the reaction. The study of the Ph/Cl transmetalation, using Sn:Au = 20:1 in order to simplify the handling of data and to ensure that the equilibrium

is established in a reasonable time, affords $K_{\text{eq}} = 1.1$ at 298 K. Kinetic experiments at 303 K show that the reaction is first order in $[\text{AuPh}(\text{PMe}_3)]$ (Figure II-2).

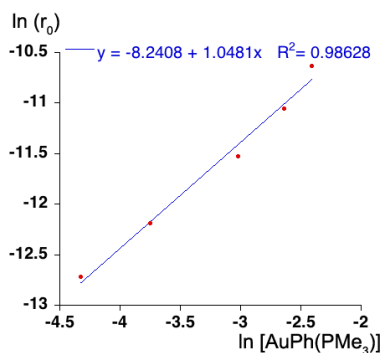


Figure II-2. Plot of $\ln[r_0]$ vs $\ln[\text{AuPh}(\text{PMe}_3)]$.

The exchange rates measured in the temperature range 250-330 K afford the activation parameters $\Delta H^\ddagger = 27(\pm 2)$ k J mol⁻¹, $\Delta S^\ddagger = -223(\pm 23)$ J K⁻¹ mol⁻¹, $\Delta G^\ddagger_{298} = 22.3$ kcal mol⁻¹ (Figure II-3). For comparison with experiments and calculations to come, ΔG^\ddagger_{323} in THF is 23.7 kcal mol⁻¹. The strongly negative ΔS^\ddagger value clearly supports an associative exchange process. The same reaction was also studied in toluene, resulting in a very similar activation Gibbs energy ($\Delta G^\ddagger_{298} = 22.0$ kcal.mol⁻¹), which discards the possible participation in the first of THF as coordinating agent. These values fit well with an associative process.

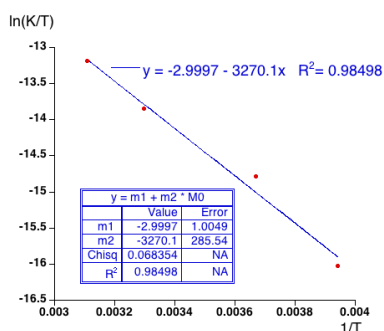


Figure II-3. Eyring plot for the reaction between $[\text{AuPh}(\text{PMe}_3)]$ and SnBu_3Cl .

DFT calculations for the reaction between $[\text{AuPh}(\text{PMe}_3)]$ and SnBu_3Cl shown in Figure II-3 match well the experimental activation energy $\Delta G_{323}^\ddagger = 24.2 \text{ kcal mol}^{-1}$ and predict a balanced equilibrium, as observed experimentally. They also match the experimental result that the phosphine ligand remains coordinated to gold along the reaction pathway. The mechanism basically consists in a double group exchange via single (TS1) or double-bridged intermediates (TS2) or transition states, as typically found in Pd. At variance with Pd^{II} , the transmetalation involving Au^{I} does not require releasing the ancillary ligand, and the coordination number of gold increases from 2 to 3 at the transition state.

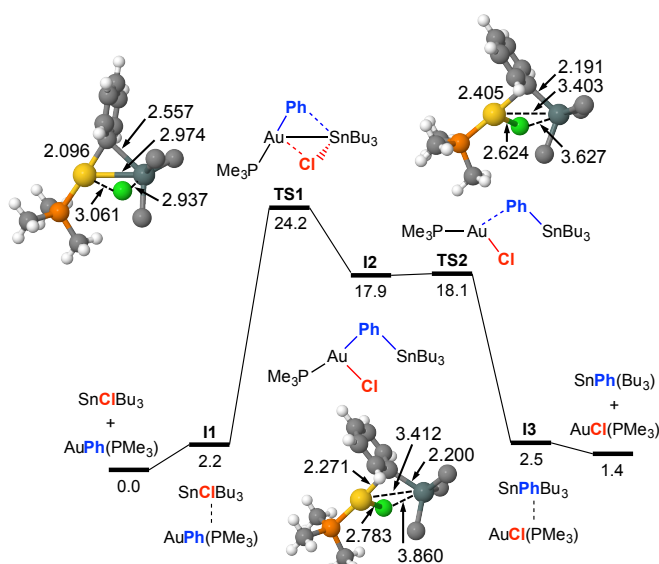


Figure II-4. Calculated Gibbs energy profile ($\text{kcal}\cdot\text{mol}^{-1}$, at 323 K and $p = 301 \text{ atm}$, see SI for details) in THF for the reaction of $[\text{AuPh}(\text{PMe}_3)]$ with SnBu_3Cl to produce $[\text{AuCl}(\text{PMe}_3)]$ and SnBu_3Ph . The optimized structures for TS1 and TS2 are shown (bond distances in Å). For the sake of clarity, the *n*-Bu moieties have been simplified in the figures. Color code: C (gray), H (white), P (orange), Cl (light green), Au (gold), Sn (dark green). I2 might not be a real intermediate.

2.2.2.4 Reaction between $[\text{AuPh}(\text{PMe}_3)]$ and $\text{SnBu}_3(\text{OTf})$

For $\text{Bu}_3\text{Sn}(\text{OTf})$ the reaction was too fast to be measured by NMR in both solvents, thus OTf is a better leaving group than Cl. As for the nature of the solutions in THF, it is not straightforward. In MeCN solution, tributyltin

triflate and $[\text{Au}(\text{OTf})(\text{PMe}_3)]$ have a molar conductivity similar to that of $(\text{NBu}_4)\text{Br}$, thus they are better described as the ionic species $[\text{SnBu}_3(\text{NCMe})]\text{OTf}$ and $[\text{Au}(\text{NCMe})\text{L}]\text{OTf}$, respectively. In THF, however, the conductivity measurements are confusing because the very low dielectric constant of the solvent leads usually to the formation of ion pairs in solution. NMR experiments are not very informative either, mainly because of the fast exchange of coordinated and dissociated triflate groups in solution. IR spectroscopy is more informative. The IR spectra of coordinated and non-coordinated triflate have been discussed elsewhere.² The triflate anion has two observable S–O stretching modes (E and A1 symmetries at about 1260 and 1030 cm^{-1}) for the SO_3 group and two ν_{st} C–F for the CF_3 moiety (E and A1 symmetries at about 1215 and 1170 cm^{-1}). The C–S stretching band has much lower frequency, below 800 cm^{-1} . The coordinated group shows three S–O (the band at 1260 splits into two) and three C–F stretching bands (the splitting of the E mode at 1215 is not always clearly observable). IR experiments support that $\text{SnBu}_3(\text{OTf})$ is mainly a neutral compound with the triflate coordinated to tin (Figure II-5), while $[\text{Au}(\text{OTf})(\text{PMe}_3)]$ produces an equilibrium mixture of $[\text{Au}(\text{OTf})(\text{PMe}_3)]$ and $[\text{Au}(\text{PMe}_3)(\text{THF})]\text{OTf}$ (Figure II-6).

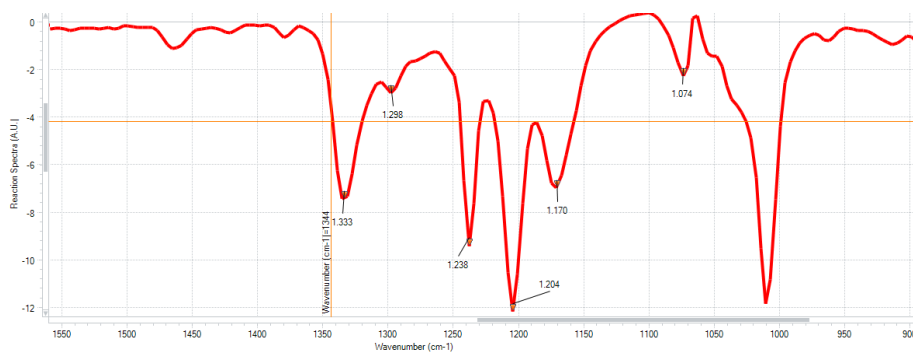


Figure II-5. IR spectrum in THF solution of SnBu_3OTf . Of note is the absence of the strong S–O band at about 1265 cm^{-1} , which is characteristic of non-coordinate triflate group. The two ν_{st} S–O bands at 1333 and 1238 cm^{-1} are indicative of coordinated triflate.

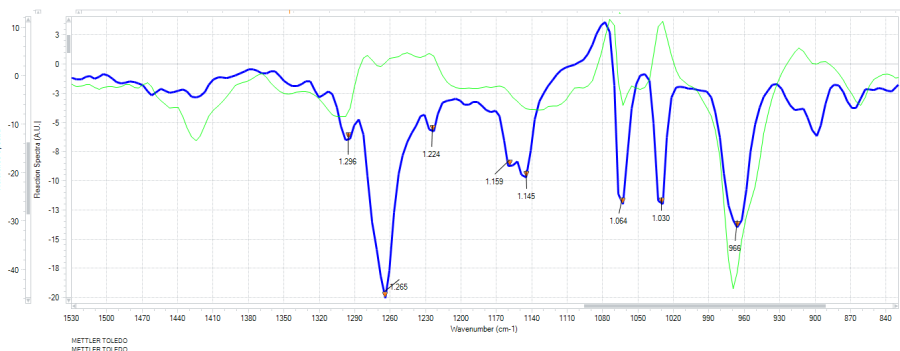


Figure II-6. IR spectrum in THF solution of [Au(OTf)(PMe₃)] (blue line) and [AuCl(PMe₃)] (green line). Two bands at 1265 cm⁻¹ and 1030 cm⁻¹ correspond to the S–O stretching modes; also two ν_{st} C–F at 1224 cm⁻¹ and 1159 cm⁻¹ are consistent with non-coordinated triflate. Additional S–O bands at 1296 cm⁻¹ and 1064 cm⁻¹ and one band at 1145 cm⁻¹ for the C–F are attributed to coordinated triflate.

We assume that the mechanism is the same produced when X = Cl, so DFT calculations were not performed for this case.

2.2.2.5 Reaction between [AuPh(PMe₃)] and SnBu₃(vinyl)

The Ph/vinyl exchange between gold and tin was also studied using a 20 fold proportion of SnBu₃(vinyl) to produce [Au(vinyl)(PMe₃)] and SnBu₃Ph. No conversion was observed at room temperature, but it took place at a low rate of $1.7 (\pm 0.2) \times 10^{-6} \text{ L mol}^{-1} \text{ s}^{-1}$ when heated 323 K ($\Delta G^{\ddagger}_{323} = 27.5 \text{ kcal/mol}$). For this exchange, DFT calculations prove that the double group exchange mechanism via bridged intermediates, proposed for X = Cl, has to be discarded for X = vinyl because it has a very high energetic barrier (42.1 kcal mol⁻¹) at the rate-determining step. Simulations also provide a reasonable and much lower energy highly symmetrical pathway that matches very well the experimental ΔG^{\ddagger} value and uncovers a dramatic mechanistic change (Figure II-7). It involves the oxidative addition of the Sn–C_{vinyl} bond to Au via **TS3**, to produce a square-planar Au^{III} intermediate *trans*-[Au(SnBu₃)Ph(vinyl)(PPh₃)] (**15**), from which the Sn–C_{Ph} or Sn–C_{vinyl} reductive elimination via **TS4** can give rise to the respective Au^I and Sn products. The calculated $\Delta G^{\ddagger}_{323}$ values are 28.6 kcal.mol⁻¹ starting from [AuPh(PMe₃)], and 28.9 starting from

[Au(vinyl)(PMe₃)]. We also carried out, as caution, a calculation of the TS energy in an oxidative addition/reductive elimination pathway for Ph/Cl exchange, which afforded an energetic barrier of 34.2 kcal/mol, confirming its unlikelihood.

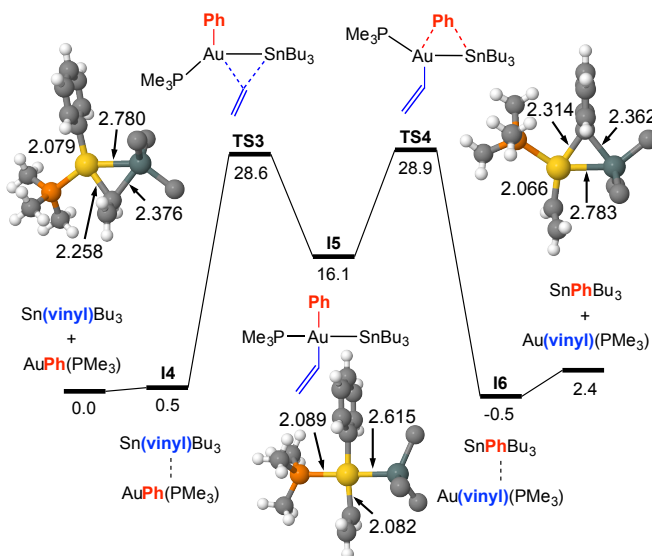


Figure II-7. Calculated Gibbs energy profile (kcal.mol⁻¹ at 323 K and p = 301 atm, in THF for the reaction of [AuPh(PMe₃)] with SnBu₃(vinyl) to produce [Au(vinyl)(PMe₃)] and Bu₃SnPh. The optimized structures for **TS3** and **TS4** are shown (bond distances in Å). For the sake of clarity, the *n*-Bu groups of the stannane have been simplified. Color code: C (gray), H (white), P (orange), Au (gold), Sn (dark green).

2.2.3 Discussion of the results

Now, the transmetalation between [AuPhL] and SnBu₃X (X = Cl, OTf and vinyl) will be compared. If we look at the figures of the calculated Gibbs energy profiles, the closely linear arrangement (P-Au-X almost 180°) present in all the starting [AuXL] complexes is very differently altered in the transition states. **TS3** shows a large alteration (P-Au-Ph = 116°) at the initial interaction, while the change in **TS1** is smaller 171°. It is also interesting to note the different Au-Sn distances in the transition states. In **TS3** (2.780 Å) and **TS4** (2.783 Å) the bond distance indicates a covalent bond (sum of the covalent radii is 2.75 Å), whereas in **TS1** the distances indicate a weaker interaction.

These results are indicative of the different orbital implications of the gold fragment at the initial interaction of the reagents in the two pathways.

Because of the very different behavior of these two reactions, we decided to make a more detailed analysis. It is well known that Sn can expand its coordination number beyond four with common coordinating molecules.³ In SnBu_3X compounds, tin center have three low energy σ^* (Bu-Sn) orbitals from what the metal can expand its coordination number (Figure II-8a). Its acceptor capacity depends on the electronegativity of X (more electronegative groups would stabilize the C-Sn σ^* orbitals, making them better acceptors), and also on the involvement of the σ^* (Bu-Sn) orbitals in negative hyperconjugation. The tin center is a stronger Lewis acid with X = Cl than with X = vinyl because of the electronegativity of the chloride and also because of the hyperconjugation of the vinyl group.

Gold can also expand its coordination number as was shown by Bourissou in a bimetallic Au/Sn system where Sn becomes pentacoordinated by an intramolecular interaction with Au as a donor ligand (experimental Au-Sn bond distance 2.891 Å).⁴ In this case gold uses its 6s orbitals. Additionally, gold also shows metallobasicity implicating the electron density of the 5d electrons (Figure II-8a). This metallobasicity is higher when the group linked to the gold center has more electron density vinyl > Cl. The ability of $[\text{AuXL}]$ complexes to act as metallobases should follow the trend vinyl > Ph > Cl, whereas the tendency of gold(I) to increase its coordination number is the opposite.

Changes in acidity and basicity of gold and tin centers allow us to understand the mechanistic change produced for X = Cl, OTf or X= vinyl. Analyzing the situations independently:

In our first case, Cl is bonded to the tin center and the phenyl group is on the gold center (Figure II-8b, **TS1**). Thus, the tin center is very acidic whereas gold, having a good donating group Ph, is more basic. In this situation

the electron density of the Ph-Au bond favors the attack of phenyl to the tin center, which becomes 5-coordinated and the lone electron pair of the Cl interacts with the gold center. When Cl is on the gold and the phenyl is bonded to tin (Figure II-8b, **TS2**), gold center accept the electrondensity of the Sn-Ph bond in its unoccupied p orbitals, becoming 3-coordinated, while the Sn atom remains 4-coordinated.

In the second case, the vinyl by aryl exchange, both, gold and tin centers are basic (Figure II-8c, **TS3**). The electron density of the Sn-vinyl bond intact with the unoccupied 6p orbitals of the gold center and also the 5d electrons interact with the σ^* tin orbitals, producing an oxidative addition of Au(I) to Au(III).

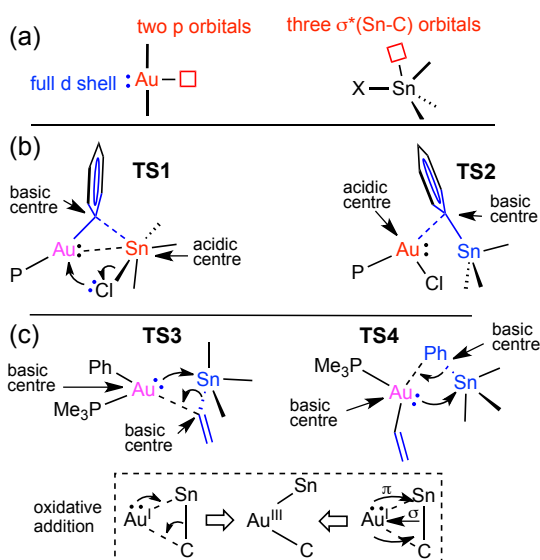


Figure II-8. Schematic orbital availability (a) and analysis of the electronic interactions involved in the transition states for exchange *via*: b) transmetalation; c) oxidative addition. Red is used for acidic centers, blue for basic, and pink for bifunctional. In the lower part of the figure two schematic representations of the electron redistribution leading to the gold intermediate **I5** are shown. Both are similar although the one at the left indicates that the donating σ (Sn-C) orbital has more contribution of C, and the σ^* (Sn-C) accepting orbital has more participation of Sn.

To investigate in detail this Au-Sn interaction in **TS1**, Dr. García-Melchor carried out a second order perturbation theory analysis of the Fock

matrices in the Natural Bond Orbital (NBO) basis (Figure II-9) that is included here for the sake of completeness.⁵

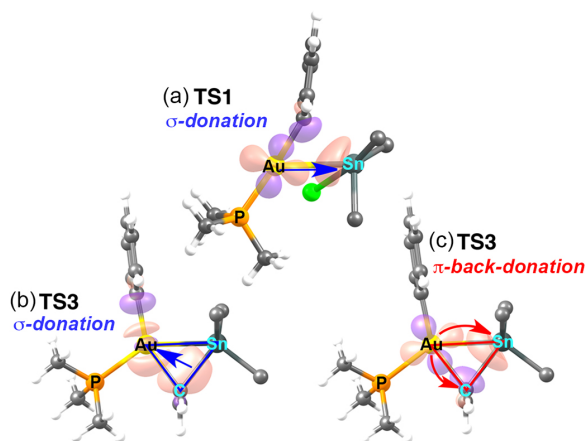


Figure II-9. Representation of the NBOs involved in: (a) donation from gold to tin in **TS1**; (b) the donation of the Sn-C_{vinyl} bond to the Au-C_{Ph} unit in **TS3**; and (c) the back-donation from Au to the Sn-C_{vinyl} bond in **TS3**. A schematic representation of these interactions in blue (b) and red (c) is superimposed.

This analysis reveals an electron donation from d orbitals of gold to a $\sigma^*(\text{Sn-Bu})$ orbital. The highly donor hydrocarbyl group R (R = Ph, vinyl) attached to Sn saturates its potential acidity and the Sn-R moiety behaves as a nucleophile attacking the gold center with the electron density of the σ (Sn-C_R) bond, more participated by the C atom. This leads to an electronically enriched 3-coordinated AuI bearing two hydrocarbyl groups, which markedly enhances its metallobasicity from the 5d(Au) orbitals.

To our knowledge, this is the first time that the oxidative addition of an Sn-C bond to gold has been proposed. The Au^{III} complexes bearing Au-Sn bonds reported to date have been obtained by oxidative addition of a fairly weak Sn-Sn bond to gold(I).^{6,7} It is worth mentioning that experimentally we do not detect any Ph-vinyl coupling product by NMR, and only traces by GC. This coupling would require the Ph and vinyl groups to achieve a *cis* disposition, either directly from the oxidative addition, or by isomerization of **I5** to any of the two possible *cis*-C,C isomers. Calculations show that *cis*-Ph/vinyl *trans*-Ph/Sn isomer (the other *cis*-C,C isomer is expected to have very similar energy)

is 8.2 kcal.mol⁻¹ less stable than the *trans* intermediate **I5**, and the calculated reductive elimination barrier to give Ph-vinyl is prohibitively high (*ca.* 44 kcal.mol⁻¹).

In summary, we find that the Sn/Au transmetalation is very much influenced by the acidity of the tin center and the metallobasicity of the gold center. When electron donor groups on tin quench the acidity of the low-lying $\sigma^*(\text{Sn-C}_{\text{Bu}})$ orbitals by hyperconjugation and the aurobasicity increases in the TS, the transmetalation switches from the classical bridge mechanism to an oxidative addition pathway. This mechanism becomes effective by participation, as acceptor of the electron density from gold, of the $\sigma^*(\text{Sn-C}_{\text{R}})$ orbital of the group being transmetalated.

2.3 EXPERIMENTAL SECTION

General methods are the same as described in Chapter I. IR spectra in solution were measured with a ReactIR (Metler-Toledo) spectrometer. The compounds [Au(C₆F₅)(tht)],⁸ [Au(C₆F₅)(PMe₃)],⁹ [AuCl(PMe₃)],¹⁰ [AuPh(PPh₃)],¹¹ [Au(C₆Cl₂F₃)(PMe₃)],¹² methyl-1-naphtyltributyltin,¹³ 3,5-dichloro-2,4,6-trifluorophenyltributyltin¹⁴ and tributylpentafluorophenyltin¹⁵ were prepared as reported in the literature. Stock solutions of SnBu₃OTf in different concentrations were prepared in dry THF under argon atmosphere and subsequently dried with zeolites for three days before their use.

2.3.1 Synthesis and characterization of the complexes

[AuI(PMe₃)] KI (2.15 g, 12.9 mmol) was added to a stirred solution of [AuCl(PMe₃)] (200 mg, 0.65 mmol) in acetone (50 mL) at room temperature. After 24 h the solution was filtered and the solvent was evaporated. The solid obtained was dissolved in dichloromethane, filtered and crystallized from dichloromethane/pentane. Yield: 200 mg. (77 %). ¹H NMR (CDCl₃, 298 K): δ 1.75 (d, *J* = 7.8 Hz, 9H). ³¹P NMR (CDCl₃, 298 K): δ 1.85 (s, 1P). ¹³C NMR

(CDCl₃, 298 K): δ 16.15 (d, $J = 37$ Hz). Cald. for C₃H₉AuIP: C, 9.00; H, 2.27. Found: C, 9.30; H, 2.16.

[Au(C₆H₅)(PMe₃)] A two-necked flask was charged with [AuCl(PMe₃)] (700 mg, 2.27 mmol) and 100 mL of THF. To this solution was added dropwise 2.6 mL, of a 1M solution of phenylmagnesium bromide in THF (2.6 mmol). The reaction was stirred during 4 hours and then three drops of water were added to stop the reaction. The solvents were evaporated and the residue was dissolved in dichloromethane, the solution was filtered through Celite, concentrated and crystallized by addition of *n*-hexane. Yield 794.5 mg (95 %). ¹H NMR (CDCl₃, 298 K): δ 7.4–7.3 (m, $J = 6.0$ Hz, 2H) δ 7.15–7.05 (m, 2H), δ 6.90 (t, $J = 7.4$ Hz, 1H). ³¹P NMR (CDCl₃, 298 K): δ 6.38 (s). ¹³C NMR (CDCl₃, 298 K, quaternary carbons are not included): δ 15.87 (d, $J = 31$ Hz), δ 125.64 (s), δ 127.45 (d, $J = 6$ Hz), δ 139.52 (s). Cald. For C₉H₁₄AuP: C, 30.87; H, 4.03. Found: C, 30.45; H, 3.93.

[Au(2-MeC₁₀H₆)(PMe₃)] A two-necked flask was charged with 280 μ L (1.78 mmol) of 1-bromo-2-metylnaphtalene and 50 mL of THF. The mixture was cooled down to -78 °C and 0.7 mL (1.0 mmol) of a 2.5 M solution of *n*-BuLi in hexane were added dropwise. The reaction was stirred for 1h and 500 mg of [AuCl(PMe₃)] (1.62 mmol) were subsequently added. The cooling bath was removed and the mixture was stirred at room temperature for 4 hours. Next, a few drops of EtOH were added. The solvents were evaporated and then it was added a saturated aqueous solution of NH₄Cl (30 mL). The aqueous layer was decanted and extracted with Et₂O (3x30 mL). All the organic layers were combined, washed with brine (3x60 mL) and dried over MgSO₄. The solvent was removed under reduced pressure and the residue was dissolved in CH₂Cl₂, filtered and precipitated by slow addition of *n*-hexane. Yield 580 mg (86 %). ¹H NMR (acetone-*d*₆, 298 K): δ 8.48 (d, $J = 8.04$ Hz, 1H), δ 7.70 (d, $J = 7.8$ Hz, 1H), δ 7.55 (d, $J = 8.0$ Hz, 1H), δ 7.3–7.1 (m, 3H), δ 2.70 (s, 3H), δ 1.65 (d, $J = 9.6$ Hz, 9H). ³¹P NMR (acetone-*d*₆, 298 K): δ 9.49 (s). ¹³C NMR (acetone-*d*₆, 298 K, quaternary carbons are not included): δ 15.51 (d, $J = 32$ Hz), δ 26.97

(s), δ 124.09 (s), δ 124.20 (s), δ 125.33 (s), 128.43 (s), δ 128.61 (d, $J = 8$ Hz), δ 134.20 (s). Cald. For $C_{14}H_{18}AuP$: C, 40.59; H, 4.38. Found: C, 40.38; H, 4.22.

[Au(C₆H₅)(PCy₃)] A two-necked flask was charged with 400 mg of [AuCl(PCy₃)] (0.78 mmol), 20 mL of THF, and 0.90 mL of a 1M solution (0.90 mmol) of phenylmagnesium bromide in THF dropwise. The reaction was stirred during 4 hours and three drops of water were added. The solvents were evaporated and the white solid was re-crystallized in CH₂Cl₂/hexane. Yield 226 mg (53 %). ¹H NMR (CDCl₃, 298 K): δ 7.40–7.30 (m, 2H), δ 7.15–7.00 (m, 2H), δ 6.88 (t, $J = 7.4$ Hz, 1H), δ 2.10–1.00 (m, 33 H). ³¹P NMR (CDCl₃, 293 K): δ 57.1 (s). ¹³C NMR (CDCl₃, 298 K, quaternary carbons are not included): δ 26.05 (s), δ 27.21 (d, $J = 12$ Hz), δ 30.69 (s), δ 33.24 (d, $J = 23.64$ Hz), δ 125.36 (s), δ 127.43 (d, $J = 6$ Hz), δ 139.26 (s). Cald. for $C_{24}H_{38}AuP$: C, 51.99; H, 6.91. Found: C, 51.64; H, 6.77.

[AuOTf(PMe₃)]. To a stirred solution of [AuCl(PMe₃)] (400 mg, 1.29 mmol) in CH₂Cl₂ (20 mL) 333 mg of Ag(OTf) (1.29 mmol) were added. After 1 h, the AgCl was filtered out and the solution was concentrated to 5 mL. To this solution, 10 mL of pentane were added producing the crystallization of the product. Yield: 243 mg. (44.00 %). ¹H NMR (acetone-*d*₆, 298 K): δ 1.87–1.84 (d, 9H). ³¹P NMR (acetone-*d*₆, 298 K): δ -12.82 (s, 1P), ¹⁹F NMR (acetone-*d*₆, 298 K): δ -78.25 (s, 3F). Cald. for $C_4H_9AuF_3O_3PS$: C, 11.38; H, 2.15. Found: C, 10.90; H, 2.36.

[Au(vinyl)(PMe₃)] This complex could not be isolated in a pure form due to extensive decomposition, but was prepared in solution to identify its NMR signals. [AuCl(PMe₃)] (1.00 g, 3.24 mmol) was dissolved in 30 mL of THF and the solution was cooled down to -20 °C. To this solution, 3.20 mL of a solution 1M of vinylmagnesium bromide in THF (3.20 mmol) were added dropwise. The reaction was stirred during 0.5 hours and 0.50 mL (0.50 mmol) of vinylmagnesium bromide was subsequently added. The solvents were evaporated, the residue was dissolved in CDCl₃, filtered, and the NMR was registered under nitrogen. ¹H NMR (CDCl₃, 298 K): δ 7.0–7.8 (m, 1H), δ 5.8–

5.6 (m, 1H), δ 5.2–5.0 (m, 1H), δ 1.5–1.42 (d, $J = 9.4$ Hz 9H). ^{31}P NMR (CDCl_3 , 298 K): δ 7.92 (s).

2.3.2 Characterization of the triflate derivatives in solution

2.3.2.1 Conductivity measurements

a) In THF. The conductivities of SnBu_3OTf and $[\text{Au}(\text{OTf})(\text{PMe}_3)]$ solutions in THF (10^{-4} M) were measured and compared with the conductivity of a THF pure solution and a $[\text{NBu}_4](\text{Br})$ solution in THF (10^{-4} M). The value obtained for the SnBu_3OTf was $2.1 \text{ S cm}^2 \text{ mol}^{-1}$, $2.4 \text{ Scm}^2\text{mol}^{-1}$ for $[\text{Au}(\text{OTf})(\text{PMe}_3)]$, $3.5 \text{ Scm}^2\text{mol}^{-1}$ for $[\text{NBu}_4](\text{Br})$ (10^{-4} M) and $0.04 \text{ Scm}^2\text{mol}^{-1}$ for the THF pure solution. The large formation of ion-pair complexes in solution precluded the measurement of more accurate and relevant data.

b) In acetonitrile. The conductivities of SnBu_3OTf , SnBu_3Cl , and SnBu_3I solutions in acetonitrile (10^{-4} M) were measured and compared with the conductivity of an acetonitrile pure solution and a $[\text{NBu}_4](\text{Br})$ solution in THF (10^{-4} M). The value obtained for SnBu_3OTf was $129.2 \text{ Scm}^2\text{mol}^{-1}$, $9.8 \text{ Scm}^2\text{mol}^{-1}$ for SnBu_3Cl , $9.8 \text{ Scm}^2\text{mol}^{-1}$ for SnBu_3I , $156.1 \text{ Scm}^2\text{mol}^{-1}$ for $[\text{NBu}_4](\text{Br})$ (10^{-4} M) and $6.3 \text{ Scm}^2\text{mol}^{-1}$ for the acetonitrile pure solution.

2.3.2.2 NMR experiments

We tried to differentiate free triflate and coordinate triflate by NMR experiments. The chemical shift of the ^{19}F NMR signal of complex $[\text{Au}(\text{OTf})(\text{PMe}_3)]$ in THF were recorded at different temperatures. At the lowest temperature available in the spectrometer used, the signal remained sharp and no signals of coalescence were observed. The chemical shift is very close to that of the solutions of $[\text{NBu}_4](\text{OTf})$ at the same temperature. A solution containing $[\text{Au}(\text{OTf})(\text{PMe}_3)]$ and $[\text{NBu}_4](\text{OTf})$ shows just one fluorine signal at an intermediate position (Figure II-10). Thus, it can be concluded that there is a fast exchange of triflate between gold and the solution.

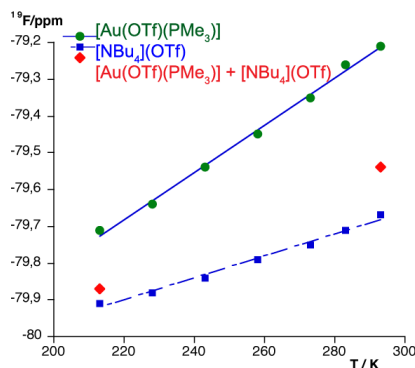


Figure II-10. Observed chemical shifts for a solution of $[\text{Au}(\text{OTf})(\text{PMe}_3)]$ (green markers), $[\text{NBu}_4](\text{OTf})$ (blue markers) and a mixture of both solutions (red marker).

The ^{19}F chemical shift of the stock solution of SnBu_3OTf in THF is almost the same (-79.84 ppm at rt) than that of $[\text{Au}(\text{OTf})(\text{PMe}_3)]$. To this sample, $[\text{NBu}_4](\text{Cl})$ was added to produce $[\text{NBu}_4](\text{OTf})$ and SnBu_3Cl . The formation of SnBu_3Cl was confirmed by ^{119}Sn NMR and because of the movement of the chemical shift in ^{19}F NMR to -79.70 . The same experiment performed in CD_2Cl_2 produced a movement in the chemical shift of about 1 ppm (from -78.99 to -79.92 ppm).

2.3.2.3 IR spectroscopy

The IR spectra of coordinated and non-coordinated triflate have been discussed elsewhere.¹⁶ The triflate anion has two observable S–O stretching modes (E and A_1 symmetries at about 1260 and 1030 cm^{-1}) for the SO_3 group and two C–F for the CF_3 moiety (E and A_1 symmetries at about 1215 and 1170 cm^{-1}). The C–S stretching band has much lower frequency, below 800 cm^{-1} . The coordinated group shows three S–O (the band at 1260 splits into two) and three C–F stretching bands (the split of the E mode at 1215 is not always straightforward).

2.3.3 Kinetic experiments

Kinetic experiments were monitored by ^{31}P NMR. A NMR tube (5mm), placed in a bath at $-78\text{ }^\circ\text{C}$, was charged with $[\text{AuPh}(\text{PPh}_3)]$, $[\text{AuPh}(\text{PMe}_3)]$ or $[\text{AuPh}(\text{PCy}_3)]$ and SnBu_3Cl and a small amount of THF (about 0.5 mL) was added to dissolve the solids. Next, an additional amount of THF was added to reach a fixed volume of 0.6 mL. The tube was subsequently charged with an acetone- d_6 capillary for NMR lock and placed in a thermostated probe. ^{31}P NMR spectra were recorded at fixed time intervals of 6 or 15 min. Concentration–time data were obtained from the integrated areas of NMR signals of the gold complexes $[\text{AuPh}(\text{PPh}_3)]$, $[\text{AuPh}(\text{PMe}_3)]$, and $[\text{AuPh}(\text{PCy}_3)]$. The initial rate was obtained by linear fitting of the concentration–time curves in the interval 0–15% of consumption of the starting reagents. In a typical experiment at 303 K, a NMR tube was charged with $[\text{AuPh}(\text{PMe}_3)] = 0.049\text{ mol L}^{-1}$ and $[\text{SnBu}_3\text{Cl}] = 0.95\text{ mol L}^{-1}$.

2.3.3.1 Experimental kinetic order on $[\text{AuPh}(\text{PMe}_3)]$

Table II-2. Starting conditions for the transmetalation reaction between $[\text{AuPh}(\text{PMe}_3)]$ and SnBu_3Cl in THF at 303 K.

$[\text{AuPh}(\text{PMe}_3)] / \text{mol L}^{-1}$	Initial rates (r_0) / $\text{mol L}^{-1} \text{s}^{-1}$
1.32×10^{-2}	$3.0(\pm 6) \times 10^{-6}$
2.36×10^{-2}	$5.1(\pm 5) \times 10^{-6}$
4.88×10^{-2}	$9.8(\pm 8) \times 10^{-6}$
7.13×10^{-2}	$1.6(\pm 1) \times 10^{-5}$
8.98×10^{-2}	$2.40(\pm 9) \times 10^{-5}$
$[\text{SnBu}_3\text{Cl}]_0 = 0.95\text{ mol L}^{-1}$	

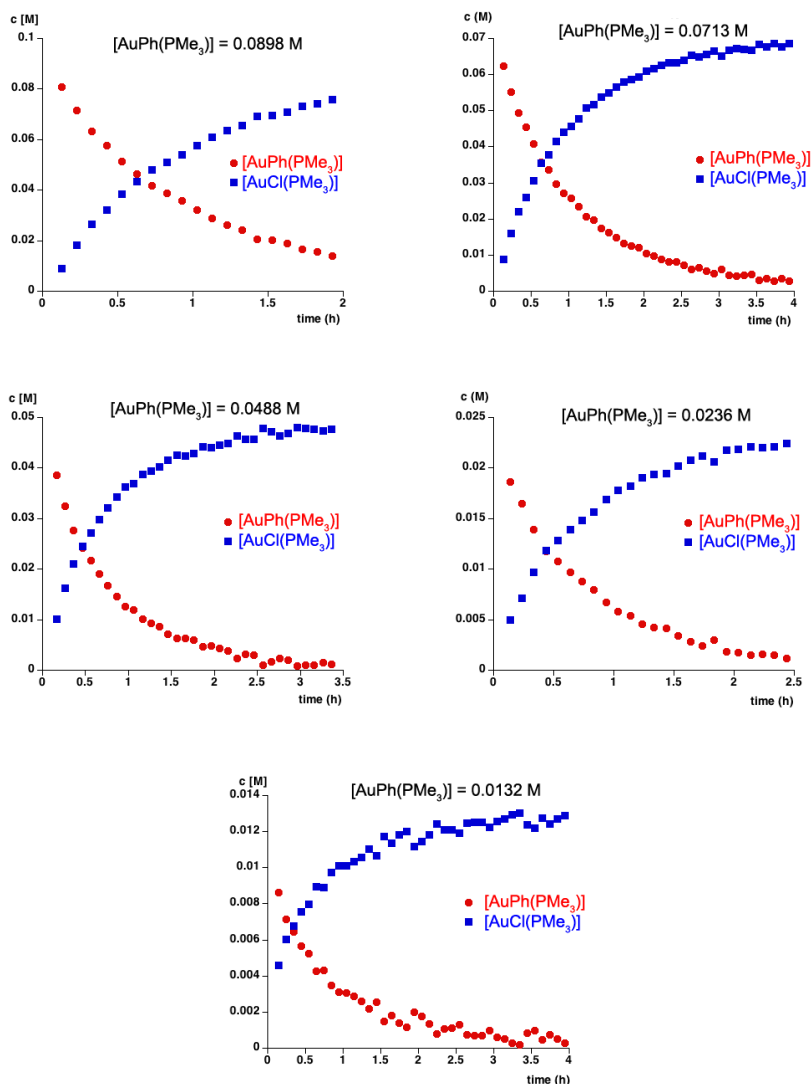


Figure II-11. Representation of the concentrations of $[\text{AuPh}(\text{PMe}_3)]$ and $[\text{AuCl}(\text{PMe}_3)]$ vs time. Starting conditions: $[\text{SnBu}_3\text{Cl}]_0 = 0.95 \text{ mol L}^{-1}$ in THF at 303 K.

The experimental representation of $\ln(r_0)$ vs $\ln[\text{AuPh}(\text{PMe}_3)]$ for different concentrations of $[\text{AuPh}(\text{PMe}_3)]$ leads to a straight line with slope +1.05.

2.3.3.2 Activation parameters for the transmetalation between [AuPh(PMe₃)] and SnBu₃Cl

Table II-3. Values of the rate constants for the transmetalation reaction between [AuPh(PMe₃)] and SnBu₃Cl in THF at different temperatures.

T / K	Rate constant / L mol ⁻¹ s ⁻¹
254	2.78(±1) x10 ⁻⁵
273	1.04(±1) x10 ⁻⁴
303	2.95(±1) x10 ⁻⁴
322	6.02(±2) x10 ⁻⁴

[AuPh(PMe₃)]₀ = 0.07 mol L⁻¹
[SnBu₃Cl]₀ = 0.95 mol L⁻¹

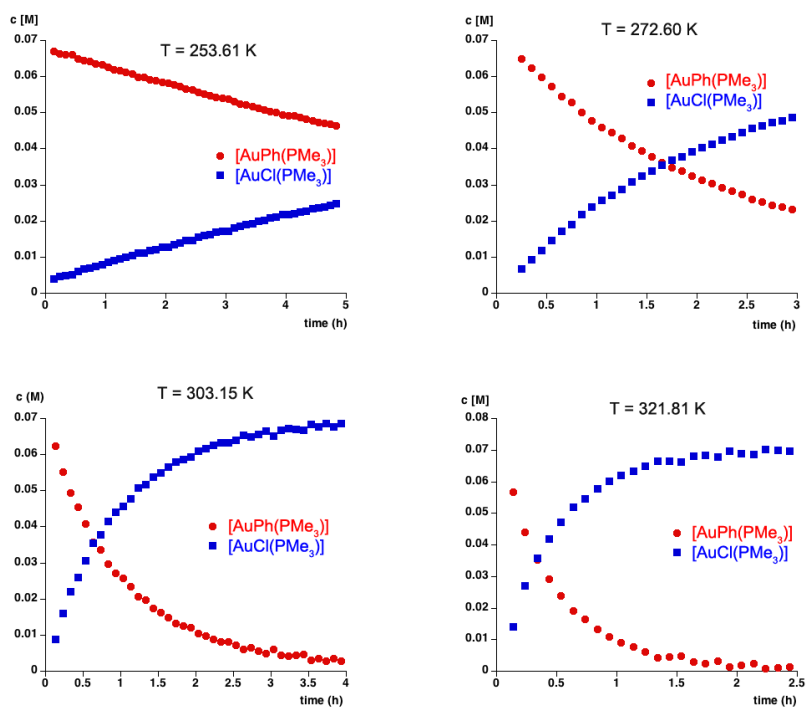


Figure II-12. Representation of the concentrations of [AuPh(PMe₃)] and [AuCl(PMe₃)] as a function of time. Starting conditions: [SnBu₃Cl]₀ = 0.95 mol L⁻¹ in THF at different temperatures.

With the data obtained in the representation shown in Figure 3, the following activation parameters were determined: $\Delta H^\ddagger = 27(\pm 2) \text{ kJ mol}^{-1}$ and $\Delta S^\ddagger = -223(\pm 23) \text{ J K}^{-1} \text{ mol}^{-1}$.

2.3.4 Vinyl by phenyl exchange



The kinetic experiment was monitored by ^{31}P NMR at 323 K. A NMR tube (5mm) was charged with $\text{SnBu}_3(\text{vinyl})$ (0.953 mol L^{-1}) and $[\text{AuPh}(\text{PMe}_3)]$ (0.048 mol L^{-1}). The NMR tube was cooled to $-78 \text{ }^\circ\text{C}$, and a small amount of THF (about 0.5 mL) was added to dissolve the solids. Next, an additional amount of THF was added to reach a fixed volume of 0.6 mL. The tube then was charged with an acetone- d_6 capillary for NMR lock and placed in a thermostated probe. The rate constant obtained was $k = (1.7 \pm 0.02) \times 10^{-6} \text{ (}\Delta G^\ddagger = 115.09 \text{ kJ mol}^{-1}; = 27.49 \text{ kcal mol}^{-1}\text{)}$.

In the same reaction, after 48 hours in THF- d_8 at 323 K, the presence of a small amount of styrene was detected in the Gas Chromatography-Mass.

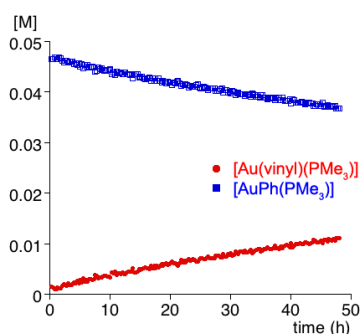
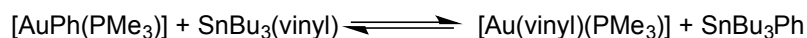


Figure II-13. Observed concentrations of $[\text{Au}(\text{vinyl})(\text{PMe}_3)]$ and $[\text{AuPh}(\text{PMe}_3)]$ as a function of time. Starting conditions: $[\text{SnBu}_3(\text{vinyl})]_0 = 0.953 \text{ mol L}^{-1}$ and $[\text{AuPh}(\text{PMe}_3)]$ (0.048 mol L^{-1}) at 323 K.

2.3.5 Experiments between [AuPh(PMe₃)] with SnBu₃Cl and SnBu₃I

In a typical experiment, a NMR tube (5mm) was charged with SnBu₃X (0.24 mol L⁻¹) and [AuPh(PMe₃)] (0.024 mol L⁻¹) in THF or acetonitrile. The NMR tube was cooled to -78 °C, and a small amount of solvent (about 0.5 mL) was added to dissolve the solids. Next, an additional amount of solvent was added to reach a fixed volume of 0.6 mL. The tube was charged with an acetone-*d*₆ capillary for NMR lock and placed in a thermostated probe. The kinetic experiments were monitored by ³¹P NMR. NMR spectra were recorded at fixed time intervals of 6 minutes at 253 K. Concentration-time data were obtained from the integrated areas of the signals of [AuPh(PMe₃)], [AuCl(PMe₃)] and [AuI(PMe₃)].

- ¹ Mechanistic studies on transmetalation involving Sn: a) Cordovilla, C.; Bartolomé, C.; J. M. Martínez-Irarduya and Espinet, P. *ACS Catal.*, **2015**, *5*, 3040–3053; b) Espinet, P. and Echavarren, A. M. *Angew. Chem. Int. Ed.*, **2004**, *43*, 4704–4734; c) Pérez–Temprano, M. H.; Nova, A.; Casares, J. A. and Espinet, P. *J. Am. Chem. Soc.*, **2008**, *130*, 10518–10520; d) Pérez–Temprano, M. H.; Gallego, A. M.; Casares, J. A. and Espinet, P. *Organometallics*, **2011**, *30*, 611–617.
- ² Angus-Dunne, S. J.; Lee-Chin, L. E. P.; Burns R. C.; Lawrance G. A. *Trans. Met. Chem.* **2006**, *31*, 268–275.
- ³ Elschenbroich, C. *Organometallics*, 3rd, edition. Wiley–VCH Verlag GmbH&Co. KGaA, Weinheim, 2006.
- ⁴ Gualco, P.; Lin, T. P.; Sircoglou, M.; Mercy, M.; Ladeira, S.; Bouhadir, G.; Pérez, L. M.; Amgoune, A.; Maron, L.; Gabbai, F. P. and Bourissou, D. *Angew. Chem. Int. Ed.* **2009**, *48*, 9892–9895.
- ⁵ NBO 6.0. Glendening, E. D.; Badenhoop, J. K.; Reed, A. E.; Carpenter, J. E.; Bohmann, J. A.; Morales, C. M.; Landis, C. R. and Weinhold, F. Theoretical Chemistry Institute, University of Wisconsin, Madison (2013).
- ⁶ Lassauque, N.; Gualco, P.; Mallet-Ladeira, S.; Miqueu, K.; Amgoune, A. and Bourissou, D. *J. Am. Chem. Soc.* **2013**, *135*, 13827–13834.
- ⁷ Reviews about transition metal-tin chemistry: a) Agustin, D.; Ehses, M. *Compt. Rend. Chim.* **2009**, *12*, 1189–1227. b) Holt, M. S.; Wilson, W. L. and Nelson, J. H. *Chem. Rev.* **1989**, *89*, 11–49.
- ⁸ Espinet, P.; Echavarren, A. M.; Rosellón, A.; Livendahl, M. and Lauterbach, T., *Organic Letters*, **2010**, *12* (13), 3006–3009.
- ⁹ López–de–Luzuriaga, J. M.; Monge, M.; Olmos, M. E.; Pascual, D. and Lasanta, T., *Chem. Commun.* **2011**, *47*, 6795–6797.
- ¹⁰ Isab, A.; Fettouhi, M.; Ahmad, S. and Ouahab, L., *Polyhedron*, **2003**, *22*(10), 1349–1354.
- ¹¹ Peña–López, M. Ayán–Varela, L. A. Sarandeses, J. Sestelo, *Chem. Eur. J.* **2010**, *16*, 9905–9909.
- ¹² Lasanta, T.; López–de–Luzuriaga, J. M.; Monge, M.; Olmos, M. E.; Pascual, D. *Chem. Eur. J.* **2013**, *19*, 4754–4766.
- ¹³ Weisemann, C.; Schmidtberg, G. and Brune, H. *J. Organomet. Chem.* **1988**, *361*, 3, 299–307.
- ¹⁴ Casado, A. L.; Gallego, A. M. and Espinet, P. *J. Am. Chem. Soc.* **2000**, *122*, 11711–11782.

¹⁵ Deacon, G. B.; Gatehouse B. M. and Nelson–Reed, K. T. *J. Organomet. Chem.* **1989**, *359*, 267–283.

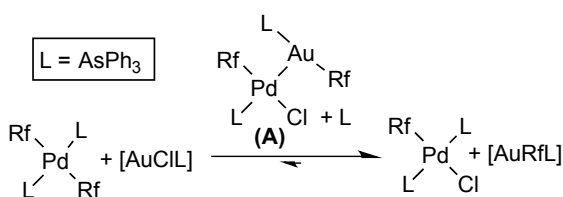
¹⁶ Angus–Dunne, S. J.; Lee–Chin, L. E. P.; Burns, R. C. and Lawrance, G. A. *Trans. Met. Chem.* **2006**, *31*, 268–275.

CHAPTER III

Cross Alkyl-Aryl vs. Homo Aryl-Aryl Coupling in Pd Catalyzed Reactions

3.1 INTRODUCTION

In recent years, many metal-catalyzed processes that involve the participation of organogold derivatives have been developed.¹ The utility of gold has been extended to Pd-catalyzed cross-coupling reactions, using gold complexes as stoichiometric reagents² and as cocatalysts; for example in the gold cocatalyzed Stille reaction.³ Kinetics and thermodynamics of the transmetalation involving Au^I and Pd^{II} have not been deeply studied. A previous work from our group suggested that the formation of *trans*-[PdRf₂L₂] (Rf = C₆F₃Cl₂) from *trans*-[PdRfCl(L)₂] and [AuRfL] (L = AsPh₃) is an endergonic process that occurs via intermediates and transition states stabilized by Pd-Au metallophilic interactions (Equation III-1).



Equation III-1. Transmetalation reaction between *trans*-[PdRf₂L₂] and [AuClL].

The transmetalation occurs via replacement of one ancillary ligand in the palladium coordination sphere by the incoming gold complex.⁴ Similar conclusions have been drawn in a recent computational study of the transmetalation between vinylgold and arylpalladium complexes, suggesting that the participation of intermediates type **A** formed by associative ligand substitution can be general for Au^I/Pd^{II} catalytic systems.⁵ The displacement of the equilibrium toward the right is expected to be more marked the more nucleophilic the hydrocarbyl groups.

In spite of the disfavored equilibrium, the cross-coupling processes from [PdR¹XL₂] and [AuR²L] do work, because the formation of the product R¹-R² is irreversible. Since the transmetalation is a reversible equilibrium, some reactions (isomerizations or exchanges between metal centers) can complicate

the evolution before the coupling takes place. It is known that, for common aryl and alkyl groups, the reductive elimination occurs on *cis*-[PdR¹R²L₂] and follows the order C_{Ar}-C_{Ar} > C_{Ar}-C_{sp³} > C_{sp³}-C_{sp³}.⁶ So, Me-Ar coupling should be faster than Me-Me but slower than Ar-Ar. In spite of these undesired complications, C(sp³) systems are appealing groups for gold catalysis because of the stability of alkylgold(I) complexes that makes them potentially valuable reagents for C(sp³)-C(sp²) couplings.

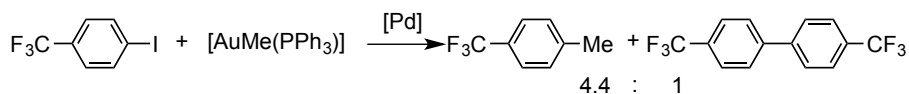
Sarandeses *et al.* have used [AuⁿBu(PPh₃)] in alkyl-aryl palladium-catalyzed cross-coupling experiments, but the results were not good for cross-coupling of [AuⁿBu(PPh₃)] with 4-iodotoluene, obtaining only the homo-coupling product.^{2g} Also, Hashmi *et al.* reported good yields in the coupling of [AuMe(PPh₃)] with 4-iodobenzonitrile.⁵

Here, we report an experimental mechanistic study of the Pd catalyzed Me-Ar coupling of AuMe and ArI systems, to better understand the circumstances of this coupling reaction.

3.2 RESULTS AND DISCUSSION

The catalytic reactions between [AuMe(PPh₃)] with different ArI, catalyzed by *trans*-[Pd(C₆H₄CF₃-*p*)I(PPh₃)₂] (Table III-1) were monitored by NMR in THF-*d*₈ at 50 °C, always obtaining the homo and hetero-coupling products.

One example is the reaction between [AuMe(PPh₃)] with *p*-CF₃C₆H₄I catalyzed by *trans*-[Pd(C₆H₄CF₃-*p*)I(PPh₃)₂] (5%), that form the cross-coupling (*p*CF₃C₆H₄Me) and the homo-coupling (4,4'-bistrifluoromethylbiphenyl) products, in 4.4:1 ratio (Equation III-2). It is important to mention that the formation of metallic gold was not observed during the reaction.



Equation III-2. Cross-coupling reaction of $[\text{AuMe}(\text{PPh}_3)]$ with $p\text{-CF}_3\text{C}_6\text{H}_4\text{I}$ catalyzed by $\text{trans-}[\text{Pd}(\text{C}_6\text{H}_4\text{CF}_3\text{-}p)\text{I}(\text{PPh}_3)_2]$.

The results of experiments with other aryl iodides are summarized in Table III-1.

Table III-1. Hetero/homocoupling ratios versus Hammett σ_p values. Reaction conditions $[\text{AuMe}(\text{PPh}_3)] = 0.021$ mmol; $[\text{ArI}] = 0.042$ mmol; $\text{trans-}[\text{Pd}(\text{C}_6\text{H}_4\text{CF}_3\text{-}p)\text{I}(\text{PPh}_3)_2]$ (5%) at 323 K.

Ar-I	Hammett σ_p	Ar-Me/Ar-Ar
$p\text{-NO}_2\text{C}_6\text{H}_4\text{I}$	0.78	6.3
$p\text{-CF}_3\text{C}_6\text{H}_4\text{I}$	0.54	4.4
$p\text{-FC}_6\text{H}_4\text{I}$	0.06	2.4
$p\text{-CH}_3\text{C}_6\text{H}_4\text{I}$	-0.17	2.8
$p\text{-CH}_3\text{OC}_6\text{H}_4\text{I}$	-0.26	2.4

A reasonable correlation is found between the percentage of cross-coupling product and the σ_p Hammett parameter for the aryls. Aryls with larger σ_p produce less Ar-Ar homocoupling.

3.2.1 Mechanism of the reaction

In order to get insight into the mechanism we moved to use $\text{C}_6\text{Cl}_2\text{F}_3$ (Rf) as aryl, which should slow down the different steps of the reaction and facilitate the detection of other possible intermediates or byproducts such as *cis* and *trans-}[\text{PdR}^1\text{R}^2(\text{PPh}_3)_2] (R^1 and $\text{R}^2 = \text{Rf}$ or Me), or $[\text{AuRf}(\text{PPh}_3)]$. The study focused on the transmetalations possibly occurring once the concerted oxidative addition to Pd(0) and subsequent *cis/trans* isomerization has formed the *trans-}Pd^{II}* intermediate.⁷ The same L (PPh_3) was used for both metals to avoid observational complications associated to L exchanges that have been studied somewhere else.⁸ The reaction of *trans-}[\text{PdRfCl}_2] (**1**) with excess of $[\text{AuMeL}]$ (**2**) in THF at 50 °C, was monitored by ^{19}F NMR (Figure III-1).**

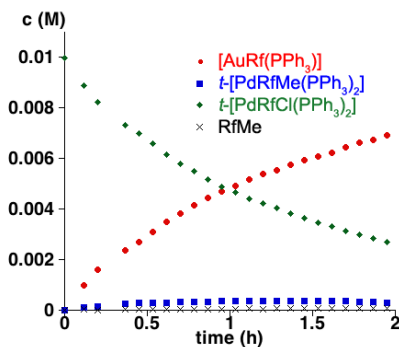
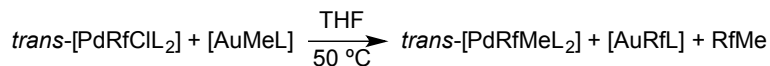


Figure III-1. Concentration/time plot of the reaction between $\text{trans-[PdRfClL}_2\text{]}_0 = 0.010\text{ M}$ and $[\text{AuMeL}]_0 = 0.030\text{ M}$ in THF at 323 K.

The disappearance of **1** and the formation of $[\text{AuRf(PPh}_3\text{)}]$ (**3**) as the main product were observed. The reaction was complete in about 10 h at rt. The presence of the other product, $\text{trans-[PdMeCl(PPh}_3\text{)}_2]$ (**4**), was confirmed by ^{31}P NMR (Figure III-2).

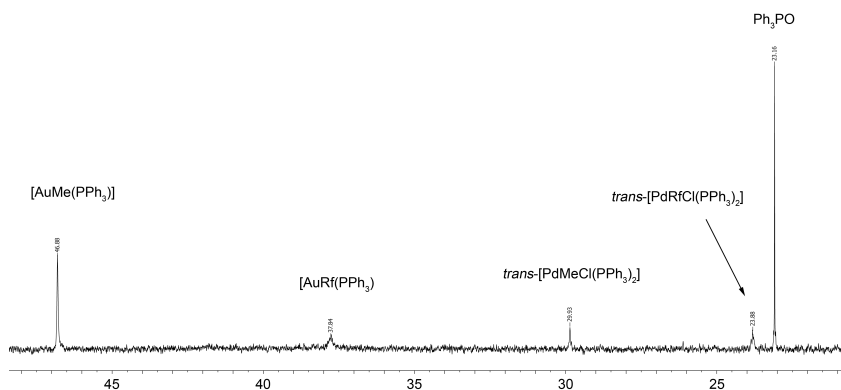


Figure III-2. ^{31}P RMN spectra of the reaction between $[\text{AuMe(PPh}_3\text{)}]_0 = 0.020\text{ mol L}^{-1}$ and $\text{trans-[PdRfCl(PPh}_3\text{)}_2]_0 = 0.010\text{ mol L}^{-1}$ with $[\text{PPh}_3]_0 = 0.025\text{ mol L}^{-1}$ in THF at 324.15 K after 15 hours.

It is interesting to note that only a small amount of cross-coupling product RfMe and none of the homo-coupling Rf-Rf product was observed, as expected from the reluctance of Rf to participate in reductive elimination. After

17 h a small amount of ethane was also observed in the ^1H NMR. The high activation energy of these coupling processes (Rf-Rf, Rf-Me or Me-Me), and the different nature of the two organic radicals allow for observation of some exchange processes in solution.

A kinetic study (initial rates method), based on the rate of consumption of **1**,^a showed that the reaction kinetics is close to first order in gold complex (kinetic order for **[2]** = 0.8) (Figure III-3), and is retarded by addition of phosphine to the solution (kinetic order for $[\text{PPh}_3]$ = -1) (Figure III-4).

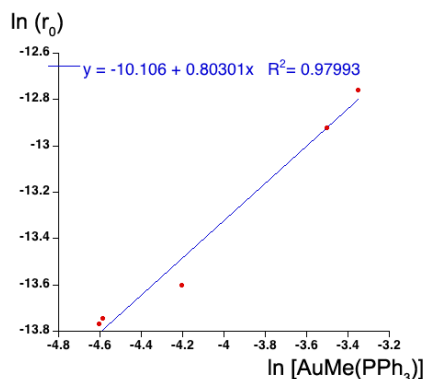


Figure III-3. Plot of $\ln[r_0]$ vs $\ln[\text{AuMe}(\text{PPh}_3)]$.

^a The kinetic order of the reagents and the activation parameters have been obtained by the initial rates method in order to prevent the influence of possible changes in the composition of the system due to subsequent reactions of the products with the reagents. Also, because a slight decomposition of the reagents is observed at reaction times larger than 6 h. The data can be fitted to a pre-equilibrium model, or to a steady state model of formation of intermediate **B** followed by the irreversible formation of the products.

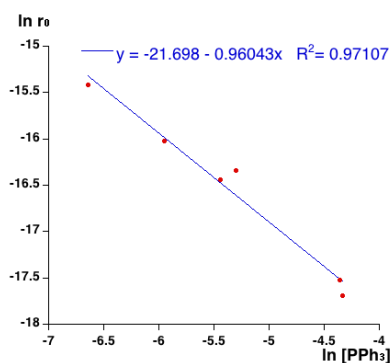


Figure III-4. Plot of $\ln[r_0]$ vs $\ln[\text{PPh}_3]$.

Moreover, the plot of $1/k_{\text{obs}}$ vs. $[\text{PPh}_3]$ gives a straight line. Applying the *steady state* approximation to an intermediate **B** (Equation 3) in which one phosphine has been displaced, a rate constant $k_1 \approx 1.2 \cdot 10^{-3}$ is found, which affords $\Delta G^\ddagger_{323} = 23.3 \text{ kcal mol}^{-1}$. The study of the reaction in the temperature range 280-327 K supports an associative phosphine substitution process with $\Delta H^\ddagger = 63.9 \text{ kJ mol}^{-1}$ and $\Delta S^\ddagger = -95.5 \text{ J K}^{-1} \text{ mol}^{-1}$ (Figure III-5). This fits the expectations from our previous study on Au(aryl)/Pd(aryl) transmetalation.⁴

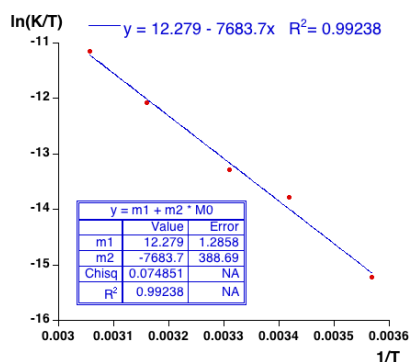
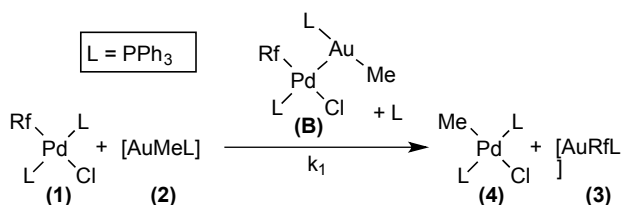
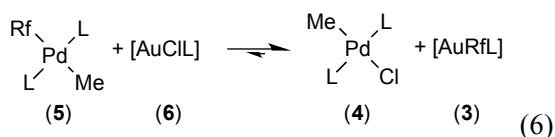
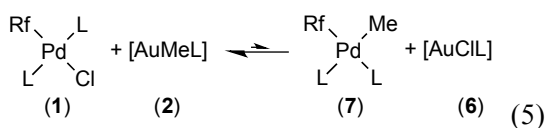
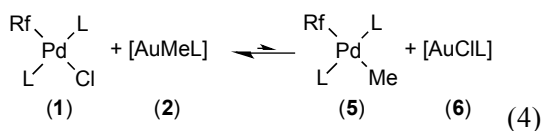


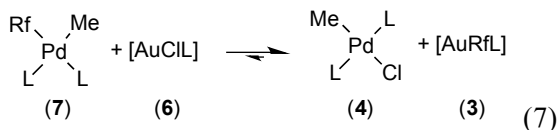
Figure III-5. Eyring plot corresponding to the reaction between *trans*-[PdRfCl(PPh₃)₂] with [AuMe(PPh₃)]. $\Delta H^\ddagger = 64(\pm 3) \text{ KJ / mol}$; $\Delta S^\ddagger = -95(\pm 22) \text{ J / K mol}$.



Equation III-3. Transmetalation reaction between *trans*-[PdRfClL₂] and [AuMeL]. (B) represents the composition of the intermediate, no its structure.

The formation of **3** and **4** indicates the thermodynamic result of group exchange in the absence of coupling, but it does not mean that Equation 3 is the only pathway from **1** and **2** to **3** and **4**. For instance, the observation of some Rf-Me proves that undetected *cis*-[PdRfMe(PPh₃)₂] (**7**) must have been formed too during the reaction, but having a high activation energy toward coupling and being high in energy compared to alternative products it never reaches observable concentration. Similarly, a small amount of the exchange product [Au(C₆H₄CF₃-*p*)(PPh₃)] was detected by ³¹P NMR at early stages of the catalysis in Eq. 1. Overall, the molecules that are known to participate, either because they are observed directly or because they are deduced indirectly through observation of their byproducts, suggest that the reactions in equations 3-7 (L = PPh₃) are competitively operating in the process, even if some of them involve undetected products.

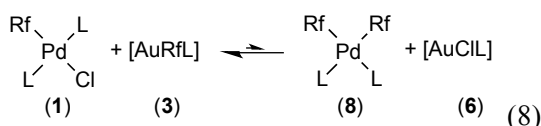




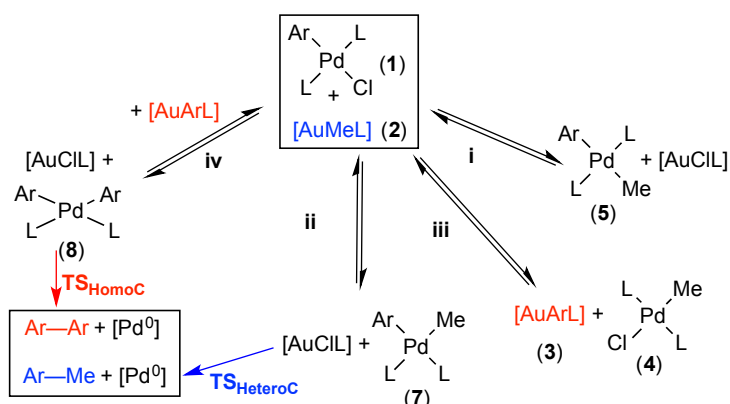
Direct kinetic data can be obtained only for some equations. Thus, complexes **5** and **7** can be prepared by alternative methods,⁹ and the reactions in equations 6 and 7 can be studied. The reaction of **5** with $[\text{AuCl}(\text{PPh}_3)]$ (**6**) (Eq. 6) takes place smoothly at 50 °C (for $[\mathbf{5}]_0 = 0.01 \text{ M}$, $k_{\text{obs}} = 3.4 \cdot 10^{-2} \text{ Lmol}^{-1}\text{s}^{-1}$; $\Delta G_{323}^\ddagger = 21.2 \text{ kcal mol}^{-1}$). Not unexpectedly, the reaction is retarded by addition of PPh_3 (for $[\text{PPh}_3] = [\mathbf{5}]_0 = 0.01 \text{ M}$, $k_{\text{obs}} = 2.1 \cdot 10^{-2} \text{ Lmol}^{-1}\text{s}^{-1}$). The reaction of the *cis* isomer **7** (Eq. 7) is too fast to be measured by NMR at this temperature, even in the presence of added $[\text{PPh}_3]$, as in the time required to record a ^{19}F NMR spectrum the reaction is finished. In the context of the reaction of **1** with **2**, this confirms that complex **7**, although formed during the reaction, will not be detected in the experiment due to its very high reactivity with the gold species.

Four other complexes, the precursors of the non-observed homocoupling products Rf-Rf and Me-Me, should be considered in order to have a complete picture of the exchanges. Homo-coupling product Rf-Rf was not observed in the experiment in Figure III-1, as expected from the well-known inertness of *cis*- $[\text{PdRf}_2\text{L}_2]$. In fact this inertness made it possible our previous study using *trans*- $[\text{PdRf}_2(\text{AsPh}_3)_2]$ and $[\text{AuCl}(\text{AsPh}_3)]$ as reagents.⁴ Although that study suggests that the equilibrium *trans*- $[\text{PdRfClL}_2] + [\text{AuRfL}]$ to give *cis*- $[\text{PdRf}_2\text{L}_2]$ (**8**) and $[\text{AuClL}]$ (Eq. III-8) should not produce NMR detectable concentrations of *cis*- $[\text{PdRf}_2\text{L}_2]$, this equilibrium has to be taken into account for aryls less inert than Rf (Ar in place of Rf, such $\text{C}_6\text{H}_4\text{CF}_3$), because then a faster reductive elimination from the intermediate *cis*- $[\text{PdAr}_2(\text{PPh}_3)_2]$ will produce biphenyls, as observed (Eq. III-1). For the shake of simplicity the pathways leading to $[\text{PdMe}_2\text{L}_2]$ (similar to Eq. III-8, with Me instead of Pf) will be omitted on the reasonable assumption that Me-Me coupling will be slower compared to any other coupling in the systems with conventional aryls and, in

addition, the equilibrium for formation of the electron rich $[\text{PdMe}_2\text{L}_2]$ should be the most unfavorable one. Note, however, that some ethane is observed in our experimental reaction were the fluorinated aryl does not couple fast. Finally, isomerizations of the $[\text{PdRf}_2(\text{PPh}_3)_2]$ and $[\text{PdRfMe}(\text{PPh}_3)_2]$ complexes are not considered because they are usually slower processes than transmetalations.



The previous analysis shows that, in a general case, the Pd catalyzed reaction of aryl halides with alkyl gold complexes is a complicated process involving several competitive transmetalation pathways. This complex system can be simplified as shown in Scheme 1, where the formation of different intermediates *via* Au/Pd transmetalation is represented. From these, coupling should take place according to their respective rates for reductive elimination. All the equilibria have $[\text{PPh}_3]$ dependent rates. Pathway (i) is unproductive as it forms, in a reversible way, *trans*- $[\text{PdArMe}(\text{PPh}_3)_2]$ which will not couple (a *cis* arrangement is required for coupling); pathway (ii) leads to *cis*- $[\text{PdArMe}(\text{PPh}_3)_2]$, producing cross-coupling; pathway (iii) produces $[\text{AuArL}]$, which eventually leads *via* the fourth pathway (iv) to *cis*- $[\text{PdAr}_2(\text{PPh}_3)_2]$ and explains the Ar-Ar homo-coupling observed in Eq. III-1.

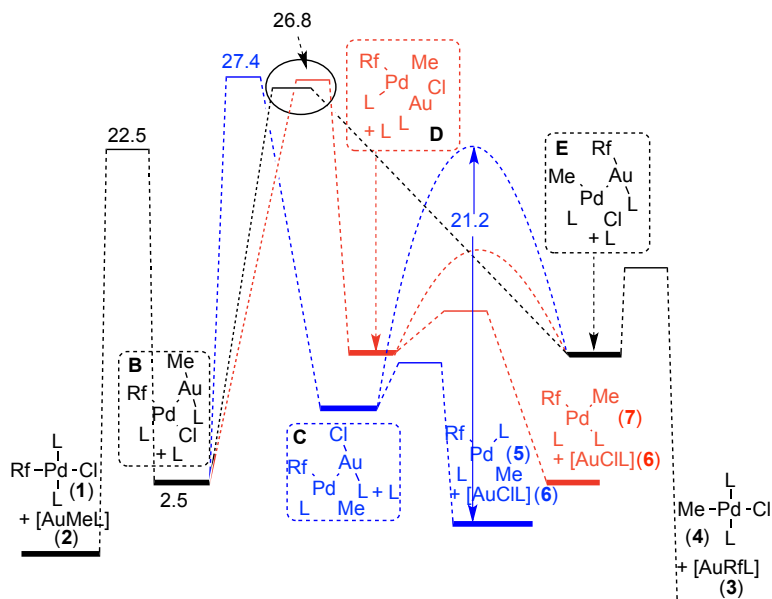


Scheme III-1. Competitive pathways to homo and heterocoupling. The pathways can represent more than one step.

In fact the exchanges are more complex than shown in Scheme III-1, as the transformations are not direct and involve the formation of bimetallic transition states and intermediates,¹⁰ related to the existence of more than one step. In this intricate scheme, the number of unknowns is much larger than the number of parameters that can be experimentally modified, so determining all elementary rate constants from experimental measures on the overall reaction is not possible. However, some reasonable approximations can be made for our model reaction in the light of the kinetic data obtained.

3.2.2 Analysis of the kinetic data

The collection of experimental data was fitted to kinetic models using a non-linear fitting software package.¹¹ The kinetic models consider a substitution of the ligand by the incoming [AuMe(PPh₃)] consistent with the -1 reaction order on [PPh₃] observed for Eq. III-3. The activation energy for this substitution is 22.5 kcal mol⁻¹ good agreement with the experimental values obtained above ($\Delta G_{323}^{\ddagger} = 23.3$ kcal mol⁻¹; $\Delta H^{\ddagger} = 63.9$ kJ mol⁻¹ and $\Delta S^{\ddagger} = -95.5$ J.K⁻¹ mol⁻¹) and with similar activation energy values in our previous studies on gold/Pd systems.⁴ The negative activation entropy for the reaction supports an associative substitution process of PPh₃ by the entering gold complex. From intermediate B, formed in this step, the reaction may proceed through different competitive pathways, which have different consequences when translated to a catalytic process. The possibilities considered are depicted in Scheme III-2.¹²



Scheme III-2. Proposed competitive transmetalations. $\Delta G_{323}^{\ddagger}$ values in kcal mol. The three activation energies (22.5, 27.4, and 26.8) are given by the kinetic fitting, taking as zero the stage 1 + 2. The value 21.1 is an experimental value, as explained in the text, which is imposed in the fitting as a fixed value. The exact structures of the bimetallic Pd/Au intermediates are to be determined.

First, the transmetalation may produce *trans*-[PdRfMeL₂] (5) via intermediate C. This is an unproductive transmetalation since the cross-coupling product cannot be formed from this isomer. In addition, since the *cis* to *trans* isomerization is slow, it cannot easily reenter the catalytic cycle, except by a reversal transmetalation. Thus, 5, if formed, will react with [AuCIL] (6) to go back to C and eventually produce the byproducts *trans*-[PdMeCIL₂] (4) and [AuRfL] (3) (blue lines in Scheme 2). In the kinetic model, the known value of the rate constant was assigned to this transformation, with activation energy of 21.2 kcal·mol⁻¹. This pathway is clearly detrimental for cross-coupling purposes since 3 is responsible (via transmetalation to 1; see pathway IV in Scheme 1) for the formation of homocoupling products and also because 4 further reacts with [AuMeL] (2) to produce ethane, consuming unproductively the organogold reagent.

According to the experimental data, a second pathway of reaction has to be proposed to account for a consumption of intermediate B, with an activation energy value of 26.8 kcal mol⁻¹. This second pathway can lead to the unobserved *cis*-[PdRfMeL₂] (7) through intermediate D (red lines in Scheme 2). From 7, the reductive elimination can proceed to the cross-coupling product Rf-Me. However, if the reductive elimination is slow, *cis* aryl-alkyl palladium(II) complexes can alternatively react with [AuCIL] (6) via intermediate E, to produce the undesired aryl gold complex, which eventually gives rise to homocouplings Rf-Rf and Me-Me. This is the case for our model experimental system because fluoroaryls make fluoroaryl-alkyl coupling particularly difficult. Since the reductive elimination does not take place at a significant rate, almost all our *cis* product is consumed in a very fast reaction with [AuCIL] to produce *trans*-[PdMeCIL₂] (4) and [AuRfL] (3).

Finally, a third pathway for the evolution of intermediate B can be considered: its transformation to intermediate E in an aryl/methyl exchange reaction, which eventually produces *trans*-[PdMeCIL₂] (4) and [AuRfL] (3) (black lines in Scheme III-2). Unfortunately, the existence of this pathway cannot be proved or disproved with the experimental data available. In case it effectively exists as a competitive pathway, the experimental activation energy 26.8 kcal mol⁻¹ would in fact correspond to the averaged rate of both pathways (red and black).

Thus, the selectivity to the desired cross-coupling product Ar-Me depends at least on two critical steps: (i) the transmetalation rate from intermediate B to produce *cis*-[PdArMeL₂], since the other pathways lead to the undesired [AuArL], and (ii) the reductive elimination rate of *cis*-[PdArMeL₂] because its accumulation in solution opens the possibility of a fast exchange with [AuCIL] to produce again [AuArL].

The model proposed in Scheme III-2 provides qualitative information to understand why the cross-coupling of alkylgold complexes with aryl halides

is difficult. An obvious reason is that the Ar-alkyl reductive elimination has higher activation energy than Ar-Ar coupling for conventional aryls.¹³ This should allow for the formation of *cis*-[PdArL₂] via successive transmetalations (eqs III-3 and III-6-8) with Ar in place of Rf, leading to the precursor on which a faster Ar-Ar homocoupling can occur. The efficiency of this undesired process should depend, in a general case, on the transmetalation rates as compared to the cross-coupling rates. In addition, the preference of palladium for the Me group and gold for the Ar group, noted in Figure 1 and in eqs III-5 and III-6, suggests that using [AuⁿBu(PPh₃)] or alkyl complexes other than Me should produce alkylpalladium complexes similar to 4, allowing for easy β -H elimination. Although the addition of phosphine could help to prevent this and slow the undesired transmetalation reactions, it should have the same effect on the desired transmetalations, so it does not look that this could help to drive the reaction more selectively.

In our experience, more electronegative aryl groups are slower toward coupling (an extreme case is Rf for which Rf-Rf coupling does not occur) and also slower toward transmetalation. Both effects help to make the undesired transmetalation/homocoupling sequence less competitive for more electronegative groups. The literature case of aryl-vinyl coupling, studied by the Hashmi, Blum and Sarandeses groups,¹⁴ is also easily understood; vinyl transmetalations are very fast and under these conditions the reactions are dominated by the faster coupling rate (aryl-vinyl > aryl-aryl).

3.3 EXPERIMENTAL SECTION

General methods are the same as described in Chapter I. The compounds *trans*-[PdRfCl(PPh₃)₂],¹⁵ [AuRf(PPh₃)],¹⁶ *cis* and *trans*-[PdRfMe(PPh₃)] and RfMe,¹⁷ and *trans*-[Pd(C₆H₄CF₃-p)I-(PPh₃)₂]¹⁸ were prepared as reported in the literature.

3.3.1 Synthesis of the Complexes

[AuMe(PPh₃)]. This synthesis is a modification of the procedure reported in the literature.¹⁹ [AuCl(PPh₃)] (1.5 g, 3.03 mmol) was dissolved in THF (20 mL). The solution was cooled to -78 °C, and 7.58 mL of ZnMe₂ 2.0 M in toluene (15.2 mmol) was added. The reaction was stirred for 4 h. After this time, the solution was heated to -20 °C, the solvent was removed in vacuum, and 20 mL of cold hexane was added, causing the precipitation of the gold complex as a white solid that was filtered, washed with cold hexane, and vacuum-dried. Yield: 1.30 g (60%). ¹H NMR (acetone-*d*₆): δ 7.62–7.53 (m, 15H, Ph), δ 0.42 (d, ³J_{P-H} = 8.3 Hz, 3H, Me). ³¹P NMR (acetone-*d*₆): δ 46.7 (s). Anal. Calcd for C₁₉H₁₈AuP: C, 48.12; H, 3.83. Found: C, 47.93; H, 3.85.

3.3.2 Reactions of *trans*-[PdRfCl(PPh₃)₂] and [AuMe(PPh₃)]. Kinetic procedure

The kinetic experiments were studied by ¹⁹F NMR. A volumetric NMR tube (5 mm) was charged with weighted amounts of *trans*-[PdRfCl(PPh₃)₂], [AuMe(PPh₃)], and PPh₃. The NMR tube was cooled to -78°C, and a small amount of THF (about 0.5 mL) were added to dissolve the solids. Then an additional amount of THF was added to reach a fixed volume of 0.6 mL. The tube was charged with an acetone-*d*₆ capillary for NMR lock and placed in a thermostated probe. A series of NMR spectra (64 transients) were recorded at fixed time intervals of 5 min. Concentration-time data were obtained from the

integrated areas of *trans*-[PdRfCl(PPh₃)₂], [AuRf(PPh₃)], *trans*-[PdRfMe(PPh₃)₂], and Rf-Me.

3.3.3 Cross-Coupling experiments. Typical procedure

An NMR tube was charged with [AuMe(PPh₃)] (10.0 mg, 0.021 mmol), p-CF₃C₆H₄I (0.042 mmol), and *trans*-[Pd(p-CF₃C₆H₄)I(PPh₃)₂] as catalyst (0.95 mg, 0.0011 mmol). The solids were dissolved in 0.6 mL of THF-*d*₈, and the tube was placed in a thermostated bath at 50 °C. The evolution of the reaction was monitored by ³¹P NMR and ¹H NMR and by ¹⁹F NMR when possible. The relative amount of homo- and cross-coupling products was taken from integrated areas of clean signals. The products were characterized according to the known NMR data: p-CF₃C₆H₄C₆H₄CF₃,²⁰ p-NO₂C₆H₄C₆H₄NO₂,²¹ and p-FC₆H₄C₆H₄F.²²

3.3.4 Kinetic studies. Reaction of *trans*-[PdRfCl(PPh₃)₂] with [AuMe(PPh₃)]

The kinetic experiments were monitored by ¹⁹F NMR. A volumetric NMR tube (5mm) was charged with weighted amounts of *trans*-[PdRfCl(PPh₃)₂], [AuMe(PPh₃)] and PPh₃. The NMR tube was cooled to -78 °C and a small amount of THF (about 0.5 mL) was added to dissolve the solids. Then an additional amount of THF was added to reach a fixed volume of 0.6 mL. The tube was charged with an acetone-*d*₆ capillary for NMR lock, and placed into a thermostated probe. Series of NMR spectra (64 transients) were recorded at fixed time intervals of 5 minutes. Concentration-time data were obtained from the integrated areas of *trans*-[PdRfCl(PPh₃)₂], [AuRf(PPh₃)], *trans*-[PdRfMe(PPh₃)₂] and Rf-Me (Figure III-2). The initial rates were obtained by linear fitting of the concentration-time curves in the interval 0-15% of consumption of the starting reagents. After recording the kinetic data, a ³¹P NMR of each sample was recorded.

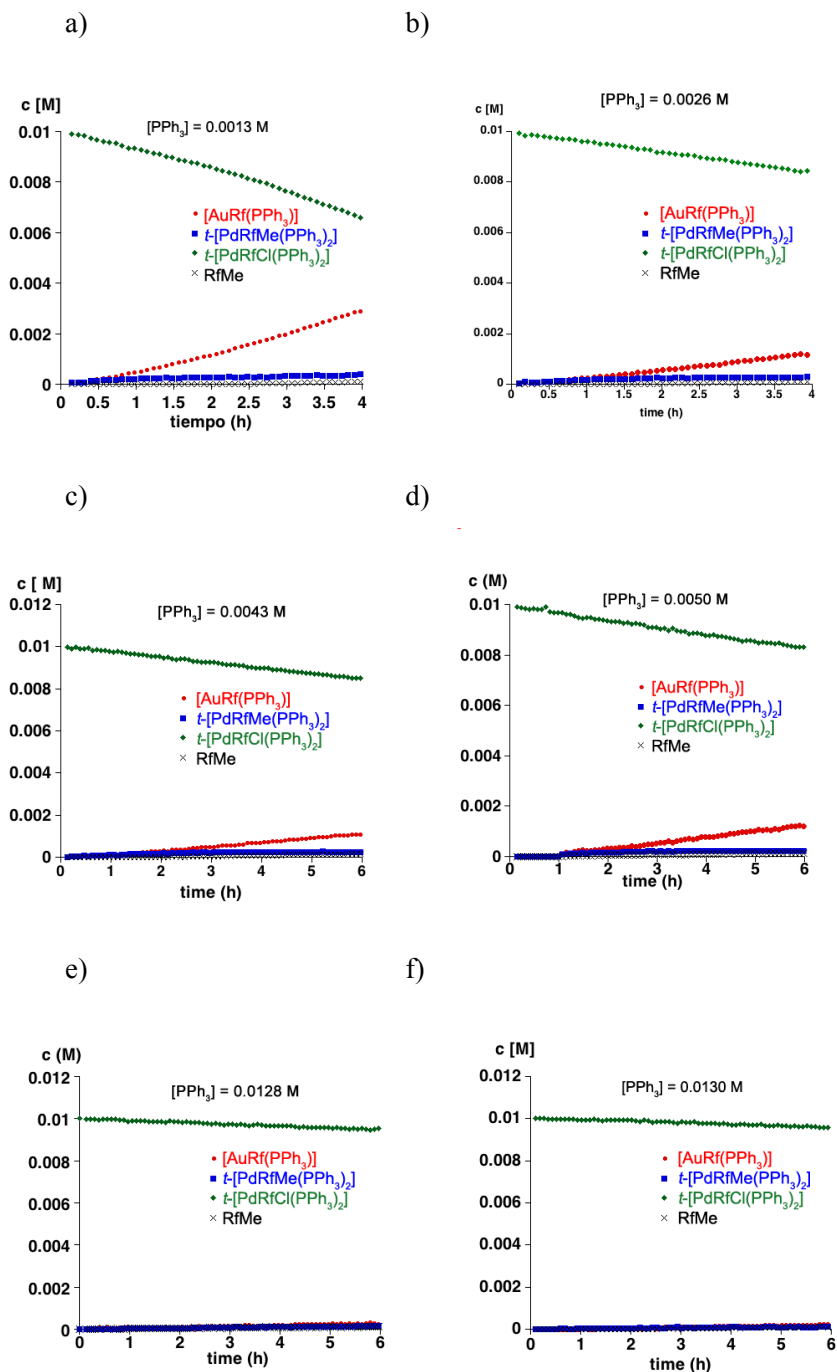


Figure III-6. Observed concentrations as a function of time. $[\text{AuMe}(\text{PPh}_3)]_0 = 0.020 \text{ mol L}^{-1}$ and $\text{trans-}[\text{PdRfCl}(\text{PPh}_3)_2]_0 = 0.010 \text{ mol L}^{-1}$. a) $[\text{PPh}_3] = 0.0013 \text{ mol L}^{-1}$, b) $[\text{PPh}_3] = 0.0026 \text{ mol L}^{-1}$, c) $[\text{PPh}_3] = 0.0043 \text{ mol L}^{-1}$, d) $[\text{PPh}_3] = 0.0050 \text{ mol L}^{-1}$, e) $[\text{PPh}_3] = 0.0128 \text{ mol L}^{-1}$, f) $[\text{PPh}_3] = 0.0130 \text{ mol L}^{-1}$.

Table III-2. Kinetic data obtained for the transmetalation reaction between *trans*-[PdRfCl(PPh₃)₂] and [AuMe(PPh₃)] in THF at 324.15 K with different amounts of PPh₃.

[Au]	[Pd]	[PPh ₃]	r_0 (st. dv)/ mol L ⁻¹ s ⁻¹	k_{obs} / s ⁻¹
0.0210	0.010	0.00131	$2.01(\pm 2) \cdot 10^{-7}$	$9.57 \cdot 10^{-4}$
0.0210	0.010	0.00261	$1.101(\pm 8) \cdot 10^{-7}$	$5.23 \cdot 10^{-4}$
0.0210	0.010	0.00435	$7.23(\pm 4) \cdot 10^{-8}$	$3.44 \cdot 10^{-4}$
0.0199	0.0099	0.00500	$8.02(\pm 9) \cdot 10^{-8}$	$4.07 \cdot 10^{-4}$
0.0198	0.010	0.0128	$2.45(\pm 1) \cdot 10^{-8}$	$1.23 \cdot 10^{-4}$
0.0200	0.010	0.0130	$2.07(\pm 1) \cdot 10^{-8}$	$1.04 \cdot 10^{-4}$

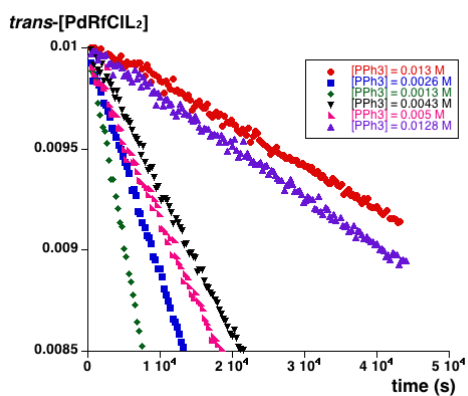


Figure III-7. Plot of *trans*-[PdRfCl(PPh₃)₂] vs. time (s) in the interval 0-15% of consumption of the starting reagent. [AuMe(PPh₃)]₀ = 0.020 mol L⁻¹ and *trans*-[PdRfCl(PPh₃)₂]₀ = 0.010 mol L⁻¹.

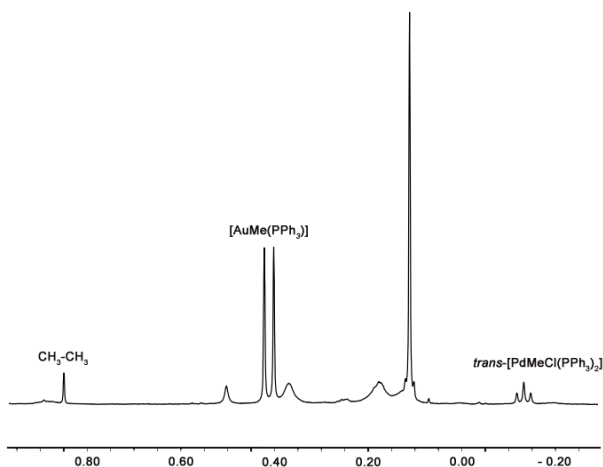
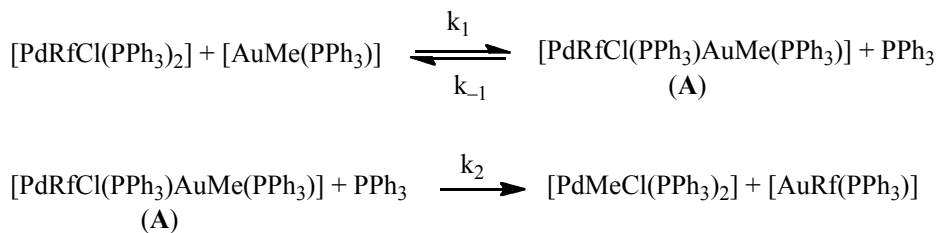


Figure III-8. ¹H RMN spectra of the reaction between [AuMe(PPh₃)]₀ = 0.020 mol L⁻¹ and trans-[PdRfCl(PPh₃)₂]₀ = 0.010 mol L⁻¹ in THF-*d*₈ at 323.15 K after 17 hours.

3.3.4.1 Experimental kinetic order on [PPh₃]

The experimental dependence of $\ln(r_0)$ vs. $\ln[\text{PPh}_3]$ for different amounts of added phosphine leads to a straight line with slope -0.96 .

The kinetic behavior is compatible with a two-step mechanism consisting in equilibrium of substitution of PPh₃ followed by an irreversible reaction:



The steady-state approximation to intermediate A gives:

$$r_0 = \frac{k_1 k_2 [\text{PdRfCl}(\text{PPh}_3)_2] [\text{AuMe}(\text{PPh}_3)]}{k_2 + k_{-1} [\text{PPh}_3]} \quad \text{and} \quad k_{obs} = \frac{k_1 k_2}{k_2 + k_{-1} [\text{PPh}_3]}$$

A plot of $1/k_{\text{obs}}$ vs $[\text{PPh}_3]$ gives a straight line with a intercept $1/k_1$ and slope k_{-1}/k_1k_2 (Figure III-9).

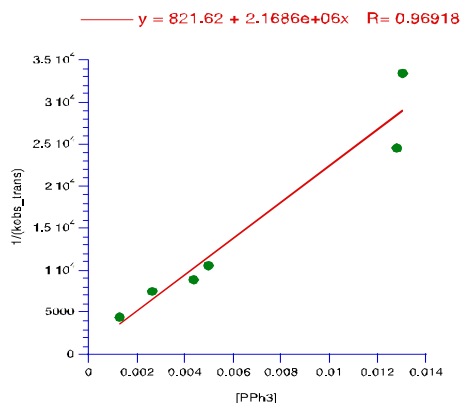


Figure III-9. Plot of $1/(k_{\text{obs_trans}})$ vs. $[\text{PPh}_3]$.

$$k_1 = 1.2 \cdot 10^{-3} \text{ s}^{-1} \text{ L mol}^{-1} ; k_{-1}/k_2 = 2.6 \cdot 10^3 \text{ mol}^{-1} \text{ L}.$$

3.3.4.2 Experimental kinetic order on $[\text{AuMe}(\text{PPh}_3)]$

Table III-3. Starting conditions for the kinetics of the transmetalation reaction between *trans*- $[\text{PdRfCl}(\text{PPh}_3)_2]$ and $[\text{AuMe}(\text{PPh}_3)]$ in THF at 320 K and rates obtained.

$[\text{AuMe}(\text{PPh}_3)]_{\text{added}} / \text{mol L}^{-1}$	Initial rate (r_0) / $\text{mol L}^{-1} \text{ s}^{-1}$
0.0100	$1.0(\pm 2) \cdot 10^{-6}$
0.0102	$1.0(\pm 2) \cdot 10^{-6}$
0.0149	$1.2(\pm 2) \cdot 10^{-6}$
0.0302	$2.4(\pm 2) \cdot 10^{-6}$
0.0349	$2.8(\pm 2) \cdot 10^{-6}$
<i>trans</i> - $[\text{PdRfCl}(\text{PPh}_3)_2]_0 = 0.01 \text{ mol L}^{-1}$. T: 323 K	

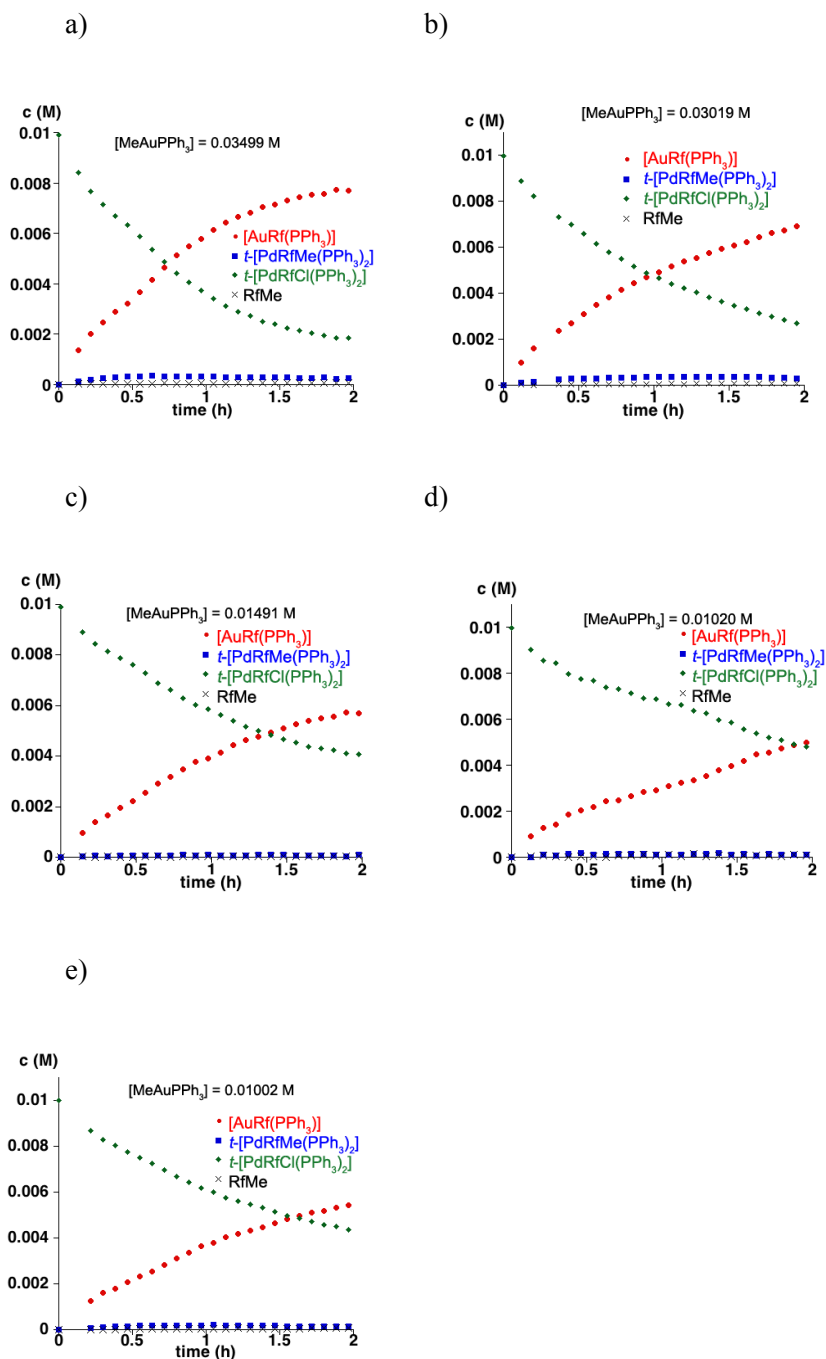


Figure III-10. Observed concentrations as a function of time. Starting conditions: $\text{trans-[PdRfCl(PPh}_3\text{)}_2\text{]}_0 = 0.010 \text{ mol L}^{-1}$. a) $[\text{AuMe(PPh}_3\text{)}] = 0.0349 \text{ mol L}^{-1}$, b) $[\text{AuMePPh}_3] = 0.0302 \text{ mol L}^{-1}$, c) $[\text{AuMePPh}_3] = 0.0149 \text{ mol L}^{-1}$, d) $[\text{AuMePPh}_3] = 0.0102 \text{ mol L}^{-1}$, e) $[\text{AuMePPh}_3] = 0.0100 \text{ mol L}^{-1}$.

The experimental dependence of $\ln(r_0)$ vs. $\ln[\text{AuMe}(\text{PPh}_3)]$ for different amounts of added phosphine leads to a straight line with slope +0.8.

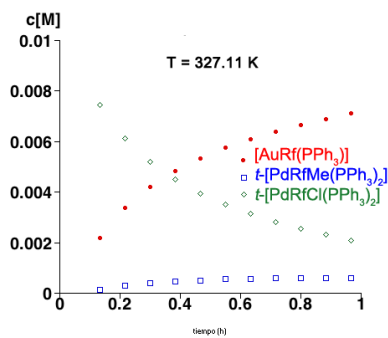
3.3.4.3 Calculation of the activation parameters in the reaction between $[\text{AuMe}(\text{PPh}_3)]$ and *trans*- $[\text{PdRfCl}(\text{PPh}_3)_2]$

Table III-4. Reactions between $[\text{AuMe}(\text{PPh}_3)]_0 = 0.10 \text{ mol L}^{-1}$ and *trans*- $[\text{PdRfCl}(\text{PPh}_3)_2]_0 = 0.010 \text{ mol L}^{-1}$ in THF at different temperatures

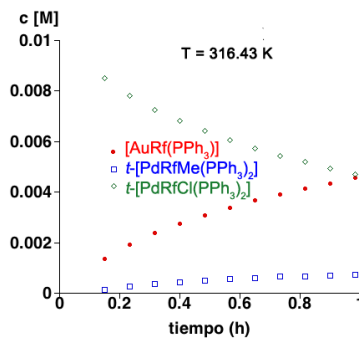
T/ K	Rate constant/ $\text{L mol}^{-1} \text{ s}^{-1}$
280.17	$6.91(\pm 3) \cdot 10^{-5}$
292.50	$3.0(\pm 3) \cdot 10^{-4}$
302.15	$5.14(\pm 5) \cdot 10^{-4}$
316.43	$1.80(\pm 2) \cdot 10^{-3}$
327.11	$4.70(\pm 7) \cdot 10^{-3}$



a)



b)



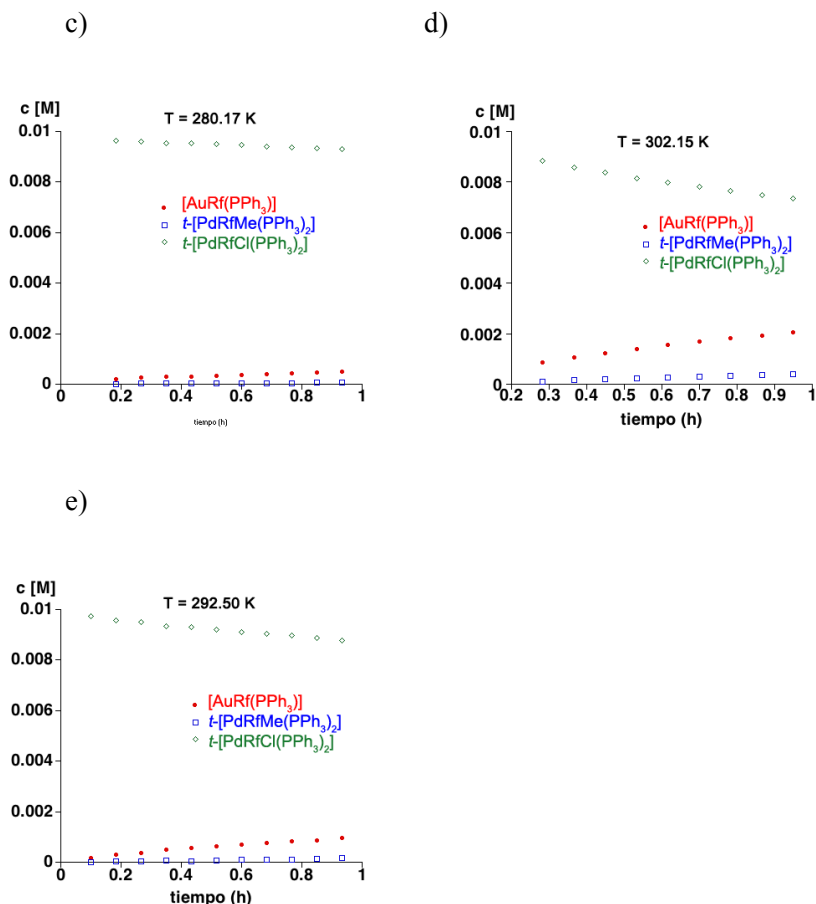


Figure III-11. Observed concentrations as a function of time. a) $T = 327.11 \text{ K}$, b) $T = 316.43 \text{ K}$, c) $T = 280.17 \text{ K}$, d) $T = 302.15 \text{ K}$ y e) $T = 292.50 \text{ K}$.

3.3.5 Experiments between *cis* or *trans*- $[\text{PdRfMe}(\text{PPh}_3)_2]$ and $[\text{AuCl}(\text{PPh}_3)]$

A NMR tube placed in a bath at $-78 \text{ }^\circ\text{C}$ was charged with *trans*- $[\text{PdRfMe}(\text{PPh}_3)_2]$ (5.08 mg, 0.010 mol L^{-1}), $[\text{AuCl}(\text{PPh}_3)]$ (5.93 mg, 0.020 mol L^{-1}), and the weighted amount of PPh_3 (1.57 mg, 0.010 mol L^{-1}). THF was added to a fixed volume of $600 \pm 5 \text{ } \mu\text{L}$. When the solids were dissolved, the tube was charged with an acetone- d_6 capillary for NMR lock and was placed into a thermostated probe. Concentration-time data were the obtained from the integrated areas of $[\text{AuRf}(\text{PPh}_3)]$, *cis* or *trans*- $[\text{PdRfMe}(\text{PPh}_3)_2]$ and *trans*- $[\text{PdRfCl}(\text{PPh}_3)_2]$.

In the reaction between $trans$ -[PdRfMe(PPh₃)₂] + [AuCl(PPh₃)] (**1**) the rate constant is 0.034(1) (s⁻¹Lmol⁻¹) and for the reaction $trans$ -[PdRfMe(PPh₃)₂] + [AuCl(PPh₃)] + PPh₃ (**2**), with [PPh₃]₀ = 0.010 mol L⁻¹ the rate constant is 0.021(1) (s⁻¹Lmol⁻¹). The kinetic model was fitted to the measured concentration vs. time data by nonlinear least-squares (NLLS) regression, using the program Copasi.²³

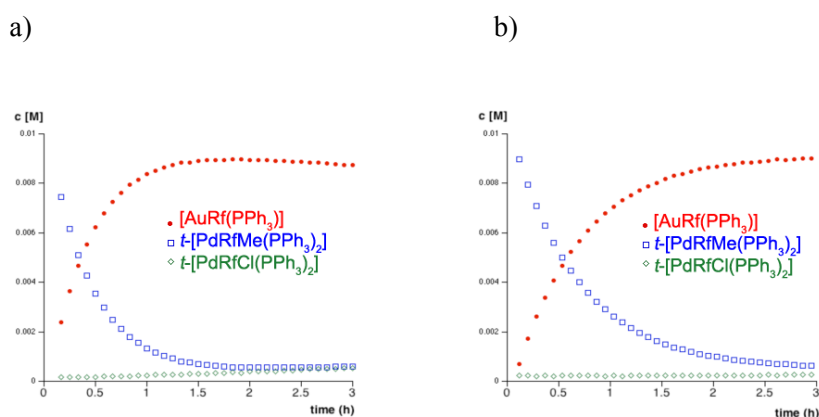


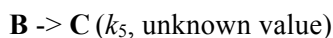
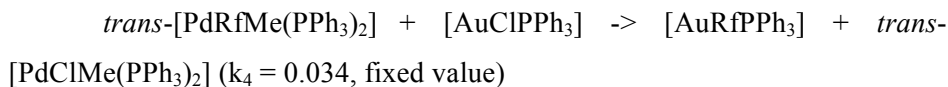
Figure III-12. Observed concentrations as a function of time. Starting conditions: a) [AuCl(PPh₃)]₀ = 0.020 mol L⁻¹, $trans$ -[PdRfMe(PPh₃)₂]₀ = 0.010 mol L⁻¹; b) [AuCl(PPh₃)]₀ = 0.020 mol L⁻¹, $trans$ -[PdRfMe(PPh₃)₂]₀ = 0.010 mol L⁻¹, [PPh₃]₀ = 0.010 mol L⁻¹.

3.3.6 Kinetic model used for the no linear least square fitting of the data obtained at 323 K

The kinetic model was fitted to the measured concentration vs. Time experimental data by nonlinear least-squares (NLLS) regression, using the program Copasi. The proposed kinetic model was entered into the software program.

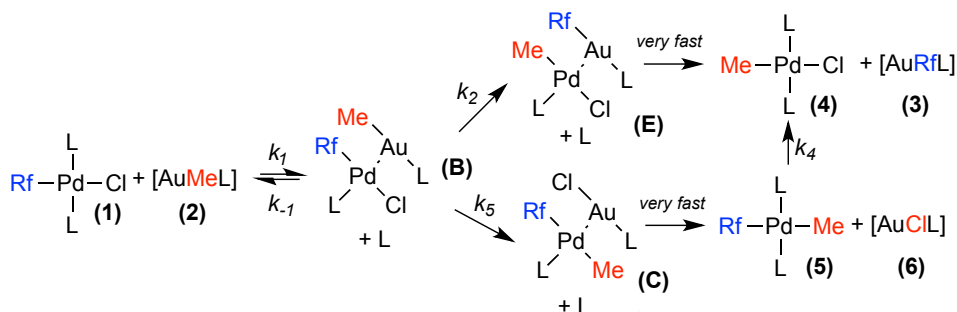
MeAuPPh₃ + $trans$ -[PdRfCl(PPh₃)₂] = **B** + PPh₃ (k_1 , k_{-1} , unknown value)

B -> **E** (k_2 , unknown value)



Where **B**, **C**, and **E** are the intermediates shown in Scheme 2.

Rate constant k_4 has been fixed to its known values 0.034 and a very large value (10^3) has been assigned to k_3 , and k_6 meaning that they are fast irreversible reactions under the conditions of the study.



Scheme III-3. Mechanism of the reaction between $[\text{AuMeL}]$ and $\text{trans-}[\text{PdRfCl}(\text{PPh}_3)_2]$.

The following values have been obtained (standard deviation). :

$$k_1 = 4.4(\pm 8) \cdot 10^{-3} \text{ (} \Delta G^\ddagger = 22.5 \pm 0.2 \text{ kcal/mol),}$$

$$k_{-1} = 2.2(\pm 5) \cdot 10^{-1} \text{ (} \Delta G^\ddagger = 19.9 \pm 0.2 \text{ kcal/mol),}$$

$$k_2 = 2.43(\pm 8) \cdot 10^{-4} \text{ (} \Delta G^\ddagger = 24.31 \pm 0.02 \text{ kcal/mol)}$$

$$k_5 = 9.1(\pm 4) \cdot 10^{-5} \text{ (} \Delta G^\ddagger = 24.94 \pm 0.02 \text{ kcal/mol).}$$

¹ Recent reviews: a) Peñez–Temprano, M. H.; Casares, J. A.; Espinet, P. *Chem. Eur. J.* **2012**, *18*, 1864–1884; b) Hirner, J. J.; Shi, Y.; Blum, S. A. *Acc. Chem. Res.* **2011**, *44*, 603–613; c) Wegner, H. A.; Auzias, M. *Angew. Chem.* **2011**, *123*, 8386; *Angew. Chem. Int. Ed.* **2011**, *50*, 8236–8247; d) Garcia, P.; Malacria, M.; Aubert, C.; Gandon, V.; Fensterbank, L. *Chem. Cat. Chem.* **2010**, *2*, 493–497.

² Use of organogold complexes as stoichiometric reagents in Pd-catalyzed cross-coupling reactions: a) Shi, Y.; Ramgren, S. D.; Blum, S. A. *Organometallics* **2009**, *28*, 1275–1277; b) Hashmi, A. S. K.; Lothschütz, C.; Döpp, R.; Rudolph, M.; Ramamurthi, T. D.; Rominger, F. *Angew. Chem. Int. Ed.* **2009**, *48*, 8243–8246; c) Hashmi, A. S. K.; Döpp, R.; Lothschütz, C.; Rudolph, M.; Riedel, D.; Rominger, F. *Adv. Synth. Catal.* **2010**, *352*, 1307–1314; d) Peña–López, M.; Ayañ–Varela, M.; Sarandeses, L. A.; Peñez–Sestelo, J. *Chem. Eur. J.* **2010**, *16*, 9905–9909; e) Roth, K. E.; Blum, S. A. *Organometallics*, **2011**, *30*, 4811–4813; f) Peña–López, M.; Ayañ–Varela, M.; Sarandeses, L. A.; Peñez–Sestelo, J. *Org. Biomol. Chem.* **2012**, *10*, 1686–1694; g) Peña–López, M.; Sarandeses, L. A.; Peñez–Sestelo, J. *Eur. J. Org. Chem.* **2013**, 2545–2554.

³ a) delPozo, J.; Carrasco, D.; Peñez–Temprano, M. H.; García–Melchor, M.; Álvarez, R.; Casares, J. A.; Espinet, P. *Angew. Chem. Int. Ed.* **2013**, *52*, 2189–2193; b) delPozo, J.; Casares, J. A.; Espinet, P. *Chem. Commun.* **2013**, *49*, 7246–7248.

⁴ Peñez–Temprano, M. H.; Casares, J. A.; deLera, A. R.; Álvarez, R. and Espinet, P. *Angew. Chem. Int. Ed.* **2012**, *20*, 4917–4920.

⁵ Hansmann, M. M.; Pernpointner, M.; Döpp, R. and Hashmi, A. S. K. *Chem. Eur. J.* **2013**, *19*, 15290–15303.

⁶ a) Peñez–Rodríguez, M.; Braga, A. A. C.; García–Melchor, M.; Peñez–Temprano, M. H.; Casares, J. A.; Ujaque, G.; deLera, A. R.; Álvarez, R.; Maseras, F. and Espinet, P. *J. Am. Chem. Soc.* **2009**, *131*, 3650–3657 and references cited therein; b) Salas, G.; Fuentes, B.; Casares, J. A. and Espinet, P. *J. Am. Chem. Soc.* **2007**, *129*, 3508–3509; c) Ananikov, V. P.; Musaev, D. G. and Morokuma, K. *Organometallics*, **2005**, *24*, 715–723.

⁷ This oxidative addition is a well-known step. The oxidative addition of Rf–I gives initially *cis*-[PdRfIL₂] but, in the conditions of this reaction, this intermediate isomerizes to *trans*-[PdRfIL₂] at a much faster rate than the observed rate of transmetalation. Casado, A. L. and Espinet, P. *Organometallics*, **1998**, *17*, 954–959.

⁸ delPozo, J.; Casares, J. A. and Espinet, P. *Chem. Commun.* **2013**, *49*, 7246–7248.

⁹ Salas, G.; Fuentes, B.; Casares, J. A. and Espinet, P. *J. Am. Chem. Soc.* **2007**, *129*, 3508–3509.

¹⁰ For related calculations in Zn/Pd transmetalations, including the competitive formation of *cis* and *trans* Pd complexes from a common precursor see: a) Fuentes, B.; García–Melchor, M.; Lledós, A.; Maseras, F.; Casares, J. A.; Ujaque, G. and Espinet, P. *Chem. Eur. J.*, **2010**, *16*, 8596–8599; b) García–Melchor, M.; Fuentes

B.; Lledós, A.; Casares, J. A.; Ujaque, G. and Espinet, P. *J. Am. Chem. Soc.* **2011**, *133*, 13519–13526.

¹¹ Hoops S., Sahle S., Gauges R., Lee C., Pahle J., Simus N., Singhal M., Xu L., Mendes P. and Kummer U. *Bioinformatics*, **2006**, *22*, 3067–3074.

¹² The structures of intermediates B and C in Scheme 2 are proposed with a Pd-Au bond according to the calculated structures found in all DFT studies available. An alternative Pd-X-Au structure with bridging X ligand (X = Cl, Me), which would be kinetically equivalent, has not been found in the calculations. Structures with Pd interacting with both components of the X-Au bond have been found in the transition states of the associative substitution of the Pd leaving ligand by the entering complex [AuXL].

¹³ a) Peñez-Rodríguez, M.; Braga, A. A. C.; García-Melchor, M.; Peñez-Temprano, M. H.; Casares, J. A.; Ujaque, G.; deLera, A. R.; Álvarez, R.; Maseras and F.; Espinet, P. *J. Am. Chem. Soc.* **2009**, *131*, 3650–3657 and references cited therein; b) Salas, G.; Fuentes, B.; Casares, J. A. and Espinet, P. *J. Am. Chem. Soc.* **2007**, *129*, 3508–3509; c) Ananikov, V. P.; Musaev, D. G. and Morokuma, K. *Organometallics*, **2005**, *24*, 715–723.

¹⁴ a) Hansmann, M. M.; Pernpointner, M.; Döpp, R.; Hashmi, A. S. K. *Chem. Eur. J.* **2013**, *19*, 15290–15303; b) Shi, Y.; Peterson, S. M.; Haberaecker, W. W.; Blum, S. A. *J. Am. Chem. Soc.* **2008**, *130*, 2168–2169; c) Shi, Y.; Ramgren, S. D.; Blum, S. A. *Organometallics*, **2009**, *28* (5), 1275–1277; d) Hashmi, A. S. K.; Lothschütz, C.; Döpp, R.; Ackermann, M.; Becker, J. D. B.; Rudolph, M.; Scholz, C.; Rominger, F. *Adv. Synth. Catal.* **2012**, *354*, 133–147; e) Peña-López, M.; Sarandeses, L. A.; Peñez-Sestelo, *J. Eur. J. Org. Chem.* **2013**, 2545–2554.

¹⁵ Casado, A. L.; Casares, J. A.; Espinet, P. *Inorg. Chem.* **1998**, *37*, 4154–4156.

¹⁶ Byabartta, P. *Trans. Met. Chem.* **2007**, *32*, 716–726.

¹⁷ Salas, G.; Fuentes, B.; Casares, J. A.; Espinet, P. *J. Am. Chem. Soc.* **2007**, *129*, 3508–3509.

¹⁸ Wallow, T. I.; Goodson, F. E.; Novak, B. M. *Organometallics*, **1996**, *15*, 3708–3716.

¹⁹ Mizushima, E.; Cui, D. M.; DebNath, D. C.; Hayashi, T.; Tanaka, M. *Org. Synth.* **2006**, *83*, 55–60.

²⁰ Ma, N.; Zhu, Z.; Wu, Y. *Tetrahedron*, **2007**, *63*, 4625–4629.

²¹ Nising, C. F.; Schmid, U. K.; Nieger, M. *J. Org. Chem.* **2004**, *69*, 6830–6833.

²² Goldstein, J. H.; Tarpley, A. R. *J. Phys. Chem.* **1971**, *75*, 421–430.

²³ Hoops, S.; Sahle, S.; Gauges, R.; Lee, C.; Pahle, J.; Simus N.; Singhal, M.; Xu, L.; Mendes, P. and Kummer, U. *Bioinformatics* **2006**, *22*, 3067–3074.

CHAPTER IV

**Similarities between gold and zinc in
Aryl by Alkyl exchange reaction with
palladium dimers**

4.1 INTRODUCTION

Along the development of this doctoral thesis we have been interested not only in the study of Au-Pd and Au-Sn transmetalation reactions, but also in the study of the Zn to Pd transmetalation reactions as is described in next Chapter, where mechanistic studies on the transmetalation of Negishi cross-coupling reaction are explained.

The electronic configuration of gold(I) and zinc(II) are, respectively, [Xe] 4f¹⁴ 5d¹⁰ and [Ar] 3d¹⁰. Gold(I) and some of the zinc(II) compounds are molecules with the same coordination number (2) and a linear geometry.

Last year our research group published a study on the *cis* to *trans* isomerization reaction of [PdMeAr(PR₃)₂] (Ar = C₆F₅, C₆Cl₂F₃) catalyzed by ZnMe₂, involving methyl exchange between Pd and Zn.¹ Revisiting previous studies, a comparison between Pd/Zn and Pd/Au intermediates and transition states was established, revealing very similar structures with intermetallic distances shorter than the sum of the Van der Waals radius in both cases. These distances are associated to the involvement of the metals in electron deficient bond formation during the transmetalation reaction of the methyl group. A similarity to the structural behavior of the main-group electron-deficient compounds was highlighted, supporting a unified view of the transmetalation processes.

In the gas phase, ZnMe₂ is a linear and symmetric molecule in which the two electron donating Me groups make the Zn center very electron rich inhibiting the acidic characteristic found in other Zn compounds, such as ZnMeCl. On the contrary, ZnMe₂ acts primarily through the electron rich C-Zn bond as a Lewis base toward the Pd acidic center.

The isomerization mechanism observed in the above mentioned study,¹ shows similarity with the Rf transmetalation previously described also by our research group between *cis*-[PdRf₂(AsPh₃)₂] and [AuCl(AsPh₃)],² where the

Au-Cl bond displaces a ligand from Pd, with a Pd-Au strong bond interaction in the intermediates and the transition states.

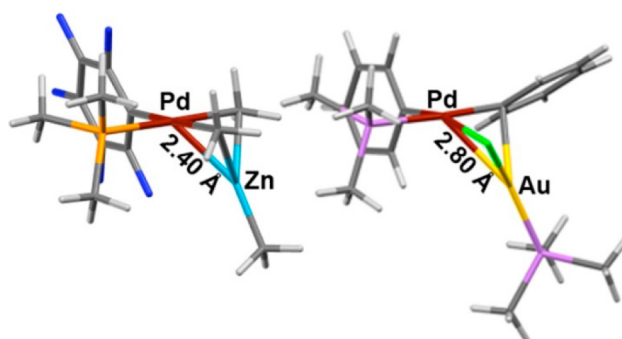
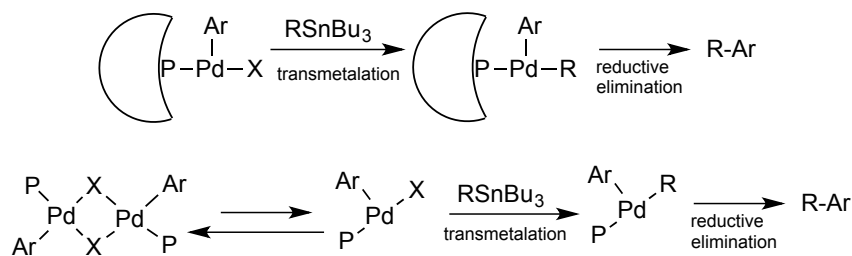


Figure IV-1. Structural similarity of $[(\text{Me}_3\text{P})\text{P}(\mu\text{-Me})_2\text{ZnMe}]$ and $[(\text{Me}_3\text{As})\text{PhPd}(\mu\text{-Ph})(\mu\text{-Cl})\text{Au}(\text{AsMe}_3)]$ in transmetalation processes. The figure is taken as published in reference 1.

One more similarity found in transmetalation reactions with gold and zinc is its capability to produce carbon for carbon exchange reactions with palladium compounds. These reactions are the responsible for the formation of undesired homocoupling products in the Negishi reaction,³ and in cross-coupling reactions in which gold compounds are used as the nucleophilic agent, as described in the previous Chapter. One possibility to avoid the problem is to use systems from which the reductive elimination is quickly produced, such as tricoordinate intermediates (Scheme IV-1).⁴



Scheme IV-1. Sketch of the performance of mononuclear and dimeric palladium complexes with bulky phosphines in cross-coupling reactions.

However, regarding their alkylating capability, both reagents (ZnMe_2 and $[\text{AuMeL}]$) behave very differently. Whereas organogold complexes produce preferably aryl by alkyl exchange when reacting with *trans*- $[\text{PdRfCl}(\text{PPh}_3)_2]$ to give *trans*- $[\text{PdMeCl}(\text{PPh}_3)_2]$, dimethylzinc produces *trans*- $[\text{PdRfMe}(\text{PPh}_3)_2]$, as main product.⁵ Both reactions take place via substitution of one PPh_3 ligand by the metallating reagent, and their reaction rates are not very different, but the thermodynamics of the equilibria govern the selection of the exchange produced.

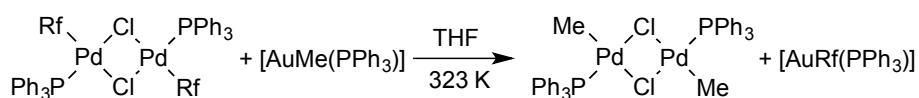
The main objective of this Chapter is the study of transmetalation reactions between palladium dimers with halogen bridges of the type *trans*- $[\text{Pd}_2(\mu\text{-X})_2\text{Rf}_2\text{L}_2]$ and organozinc and organogold(I) complexes. It is surprising that studies on reaction mechanisms of palladium dimers have not been reported yet, in spite of its importance in platinum group chemistry. One of the few things that it is known about the behavior of these dimers in transmetalation reactions is that the bridging halogens are difficult to substitute using magnesium reagents. For instance, the reaction of $[\text{Pd}_2(\mu\text{-Br})_2\text{Br}_4]^{2-}$ with $\text{C}_6\text{F}_5\text{MgBr}$ leads, by selective substitution of the terminal Pd-Br bonds, to $[\text{Pd}_2(\mu\text{-Br})_2(\text{C}_6\text{F}_5)_4]^{2-}$, even in the presence of an excess of $\text{C}_6\text{F}_5\text{MgBr}$.⁶ This lack of reactivity toward transmetalation is in contrast with the well known lability and weakness of bridging halide ligands when compared with terminal halide ligands in other substitution reactions. Probably it is this inertness is what has limited the use of these dimers as catalysts, in spite of the fact that they can generate in solution highly reactive species by bridge splitting.

In the following pages, the reactivity between $[\text{AuMeL}]$ and ZnMe_2 with different palladium dimers of the type *trans*- $[\text{Pd}_2(\mu\text{-X})_2\text{Rf}_2\text{L}_2]$ is described and compared.

4.2 RESULTS AND DISCUSSION

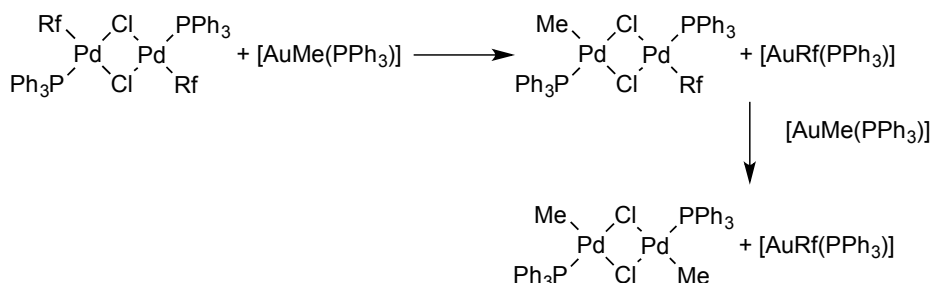
4.2.1 Reactions between *trans*-[Pd₂(μ-X)₂Rf₂L₂] and [AuMeL]

First we studied the reaction between the dimer *trans*-[Pd₂(μ-Cl)₂Rf₂(PPh₃)₂] and [AuMe(PPh₃)] (4 equivalents) in THF at 323 K. After 5 minutes the reaction was completed, producing only [AuRf(PPh₃)] and the dimer *trans*-[Pd₂(μ-Cl)₂Me₂(PPh₃)₂]. Thus, at this temperature the exchange Me/Rf between gold and palladium is much faster than on complexes *trans*-[PdRfCl(PPh₃)₂] described in Chapter III.



Scheme IV-2. Scheme for the exchange reaction between *trans*-[Pd₂(μ-Cl)₂Rf₂(PPh₃)₂] and [AuMe(PPh₃)].

It was necessary to cool down the system below 258 K, to get a reaction rate slow enough to monitor the reaction and to obtain kinetic data. The spectrum in Figure 2 shows the exchange reaction between Rf and Me groups, which is produced sequentially in two steps, first affording the dimer with the Rf and Me groups and then, the dimer with two Me groups also in *trans* position (Scheme IV-3).



Scheme IV-3. Scheme of the two steps for the exchange reaction between *trans*-[Pd₂(μ-Cl)₂Rf₂(PPh₃)₂] and [AuMe(PPh₃)].

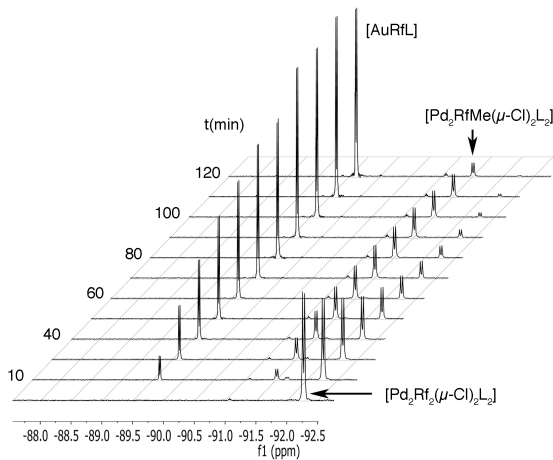


Figure IV-2. ^{19}F NMR at different times of the reaction of *trans*- $[\text{Pd}_2(\mu\text{-Cl})_2\text{Rf}_2(\text{PPh}_3)_2]$ with $[\text{AuMe}(\text{PPh}_3)]$ in THF at 258 K to give *trans*- $[\text{Pd}_2(\mu\text{-Cl})_2\text{MeRf}(\text{PPh}_3)_2]$ and $[\text{AuRf}(\text{PPh}_3)]$. Starting conditions: *trans*- $[\text{Pd}_2(\mu\text{-Cl})_2\text{MeRf}(\text{PPh}_3)_2]_0 = 0.0050 \text{ mol L}^{-1}$ and $[\text{AuMe}(\text{PPh}_3)]_0 = 0.020 \text{ mol L}^{-1}$.

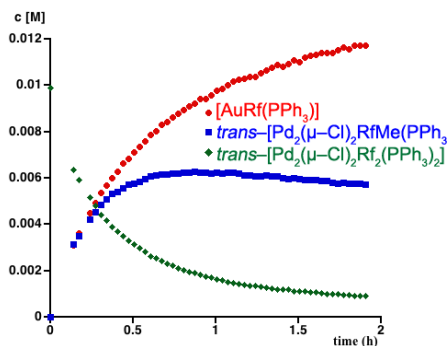
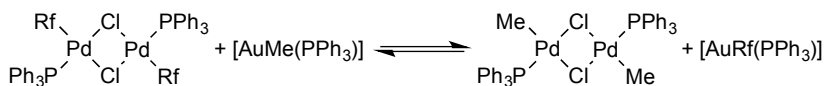


Figure IV-3. Concentration/time plot of the reaction of *trans*- $[\text{Pd}_2(\mu\text{-Cl})_2\text{Rf}_2(\text{PPh}_3)_2]_0 = 0.010 \text{ mol L}^{-1}$ with $[\text{AuMe}(\text{PPh}_3)]_0 = 0.020 \text{ mol L}^{-1}$ in THF at 258 K.

The kinetic orders of the reaction on palladium and gold were measured from the initial rates, obtaining values of 1.2 and 0.8 for *trans*-[Pd₂(μ-Cl)₂Rf₂(PPh₃)₂] and [AuMe(PPh₃)], respectively.

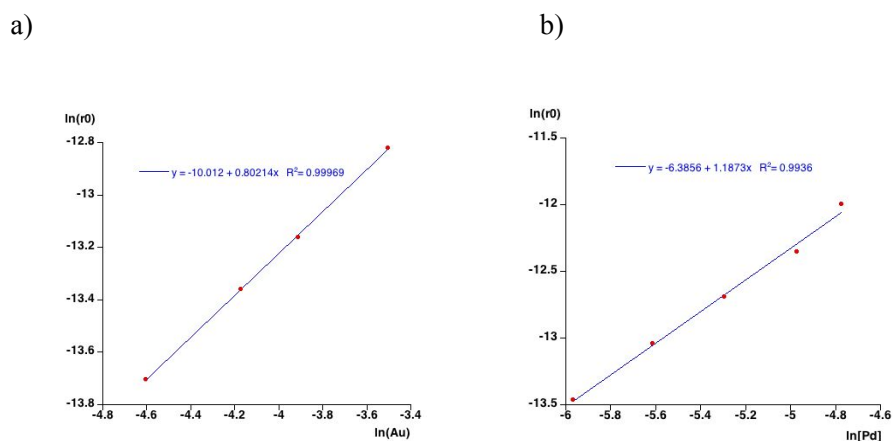


Figure IV-4. a) Plot of $\ln[r_0]$ vs $\ln[\text{AuMe}(\text{PPh}_3)]$, b) Plot of $\ln[r_0]$ vs $\ln[\text{trans-}[\text{Pd}_2(\mu\text{-Cl})_2\text{Rf}_2\text{L}_2]]$.

Also by measuring the reaction rate constants at temperatures between 219-248 K the activation parameters ΔH^\ddagger and ΔS^\ddagger were obtained, giving values of $10.9 \pm 1.3 \text{ kcal mol}^{-1}$ and $-21 \pm 5 \text{ cal mol}^{-1} \text{ K}^{-1}$, respectively. The ΔG^\ddagger_{323} value is $17.7 \text{ kcal mol}^{-1}$. The negative activation entropy supports an associative process, as expected for the transmetalation mechanism.

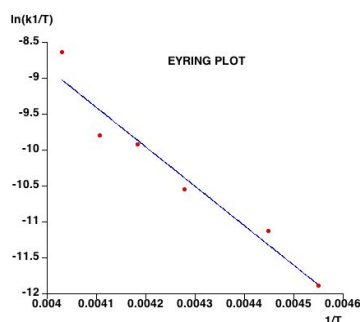
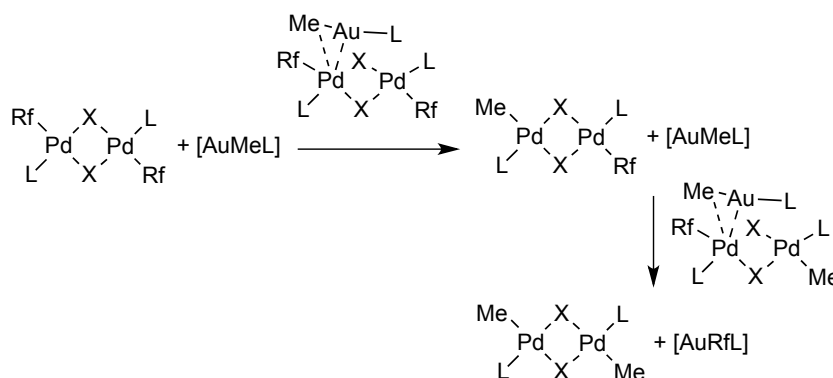


Figure IV-5. Eyring plot corresponding to the reaction between *trans*-[Pd₂(μ-Cl)₂Rf₂L₂] with [AuMe(PPh₃)] at temperatures between 219 and 248 K.

The previously reported mechanism for the Rf transmetalation between *cis*-[PdRf₂(AsPh₃)₂] and [AuCl(AsPh₃)]₂² requires the displacement of one ligand coordinated to palladium by the incoming gold complex. Considering the large difference in activation energy for this reaction between these dimers and the monomers studied in the Chapter III, the most likely hypothesis is that the mechanism goes through the rupture of just one of the chloro bridges in the dimer. The substitution of the phosphine should provide a ΔG_{323}^\ddagger value about 23 kcal mol⁻¹ while the halogen-bridge rupture should be much less energetic, consistent with the ΔG_{323}^\ddagger value found for this reaction (17.7 kcal mol⁻¹). Thus, the kinetic behavior is compatible with a two-step mechanism where the first step is the rupture of one bridging halogen by the incoming gold complex, to form an intermediate, followed by the methyl for aryl exchange between gold and palladium (Scheme IV-4).

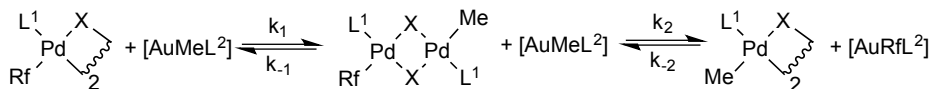


Scheme IV-4. Proposed mechanism for the reaction between [AuMeL] and *trans*-[Pd₂(μ -X)₂Rf₂(L)₂] with the cleavage of one bridged halogen in each exchange reaction. The Au-Me bond is initially coordinated to the palladium center, before the Au-Pd interaction.

Unfortunately, the system does not allow us to obtain the kinetic dependence of the reaction on the concentration of PPh₃, because the addition of an excess of the PPh₃ ligand to the dimer *trans*-[Pd₂(μ -Cl)₂Rf₂(PPh₃)₂] would split the bridging chlorines, rendering the corresponding monomer *trans*-[PdClRf(PPh₃)₂]. It might be expected not to have a mechanistic role,

according to our proposal, although this does not exclude electronic and steric influences.

As expected, the reaction is an equilibrium and, the second transmetalation is not always completed, thus K_{eq} between $[AuMeL]$ and $trans-[Pd_2(\mu-X)_2RfMe(L)_2]$ were calculated from the concentrations in the equilibrium (Scheme IV-5, Table IV-1) and k_1 , k_{-1} were calculated using the kinetic model. For the pair $L^1 = PCy_3$ and $L^2 = PPh_3$, an equilibrium is also reached for the first exchange process. The direct rate constants for the first substitution (k_1) are higher than for the second substitution (k_2) in every case. Note that there is a statistical effect, since complexes $trans-[Pd_2(\mu-X)_2Rf_2(PPh_3)_2]$ have double number reactive sites than complexes $trans-[Pd_2(\mu-X)_2RfMe(PPh_3)_2]$. When the ligand is PMe_3 in palladium and gold compounds the reaction is so fast that it was not possible to measure the rate constants.



Scheme IV-5. Equilibrium reaction between $[\text{AuMeL}]$ and $\text{trans-}[\text{Pd}_2(\mu\text{-X})_2\text{Rf}_2(\text{L})_2]$.

Table IV-1. Constants for the reactions between $[\text{AuMeL}]_0 = 0.020 \text{ molL}^{-1}$ and $\text{trans-}[\text{Pd}_2(\mu\text{-X})_2\text{Rf}_2\text{L}_2]_0 = 0.010 \text{ molL}^{-1}$ at 258 K^a. $K_{2\text{eq}}$ is defined for the reaction between $[\text{AuMeL}]$ and $\text{trans-}[\text{Pd}_2(\mu\text{-X})_2\text{RfMeL}_2]$ studied independently.

Entry	L ¹	L ²	X	$k_1/\text{L mol}^{-1} \text{ s}^{-1}$	$k_{-1}/\text{L mol}^{-1} \text{ s}^{-1}$	$k_2/\text{L mol}^{-1} \text{ s}^{-1}$	$k_{-2}/\text{L mol}^{-1} \text{ s}^{-1}$	$K_{2\text{eq}}$
1	PPh ₃	PPh ₃	Cl	$4.27(\pm 1) \cdot 10^{-2}$	$4.0(\pm 1) \cdot 10^{-3}$	$8.06 \cdot 10^{-3}$	$8.95(\pm 4) \cdot 10^{-5}$	90.08
2	PPh ₃	PPh ₃	I	$7.12(\pm 1) \cdot 10^{-3}$	0	$1.335 \cdot 10^{-3}$	$2.424(\pm 8) \cdot 10^{-4}$	5.51
3	PCy ₃	PCy ₃	Cl	$1.594(\pm 7) \cdot 10^{-2}$	$7.5(\pm 1) \cdot 10^{-4}$	$2.406 \cdot 10^{-3}$	$1.930(\pm 7) \cdot 10^{-4}$	12.47
4	PMe ₃	PMe ₃	Cl	Fast	Fast	Fast	Fast	4.85
5*	PCy ₃	PPh ₃	Cl	$1.02 \cdot 10^{-3}$	$5.14(\pm 1) \cdot 10^{-3}$	$1.7 \cdot 10^{-4}$	$9.1(5) \cdot 10^{-4}$	0.19

* For the reaction with L¹ = PCy₃ and L² = PPh₃ was possible to measure $K_{1\text{eq}} = 0.20$ for the reaction between $[\text{AuMeL}]$ and $\text{trans-}[\text{Pd}_2(\mu\text{-Cl})_2\text{Rf}_2\text{L}_2]$.

Some conclusions can be extracted from the table:

- The equilibrium is more shifted to the products with Cl than with I (entries 1 and 2). This can be explained because the chloro ligand is more electrowithdrawing than the iodo one, so the dimer with chloro is comparatively more stabilized with two electrodonating Me groups than the dimer with the more electrodonating iodo.
- The equilibrium is more shifted to the products with PPh₃ than with PCy₃, and these more than with PMe₃ (entries 1, 3 and 4). The reason for this is

^aAll the equilibria constants were calculated at 258 K and using decafluorobiphenyl as a patron. In all of the reactions the equilibrium is reached 20 hours after the beginning of the reaction except for the reaction with bridging iodine that the equilibrium was reached after a few days. K_{eq} were measured by the concentrations in the equilibrium.

related to the σ -donor ability of each ligand: PCy₃ is more electrodonating than PPh₃, making the dimer with the electrowithdrawing Rf group more stable. As PMe₃ is also electrodonating, the dimer with this phosphine and Rf groups is also a good electronic combination, making less likely the formation of the final dimer with two electrodonating Me groups. Although PCy₃ is more electrodonating than PMe₃, this favoring the dimer with two Me groups and PMe₃, the smaller size of the PMe₃ reduces the contribution of ligand repulsions and makes the dimer with Rf groups more stable than the alternative dimer with PCy₃, which turns out to be decisive for the overall balance of the equilibrium in this case.

- The reaction is slower when the bridging halogen is iodine (entry 2). This result can be rationalized considering the relative strength of the different halogen bridges. Fagnou studied that the stability of the dimers changes dramatically with the nature of the halide, being more stable the dimer with bridging iodine than the one with bridging chlorine.⁷ Buchwald also found that the nature of the halide affects the cleavage of the bridges in the dimers. He found that the splitting of chloro bridges is faster than for iodo bridges in the reaction between amines with palladium halide dimers via cleavage of the halide bridge, to produce monomeric palladium amine complexes (Scheme IV-6).⁸

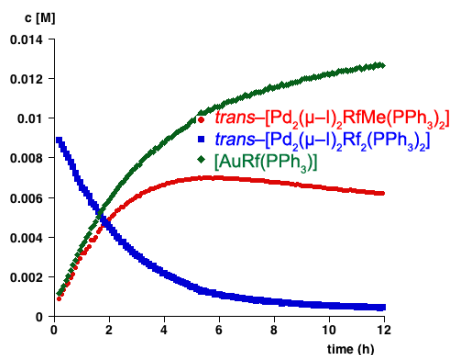
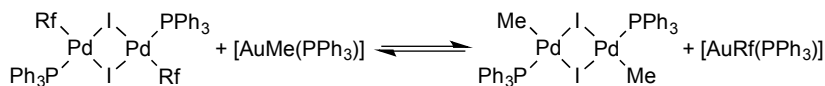
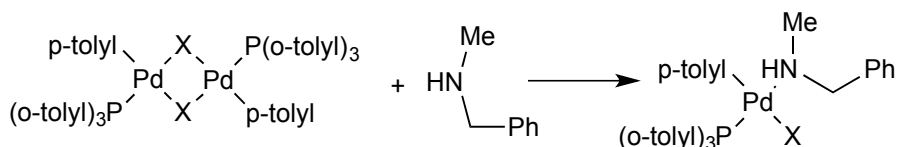


Figure IV-6. Observed concentrations as a function of time. Starting conditions: $[\text{AuMe}(\text{PPh}_3)] = 0.020 \text{ molL}^{-1}$, $\text{trans-}[\text{Pd}_2(\mu\text{-I})_2\text{Rf}_2(\text{PPh}_3)_2] = 0.010 \text{ molL}^{-1}$ at 258 K.



Scheme IV-6. Synthesis of monomeric palladium amine complexes. The reaction is faster for X = Cl than for X = I (Ref.8).

He explained this tendency with the relative polarizability and the size of the halides. Towards palladium(II), iodine is more electrodonating than chlorine, giving Pd-($\mu\text{-X}$) higher bond strengths. Palladium dimers are more stable with iodine, being the reactions in which a cleavage of the bridges is produced, slower.

In our experiments, as the reaction is one order of magnitude faster with chloro bridges than with iodo bridges, we might conclude with Buchwald's analysis that the concomitant bridge cleavage of the bridging halide has a large contribution to the ΔG^\ddagger . However, we should not forget another important contribution to an associative ligand substitution, that is the

fact that the electrophilicity of the Pd center is larger for Cl ligands than for I ligands.

- When considering the effect of the neutral ligands L in the reaction (entries 1, 3 and 4), two effects have to be taken into account: i) the trans labilization of the Pd-X bond that is broken during the reaction, which depends on the σ -donor capability of each ligand L, and ii) the bulkiness of the ligand, measured by its Tolman's Cone Angle, that will largely influence the energy of the TS in associative processes.

Table IV-2. Tolman's Cone Angle and Tolman's Electron Parameter for different phosphines: PMe_3 , PPh_3 and PCy_3 .^b

Phosphine	Tolman Cone Angle	Tolman Electronic Parameter
PMe_3	118°	2064.1 cm^{-1}
PPh_3	145°	2068.9 cm^{-1}
PCy_3	170°	2056.4 cm^{-1}

When other phosphines are used in the two metals, the electrophilicity in Pd and the nucleophilicity of the Me-Au bond change. In the case of PMe_3 the two effects are added; a better nucleophilicity of the Au reagent, a better trans labilization of the Pd-X and a small Tolman Cone Angle, so the reaction is really fast. In the case of PCy_3 its large size counteracts the electronic effects, which points to a very important participation of the electrophilicity of the Pd center, which is largely affected by the size effect of the ligand.

^b The Tolman Cone Angle is a measure of the size of a phosphine ligand, while the TEP (Tolman Electronic Parameter) is a measure of the electron donating or withdrawing ability of a ligand.

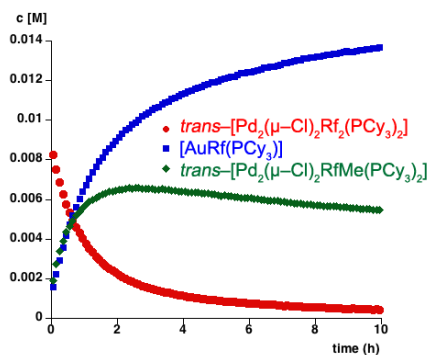
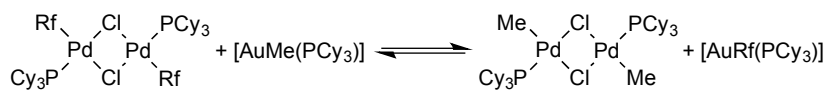


Figure IV-7. Observed concentrations as a function of time. Starting conditions: $[\text{AuMe}(\text{PCy}_3)] = 0.020 \text{ molL}^{-1}$, $\text{trans-}[\text{Pd}_2(\mu\text{-Cl})_2\text{Rf}_2(\text{PCy}_3)_2] = 0.010 \text{ molL}^{-1}$ at 258 K.

Considering only the bulkiness of the ligands, the phosphine with the smallest Tolman Cone Angle provide faster reactions, because the steric hindrance produced in the intermediate of the reaction is lower than when a bulkier phosphine is used. But taking into account the trans effect for each phosphine ligand, the trans labilization of the Pd-X bond that is broken during the reaction depends on the σ -donor capability of each ligand, being easier to break the Pd-X bond if the phosphine is more electrodonating.

The order obtained for the reaction rates is the following: $\text{PMe}_3 \gg \text{PPh}_3 \approx \text{PCy}_3$. In the case of the PMe_3 the reaction is so fast because it has a high trans labilization of the Pd-X bond broken during the reaction and small steric requirements. Thus, in this case the labilization seems to predominate. For $\text{L} = \text{PCy}_3$, although the trans effect is higher the steric bulkiness of the ligand predominates.

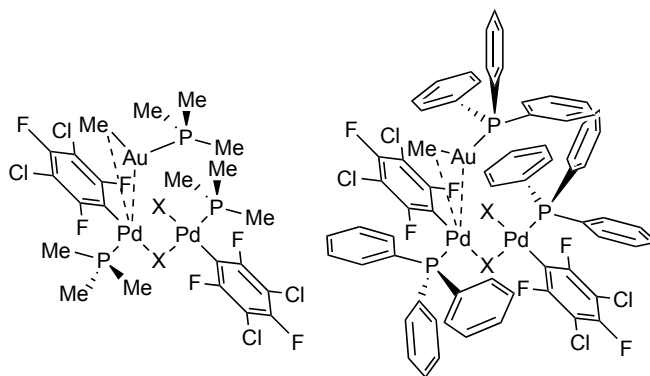


Figure IV-8. Steric hindrance produced between the ligand of the gold compound and the ligand in palladium dimer in the associative intermediate of the reaction.

In the reaction between $trans\text{-}[\text{Pd}_2(\mu\text{-Cl})_2\text{Rf}_2(\text{PCy}_3)_2]$ and $[\text{AuMe}(\text{PPh}_3)]$ (Figure IV-9) we found some ligand exchange. The reaction was slower than when PCy_3 was used in both metal complexes. The steric bulk in the palladium dimer is the same, but $[\text{AuMe}(\text{PPh}_3)]$ is a worse nucleophile than $[\text{AuMe}(\text{PCy}_3)]$, because PPh_3 gives less electron density to the gold compound than PCy_3 .

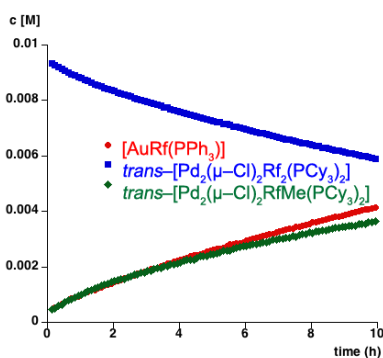
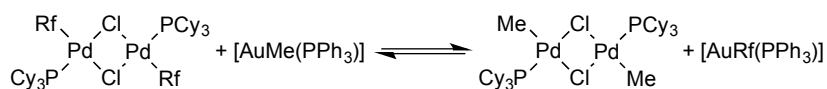


Figure IV-9. Observed concentrations as a function of time. Starting conditions: $[\text{AuMe}(\text{PPh}_3)] = 0.020 \text{ molL}^{-1}$, $trans\text{-}[\text{Pd}_2(\mu\text{-Cl})_2\text{Rf}_2(\text{PCy}_3)_2] = 0.010 \text{ molL}^{-1}$ at 258 K.

4.2.2 Reactions between *trans*-[Pd₂(μ-X)₂Rf₂L₂] and ZnMe₂

In order to compare the differences between the reactivity of the gold and zinc compounds in the reaction with *trans*-[Pd₂(μ-X)₂Rf₂L₂], we moved to study the same reaction but using ZnMe₂ instead of [AuMeL]. With organozinc the reactions are faster than with gold complexes, so the study had to be performed at lower temperature (219 K, in THF). The reaction is more complex than with [AuMeL], the spectrum of the Figure IV-10 shows that the first reaction is a very fast exchange of the Me and Rf groups to form ZnRfMe and [Pd₂(μ-Cl)₂Me₂(PPh₃)₂], the last was detected by ³¹P.^c Eventually, the system evolves to produce *cis*-[PdRfMeL(thf)].^d The known compound [Pd₂(μ-Cl)₂RfMe(PPh₃)₂] was not detected.

^c In addition, two minor unidentified compounds were detected by ¹⁹F during the experiment.

^d *cis*-[PdRfMe(PPh₃)(thf)] was characterized by adding an excess of PPh₃ to the NMR tube at low temperature.

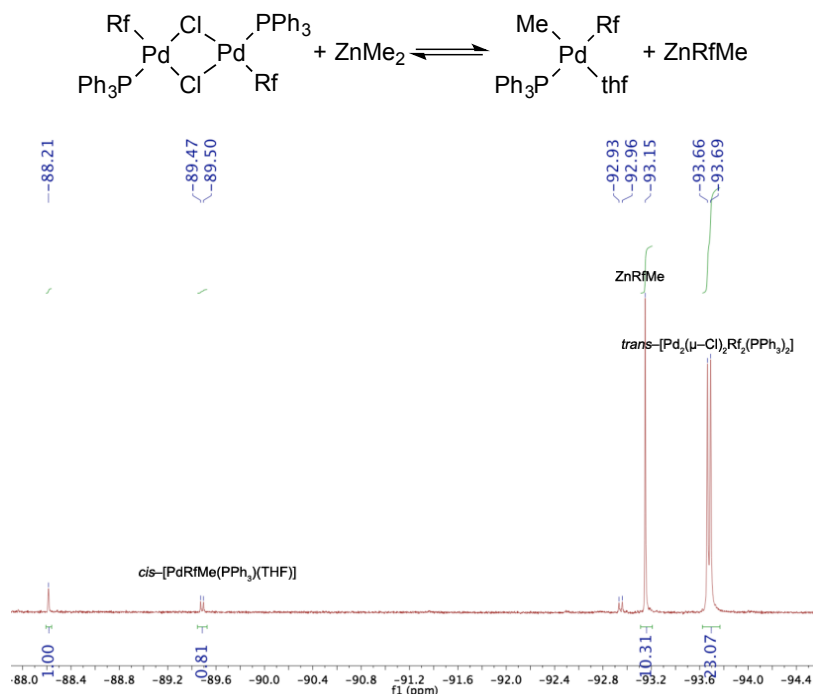


Figure IV-10. ^{19}F NMR spectra after seven minutes of the reaction between ZnMe_2 and $\text{trans-}[\text{Pd}_2(\mu\text{-Cl})_2\text{Rf}_2(\text{PPh}_3)_2]$ at 219 K. Starting conditions: $[\text{ZnMe}_2] = 0.015 \text{ molL}^{-1}$, $\text{trans-}[\text{Pd}_2(\mu\text{-Cl})_2\text{Rf}_2(\text{PPh}_3)_2] = 3.0 \times 10^{-3} \text{ molL}^{-1}$. Signals at -88.21 and -92.9 are unknown products.

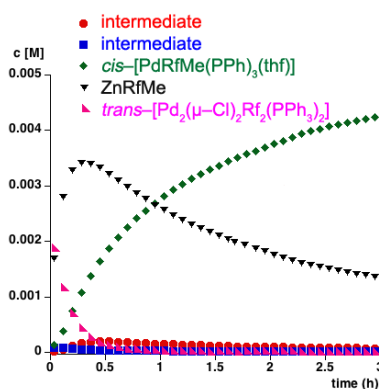
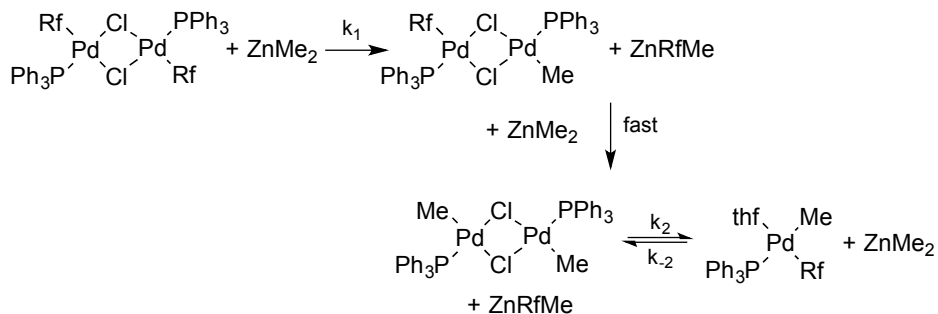


Figure IV-11. Observed concentrations as a function of time. Starting conditions: $[\text{ZnMe}_2] = 0.015 \text{ molL}^{-1}$, $\text{trans-}[\text{Pd}_2(\mu\text{-Cl})_2\text{Rf}_2(\text{PPh}_3)_2] = 3.0 \times 10^{-3} \text{ molL}^{-1}$ at 219 K.

The transmetalation of $[\text{Pd}_2(\mu\text{-Cl})_2\text{RfMe}(\text{PPh}_3)_2]$ with ZnMe_2 is so fast that it is not observable (Scheme IV-7). No cross-coupling product was detected during the reaction.

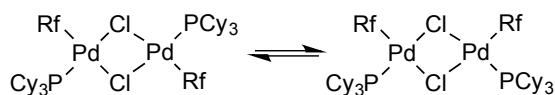


Scheme IV-7. Reaction between ZnMe_2 and $\text{trans-}[\text{Pd}_2(\mu\text{-Cl})_2\text{Rf}_2(\text{PPh}_3)_2]$. $k_1 = 0.169(\pm 9) \text{ L mol}^{-1} \text{ s}^{-1}$; $k_2 = 0.24(\pm 1) \text{ L mol}^{-1} \text{ s}^{-1}$; $k_{-2} = 173.3(\pm 1) \text{ L mol}^{-1} \text{ s}^{-1}$.

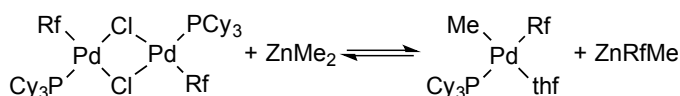
No ZnRf_2 is observed. This is due to the presence of a large excess of ZnMe_2 under the reaction conditions. In addition, because once one Me group of the ZnMe_2 is exchanged for the Rf group of the $\text{trans-}[\text{Pd}_2(\mu\text{-Cl})_2\text{Rf}_2(\text{PPh}_3)_2]$, the resulting ZnRfMe formed is less reactive than ZnMe_2 because of the presence of the Rf electrowithdrawing group.

The reaction rate did not allow us to expand the temperature interval to obtain the activation parameters ΔH^\ddagger and ΔS^\ddagger .

The study of the reaction between $[\text{Pd}_2(\mu\text{-Cl})_2\text{Rf}_2(\text{PCy}_3)_2]$ and ZnMe_2 in THF at 219 K is obscured by the spontaneous breaking of the bridges to produce the exchange $\text{cis/trans-}[\text{Pd}_2(\mu\text{-Cl})_2\text{Rf}_2(\text{PCy}_3)_2]$ (Scheme IV-8), precluding also the observation of the species $[\text{Pd}_2(\mu\text{-Cl})_2\text{MeRf}(\text{PCy}_3)_2]$ during the reaction because the signals from the F_{ortho} are close to coalescence at 219 K (see spectrum in Figure IV-12, $L = \text{PCy}_3$).



Scheme IV-8. Scheme for the equilibrium between $\text{trans-}[\text{Pd}_2(\mu\text{-Cl})_2\text{Rf}_2(\text{Cy}_3)_2]$ and $\text{cis-}[\text{Pd}_2(\mu\text{-Cl})_2\text{Rf}_2(\text{Cy}_3)_2]$.



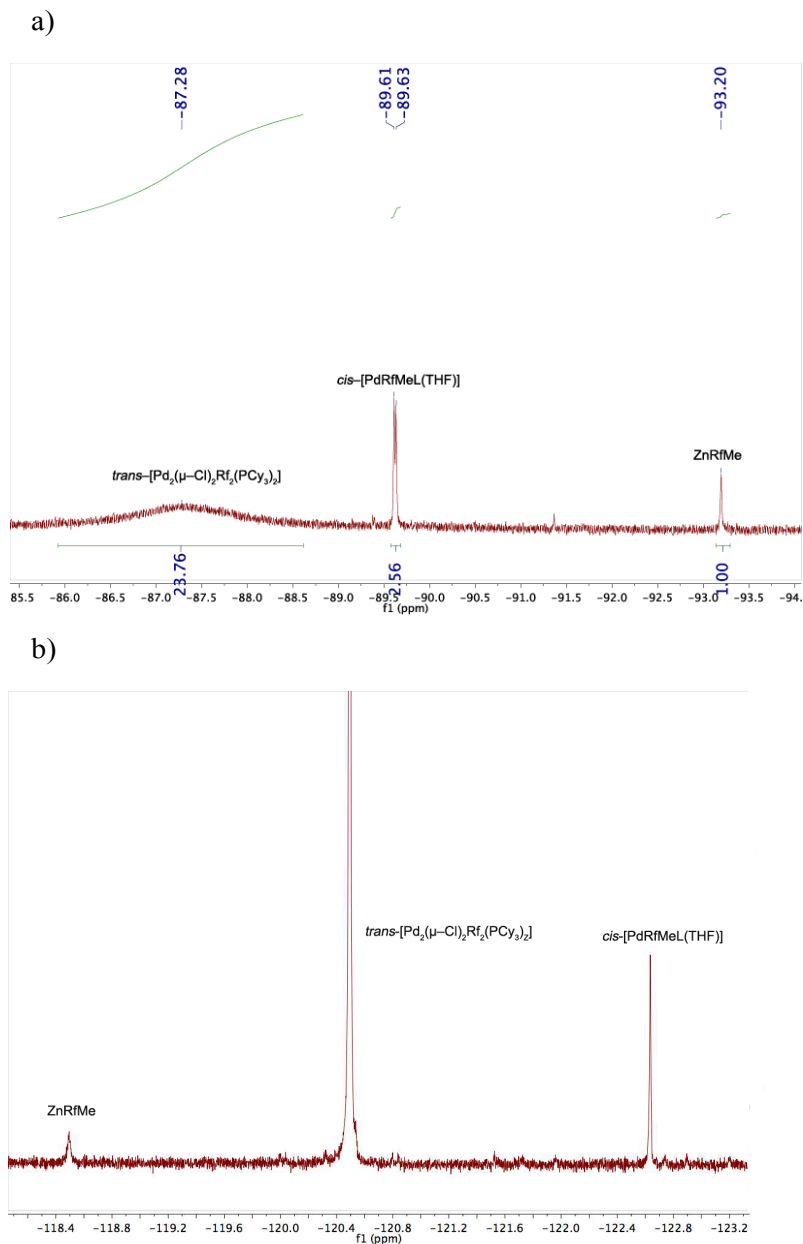


Figure IV-12. ^{19}F NMR spectra after seven minutes of the reaction between ZnMe_2 and $\text{trans-}[\text{Pd}_2(\mu\text{-Cl})_2\text{Rf}_2(\text{PCy}_3)_2]$, at 219 K. Starting conditions: $[\text{ZnMe}_2] = 0.015 \text{ molL}^{-1}$ and $\text{trans-}[\text{Pd}_2(\mu\text{-Cl})_2\text{Rf}_2(\text{PCy}_3)_2] = 3.0 \times 10^{-3} \text{ molL}^{-1}$. a) F-ortho, b) F-para. The wide signal at -87.28 ppm corresponds with the F-ortho of $\text{trans-}[\text{Pd}_2(\mu\text{-Cl})_2\text{Rf}_2(\text{PCy}_3)_2]$.

The behaviour is the same that with PPh_3 . First, the exchange reaction of the Me and Rf groups is produced, forming ZnRfMe and $[\text{Pd}_2(\mu\text{-Cl})_2\text{Me}_2(\text{PCy}_3)_2]$. The detection of $[\text{Pd}_2(\mu\text{-Cl})_2\text{RfMe}(\text{PCy}_3)_2]$ was not possible. Then, ZnRfMe gives back the Rf group to the $[\text{Pd}_2(\mu\text{-Cl})_2\text{Me}_2(\text{PCy}_3)_2]$ to form *cis*- $[\text{PdRfMe}(\text{PCy}_3)(\text{thf})]$. During the preparation of the sample the reaction of 15% of the reagents is produced. For the kinetic fitting, the first spectrum is considered to be at time zero, and the concentrations have been recalculated taking into account the amount of the compounds that has already reacted. The concentration of ZnRfMe remains constant during the reaction.

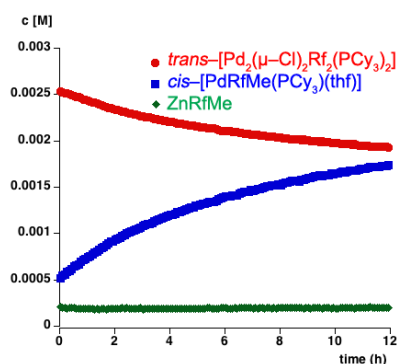
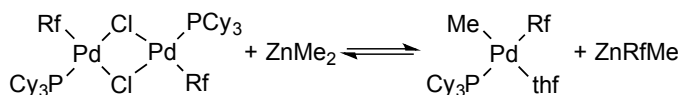


Figure IV-13. Observed concentrations as a function of time. Starting conditions: $[\text{ZnMe}_2] = 0.015 \text{ mol L}^{-1}$, $[\text{trans-}[\text{Pd}_2(\mu\text{-Cl})_2\text{Rf}_2(\text{PCy}_3)_2]] = 3.0 \times 10^{-3} \text{ mol L}^{-1}$ at 219 K. $k_1 = 8.18(\pm 2) \cdot 10^{-4} \text{ L mol}^{-1} \text{ s}^{-1}$; $k_2 = 3.3(\pm 1) \text{ L mol}^{-1} \text{ s}^{-1}$; $k_3 = 24.2(\pm 9) \text{ L mol}^{-1} \text{ s}^{-1}$.

The reaction between *trans*- $[\text{Pd}_2(\mu\text{-Cl})_2\text{Rf}_2(\text{PMe}_3)_2]$ and ZnMe_2 in THF at 219 K, is much faster than the reaction with PPh_3 or PCy_3 . Using *trans*- $[\text{Pd}_2(\mu\text{-Cl})_2\text{Rf}_2(\text{PMe}_3)_2]$, seven minutes after the beginning of the reaction the initial palladium compound is not observed anymore, and only ZnRfMe and *cis*- $[\text{PdRfMe}(\text{PMe}_3)(\text{thf})]$ are observed.

The effect of the phosphine ligand is the same as in the case of the reaction with gold. For PMe_3 the reaction is faster than with PPh_3 because PMe_3 has a high *trans* labilization effect on the Pd-X bond broken during the reaction and a smaller bulkiness.

The reaction with PCy_3 is slower than the reaction with PPh_3 , having PCy_3 a higher Tolman cone angle than PPh_3 . This is likely due to the steric hindrance produced in the intermediate of the reaction between the molecule of ZnMe_2 and the ligand in the palladium dimer. The second exchange reaction between ZnRfMe and $[\text{Pd}_2(\mu\text{-Cl})_2\text{Me}_2(\text{PCy}_3)_2]$ to form *cis*- $[\text{PdRfMe}(\text{PCy}_3)(\text{thf})]$ is also slower with PCy_3 than with PPh_3 , because of the higher electron density and the higher steric protection of the Pd center in the dimer $[\text{Pd}_2(\mu\text{-Cl})_2\text{Me}_2\text{L}_2]$ with PCy_3 , making it less electrophilic towards ZnRfMe .

The first exchange reaction between the Me group of $[\text{AuMeL}]$ and the Rf group of the *trans*- $[\text{Pd}_2(\mu\text{-X})_2\text{Rf}_2\text{L}_2]$ is really fast, whereas the second exchange reaction between $[\text{AuMeL}]$ and *trans*- $[\text{Pd}_2(\mu\text{-X})_2\text{RfMeL}_2]$ is slower. This is probably because of the electronic effect that the Me group has on the substitution of the Rf in the other Pd center, which can be explained by the *trans influence* that the Me group has on the bridging chlorine in *trans* position, allowing the Cl-Pd bond of the other Pd center to be shorter, and making that Cl bridging group a better electron donor towards the PdRf center, thus reducing its electrophilicity. Moreover, as this bond is shorter than the other bridging chlorine, it will be more difficult for the gold compound to break it to form the intermediate with an Au-Pd interaction from which the exchange reaction is produced. It is also possible the breaking of the other bridging chlorine but this pathway is unproductive because the Rf group of the palladium dimer and the incoming Me group of the gold compound would be in mutual *trans* position from which it is not possible the exchange reaction (Figure IV-14).

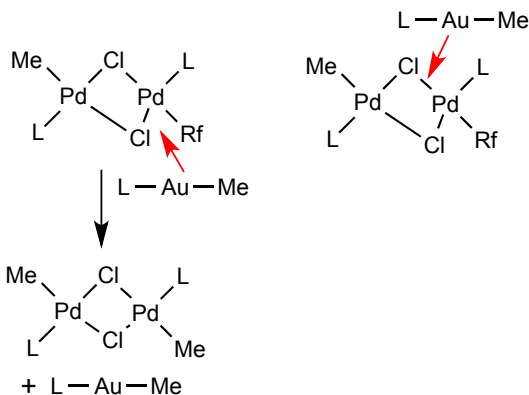


Figure IV-14. Splitting of the bridging chlorine forming the intermediate from what the exchange reaction is produced vs. unproductive splitting of the other bridging chlorine.

Some conclusions can be drawn from this study:

- With both reagents ZnMe_2 and $[\text{AuMeL}]$, the exchange reaction between Me and Rf groups with the dimer $\text{trans}-[\text{Pd}_2(\mu\text{-X})_2\text{Rf}_2\text{L}_2]$ is produced but the reaction with ZnMe_2 is faster than with $[\text{AuMeL}]$ because of its higher nucleophilicity.

- In the reaction with ZnMe_2 , the transmetalation of $[\text{Pd}_2(\mu\text{-Cl})_2\text{RfMe}(\text{PPh}_3)_2]$ with ZnMe_2 is so fast that it is not observable. Once the exchange between Rf and Me is produced, ZnRfMe gives back the Rf group to the $[\text{Pd}_2(\mu\text{-Cl})_2\text{Me}_2(\text{PCy}_3)_2]$ to form $\text{cis}-[\text{PdRfMe}(\text{PCy}_3)(\text{thf})]$ and ZnMe_2 .

4.3 EXPERIMENTAL SECTION

General methods are the same as described in Chapter I. The compounds $[\text{AuMe}(\text{PPh}_3)]$,⁹ $[\text{AuMe}(\text{PMe}_3)]$,¹⁰ $[\text{AuMe}(\text{PCy}_3)]$,¹¹ $[\text{AuRf}(\text{PPh}_3)]$,¹² $[\text{AuRf}(\text{PMe}_3)]$,¹³ $\text{trans}-[\text{Pd}_2(\mu\text{-Cl})_2\text{Me}_2(\text{PPh}_3)_2]$,¹⁴ $\text{trans}-[\text{Pd}_2(\mu\text{-Cl})_2\text{Me}_2(\text{PMe}_3)_2]$,¹⁵ $\text{trans}-[\text{Pd}_2(\mu\text{-I})_2\text{Me}_2(\text{PPh}_3)_2]$,¹⁶ were prepared as reported in the literature.

4.3.1 Synthesis of the Complexes

[AuRf(PCy₃)] 300 mg de [AuRf(tht)] (0.62 mmol) and 191 mg of PCy₃ (0.68 mmol) were dissolved in 30 ml of dry DCM. The solution was stirred for 1 hour under nitrogen. Then, it was concentrated and the product was obtained as a white solid by precipitation with 15 ml of hexane, filtered and dried under vacuum. Yield: 247 mg (59 %). ¹H NMR (CDCl₃, 298 K): δ 1.2–2.2 (m, 30 H). ¹⁹F NMR (CDCl₃, 298 K): δ -91.43 (d, ⁴J_{P-F} = 6.8 Hz, *o*-CF), -119.25 (s, *p*-CF). ³¹P NMR (CDCl₃, 298 K): δ 57.00 (t, ⁴J_{P-F} = 6.8 Hz). ¹³C NMR (CDCl₃, 298 K, quaternary carbons are not included): δ 25.95 (s), δ 27.12 (d, *J* = 11,82 Hz), δ 30.78 (s), δ 33.30 (d, *J* = 27.08 Hz). Cald. for C₂₄H₃₃AuCl₂F₃P: C 42.56; H 4.91. Found: C 42.01; H 4.81.

***trans*-[Pd₂(μ-Cl)₂Rf₂(PPh₃)₂]** 303.8 mg of *trans*-[PdRf₂(PPh₃)₂] (0.30 mmol) and 52.3 mg of PdCl₂ (0.30 mmol) were dissolved in acetone (40 mL). The solution was heated to reflux. After 18 hours the solvent was removed *a vacuum* and the product of the reaction was washed with EtOH. The product was purified by chromatography in silica, with CHCl₃ as eluent, to give a yellow solution. The CHCl₃ was evaporated to the yellow solution, obtaining the desired product as a yellow solid. Yield: 170 mg (48 %). ¹H NMR (CDCl₃, 298 K): δ 7.68 (m, 12 H), δ 7.44 (m, 6 H), δ 7.36 (m, 12 H). ¹⁹F NMR (CDCl₃, 298 K): δ -92.14 (d, ⁴J_{P-F} = 12.2 Hz, *o*-CF), -118.49 (s, *p*-CF). The ³¹P NMR is ³¹P {¹H} NMR (CDCl₃, 298 K): δ 32.40 (t, ⁴J_{P-F} = 11.9 Hz). ¹³C NMR (CDCl₃, 298 K, quaternary carbons are not included): δ 128.36 (d, *J* = 11.71 Hz), δ 131.42 (s), δ 134.18 (d, *J* = 11.16 Hz). Cald. for C₄₈H₃₀Cl₆F₆P₂Pd₂: C 47.72; H 2.50. Found: C 47.30; H 2.49.

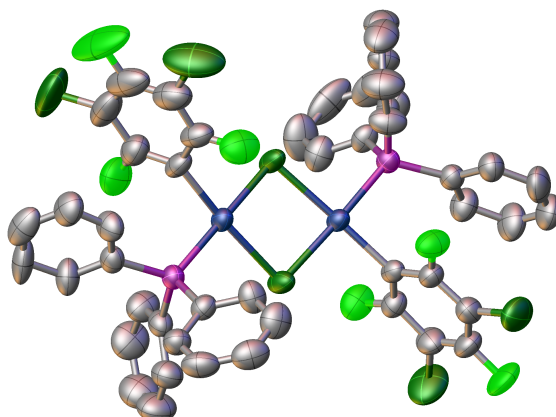


Figure IV-15. X-Ray structure of *trans*-[Pd₂(μ-Cl)₂Rf₂(PPh₃)₂]. Blue: Pd; Dark green: Cl; Light green: F; Pink: P and Grey: C. H atoms are omitted for clarity.

***trans*-[Pd₂(μ-I)₂Rf₂(PPh₃)₂]** 1.40 g of *trans*-[PdI₂(PPh₃)₂] (1.58 mmol) and 1.18 g of *cis*-[PdRf₂(THF)₂] (1.82 mmol) were dissolved in dry THF (40 mL). The suspension was stirred for 5 hours. The solvent was evaporated to dryness and the residue was extracted with CH₂Cl₂ (3x70 mL). The dark solution was evaporated to dryness and the solid was filtered and washed with EtOH. The crude product was recrystallized from CH₂Cl₂/EtOH. Yield: 1.8 g (81 %). ¹H NMR (CDCl₃, 298 K): δ 7.77–7.20 (m, 30 H). ¹⁹F NMR (CDCl₃, 298 K): δ -90.93 (s, *o*-CF), -120.30 (s, *p*-CF). The ³¹P NMR is ³¹P NMR (CDCl₃, 298 K): δ 31.26 (s). ¹³C NMR (CDCl₃, 298 K, quaternary carbons are not included): δ 128.22 (d, *J* = 10.13 Hz), δ 131.13 (s), δ 134.35 (d, *J* = 10.51 Hz). Cald. for C₄₈H₃₀Cl₄F₆I₂P₂Pd₂: C 41.44; H 2.17. Found: C 41.19; H 1.87.

***trans*-[Pd₂(μ-Cl)₂Rf₂(PCy₃)₂]** 401.6 mg of *trans*-[PdCl₂(PCy₃)₂] (0.54 mmol) were dissolved in dried THF (30 mL). The solution was cooled to 273 K and 353.9 mg of *cis*-[PdRf₂(THF)₂] (0.54 mmol) were added. After 5 hours the solvent was removed *a vacuum* and was recrystallized from CH₂Cl₂/EtOH. The palladium complex was obtained as a yellow solid, filtered and vacuum dried. Yield: 401.3 mg (60 %). ¹H NMR (CDCl₃, 298 K): δ 2.2–0.8 (m, 66 H). ¹⁹F NMR (CDCl₃, 298 K): δ -86.28 (d, ⁴*J*_{P-F} = 7.9 Hz, *o*-CF), -117.93 (s, *p*-CF). ³¹P {¹H} NMR (CDCl₃, 298 K): δ 49.70 (t, ⁴*J*_{P-F} = 10 Hz). ¹³C NMR (CDCl₃,

298 K, quaternary carbons are not included): δ 26.06 (s), δ 27.46 (d, $J = 11.53$ Hz), δ 29.68 (s), δ 35.88 (s). Cald. for $C_{48}H_{66}Cl_6F_6P_2Pd_2$: C 46.32; H 5.35. Found: C 45.84; H 4.86.

***trans*-[Pd₂(μ -Cl)₂Rf₂(PMe₃)₂]** 263.5 mg of *trans*-[PdCl₂(PMe₃)₂] (0.80 mmol) were dissolved in dried THF (45 mL). The solution was cooled to 273 K and 520.3 mg of *cis*-[PdRf₂(THF)₂] (0.80 mmol) were added. After 5 hours the solvent was removed *a vacuum* and was recrystallized from CH₂Cl₂/EtOH. The palladium complex was obtained as a green solid, filtered and vacuum dried. Yield: 440 mg (33 %). ¹H NMR (CDCl₃, 298 K): δ 1.79 (d, $J = 10.21$, 18 H). ¹⁹F NMR (CDCl₃, 298 K): δ -89.10 (s, *o*-CF), -119.49 (s, *p*-CF). ³¹P NMR (CDCl₃, 298 K): δ 4.87 (s). ¹³C NMR (acetone-*d*₆, 298 K, quaternary carbons are not included): δ 15.62 (d, $J = 37.86$ Hz). Cald. for $C_{18}H_{18}Cl_6F_6P_2Pd_2$: C 25.87; H 2.17. Found: C 25.33; H 2.05.

***trans*-[Pd₂(μ -Cl)₂Me₂(PCy₃)₂]** 573 mg of [PdClMe(COD)] (2.17 mmol) were dissolved in CH₂Cl₂ (5 mL) and 569 mg of PCy₃ (2.17 mmol) were added. After 4 hours, the white product was precipitated with hexane, filtered and vacuum dried. Yield: 1.12 g (60 %). ¹H NMR (CDCl₃, 298 K): δ 2.2–1.1 (m, 72 H). The ³¹P NMR is ³¹P {¹H} NMR (CDCl₃, 298 K): δ 45.51. ¹³C NMR (CDCl₃, 298 K, quaternary carbons are not included): δ 26.06 (s), δ 27.47 (d, $J = 11.68$ Hz), δ 29.68 (s), δ 35.97 (d, $J = 23.24$ Hz), δ 36.47 (d, $J = 30.23$ Hz). Cald. for $C_{38}H_{72}Cl_2P_2Pd_2$: C 52.18; H 8.30. Found: C 51.83; H 8.14.

4.3.2 Synthesis in solution of *trans*-[Pd₂(μ -Cl)₂RfMe(PPh₃)₂], *trans*-[Pd₂(μ -Cl)₂RfMe(PCy₃)₂], *trans*-[Pd₂(μ -Cl)₂RfMe(PMe₃)₂] and [Pd₂(μ -I)₂RfMe(PPh₃)₂]

trans-[Pd₂(μ -X)₂Rf₂(L)₂] (1 eq.) and *trans*-[Pd₂(μ -X)₂Me₂(L)₂] (1 eq.) were dissolved in THF (0.6 mL), in a NMR tube containing a capillary tube with acetone-*d*₆ as reference, at room temperature. The ¹⁹F NMR spectrum shows signals of the starting palladium complex and the signals of the new

palladium compound. The NMR spectra were recorded at different temperatures.

trans-[Pd₂(μ-Cl)₂RfMe(PPh₃)₂]: ¹⁹F NMR (THF-acetone-*d*₆ capillary): δ -91.52 (d, ⁴J_{CSn} = 12.4 Hz, *o*-CF), -120.53 (s, *p*-CF). The ³¹P NMR is ³¹P (THF-acetone-*d*₆ capillary): δ 38.33 (s), 30.35 (s).

trans-[Pd₂(μ-Cl)₂RfMe(PCy₃)₂]: ¹⁹F NMR (THF-acetone-*d*₆ capillary): δ -87.01 (2F, d, ⁴J_{p-F} = 8.37, *o*-CF), -121.29 (1F, s, *p*-CF). The ³¹P NMR is (THF-acetone-*d*₆ capillary): δ 47.65 (s), 46.28 (s).

trans-[Pd₂(μ-Cl)₂RfMe(PMe₃)₂]: ¹⁹F NMR (THF-acetone-*d*₆ capillary): δ -92.31 (2F, d, ⁴J_{p-F} = 11.40, *o*-CF), -120.53 (1F, s, *p*-CF). The ³¹P NMR is (THF-acetone-*d*₆ capillary): δ 1.43 (s), -1.11 (s).

trans-[Pd₂(μ-I)₂RfMe(PMe₃)₂]: ¹⁹F NMR (THF-acetone-*d*₆ capillary): δ -91.06 (2F, d, ⁴J_{p-F} = 9.96, *o*-CF), -121.93 (1F, s, *p*-CF). The ³¹P NMR is ³¹P (THF-acetone-*d*₆ capillary): δ 37.94 (s), 29.37 (s).

Mixtures between the compounds *trans*-[Pd₂(μ-Cl)₂Rf₂L₂] (4.0x10⁻³ mmol) and *trans*-[Pd₂(μ-Cl)₂Me₂L₂] (0.0040 mmol) were prepared in order to know the chemical shifts of the two compounds and *trans*-[Pd₂(μ-Cl)₂RfMeL₂] in THF, at different temperatures. It was observed that the signals of F-ortho at lower temperatures become wider for all the compounds. For L = PCy₃, *trans*-[Pd₂(μ-Cl)₂Rf₂(PCy₃)₂] and *trans*-[Pd₂(μ-Cl)₂RfMe(PCy₃)₂] have the same F-ortho chemical shift at -87.11 ppm.

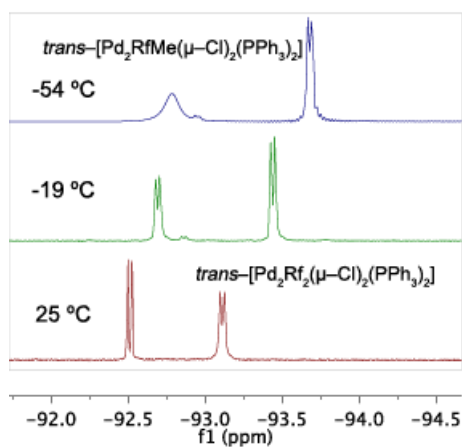


Figure IV-16. ^{19}F NMR spectra of the F-ortho in the reaction between $\text{trans-}[\text{Pd}_2(\mu\text{-Cl})_2\text{Rf}_2(\text{PPh}_3)_2]$ and $\text{trans-}[\text{Pd}_2(\mu\text{-Cl})_2\text{Me}_2(\text{PPh}_3)_2]$ at different temperatures.

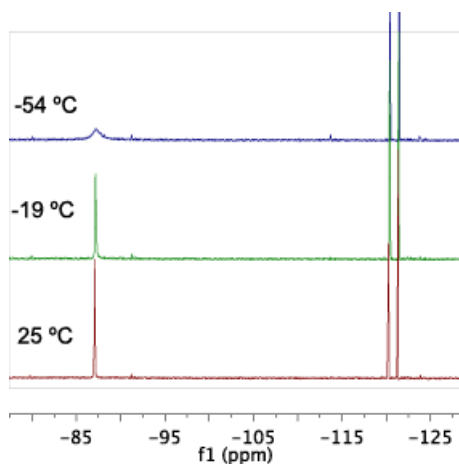


Figure IV-17. ^{19}F NMR spectra in the reaction between $\text{trans-}[\text{Pd}_2(\mu\text{-Cl})_2\text{Rf}_2(\text{PCy}_3)_2]$ and $\text{trans-}[\text{Pd}_2(\mu\text{-Cl})_2\text{Me}_2(\text{PCy}_3)_2]$ at different temperatures. $\text{trans-}[\text{Pd}_2(\mu\text{-Cl})_2\text{Rf}_2(\text{PCy}_3)_2]$ (-87.05 and -120.26 ppm), $\text{trans-}[\text{Pd}_2(\mu\text{-Cl})_2\text{RfMe}(\text{PCy}_3)_2]$ (-87.05 and -121.34 ppm).

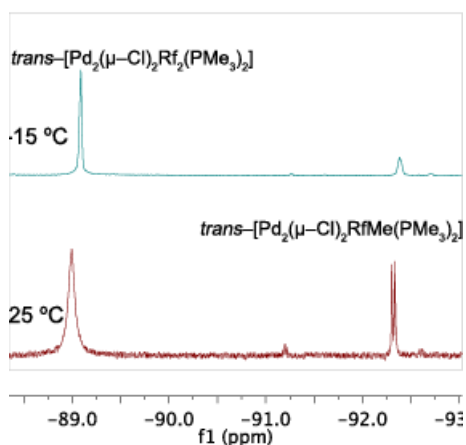


Figure IV-18. ^{19}F NMR spectra of the F-ortho in the reaction between $\text{trans-}[\text{Pd}_2(\mu\text{-Cl})_2\text{Rf}_2(\text{PMe}_3)_2]$ and $\text{trans-}[\text{Pd}_2(\mu\text{-Cl})_2\text{RfMe}(\text{PMe}_3)_2]$ at different temperatures.

4.3.3 Reactions of $\text{trans-}[\text{Pd}_2(\mu\text{-X})_2\text{Rf}_2(\text{L})_2]$ ($\text{X} = \text{Cl, I}$; $\text{L} = \text{PPh}_3, \text{PCy}_3, \text{PMe}_3$) and $[\text{AuMeL}]$ ($\text{X} = \text{PPh}_3, \text{PMe}_3, \text{PCy}_3$). Kinetic Procedure

NMR tubes (5mm) are charged with palladium dimer ($5.0 \times 10^{-3} \text{ mol} \cdot \text{L}^{-1}$ or $0.010 \text{ mol} \cdot \text{L}^{-1}$) and $[\text{AuMeL}]$ ($0.020 \text{ mol} \cdot \text{L}^{-1}$). The kinetic experiments were monitored by ^{19}F NMR. The NMR tube was cooled to $-78 \text{ }^\circ\text{C}$ and THF was added to a fixed volume of $600 \pm 5 \text{ } \mu\text{L}$, charged with an acetone- d_6 capillary for NMR lock, and placed into a thermostated probe at the desired temperature (the temperature was calibrated by a methanol standard method). Concentration-time data were then acquired from ^{19}F signals areas of $\text{trans-}[\text{Pd}_2(\mu\text{-X})_2\text{Rf}_2(\text{L})_2]$, the product $[\text{AuRfL}]$ and the intermediate $\text{trans-}[\text{Pd}_2(\mu\text{-X})_2\text{RfMe}(\text{L})_2]$. The initial rates were obtained by linear fitting of the concentration-time curves in the interval 0-15% of consumption of the starting reagents.

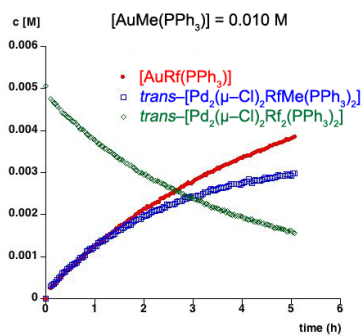
4.3.3.1 Order the reaction on [AuMe(PPh₃)]

Table IV-3. Starting conditions for the kinetics of the transmetalation reaction between *trans*-[Pd₂(μ-Cl)₂Rf₂(PPh₃)₂] and [AuMe(PPh₃)] in THF at 234 K and rates obtained.

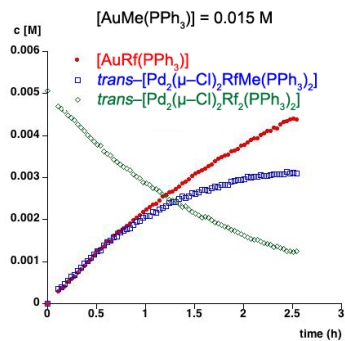
[AuMe(PPh ₃)] _{added} / mol L ⁻¹	Initial rate (r ₀) / mol L ⁻¹ s ⁻¹
0.0100	1.1179 · 10 ⁻⁶
0.0154	1.5808 · 10 ⁻⁶
0.0200	1.9265 · 10 ⁻⁶
0.0300	2.7066 · 10 ⁻⁶
<i>trans</i> -[Pd ₂ (μ-Cl) ₂ Rf ₂ (PPh ₃) ₂] ₀ = 0.0050 mol L ⁻¹	
T: 234 K	



a)



b)



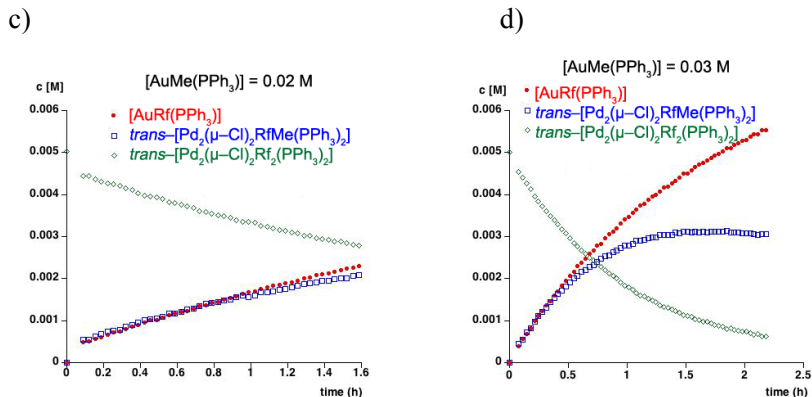


Figure IV-19. Observed concentrations as a function of time. $trans\text{-}[\text{Pd}_2(\mu\text{-Cl})_2\text{Rf}_2\text{L}_2]_0 = 0.0050 \text{ molL}^{-1}$. a) $[\text{AuMe}(\text{PPh}_3)]_0 = 0.010 \text{ molL}^{-1}$, b) $[\text{AuMe}(\text{PPh}_3)]_0 = 0.015 \text{ molL}^{-1}$, c) $[\text{AuMe}(\text{PPh}_3)]_0 = 0.020 \text{ molL}^{-1}$, d) $[\text{AuMe}(\text{PPh}_3)]_0 = 0.030 \text{ molL}^{-1}$ at 234 K.

The experimental dependence of $\ln(r_0)$ vs $\ln[\text{AuMe}(\text{PPh}_3)]$ for different amounts of $[\text{AuMe}(\text{PPh}_3)]$ leads to a straight line with slope +0.8.

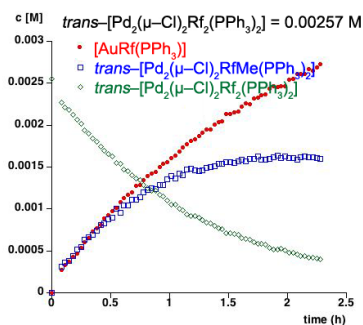
4.3.3.2 Order the reaction on $trans\text{-}[\text{Pd}_2(\mu\text{-Cl})_2\text{Rf}_2(\text{PPh}_3)_2]$

Table IV-4. Starting conditions for the kinetics of the transmetalation reaction between $trans\text{-}[\text{Pd}_2(\mu\text{-Cl})_2\text{Rf}_2(\text{PPh}_3)_2]$ and $[\text{AuMe}(\text{PPh}_3)]$ in THF at 234 K and rates obtained.

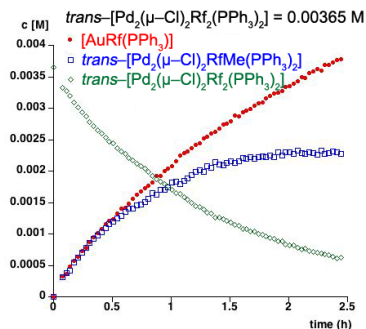
$trans\text{-}[\text{Pd}_2(\mu\text{-Cl})_2\text{Rf}_2(\text{PPh}_3)_2]_{\text{added}} / \text{molL}^{-1}$	Initial rate (r_0) / $\text{mol L}^{-1} \text{ s}^{-1}$
0.002557	$1.4246 \cdot 10^{-6}$
0.003650	$2.1740 \cdot 10^{-6}$
0.005020	$3.0802 \cdot 10^{-6}$
0.006930	$4.3179 \cdot 10^{-6}$
0.008430	$6.1731 \cdot 10^{-6}$
$[\text{MeAu}(\text{PPh}_3)]_0 = 0.02 \text{ molL}^{-1}$ T: 234 K	



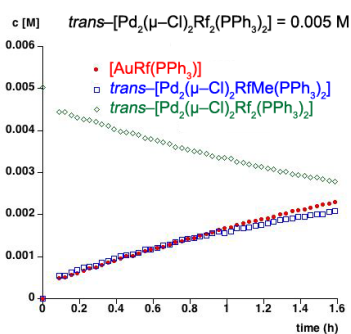
a)



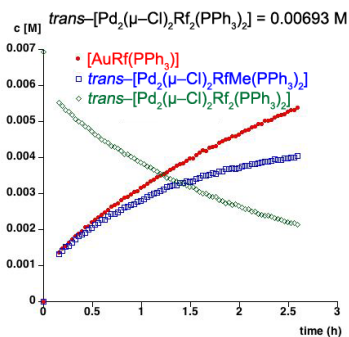
b)



c)



d)



e)

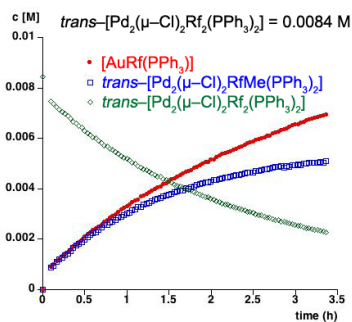


Figure IV-20. Observed concentrations as a function of time. $[\text{AuMe}(\text{PPh}_3)]_0 = 0.02 \text{ molL}^{-1}$. a) $\text{trans-}[\text{Pd}_2(\mu\text{-Cl})_2\text{Rf}_2\text{L}_2]_0 = 0.00256 \text{ molL}^{-1}$, b) $\text{trans-}[\text{Pd}_2(\mu\text{-Cl})_2\text{Rf}_2\text{L}_2]_0 = 0.00365 \text{ molL}^{-1}$, c) $\text{trans-}[\text{Pd}_2(\mu\text{-Cl})_2\text{Rf}_2\text{L}_2]_0 = 0.00502 \text{ molL}^{-1}$, d) $\text{trans-}[\text{Pd}_2(\mu\text{-Cl})_2\text{Rf}_2\text{L}_2]_0 = 0.00693 \text{ molL}^{-1}$, e) $\text{trans-}[\text{Pd}_2(\mu\text{-Cl})_2\text{Rf}_2\text{L}_2]_0 = 0.00843 \text{ molL}^{-1}$ at 234 K.

The experimental dependence of $\ln(r_0)$ vs $\ln \text{trans-}[\text{Pd}_2(\mu\text{-Cl})_2\text{Rf}_2\text{L}_2]$ for different amounts of $\text{trans-}[\text{Pd}_2(\mu\text{-Cl})_2\text{Rf}_2\text{L}_2]$ leads to a straight line with slope +1.18.

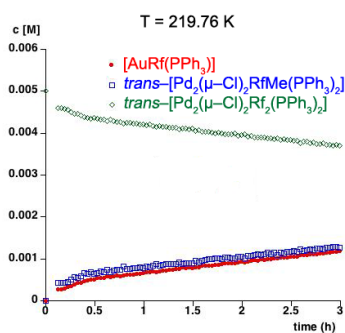
4.3.3.3 Activation parameters in the reaction between $[\text{AuMe}(\text{PPh}_3)]$ and $\text{trans-}[\text{Pd}_2(\mu\text{-Cl})_2\text{Rf}_2\text{L}_2]$

Table IV-5. Reactions between $[\text{AuMe}(\text{PPh}_3)]_0 = 0.020 \text{ molL}^{-1}$ and $\text{trans-}[\text{Pd}_2(\mu\text{-Cl})_2\text{Rf}_2\text{L}_2]_0 = 0.0050 \text{ molL}^{-1}$ in THF at different temperatures.

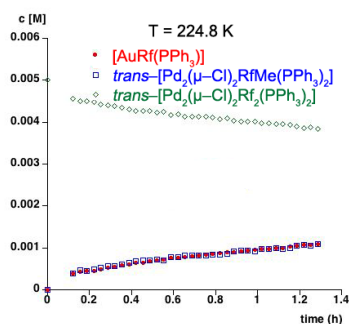
T/ K	Rate constant/ $\text{L}^2 \text{mol}^{-2} \text{s}^{-1}$
219.76	0.001520
224.80	0.003320
233.70	0.006163
238.99	0.011730
243.50	0.013620
248.10	0.044290



a)



b)



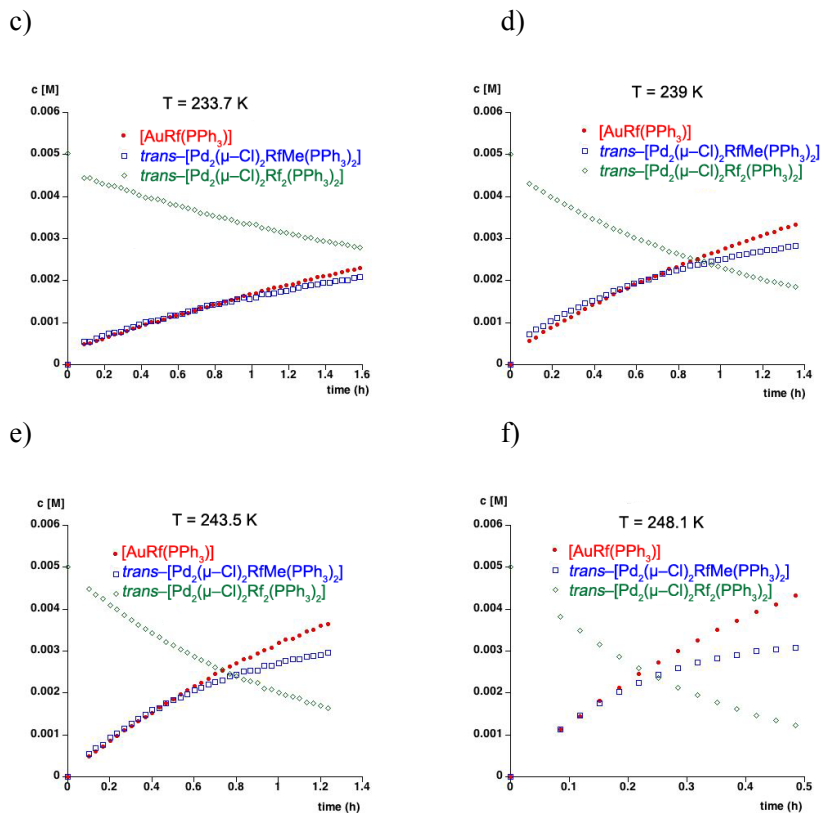


Figure IV-21. Observed concentrations as a function of time in the reaction between $[\text{AuMe}(\text{PPh}_3)]_0 = 0.020 \text{ molL}^{-1}$ and $\text{trans-}[\text{Pd}_2(\mu\text{-Cl})_2\text{Rf}_2\text{L}_2]_0 = 0.0050 \text{ molL}^{-1}$ in THF at different temperatures.

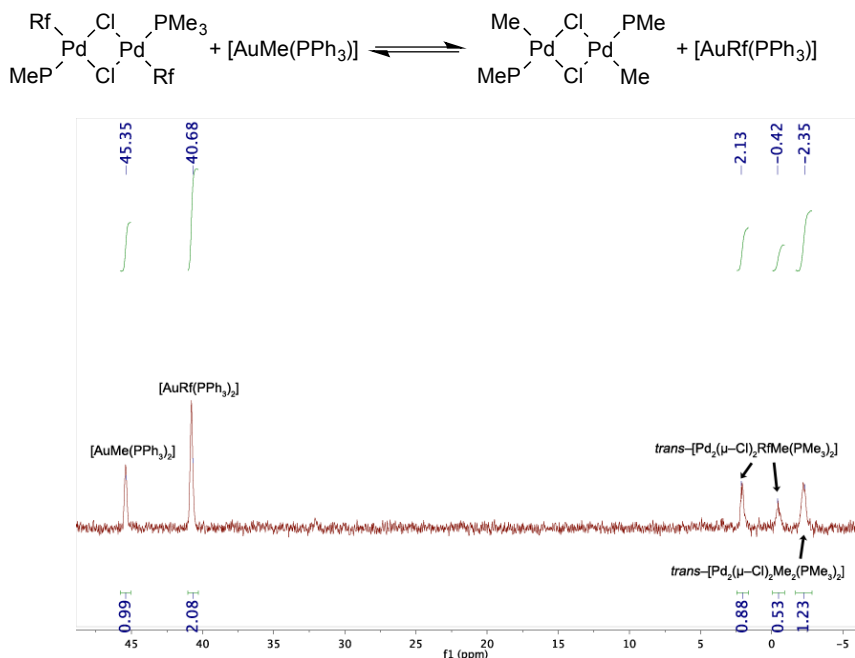
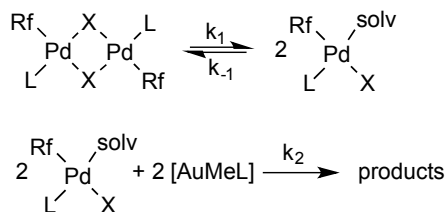


Figure IV-22. ^{31}P NMR spectra after 10 hours of the reaction between $\text{trans-}[\text{Pd}_2(\mu\text{-Cl})_2\text{Rf}_2(\text{PMe}_3)_2]_0 = 0.01\text{ M}$ and $[\text{AuMe}(\text{PPh}_3)]_0 = 0.02\text{ M}$ in THF at 258 K (it is not visible the signals of the $[\text{AuRf}(\text{PMe}_3)]$ and $\text{trans-}[\text{Pd}_2(\mu\text{-Cl})_2\text{Rf}_2(\text{PPh}_3)_2]$ because their concentrations are very low).

4.3.4 Derivation of kinetic equations in Scheme IV-9. Application of the Steady-state approximation



Scheme IV-10. Scheme for the exchange reaction between $\text{trans-}[\text{Pd}_2(\mu\text{-Cl})_2\text{Rf}_2\text{L}_2]$ and $[\text{AuMeL}]$.

The steady-state approximation was applied to lead the theoretical rate law, giving:

$$r = \frac{k_1 k_2 [\text{trans-Pd}_2\text{Rf}_2\text{Cl}_2\text{L}_2] [\text{AuMeL}]}{k_{-1} + k_2}$$

It corresponds with first order kinetics for *trans*-[Pd₂(μ-Cl)₂Rf₂L₂] and [AuMe(PPh₃)], as it was calculated experimentally.

If we consider a mechanism in which the rupture of the dimer before the reaction with the gold compound is produced:

The steady-state approximation to intermediate gives:

$$r = \frac{k_1 k_2 [\textit{trans}\text{-Pd}_2\text{Rf}_2\text{Cl}_2\text{L}_2] [\text{AuMeL}]^2}{k_{-1} + k_2 [\text{AuMeL}]^2}$$

It corresponds with a second order kinetic for [AuMeL].

4.3.5 Reactions of *trans*-[Pd₂(μ-Cl)₂Rf₂L₂] (L= PPh₃, PCy₃, PMe₃) and ZnMe₂. Kinetic Procedure

NMR tubes (5mm) are charged with palladium dimer (0.0030 mol·L⁻¹) and ZnMe₂ (0.015 mol·L⁻¹). The kinetic experiments were monitored by ¹⁹F NMR. The NMR tube was cooled to -78 °C and THF was added to a fixed volume of 600 ± 5 μL, charged with an acetone-*d*₆ capillary for NMR lock, and placed into a thermostated probe at 219 K (the temperature was calibrated by a methanol standard method). Concentration-time data are then acquired from ¹⁹F signals areas of *trans*-[Pd₂(μ-X)₂Rf₂L₂], and the products of the reaction.

-
- ¹ delPozo, J.; Gioria, E.; Casares, J. A.; Álvarez, R. and Espinet, P. *Organometallics*, **2015**, *34*, 3120–3128.
- ² Peñez–Temprano, M.; Casares, J. A.; deLera, A. R.; Alvarez, R. and Espinet, P. *Angew. Chem. Int. Ed.* **2012**, *51*, 4917–4920.
- ³ a) van Asselt, R. and Elsevier, C. J. *Organometallics*, **1994**, *13*, 1972–1980; b) Liu, Q.; Lan, Y.; Liu, J.; Li, G.; Wu, Y. D. and Lei, A. *J. Am. Chem. Soc.*, **2009**, *131*, 10201–10210; c) Fuentes, B.; García–Melchor, M.; Lledós, A.; Maseras, F.; Casares, J. A.; Ujaque, G.; Espinet, P. *Chem. Eur. J.* **2010**, *16*, 8596–8599.
- ⁴ Cordovilla, C.; Bartolomé, C.; Martínez–Ilarduya, J. M. and Espinet, P. *ACS Catal.* **2015**, *5*, 3040–3053.
- ⁵ a) Gorka Salas Doctoral Thesis. University of Valladolid, 2006; b) Juan delPozo Doctoral Thesis. University of Valladolid, 2016.
- ⁶ Usón, R.; Forniés, J.; Martínez, F. and Tomás, M. *J. Chem. Soc., Dalton Trans.*, **1980**, 888–894.
- ⁷ Fagnou, K. and Lautens, M. *Angew. Chem. Int. Ed.* **2002**, *41*, 26–47.
- ⁸ Widenhoefer, R. A. and Butchwald, S. L. *Organometallics*, **1996**, *15*, 2755–2763.
- ⁹ delPozo, J.; Carrasco, D.; Pérez–Temprano, M. H.; García–Melchor, M.; Álvarez, R.; Casares, J.A.; Espinet, P. *Angew. Chem. Int. Ed.* **2013**, *52*, 2189–2193.
- ¹⁰ Battisti, A.; Bellina, O.; Diversi, P.; Losi, S.; Marchetti, F. and Zanello, P. *Eur. J. Inorg. Chem.* **2007**, 865–875.
- ¹¹ Winston, M. S.; Wolf, W. J. and Toste, F. D. *J. Am. Chem. Soc.* **2014**, *136* (21), 7777–7782.
- ¹² Byabartta, P. *Transition Metal Chemistry*, **2007**, *32*, 716–726.
- ¹³ Lasanta, T.; López–de–Luzuriaga, J. M.; Monge, M.; Olmos, M. E. and Pascual, D. *Chem. Eur. J.* **2013**, *19*, 4754–4766.
- ¹⁴ Ladipo, F. T. and Anderson, G. K. *Organometallics*, **1994**, *13* (1), 303–306.
- ¹⁵ Stepnicka, P. and Cisarova, I. *Z. Anorg. Allg. Chem.* **2004**, *630*, 1321–1325.
- ¹⁶ Grushin, V. G.; Bensimon, C. and Alper, H. *Organometallics*, **1995**, *14*, 3259–3263.

CHAPTER V

Study of the Zn/Pd transmetalation in the Negishi cross-coupling reaction

Ray absorption spectroscopy (XAS) to study the kinetic and structural relationship between phenylzinc reagents prepared from phenyllithium reagents and zinc halides (ZnX_2 , X = Cl, Br and I),⁵ and found that the Zn-C bond distance increased upon changing the halide anion from chloride to bromide and to iodide. This was quite obviously to be expected. A higher transmetalation rate occurs with longer Zn-C bond distances, as it was also to be expected simply from the higher nucleophilicity of the Zn reagents with less electronegative halogens.

Preceding all the studies by Lei, the transmetalation step of this reaction had been studied by NMR spectroscopy in our research group. The first experimental observation was in the coupling of an alkylzinc reagent with $[\text{PdRXL}_2]$ ⁶ An unexpected observation was found in the reaction with ZnMe_2 or ZnMeCl ^a using *trans*- $[\text{PdRfCl}(\text{PPh}_3)_2]$ (Rf = 3,5-dichloro-2,4,6-trifluorophenyl), each methylating agent affording a different isomer (*cis* or *trans*) of the coupling intermediate $[\text{PdRfMe}(\text{PPh}_3)_2]$. Then, an experimental mechanistic study of the reaction between *trans*- $[\text{PdMeCl}(\text{PMePh}_2)_2]$ and ZnMeCl , afforded the first experimental determination of thermodynamic parameters of the Negishi transmetalation.⁷ In 2011 our group studied the reaction between *trans*- $[\text{PdMeCl}(\text{PMePh}_2)_2]$ and ZnMe_2 .⁸ In absence of free ligand a cationic transmetalation intermediate $[\text{PdMe}(\text{PMePh}_2)_2(\text{THF})]^+$ is formed. But in presence of excess of ligand, a stable cationic complex $[\text{PdMe}(\text{PMePh}_2)_3]^+$ is formed, which blocks the transmetalation sequestering the catalyst. Very recently, our group has also reported an experimental study onto the *cis* to *trans* isomerization reaction of $[\text{PdMeAr}(\text{PR}_3)_2]$ (Ar = C_6F_5 , $\text{C}_6\text{Cl}_2\text{F}_3$) catalyzed by ZnMe_2 , involving methyl exchange between Pd and Zn.⁹

^a All zinc species are supposed to have coordinated solvent giving a tetrahedral geometry, although we will omit the coordinated solvent in the formulas.

Should be recalled that, the most effective routes to form organozinc halides and diorganozinc compounds involve transmetalation reactions between ZnX_2 and LiR (Scheme V-3) or organomagnesium reagents. Often, the final solutions of the organotin compound are contaminated by significant amounts of LiX . The possible effect of the LiX formed during the reaction had been neglected until recent years.

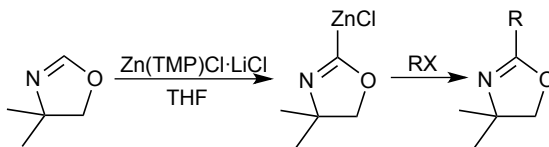


Scheme V-3. Transmetalation reactions for the obtention of organozinc compounds.

The group of Koszinowski studied the effect of $LiCl$ on solutions of $ZnRX$ ($R = Bu, Bn, Ph$) and $ZnBu_2$, investigating the formation of organozincate anions.¹⁰

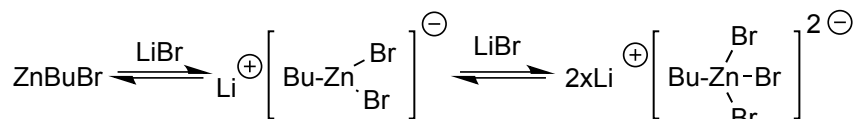
Some reputed groups have been studying the effect of the addition of Li and Mg salts to organotin halides. Firstly, Negishi and co-workers reported a better efficiency in the Pd -catalyzed cross-coupling reactions of aryl and alkenyl iodides with $ZnRX$ reagents upon addition of Li and Mg salts.¹¹

Knochel studied the Pd -catalyzed Negishi cross-coupling reaction compatible with unprotected amide or sulfonamides functions, using Zn reagents with $LiCl$ under mild conditions, for the synthesis of complex molecules and natural products.¹² In 2015, they used $Zn(TMP)Cl \cdot LiCl$ ($TMP = 2,2,6,6$ -tetramethylpiperidyl) in the metalation of 4,4-dimethyloxazoline, providing a stable oxazolinyll zincated reagent which undergoes palladium catalyzed Negishi cross-couplings allowing 2-aryloxazolines¹³ (Scheme V-4) and, in the same year they used the same organotin compound for the zincation of propynes followed by a Pd -catalyzed coupling with aryl halides providing allenes.¹⁴ The addition of $LiCl$ forms zincates that will shift the transmetalation equilibria, being the yields of the reactions higher than when were carried out in absence of Li salts.



Scheme V-4. Zincation of 4,4-dimethyloxazoline using $\text{Zn}(\text{TMP})\text{Cl}\cdot\text{LiCl}$ ($\text{R} = \text{aryl}$).

Organ *et al* have studied the addition of Li salts in the Negishi cross-coupling reaction. They first studied the addition of Li salts in the Negishi reaction, as a strategy to improve the chemical yield.¹⁵ They screened different salt additives in the alkyl-alkyl Negishi cross-coupling reaction catalyzed by NHC-Pd catalyst, finding that the addition of LiBr is the most effective in the reaction. The study reveals that a “high order”^b zincate is the active transmetalating agent (Scheme V-5).¹⁶ A possible explanation of this effect is related to the interactions between the Li salt and the ZnRX reagent. ZnRX species have a high tendency to add X anions and form zincate species, such as $[\text{ZnRX}_2]^-$ and $[\text{ZnR}_2\text{X}]^-$.

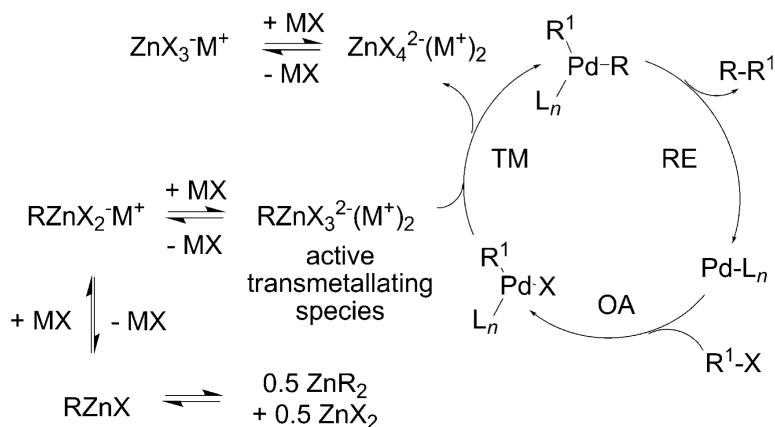


Scheme V-5. Proposed predominant organozincate species.

They identified the high order organozincate intermediate $[\text{nBuZnBr}_3]^{2-}$ involved in Negishi cross-coupling reactions, by Mass Spectrometry and NMR Spectroscopy.¹⁷ They found that highly polar solvents, such as DMI or NMP, established these zincates. They propose that it is not $[\text{ZnRX}_2]^-$ the transmetalating species; what is *necessary* to promote the transmetalation reaction is the presence of “[$\text{ZnRX}_3]^{2-}$ ” (Scheme V-6).¹⁸ It seems that the higher nucleophilicity of the zincates species accelerate the transmetalation step in the Negishi cross-coupling reaction. While the

^b The term “high order zincate” refers to a zincate $[\text{RZnX}_n]^{(n-1)-}$ ($n = 3$ or $n > 3$).

necessity of anionic species may be true for the Pd catalysts used by Organ (which imply a bulky carbene as ligand), it is out of question that using phosphines as ligands the reactions work perfectly with ZnMe_2 or ZnMeCl reagents absolutely exempt of added halides.¹⁹ Prof. Organ identified himself as one of the reviewers of this paper of our group and was suspecting of contamination in our reagents but, after interesting correspondence, accepted our conclusions that in our catalytic system there was no need of zincates for the reaction to work.



Scheme V-6. Catalytic cycle proposed for the alkyl-alkyl Negishi reaction. (R = alkyl; M = Li, Mg; X = Cl, Br) (Ref.17).

Due to the importance of the transmetalation reaction between zinc and palladium and the few studies done in this field, we decided to study mechanistically the system formed by *trans*-[PdRfCl(PPh₃)₂], with ZnMeCl and also with the zincates [ZnMeCl₂]⁻ and [ZnMeCl₃]²⁻. In order to better understand the retrometalation reaction we have studied also the reaction of *trans*- and *cis*-[PdRfMe(PPh₃)₂] with ZnCl₂.

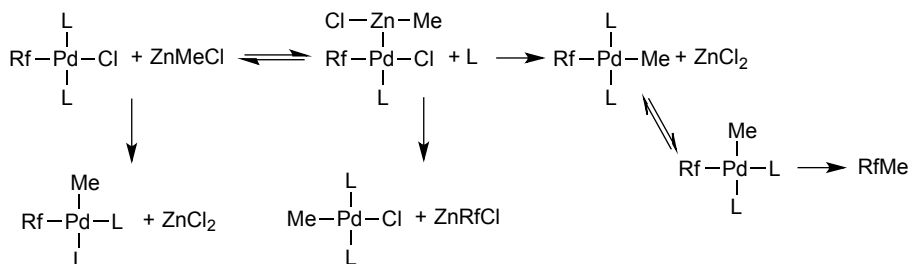
We chose these systems because the Rf-Me coupling step is slow,²⁰ and initial transmetalation isomers, *cis* and *trans*-[PdRfMe(PPh₃)₂], and other possible reaction intermediates *trans*-[PdMeCl(PPh₃)₂] and *cis*-[PdMe₂(PPh₃)₂], are easily detected in solution using ¹⁹F NMR and ³¹P NMR.

5.2 RESULTS AND DISCUSSION

5.2.1 Kinetics of transmetalation reaction between *trans*-[PdRfCl(PPh₃)₂] and ZnMeCl

In a previous work we had shown that, under a large excess of ZnMeCl that resembles catalytic conditions, the reaction between *trans*-[PdRfCl(PPh₃)₂] and ZnMeCl produces preferably *cis*-[PdRfMe(PPh₃)₂] that then it isomerizes to the *trans* isomer.⁶ The reaction also produces ZnRfCl and hypothetically *trans*-[PdMeCl(PPh₃)₂] which further reacts to produce [PdMe₂(PPh₃)₂]. The dependence of the reaction rate and the selectivity of this reaction with [PPh₃] were not studied. Now we study this dependence and the reverse reaction, namely reactions between *cis* and *trans*-[PdRfMe(PPh₃)₂] with ZnCl₂.

The kinetic experiments of the reactions between *trans*-[PdRfCl(PPh₃)₂] and ZnMeCl under different concentrations of PPh₃ (Table V-1) show that the reaction is strongly retarded by the addition of free PPh₃. The most noticeable effect is the almost complete suppression of the formation of ZnRfCl (Figure V-1) that in the presence of free PPh₃ reaches a steady state. The kinetic order on [PPh₃] on the disappearance of *trans*-[PdRfCl(PPh₃)₂] has been measured by the initial rates method, giving a value of -1.2. In addition, the reaction shows an induction period that is longer when larger is the concentration of PPh₃ (see concentration/time graphics in the experimental part). Additional information about the equilibria involved in this system can be obtained from the study of the reverse reaction.



Scheme V-7. Reaction between *trans*-[PdRfCl(PPh₃)₂] with ZnMeCl.

Table V-1. Kinetic data obtained for the transmetalation reaction between *trans*-[PdRfCl(PPh₃)₂] and ZnMeCl in THF at 298 K with different amounts of PPh₃.

[Zn]	[Pd]	[PPh ₃]	r ₀ (st. dv)/ mol L ⁻¹ s ⁻¹	k _{obs} / s ⁻¹
0.33	0.0165	0.0691	9.3007 · 10 ⁻⁰⁸	1.7081 · 10 ⁻⁰⁵
0.33	0.0165	0.0483	1.2081 · 10 ⁻⁰⁷	2.2187 · 10 ⁻⁰⁵
0.33	0.0165	0.0354	2.2016 · 10 ⁻⁰⁷	4.0433 · 10 ⁻⁰⁵
0.33	0.0165	0.0174	4.4843 · 10 ⁻⁰⁷	8.2356 · 10 ⁻⁰⁵

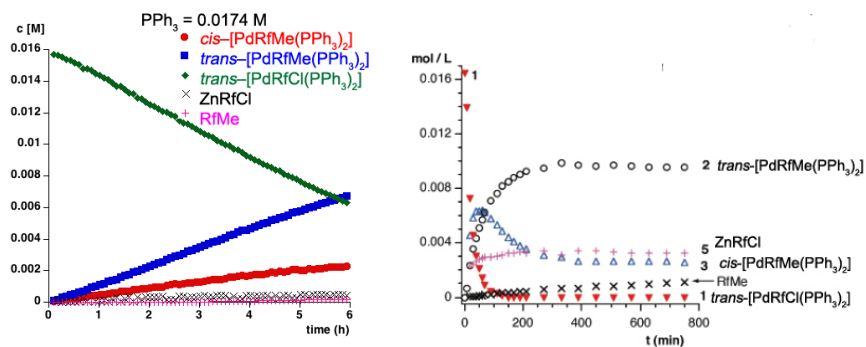


Figure V-1. ¹⁹F observed concentrations as a function of time in the reaction between [ZnMeCl]₀ = 0.33 molL⁻¹, *trans*-[PdRfCl(PPh₃)₂]₀ = 0.0165 molL⁻¹ and [PPh₃] = 0.0174 molL⁻¹ at 298 K vs. the same reaction with no [PPh₃] added (Figure taken from ref.6).

The reactions between *cis*-[PdRfMe(PPh₃)₂] or *trans*-[PdRfMe(PPh₃)₂] with ZnCl₂ have also been studied by ¹⁹F NMR

(Figure V-2), showing an exchange system in which, in addition to the known *cis/trans* isomerization equilibrium of $[\text{PdRfMe}(\text{PPh}_3)_2]$,⁶ other products are formed such as ZnRfCl (and then $[\text{PdMe}_2(\text{PPh}_3)_2]$ observed by ^{31}P RMN) and minor amounts of the product *trans*- $[\text{PdRfCl}(\text{PPh}_3)_2]$, as well as minor amounts of the reductive elimination product RfMe (Scheme V-8). The reactions are almost not retarded by the addition of free PPh_3 . The kinetic orders on $[\text{PPh}_3]$ were measured from the initial rates. For the disappearance of *cis*- $[\text{PdRfMe}(\text{PPh}_3)_2]$ and *trans*- $[\text{PdRfMe}(\text{PPh}_3)_2]$ the value is -0.2 (Figure V-2).^c

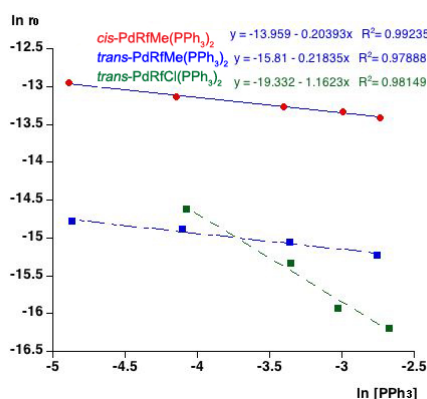
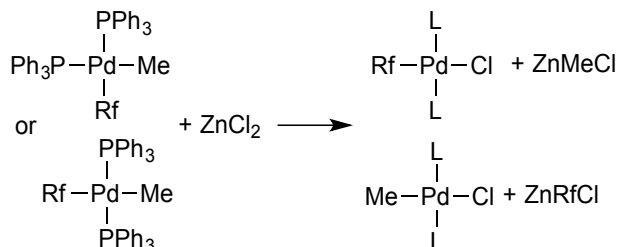


Figure V-2. Plot of $\ln[r_0]$ vs $\ln [\text{PPh}_3]$ for the disappearance of *cis*- $[\text{PdRfMe}(\text{PPh}_3)_2]$ and *trans*- $[\text{PdRfMe}(\text{PPh}_3)_2]$ in the reaction between $[\text{ZnCl}_2]_0 = 0.66 \text{ molL}^{-1}$ and $[\text{PdRfMe}(\text{PPh}_3)_2]_0 = 0.0165 \text{ molL}^{-1}$ and for the disappearance of *trans*- $[\text{PdRfCl}(\text{PPh}_3)_2]$ in the reaction between $[\text{ZnMeCl}]_0 = 0.33 \text{ molL}^{-1}$ and *trans*- $[\text{PdRfCl}(\text{PPh}_3)_2]_0 = 0.0165 \text{ molL}^{-1}$ at 298 K.

The fastest process is the formation of ZnRfCl .

^c During the reaction between *cis*- $[\text{PdRfMe}(\text{PPh}_3)_2]$ and ZnCl_2 with excess of PPh_3 , the formation of the cationic *trans*- $[\text{PdMe}(\text{PPh}_3)_3]^+$ was detected in the ^{31}P spectra at low temperature. The role of analogous cationic species inhibiting the transmetalation reaction between $[\text{PdMeXL}_2]$ and ZnMe_2 has been previously studied by our research group (reference 8).



Scheme V-8. Reaction between *cis*-[PdRfMe(PPh₃)₂] or *trans*-[PdRfMe(PPh₃)₂] with ZnCl₂.

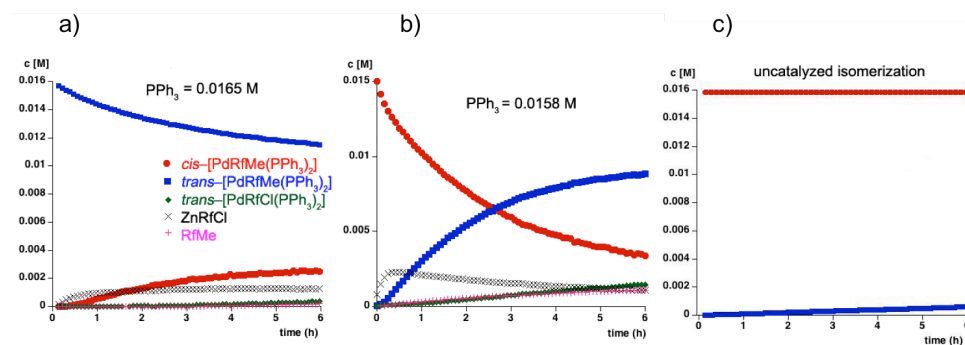
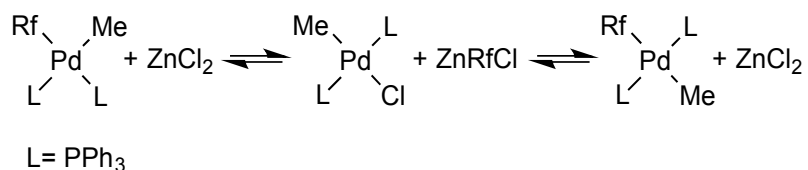


Figure V-3. ¹⁹F observed concentrations as a function of time in the reaction between a) [ZnCl₂]₀ = 0.66 mol·L⁻¹, *trans*-[PdRfMe(PPh₃)₂]₀ = 0.0165 mol·L⁻¹ and [PPh₃]₀ = 0.0165 mol·L⁻¹ at 298 K, b) *cis*-[PdRfMe(PPh₃)₂]₀ = 0.0165 mol·L⁻¹, [ZnCl₂]₀ = 0.66 mol·L⁻¹ and [PPh₃]₀ = 0.0158 mol·L⁻¹, and c) Simulated *cis*- to *trans*-[PdRfMe(PPh₃)₂] isomerization reaction with [PPh₃]₀ = 0.0165 mol·L⁻¹. Simulation was done with the rate constant values obtained from Ref.21.

The main effect of the addition of ZnCl₂ is on the *cis*/*trans* isomerization rate. Comparing the experimental graphics in Figure V-3 with the simulated isomerization without ZnCl₂ (Figure V-3c), it is clear that the isomerization from *cis*- to *trans*-[PdRfMe(PPh₃)₂] is catalyzed by ZnCl₂.

It is worth to note that, an induction period was observed for the formation of the isomerization product that is coincident with time required for the formation of the maximum amount of ZnRfMe. (See experimental part). The most likely interpretation of the induction period is that the isomerization from *cis*- to *trans*- is produced not only directly, but also

through the retrotransmetalation reaction between *cis*-[PdRfMe(PPh₃)₂] and ZnCl₂ to give *trans*-[PdMeCl(PPh₃)₂], that then reacts with ZnRfCl to give the *trans*-[PdRfMe(PPh₃)₂] isomer and ZnCl₂ (Scheme V-9).



Scheme V-9. Mechanism of *cis/trans* isomerization catalyzed by ZnCl₂ via sequential retrotransmetalation-transmetalation processes.

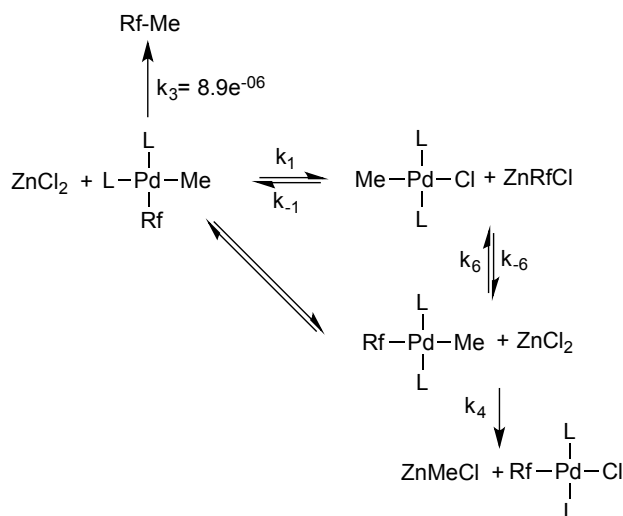
The formation rate of the retrotransmetalation products *trans*-[PdRfCl(PPh₃)₂] and ZnMeCl is slower with *trans*-[PdRfMe(PPh₃)₂] than with the *cis* isomer.

Schemes 10 and 11 are simplified models for the reactions between *trans*-[PdRfMe(PPh₃)₂] and *cis*-[PdRfMe(PPh₃)₂] with ZnCl₂. The values of the rate constants have been calculated based on them. The values of the kinetic rate constants obtained with these models agree with the experimental data (Figure V-4).^d

^d Note that the model is in fact a simplification, and other reactions, eventually dependent on the [PPh₃] are probably taking place, such as the transmetalation of *cis* or *trans*-[PdRfMe(PPh₃)₂] complexes with ZnRfCl, or ZnMeCl.

Table V-2. Calculated rate constants for the reaction between *cis*-[PdRfMe(PPh₃)₂] and ZnCl₂ under different concentrations of PPh₃. The experimental values have been least square fitted to the kinetic model shown in Scheme V-10.

[PPh ₃] added / molL ⁻¹	k ₁ / L mol ⁻¹ s ⁻¹	k ₁ ^e	k ₂ / L mol ⁻¹ s ⁻¹	k ₆ / L mol ⁻¹ s ⁻¹	k ₆
0.0647	4.24(±9)·10 ⁻⁴	2.07(±5)·10 ⁻¹	1.033(±6)·10 ⁻⁵	3.41(±4)·10 ⁻⁵	4.41(±3)·10 ⁻²
0.0502	3.3(±1)·10 ⁻⁴	2.11(±9)·10 ⁻¹	9.26(±8)·10 ⁻⁶	6.5(±4)·10 ⁻⁶	4.77(±5)·10 ⁻²
0.0332	6.7(±2)·10 ⁻⁴	6.4(±2)·10 ⁻¹	1.470(±6)·10 ⁻⁵	3.78(±4)·10 ⁻⁵	1.18(±1)·10 ⁻¹
0.0158	1.8(±3)·10 ⁻³	2.9(±5)	1.768(±7)·10 ⁻⁵	3.81(±5)·10 ⁻⁵	2.21(±2)·10 ⁻¹
0.0075	1.0(±1)·10 ⁻³	2.6(±3)	2.077(±7)·10 ⁻⁵	3.70(±7)·10 ⁻⁵	3.95(±5)·10 ⁻¹



Scheme V-11. Kinetic model used for the non-linear least squares fitting of the kinetic data of the reaction between *trans*-[PdRfMe(PPh₃)₂] and ZnCl₂. k₄ is considered irreversible because the concentration of both *trans*-[PdRfCl(PPh₃)₂] and ZnMeCl, are very low during the reaction.

^e k₋₁ and k₋₆ are pseudoconstants dependent on the concentration of PPh₃.

Table V-3. Calculated rate constants for the reaction between *trans*-[PdRfMe(PPh₃)₂] and ZnCl₂ under different concentrations of PPh₃. The experimental values have been least square fitted to the kinetic model shown in Scheme V-11. Values of k₁ were fixed with the calculated values for the *cis* isomer.

[PPh ₃] added /molL ⁻¹	k ₁ ^e	k ₄ / L mol ⁻¹ s ⁻¹	k ₆ / L mol ⁻¹ s ⁻¹	k ₆
0.0634	9.76(±2)·10 ⁻²	1.103(±9)·10 ⁻⁶	2.358(±5)·10 ⁻⁵	1.99(±1)·10 ⁻²
0.0348	3.22(±1)·10 ⁻¹	1.83(±1)·10 ⁻⁶	3.049(±9)·10 ⁻⁵	5.91(±4)·10 ⁻²
0.0165	1.66(±9)	3.03(±1)·10 ⁻⁶	3.44(±1)·10 ⁻⁵	1.36(±1)·10 ⁻¹
0.0077	2.2(±1)	4.85(±1)·10 ⁻⁶	7.05(±4)·10 ⁻⁵	6.24(±6)·10 ⁻¹

Calculated rate constants k₁, k₄ and k₆ which involve reactions with ZnCl₂, are not significantly dependent on the concentration of ligand. However k₁ and k₆, involving transmetalation reactions with organozincs, are dependent on the concentration of free ligand. Representations of ln(k₁) vs. ln[PPh₃] and ln(k₆) vs. ln[PPh₃] show a linear dependence with negative slope (between -1.0 and -1.5, see experimental part). These results agree with the experimental reaction order obtained from the initial reaction rates (see experimental part). However the data do not allow the obtention of a complete rate law.

Some conclusions can be extracted of these reactions:

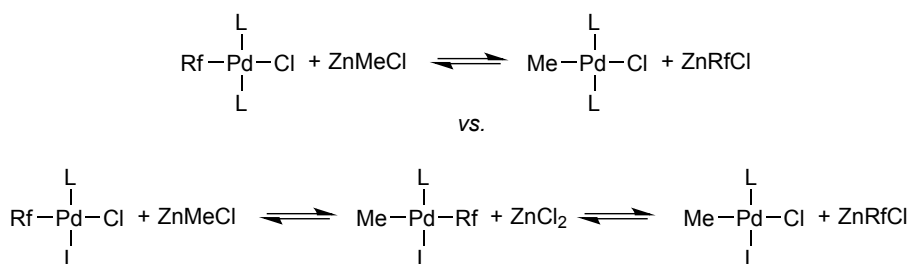
- Transmetalation equilibria are very shifted to the formation of [PdRfMe(PPh₃)₂] and ZnCl₂. The formation of the compound [PdCl₂(PPh₃)₂] was not observed even with a large excess of ZnCl₂.

- The transmetalation of the Rf group is very fast in both directions of the reaction, and the *cis* to *trans* isomerization of [PdRfMe(PPh₃)₂] is efficiently catalyzed by this species. In practice that means that no reliable information about the stereochemistry or the transmetalations can be extracted from systems in which large concentration of ZnRfCl has evolved.

- Kinetics of the transmetalation of ZnRfCl (being R = Me, Rf) with [PdRfCl(PPh₃)₂] depend on the concentration of free phosphine, but kinetics

of the transmetalation of ZnCl_2 with *cis* or *trans* $[\text{PdRfMe}(\text{PPh}_3)_2]$ do not. Note that this is not a violation of the microscopic reversibility principle because the second reaction is not the reverse of the first, since does not produce $[\text{PdRfMe}(\text{PPh}_3)_2]$ but $[\text{PdMeCl}(\text{PPh}_3)_2]$ instead.

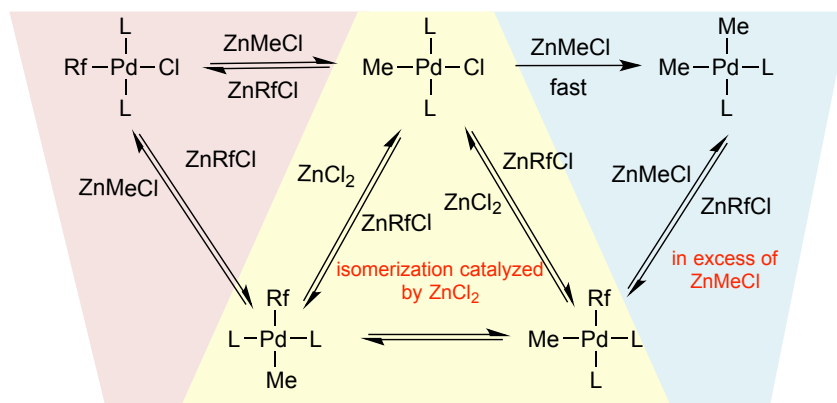
Now, it is possible to reconsider the reaction between *trans*- $[\text{PdRfCl}(\text{PPh}_3)_2]$ and ZnMeCl , and to hypothesize a mechanism. Firstly, for the fast formation of ZnRfCl , the transmetalation-retrometalation pathway is unlikely, because of the thermodynamics of the reaction. On the contrary, since the concentration of ZnRfCl grows faster than any other process, the formation of $[\text{PdMeCl}(\text{PPh}_3)_2]$ can be proposed as first step (Scheme V-12) in an analogous exchange process to that reported by Elsevier and co-workers.¹ But since the reaction is almost suppressed by addition of PPh_3 , the substitution of this ligand should take part on the mechanism.



Scheme V-12. Reaction between *trans*- $[\text{PdRfCl}(\text{PPh}_3)_2]$ and ZnMeCl vs. transmetalation-retrometalation pathway.

Under a large excess of ZnMeCl , the reaction product *trans*- $[\text{PdMeCl}(\text{PPh}_3)_2]$ suffers from fast transmetalation to give *cis*- $[\text{PdMe}_2(\text{PPh}_3)_2]$ detected by ^{31}P NMR. Finally, *cis*- $[\text{PdMe}_2(\text{PPh}_3)_2]$ reacts again with ZnRfCl to give *cis* or *trans*- $[\text{PdRfMe}(\text{PPh}_3)_2]$ (Scheme V-13). This Scheme accounts for the induction period in which ZnRfCl is formed at the beginning of the reaction, but it does not exclude the contribution of other pathways, such as the direct transmetalation or the transmetalation-retrometalation pathways. The transmetalation with ZnMeCl depends on the

concentration of PPh_3 , while the retrometalation between ZnCl_2 and $[\text{PdRfMe}(\text{PPh}_3)_2]$ does not depend on the concentration of PPh_3 . The equilibrium constants for the substitution of PPh_3 by ZnRfCl depend on the palladium reactant. Because of this, it is not possible with the available experimental data to obtain rate constants, activation energies or a simplified reaction pathway.



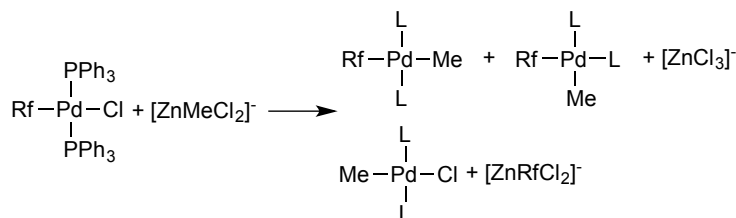
Scheme V-13. Proposed reaction mechanism for the reaction between *trans*- $[\text{PdRfCl}(\text{PPh}_3)_2]$ and ZnMeCl .

5.2.2 Kinetics of transmetalation reaction between *trans*- $[\text{PdRfCl}(\text{PPh}_3)_2]$ and $[\text{ZnMeCl}_2]^-$ or $[\text{ZnMeCl}_3]^{2-}$

The kinetics of the reactions between *trans*- $[\text{PdRfCl}(\text{PPh}_3)_2]$ and the zincates $[\text{ZnMeCl}_2]^-$ and $[\text{ZnMeCl}_3]^{2-}$ were studied.^f The profile of the reaction between *trans*- $[\text{PdRfCl}(\text{PPh}_3)_2]$ and $[\text{ZnMeCl}_2]^-$ shows the very fast formation of anion $[\text{ZnRfCl}_2]^-$.^g It is also observed the formation of transmetalation products *cis*- and *trans*- $[\text{PdRfMe}(\text{PPh}_3)_2]$ in a slower process (Figure V-5a).

^f $[\text{ZnMeCl}_2]^-$ and $[\text{ZnMeCl}_3]^{2-}$ were obtained from a solution of ZnMeCl with one or two equivalents of LiCl in THF .¹⁷

^g $[\text{ZnRfCl}_2]^-$ was identified by ^{19}F NMR being independently prepared by reaction of ZnRfCl with one equivalent of LiCl (see experimental part).



Scheme V-14. Reaction between $\text{trans}-[\text{PdRfCl}(\text{PPh}_3)_2]$ and $[\text{ZnMeCl}_2]^-$.

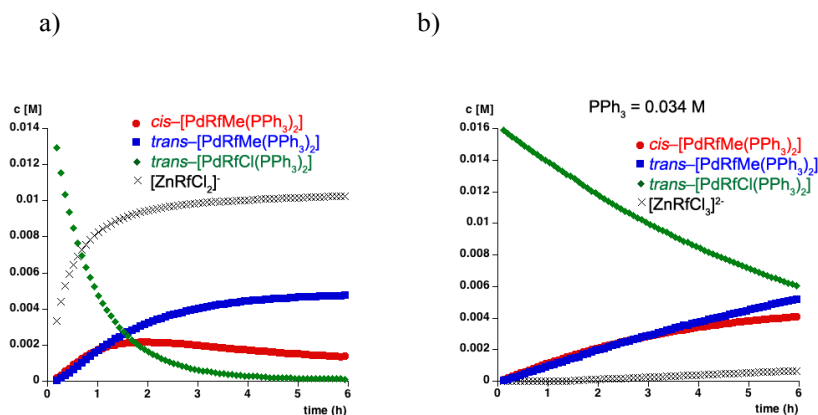
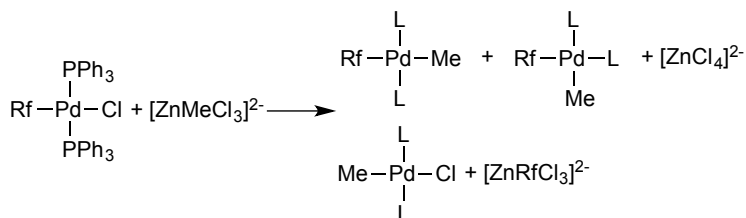


Figure V-5. ^{19}F observed concentrations as a function of time in the reaction between a) $\text{trans}-[\text{PdRfCl}(\text{PPh}_3)_2]_0 = 0.0165 \text{ mol}\cdot\text{L}^{-1}$ and $[\text{ZnMeCl}_2]_0^- = 0.33 \text{ mol}\cdot\text{L}^{-1}$ with no added ligand at 298 K, b) $\text{trans}-[\text{PdRfCl}(\text{PPh}_3)_2]_0 = 0.0165 \text{ mol}\cdot\text{L}^{-1}$ and $[\text{ZnMeCl}_3]_0^{2-} = 0.33 \text{ mol}\cdot\text{L}^{-1}$ with $[\text{PPh}_3]_0 = 0.034 \text{ mol}\cdot\text{L}^{-1}$ at 298 K.

The reaction-rate is strongly retarded by the addition of PPh_3 being the kinetic order on $[\text{PPh}_3]$ for the disappearance of $\text{trans}-[\text{PdRfCl}(\text{PPh}_3)_2]$ -0.9. The retardation affects particularly to the formation of $[\text{ZnRfCl}_2]^-$, which is almost completely suppressed.

For the reaction between $\text{trans}-[\text{PdRfCl}(\text{PPh}_3)_2]$ and $[\text{ZnMeCl}_3]^{2-}$ the same products that in the reaction with $[\text{ZnMeCl}_2]^-$ were obtained but, $[\text{ZnRfCl}_3]^{2-}$ (that was also identified by ^{19}F NMR) instead of $[\text{ZnRfCl}_2]^-$ was formed (Figure V-5 b). The reaction is also retarded by the addition of $[\text{PPh}_3]$, and the kinetic order on $[\text{PPh}_3]$ for the disappearance of $\text{trans}-[\text{PdRfCl}(\text{PPh}_3)_2]$ is also -0.9.



Scheme V-15. Reaction between *trans*-[PdRfCl(PPh₃)₂] with [ZnMeCl₃]²⁻.

In order to compare the reactions between *trans*-[PdRfCl(PPh₃)₂] with ZnMeCl, [ZnMeCl₂]⁻ and [ZnMeCl₃]²⁻, values of *k*_{obs} with different amounts of PPh₃ were measured (Tables V-1, V-4 and V-5).

Table V-4. Kinetic data obtained for the transmetalation reaction between *trans*-[PdRfCl(PPh₃)₂] and [ZnMeCl₂]⁻ in THF at 298 K with different amounts of PPh₃.

[Zn]	[Pd]	[PPh ₃]	<i>r</i> ₀ / mol L ⁻¹ s ⁻¹	<i>k</i> _{obs} / s ⁻¹
0.33	0.0165	0.0790	1.4265 · 10 ⁻⁰⁷	2.6198 · 10 ⁻⁰⁵
0.33	0.0165	0.0310	4.5119 · 10 ⁻⁰⁷	8.2863 · 10 ⁻⁰⁵
0.33	0.0165	0.0163	6.4866 · 10 ⁻⁰⁷	1.1913 · 10 ⁻⁰⁴
0.33	0.0165	0.0078	1.4075 · 10 ⁻⁰⁶	2.5849 · 10 ⁻⁰⁴

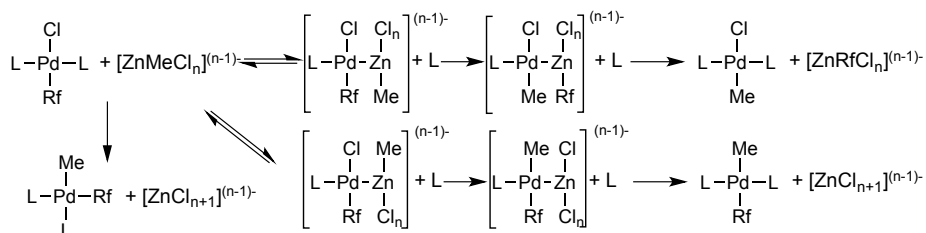
Table V-5. Kinetic data obtained for the transmetalation reaction between *trans*-[PdRfCl(PPh₃)₂] and [ZnMeCl₃]²⁻ in THF at 298 K with different amounts of PPh₃.

[Zn]	[Pd]	[PPh ₃]	<i>r</i> ₀ / mol L ⁻¹ s ⁻¹	<i>k</i> _{obs} / s ⁻¹
0.33	0.0165	0.0643	3.1325 · 10 ⁻⁰⁷	5.7529 · 10 ⁻⁰⁵
0.33	0.0165	0.0337	6.2413 · 10 ⁻⁰⁷	1.1462 · 10 ⁻⁰⁴
0.33	0.0165	0.0161	1.4471 · 10 ⁻⁰⁶	2.6577 · 10 ⁻⁰⁴
0.33	0.0165	0.0091	1.7978 · 10 ⁻⁰⁶	3.3017 · 10 ⁻⁰⁴

The values of Tables V-1, 4 and 5 show that for similar concentrations of PPh_3 , the reactions with the zincates are faster than the reaction with ZnMeCl . This is because of the higher nucleophilicity of the zincates than ZnMeCl .

In the transmetalation reactions between *trans*- $[\text{PdRfCl}(\text{PPh}_3)_2]$ with $[\text{ZnMeCl}_n]^{(n-1)-}$, the behavior of ZnMeCl , $[\text{ZnMeCl}_2]^-$ and $[\text{ZnMeCl}_3]^{2-}$ is quite similar. The formation of *trans*- $[\text{PdRfMe}(\text{PPh}_3)_2]$ and $[\text{ZnRfCl}_n]^{(n-1)-}$ depend on the concentration of $[\text{PPh}_3]$ but the formation of *cis*- $[\text{PdRfMe}(\text{PPh}_3)_2]$ does not depend on the concentration of free ligand.

A kinetic model for the reaction between *trans*- $[\text{PdRfCl}(\text{PPh}_3)_2]$ with $[\text{ZnMeCl}_n]^{(n-1)-}$ was proposed in the Scheme V-16.



Scheme V-16. Kinetic model used for the non-linear least squares fitting of the kinetic data of the reaction between *trans*- $[\text{PdRfCl}(\text{PPh}_3)_2]$ and $[\text{ZnMeCl}_n]^{(n-1)-}$.

- For the same concentration of PPh_3 , the reactions with the zincates are one magnitude order faster than the reaction with ZnMeCl as can be deduced from the values of k_{obs} . Also, it is important to note that the reaction with the zincate $[\text{ZnRfCl}_3]^{2-}$ is faster than the reaction with $[\text{ZnRfCl}_2]^-$. This is something expected because of the higher nucleophilicity of $[\text{ZnRfCl}_3]^{2-}$ vs. $[\text{ZnRfCl}_2]^-$. The same holds for the selectivity with respect to the reaction with ZnMeCl .

- The mechanisms for the reactions between *trans*- $[\text{PdRfCl}(\text{PPh}_3)_2]$ with ZnMeCl , $[\text{ZnMeCl}_2]^-$ and $[\text{ZnMeCl}_3]^{2-}$ are similar.

5.3 EXPERIMENTAL SECTION

General methods are the same as described in Chapter I. The compounds *cis*-[PdRfMe(PPh₃)₂],⁶ *trans*-[PdRfMe(PPh₃)₂]⁶ and *trans*-[PdRfCl(PPh₃)₂]²⁰ were prepared as reported in the literature.

5.3.1 Synthesis in solution of the complexes

ZnMeCl A solution of ZnMeCl (14.4 mL, 1.4 mol·L⁻¹) was prepared by comproportion of a solution of ZnCl₂ (9.4 mL, 1.1 mol·L⁻¹) in THF with a solution of ZnMe₂ (5.0 mL, 2.0 mol·L⁻¹) in toluene, under argon. ¹H NMR (THF, acetone-*d*₆ capillary, 298 K): δ -0.65 ppm (s, 3H).

Li[ZnMeCl₂] A solution of [ZnMeCl₂]⁻ (4.9 mL, 0.4 mol·L⁻¹) was prepared by reaction of a solution of ZnMeCl (1.3 mL, 1.4 mol·L⁻¹) in THF with a prepared solution of dry LiCl (3.6 mL, 0.5 mol·L⁻¹) in THF, under argon. ¹H NMR (THF, acetone-*d*₆ capillary, 298 K): δ -0.78 ppm (s, 3H).

Li₂[ZnMeCl₃] A solution of [ZnMeCl₃]²⁻ (11.5 mL, 0.4 mol·L⁻¹) was prepared by reaction of a solution of ZnMeCl (4.0 mL, 1.3 mol·L⁻¹) in THF with a prepared solution of dry LiCl (7.5 mL, 1.3 mol·L⁻¹) in THF, under argon. ¹H NMR (THF, acetone-*d*₆ capillary, 298 K): δ -0.83 ppm (s, 3H).

ZnRfCl A two-necked flask was charged with 1.1 g of C₆Cl₃F₃ (5.0 mmol) and 40 mL of Et₂O. The mixture was cooled to 195 K and 2.2 mL (5.5 mmol) of a 2.5 M solution of LiBu in hexanes were added dropwise. The solution was stirred 3h, then 5 mmol of a solution of ZnCl₂ (5.0 mL, 1 mol·L⁻¹) were added. After 12 hours at 195 K, the solution was evaporated until dryness. The solution of ZnRfCl (10.0 mL, 0.5 mol·L⁻¹) was obtained by the addition of 10 mL of THF. ¹⁹F NMR (THF, acetone-*d*₆ capillary, 298 K): δ -91.43 ppm (s, 2F), -119.74 ppm (s, 1F).

$[\text{ZnRfCl}_2]^-$ was prepared by reaction of ZnRfCl with one equivalent of a prepared solution of dry LiCl , in THF. ^{19}F NMR (THF, acetone- d_6 capillary, 298 K): δ -91.39 ppm (s, 2F), -119.43 ppm (s, 1F).

5.3.2 Kinetic experiments. Typical procedure.

In a standard experiment a NMR tube cooled to 193 K was charged with the palladium compound (9.9×10^{-3} mmol), zinc compound (0.20 mmol), and THF until a volume of 0.60 mL. When the mixture was dissolved in the THF, a coaxial capillary containing acetone- d_6 was added and the sample was placed into the NMR probe thermostated at 298 K. The evolution of the reaction was monitored by ^{19}F NMR spectroscopy. Concentration-time data were obtained by integration of the ^{19}F NMR signals.

5.3.2.1 Order on PPh_3 in the reaction between *trans*- $[\text{PdRfCl}(\text{PPh}_3)_2]$ and ZnClMe

Table V-6. Starting conditions for the transmetalation reaction between *trans*- $[\text{PdRfCl}(\text{PPh}_3)_2]$ and ZnMeCl in THF at 298 K.

$[\text{PPh}_3]_{\text{added}} / \text{molL}^{-1}$	Initial rate (r_0) / $\text{mol L}^{-1} \text{s}^{-1}$
0.0691	$9.3007 \cdot 10^{-08}$
0.0483	$1.2081 \cdot 10^{-07}$
0.0354	$2.2016 \cdot 10^{-07}$
0.0174	$4.4843 \cdot 10^{-07}$
$[\text{ZnMeCl}]_0 = 0.33 \text{ molL}^{-1}$	
<i>trans</i> - $[\text{PdRfCl}(\text{PPh}_3)_2]_0 = 0.0165 \text{ molL}^{-1}$	

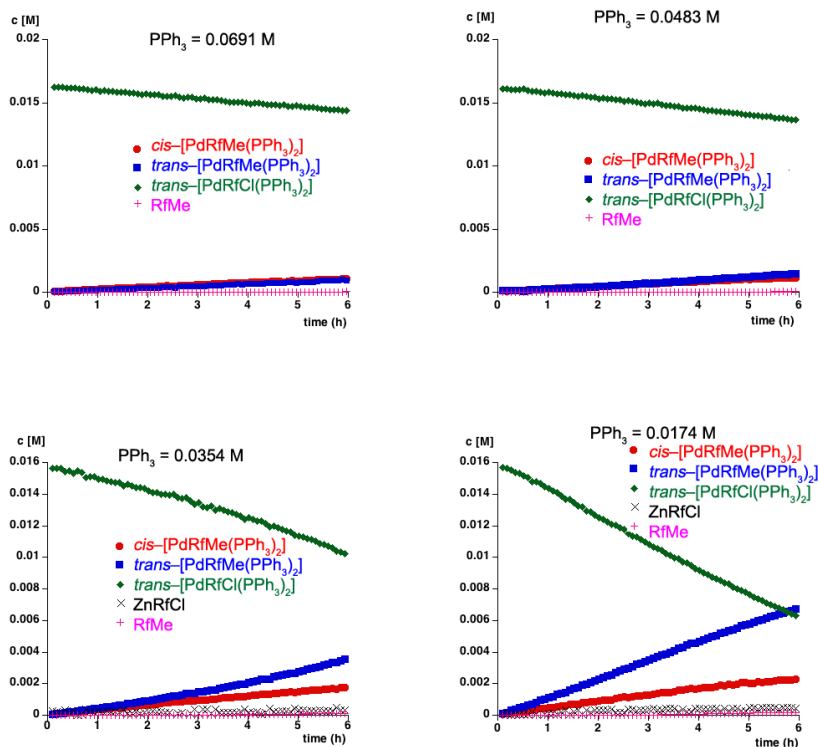
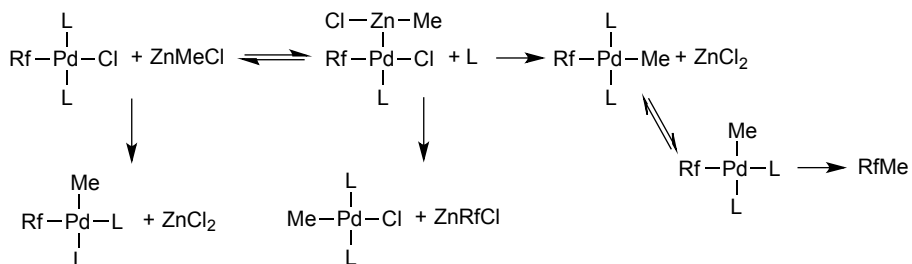


Figure V-6. Observed concentrations as a function of time. $[\text{ZnMeCl}]_0 = 0.33 \text{ molL}^{-1}$, $\text{trans-}[\text{PdRfCl}(\text{PPh}_3)_2]_0 = 0.0165 \text{ molL}^{-1}$ at 298 K.

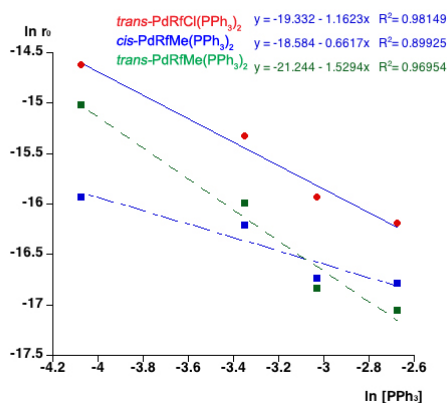


Figure V-7. Plot of $\ln[r_0]$ vs $\ln [PPh_3]$ for the formation of $trans\text{-[PdRfMe(PPh}_3)_2]$ and $cis\text{-[PdRfMe(PPh}_3)_2]$ and the disappearance of $trans\text{-[PdRfCl(PPh}_3)_2]$, in the reaction between $[ZnMeCl]_0 = 0.33 \text{ molL}^{-1}$ and $trans\text{-[PdRfCl(PPh}_3)_2]_0 = 0.0165 \text{ molL}^{-1}$ at 298 K.

5.3.2.2 Order on PPh_3 in the reaction between $cis\text{-[PdRfMe(PPh}_3)_2]$ and $ZnCl_2$.

Table V-7. Starting conditions for the kinetics of the reaction between $cis\text{-[PdRfMe(PPh}_3)_2]$ and $ZnCl_2$ in THF at 298 K and rates obtained.

$[PPh_3]_{\text{added}} / \text{molL}^{-1}$	Initial rate (r_0) / $\text{mol L}^{-1} \text{ s}^{-1}$
0.0647	$1.5050 \cdot 10^{-06}$
0.0502	$1.6275 \cdot 10^{-06}$
0.0332	$1.7223 \cdot 10^{-06}$
0.0158	$1.9818 \cdot 10^{-06}$
0.0075	$2.3783 \cdot 10^{-06}$
$[ZnCl_2]_0 = 0.66 \text{ m}$	
$cis\text{-[PdRfMe(PPh}_3)_2]_0 = 0.0165 \text{ molL}^{-1}$	

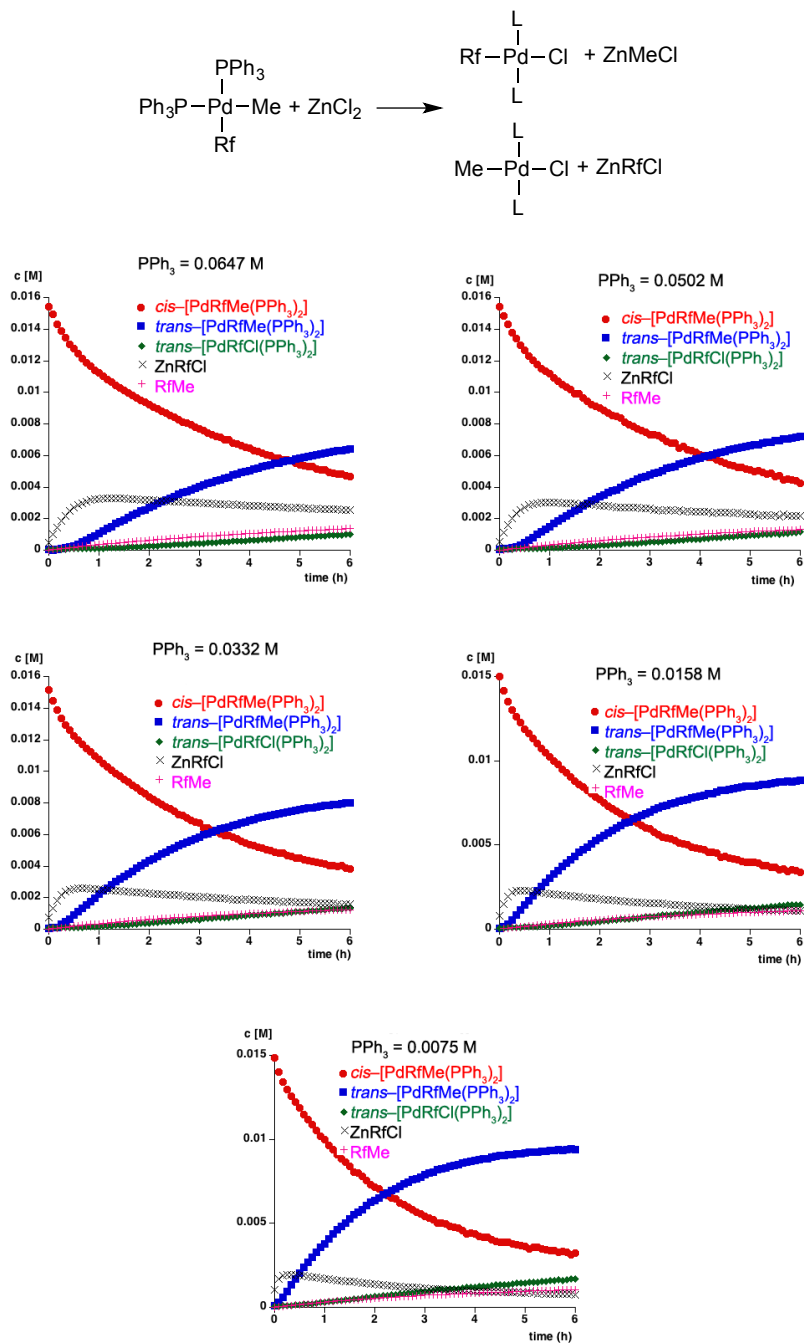


Figure V-8. ^{19}F Observed concentrations as a function of time. $[\text{ZnCl}_2]_0 = 0.66 \text{ molL}^{-1}$, $\text{cis-}[\text{PdRfMe}(\text{PPh}_3)_2]_0 = 0.0165 \text{ molL}^{-1}$ at 298 K.

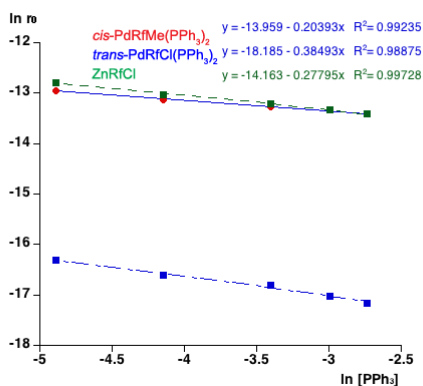


Figure V-9. Plot of $\ln[r_0]$ vs $\ln [\text{PPh}_3]$ for the formation of ZnRfCl and $\text{trans-}[\text{PdRfCl}(\text{PPh}_3)_2]$ and the disappearance of $\text{cis-}[\text{PdRfMe}(\text{PPh}_3)_2]$, in the reaction between $[\text{ZnCl}_2]_0 = 0.66 \text{ molL}^{-1}$ and $\text{cis-}[\text{PdRfMe}(\text{PPh}_3)_2]_0 = 0.0165 \text{ molL}^{-1}$ at 298 K.

5.3.2.3 Order on PPh_3 in the reaction between $\text{trans-}[\text{PdRfMe}(\text{PPh}_3)_2]$ and ZnCl_2 .

Table V-8. Starting conditions for the kinetics of the reaction between $\text{trans-}[\text{PdRfMe}(\text{PPh}_3)_2]$ and ZnCl_2 in THF at 298 K and rates obtained.

$[\text{PPh}_3]_{\text{added}} / \text{molL}^{-1}$	Initial rate (r_0) / $\text{mol L}^{-1} \text{ s}^{-1}$
0.0634	$2.4276 \cdot 10^{-07}$
0.0348	$2.8797 \cdot 10^{-07}$
0.0165	$3.4468 \cdot 10^{-07}$
0.0077	$3.8419 \cdot 10^{-07}$
$[\text{ZnCl}_2]_0 = 0.66 \text{ molL}^{-1}$	
$\text{trans-}[\text{PdRfMe}(\text{PPh}_3)_2]_0 = 0.0165 \text{ molL}^{-1}$	

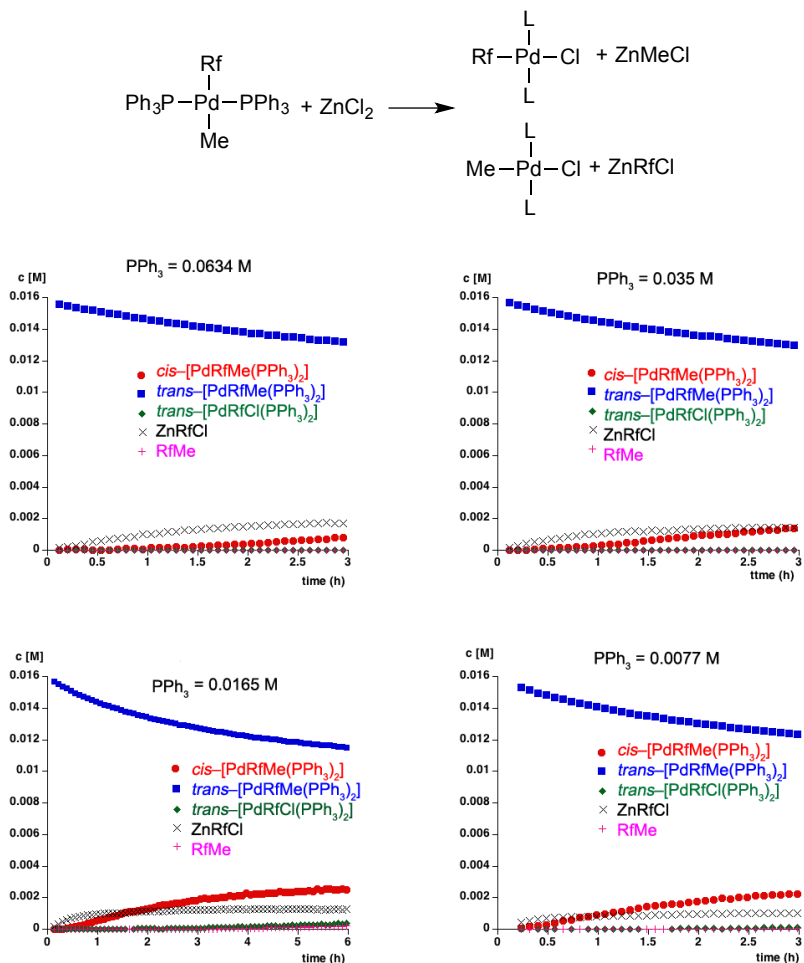


Figure V-10. Observed concentrations as a function of time. $[\text{ZnCl}_2]_0 = 0.66 \text{ molL}^{-1}$, $\text{trans-}[\text{PdRfMe}(\text{PPh}_3)_2]_0 = 0.0165 \text{ molL}^{-1}$ at 298 K.

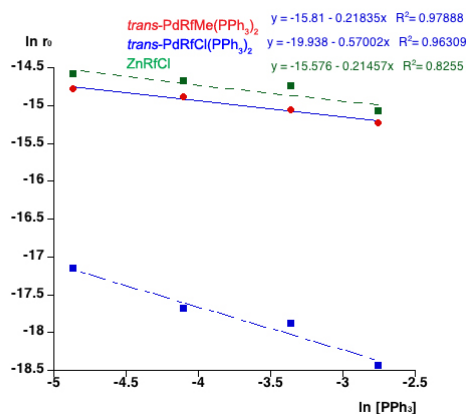


Figure V-11. Plot of $\ln[r_0]$ vs $\ln[\text{PPh}_3]$ for the formation of ZnRfCl and $\text{trans-}[\text{PdRfCl}(\text{PPh}_3)_2]$ and the disappearance of $\text{trans-}[\text{PdRfMe}(\text{PPh}_3)_2]$, in the

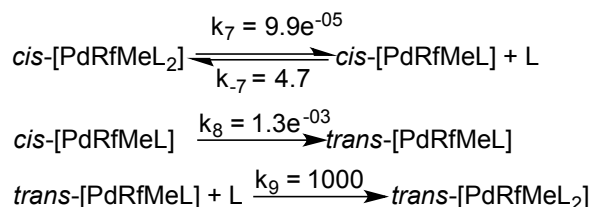
reaction between $[\text{ZnCl}_2]_0 = 0.66 \text{ molL}^{-1}$ and $\text{trans-}[\text{PdRfMe}(\text{PPh}_3)_2]_0 = 0.0165 \text{ molL}^{-1}$ at 298 K.

5.3.2.4 Kinetic model for the reactions between *cis* and *trans*- $[\text{PdRfMe}(\text{PPh}_3)_2]$ with ZnCl_2 .

For the non-linear least square fitting, rate constant for the reductive elimination reaction was fixed to the known value.⁶

In the following proposed mechanisms, the isomerization reaction from *cis*- $[\text{PdRfMe}(\text{PPh}_3)_2]$ to *trans*- $[\text{PdRfMe}(\text{PPh}_3)_2]$ is considered as dependent on the concentration of free ligand and, the reaction of the formation of ZnRfCl is considered as equilibria.

Rate constant values for the isomerization reaction were fixed to the known values from a previous work of our research group.



Scheme V-17. Isomerization reaction of *cis* to *trans*- $[\text{PdRfMe}(\text{PPh}_3)_2]$ in presence of free ligand.

From the calculated values of k_{-1} and k_{-6} shown in Table V-2, by the proposed kinetic models, can be deduced that the reactions that depend on the concentration of $[\text{PPh}_3]$ are the formation of *cis* or *trans*- $[\text{PdRfMe}(\text{PPh}_3)_2]$ and ZnCl_2 from *trans*- $[\text{PdMeCl}(\text{PPh}_3)_2]$ and ZnRfCl , but the reversal reactions are not dependent on the concentration of free phosphine.

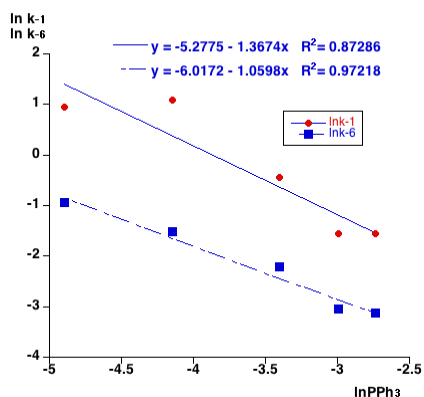


Figure V-12. Plot of the $\ln [\text{PPh}_3]$ vs. $\ln [k_{-1}$ and $k_{-6}]$ from the Table V-2 in the reaction from the *cis* isomer. Can be deduced that k_{-1} and k_{-6} for the proposed kinetic model are dependent on the concentration of free phosphine.

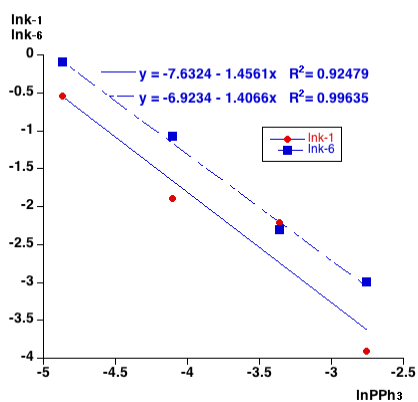


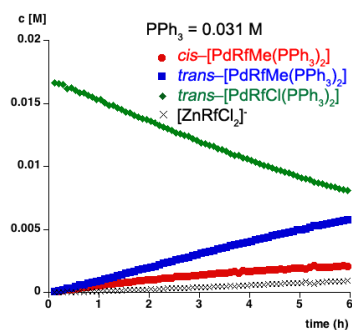
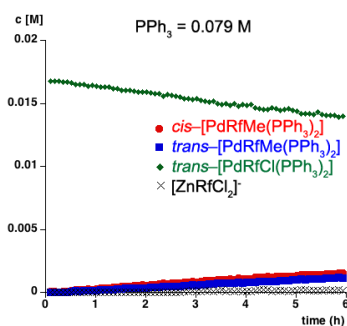
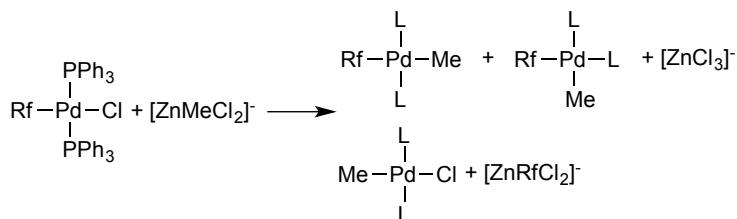
Figure V-13. Plot of the $\ln [\text{PPh}_3]$ vs. $\ln [k_{-1}$ and $k_{-6}]$ from the table 2 in the reaction from the *trans* isomer. Can be deduced that k_{-1} and k_{-6} for the proposed kinetic model are dependent on the concentration of free phosphine.

5.3.2.5 Order on PPh₃ in the reaction between *trans*-[PdRfCl(PPh₃)₂] and [ZnMeCl₂]⁻ varying the amounts of PPh₃.

Table V-9. Starting conditions for the transmetalation reaction between *trans*-[PdRfCl(PPh₃)₂] and [ZnMeCl₂]⁻ in THF at 298 K.

[PPh ₃] _{added} / molL ⁻¹	Initial rate (r ₀) / mol L ⁻¹ s ⁻¹
0.0790	1.4265 · 10 ⁻⁰⁷
0.0310	4.5119 · 10 ⁻⁰⁷
0.0163	6.4866 · 10 ⁻⁰⁷
0.0078	1.4075 · 10 ⁻⁰⁷

[ZnMeCl₂]₀⁻ = 0.33 molL⁻¹
trans-[PdRfCl(PPh₃)₂]₀ = 0.0165 molL⁻¹



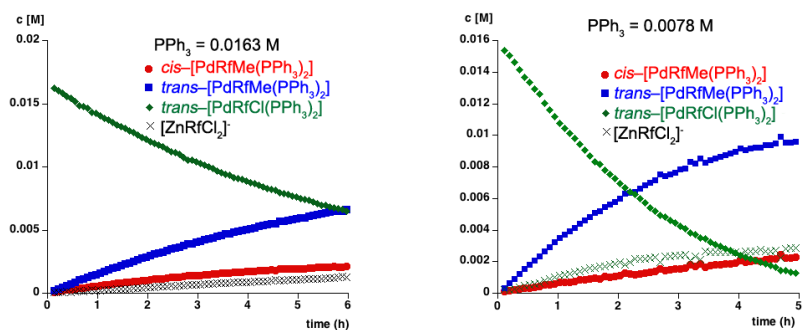


Figure V-14. Observed concentrations as a function of time. $[\text{ZnMeCl}_2]_0^- = 0.33 \text{ molL}^{-1}$, $\text{trans-}[\text{PdRfCl}(\text{PPh}_3)_2]_0 = 0.0165 \text{ molL}^{-1}$ at 298 K.

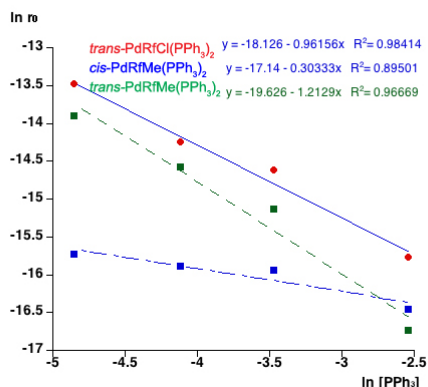


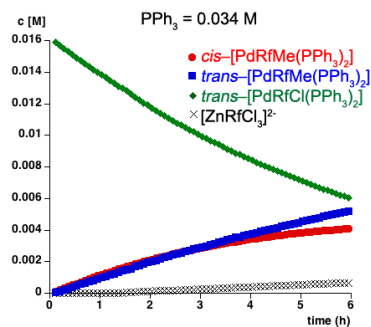
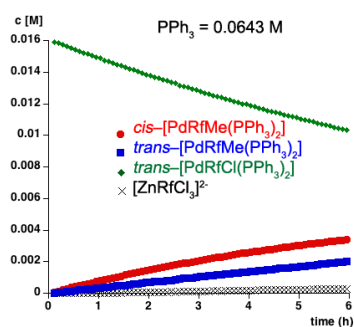
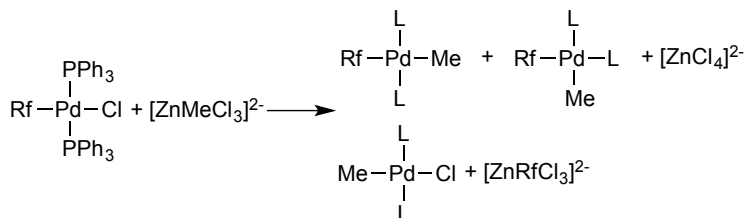
Figure V-15. Plot of $\ln[r_0]$ vs $\ln [\text{PPh}_3]$ for the formation of $\text{trans-}[\text{PdRfMe}(\text{PPh}_3)_2]$ and $[\text{ZnRfCl}_2]^-$ and the disappearance of $\text{trans-}[\text{PdRfCl}(\text{PPh}_3)_2]$, in the reaction between $[\text{ZnMeCl}_2]_0^- = 0.33 \text{ molL}^{-1}$ and $\text{trans-}[\text{PdRfCl}(\text{PPh}_3)_2]_0 = 0.0165 \text{ molL}^{-1}$ at 298 K.

5.3.2.6 Order on PPh₃ in the reaction between *trans*-[PdRfCl(PPh₃)₂] and [ZnMeCl₃]²⁻

Table V-10. Starting conditions for the transmetalation reaction between *trans*-[PdRfCl(PPh₃)₂] and [ZnMeCl₃]²⁻ in THF at 298 K.

[PPh ₃] _{added} / molL ⁻¹	Initial rate (r ₀) / mol L ⁻¹ s ⁻¹
0.0643	3.1325 · 10 ⁻⁰⁷
0.0337	6.2413 · 10 ⁻⁰⁷
0.0161	1.4471 · 10 ⁻⁰⁶
0.0091	1.7978 · 10 ⁻⁰⁶

[ZnMeCl₃]₀²⁻ = 0.33 molL⁻¹
trans-[PdRfCl(PPh₃)₂]₀ = 0.0165 molL⁻¹



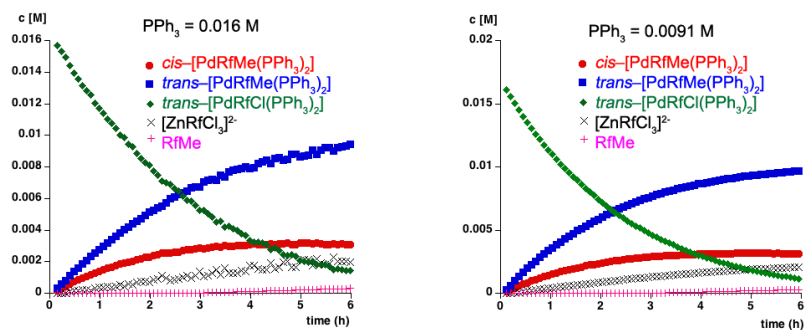


Figure V-16. Observed concentrations as a function of time. $[\text{ZnMeCl}_3]_0^{2-} = 0.33 \text{ molL}^{-1}$, $\text{trans-}[\text{PdRfCl}(\text{PPh}_3)_2]_0 = 0.0165 \text{ molL}^{-1}$ at 298 K.

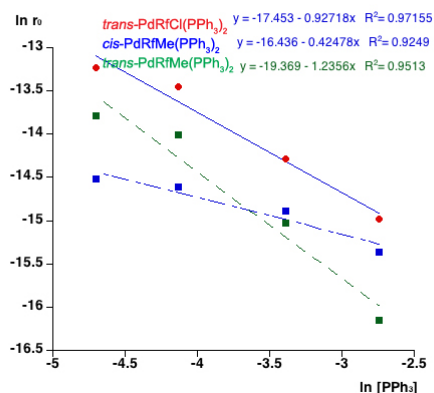


Figure V-17. Plot of $\ln[r_0]$ vs $\ln [\text{PPh}_3]$ for the formation of $\text{trans-}[\text{PdRfMe}(\text{PPh}_3)_2]$ and $[\text{ZnMeCl}_3]_0^{2-}$ and the disappearance of $\text{trans-}[\text{PdRfCl}(\text{PPh}_3)_2]$, in the reaction between $[\text{ZnMeCl}_3]_0^{2-} = 0.33 \text{ molL}^{-1}$ and $\text{trans-}[\text{PdRfCl}(\text{PPh}_3)_2]_0 = 0.0165 \text{ molL}^{-1}$ at 298 K.

- ¹ van Asselt, R. and Elsevier, C. J. *Organometallics*, **1994**, *13*, 1972–1980.
- ² Liu, Q.; Lan, Y.; Liu, J.; Li, G.; Wu, Y. D. and Lei, A. *J. Am. Chem. Soc.*, **2009**, *131*, 10201–10210.
- ³ Gioria, E.; Martínez-Ilarduya, J. M. and Espinet, P. *Organometallics* **2014**, *33*, 4394–4400.
- ⁴ a) Jin, L.; Zhang, H.; Li, P.; Sowa J. R. and Lei, A. *J. Am. Chem. Soc.*, **2009**, *131*, 9892–9893; b) Jin, L.; Xin, J.; Huang, Z.; He, J. and Lei, A. *J. Am. Chem. Soc.*, **2010**, *132*, 9607–9609; c) Xin, J.; Zhang, G.; Deng, Y.; Zhang, H. and Lei, A. *Dalton Trans.* **2015**, *44*, 19777–19781.
- ⁵ Li, J.; Jin, L.; Liu, C. and Lei, A. *Org. Chem. Front.*, **2014**, *1*, 50–53.
- ⁶ Casares, J. A.; Espinet, P.; Fuentes, B. and Salas, G. *J. Am. Chem. Soc.* **2007**, *129*, 3508–3509.
- ⁷ Fuentes, B.; García-Melchor, M.; Lledos, A.; Maseras, F.; Casares, J. A.; Ujaque, G.; and Espinet, P. *Chem. Eur. J.* **2010**, *16*, 8596–8599.
- ⁸ García-Melchor, M.; Fuentes, B.; Lledos, A.; Casares, J. A.; Ujaque, G. and Espinet, P. *J. Am. Chem. Soc.* **2011**, *133*, 13519–13526.
- ⁹ delPozo, J.; Gioria, E.; Casares, J. A.; Álvarez, R. and Espinet, P. *Organometallics*, **2015**, *34*, 3120–3128.
- ¹⁰ Fleckenstein, J. E. and Koszinowski, K. *Organometallics*, **2011**, *30*, 5018–5026.
- ¹¹ Huang, Z.; Qian, M.; Babinski, D. J. and Negishi, E. *Organometallics* **2005**, *24*, 475–478.
- ¹² Manolikakes, G.; Dong, Z.; Mayr, H.; Li, J. and Knochel, P. *Chem. Eur. J.* **2009**, *15*, 1324–1328.
- ¹³ Hass, D.; Hofmayer, M. S.; Bresser, T. and Knochel, P. *Chem. Commun.* **2015**, *51*, 6415–6417.
- ¹⁴ Quinio, P.; Francois, C.; Escribano-Cuesta, A.; Steib, A.K.; Achraimer, F.; Zipse, H.; Karaghiosoff, K. and Knochel, P. *Org. Lett.* **2015**, *17*, 1010–1013.
- ¹⁵ Avola, S.; Dubovyk, I.; Hadei, N.; Kantchev, E. A. B.; O'Brien, C. J. Valente, C.; and Organ, M. G. *Chem. Eur. J.* **2006**, *12*, 4749–4755.
- ¹⁶ Achonduh, G. T.; Hadei, N.; Valente, C.; Avola, S.; O'Brien, C. J. and Organ, M. G. *Chem. Commun.* **2010**, *46*, 4109–4111.
- ¹⁷ Hunter, H. N.; Hadei, N.; Blagojevic, V.; Patschinski, P.; Achonduh, G. T.; Avola, S.; Bohme, D. K. and Organ, M. G. *Chem. Eur. J.* **2011**, *17*, 7845–7851.

- ¹⁸ McCann, L. C. and Organ, M. G. *Angew. Chem. Int. Ed.* **2014**, *53*, 4386–4389.
- ¹⁹ Gioria, E.; Martínez-Ilarduya, J. M.; García-Cuadrado, D.; Miguel, J. A.; Genov, M. and Espinet, P. *Organometallics*, **2013**, *32* (15), 4255–4261.
- ²⁰ Casado, A. L. and Espinet, P. *Organometallics*, **1998**, *17*, 954–959.
- ²¹ delPozo, J.; Gioria, E.; Casares, J. A.; Álvarez, R. and Espinet, P. *Organometallics*, **2015**, *34*, 3120–3128.

CHAPTER VI

**Development of new ligands for the
amination of aryl halides with ammonia**

6.1 INTRODUCTION

Ammonia is among the largest volume of production and least expensive bulk chemicals. Although it is a common nitrogen source in chemical synthesis, it is rarely used as a reagent in catalytic processes. Primary arylamines are important intermediates in agrochemicals, pharmaceuticals, etc. so to form primary aromatic amines from aryl halides is a synthetically valuable catalytic transformation of ammonia.

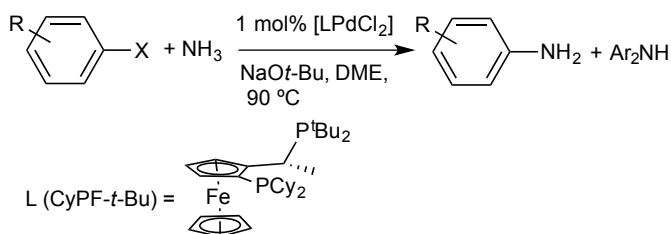
However, there are some problems that make the Pd-catalyzed amination reactions with ammonia challenging:

- The ancillary ligands can be displaced by ammonia to form an unreactive catalytic complex,
- Reductive elimination from an Ar-Pd-NH₂ complex has never been observed, because complexes with amido groups adopt stable bridging structures and,
- After the reductive elimination, an arylamine would be formed and this product would be more reactive than ammonia for further reactions.

Coupling with ammonia is also difficult because of the strong σ -donor character of the ammonia that leads to the formation of strong bonds to metals, increasing the catalyst deactivation. The moderate basicity of ammonia also discourages the proton exchange that is produced with a base before the reductive elimination.

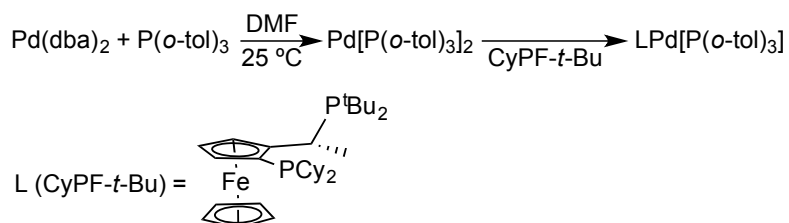
A catalyst is needed with some special characteristics, ancillary ligands resistant to the displacement by ammonia, a structure that prevents the formation of bridging structures and that induces reductive elimination from the amido complexes and the favorable reaction of ammonia over the arylamine formed as a product of the reaction.

There are some examples of amination reactions with ammonia. The first selective direct amination of aryl halides with ammonia was published in 2006 by the research group of J. F. Hartwig (Scheme VI-1),¹ employing a Pd-catalyst with a bulky Josiphos ligand. They found that complexes generated from the Josiphos ligand meet the challenges previously described and catalyze the amination reaction.



Scheme VI-1. Coupling of aryl halides with ammonia, catalyzed by [(CyPF-*t*-Bu)PdCl₂].

In 2009, the same group reported that a palladium catalyst generated from Pd[P(*o*-tol)₃]₂ and the alkylbisphosphine CyPF-*t*-Bu, could be used for the coupling of ammonia with aryl chlorides, bromides, iodides and sulfonates (Scheme VI-2).² This method is a one-pot synthesis that occurs with faster rates and higher yields than those conducted with CyPF-*t*-Bu and palladium(II) as catalyst precursors, because of the low concentration of active catalyst that is generated from the combination of palladium(II), ammonia, and base.

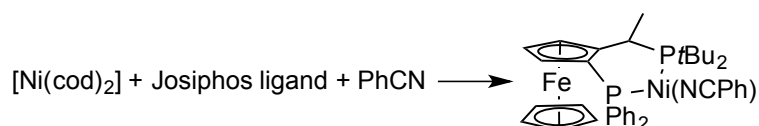


Scheme VI-2. Formation of the palladium catalyst “*in situ*” with the Josiphos ligand.

They proposed a catalytic cycle in which the oxidative addition with the aryl is the first step and then it is followed by the ligand substitution of the halogen in the palladium catalyst by NH_3 . Then, a reaction with a base to form the aminopalladium compound is produced and finally, after the reductive elimination, the ArNH_2 is formed.

They also recently developed the Pd-catalyzed amination of arylchlorides and arylbromides with ammonium salts.³ They found that ammonium salts are practical alternatives to gaseous amines for the amination of aryl halides and can occur with selectivities, distinct effects of concentration on selectivities and distinct resting states of the catalyst.

But not only palladium catalyst have been used for these transformations, very recently a nickel-catalyzed amination reaction of aryl chlorides with ammonia or ammonium sulfate has been developed.⁴ The use of a catalyst made from nickel is important because there are few examples of catalysts based on abundant and less costly metals, such as nickel. The mechanism of the palladium catalyzed amination of aryl electrophiles with ammonia has been studied,⁵ showing that the steric bulk of the ligand is important to favor the binding of ammonia over the binding of aniline. Based on this information, the research group of Hartwig developed a new nickel catalyst with the Josiphos ligand, which allows the obtention of the coupling products with high yields and selectivity. Ammonium sulfate can also be used for the same transformation.

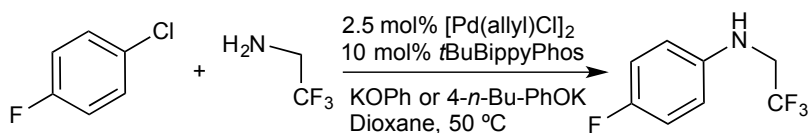


Scheme VI-3. Formation of the nickel catalyst with the Josiphos ligand.

It is also important the development of the palladium-catalyzed arylation of fluoroalkylamines by the same investigation group.⁶ Anilines with electron-withdrawing substituents on nitrogen are valuable in medicine because

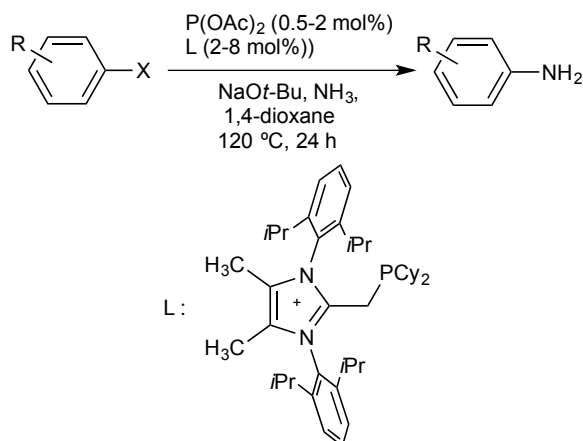
are less likely to suffer metabolic oxidation. The fluoroalkyl groups are important because they have electronic properties that should mitigate that metabolic oxidation process, but this kind of anilines had not been studied. One of the main reasons is because of the methods to prepare such structures, which are limited. The two most commonly used methods are, the reductive amination of trifluoroacetaldehyde with the corresponding aniline and Sn aryls reactions.

The research group of Hartwig reported a generally applicable coupling of aryl bromides and chlorides with primary amines containing fluorine in beta position to the nitrogen, under mild conditions and with inexpensive reagents and weak bases to promote the coupling reaction. The fluoroalkylaniline products are unstable under typical conditions for C-N coupling reactions (heat and strong bases). However, the reactions conducted with the weaker base KOPh occurred in high yield under the conditions shown in Scheme VI-4.



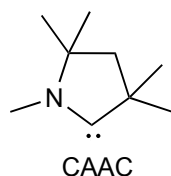
Scheme VI- 4. Conditions for the amination reaction of the arylbromides with primary amines.

Not only the research group of Hartwig has been interested in the development of this amination reactions, but also the group of Matthias Beller.⁷ They used 2-phosphanymethyl-*N,N'*-biarylimidazolium ligands in the Pd-catalyzed aminations of aryl halides as it is shown in the Scheme VI-5.



Scheme VI-5. Palladium-catalyzed amination of aryl halides with ammonia.

As previously explained, a palladium catalyst with a ligand with some special features, is needed for this kind of transformations. The research group of G. Bertrand has been developing and studying a diverse range of carbene ligands along the last years.⁸ Due to their properties, they found in cyclic(alkyl)amino carbene ligands (CAACs) good candidates for these amination reactions.



Properties of the CAACs:

- CAACs have one of the electronegative and π -donor amino substituents of diaminocarbenes replaced by a σ -donating but no π -donating alkyl group. As a consequence, CAACs are more nucleophilic (σ -donating) but also more electrophilic (π -accepting) than diaminocarbenes. The nucleophilic attack of the NH_3 in the catalytic cycle is easier when the palladium catalyst is more deactivated, and this occurs with the CAACs ligands.

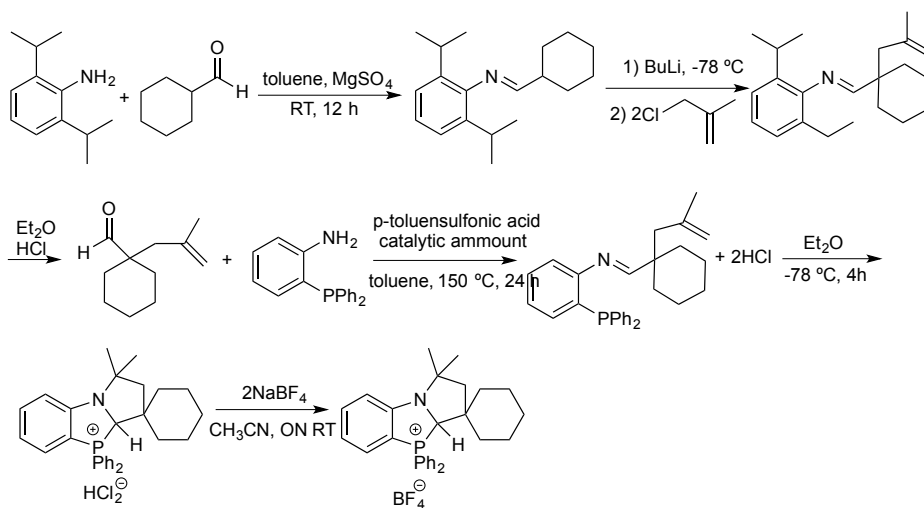
- The presence of a quaternary carbon in the position α to the carbene center provides steric environments that differentiate CAACs from all other ligands. The steric bulk of the CAACs ligands are also an important factor in order to favor the binding of ammonia over the binding of the aniline formed after the reductive elimination.
- CAAC-metal complexes are extremely thermally robust, making them perfect for using in harsh conditions. This property has been used to perform a variety of gold-catalyzed reactions in the presence of basic amines, including ammonia, which usually deactivates catalysts.
- The peculiar electronic properties of CAACs make metal-carbon bonds very strong, and therefore CAAC-transition metal complexes very robust; this property makes even more difficult the displacement of the CAAC ligand in the metal compound by ammonia to form unreactive catalytic complexes.
- Palladium catalysts with CAACs ligands have not α -hydrogens to the heteroatom so not suffer from β -elimination.

Based on these studies, the research group of Guy Bertrand has been focused on the development of new ligands and their use for amination reactions of aryl halides with ammonia. The aim was to develop a bidentate phosphino-CAAC ligand and the corresponding palladium compound to be used in catalytic reactions.

6.2 RESULTS AND DISCUSSION

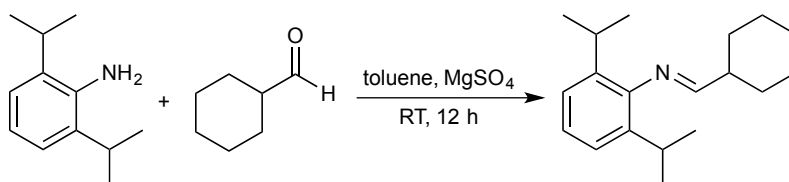
It was necessary to develop the bidentate phosphino-cyclic(alkyl)amino carbene ligand from the very beginning and then, the corresponding palladium compound was synthesized. Some of the synthesized compounds are new, while others had been synthesized before. The reactions that I set up and

improved during my stay at the research group of G. Bertrand are represented in Scheme VI-6.



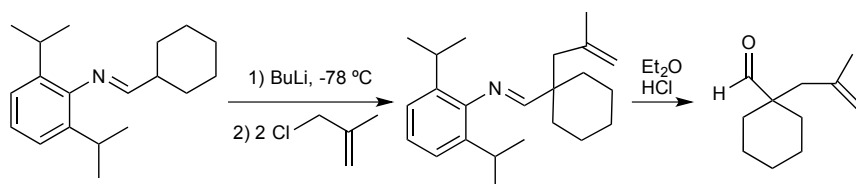
Scheme VI-6. Scheme of synthesis of a palladium compound with a phosphino-cyclic(alkyl)amino carbene ligand.

6.2.1 Condensation reaction for the synthesis of the following imine



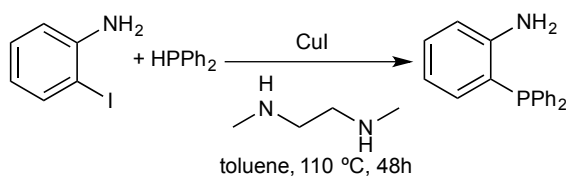
It was used the same previously described procedure on the literature, a condensation reaction between the amine and the aldehyde in toluene at room temperature, during 12 h to obtain the corresponding imine as a white solid after isolation.

6.2.2 Lithiation reaction and hydrolysis



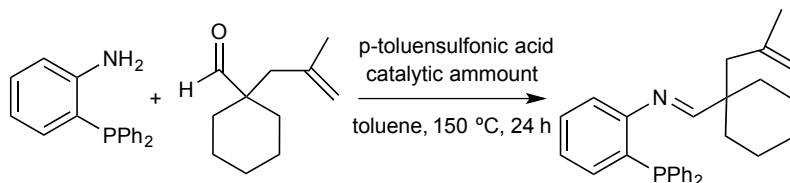
This reaction was also previously reported but in a different way, in this case a lithiation reaction between the previously synthesized imine and the 3-chloro-2-methyl-1-propene was done in dry ether to obtain the imine that then, was hydrolyzed with HCl to obtain the corresponding aldehyde.

6.2.3 Synthesis of the amine



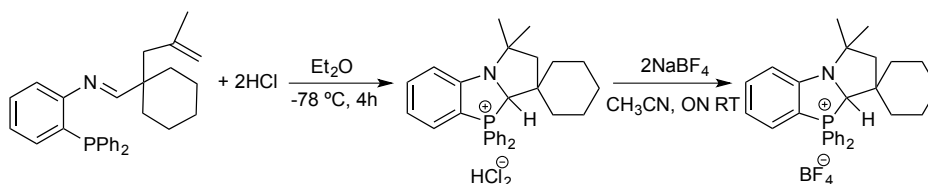
The previously described procedure in the literature was used for synthesis of amines. The reaction between 2-iodoaniline and diphenylphosphine is produced in the glove box in dry toluene, to obtain the new amine after isolation.

6.2.4 Condensation reaction to generate the new imine



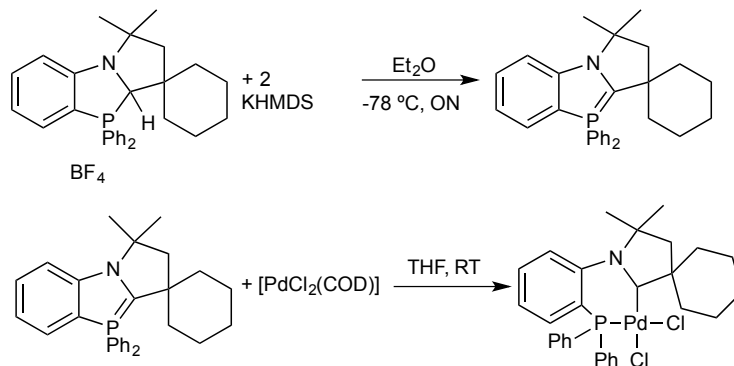
It was developed a condensation reaction between the previously reported amine and the aldehyde, using a Dean Stark system to collect the formed water during the reaction. Finally, the compound was isolated as colorless oil, by extraction with MeOH.

6.2.5 Formation of the phosphonium salt



The new compound was synthesized by dissolving the imine in dry ether under argon at $-78\text{ }^{\circ}\text{C}$ and a solution of HCl in ether was added over the imine and warmed to room temperature. Then an exchange reaction between the HCl_2^- and the BF_4^- with NaBF_4 in acetonitrile was produced, at room temperature to obtain the salt as a white solid after isolation.

6.2.6 Synthesis of the palladium complex



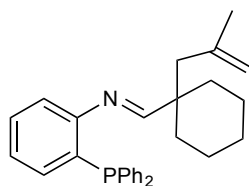
The new ylide compound was produced by reacting the BF_4^- salt with KHMDS (potassium bis(trimethylsilyl)amide) in dry ether and then, a cannula transfer of the ylide solution to a THF solution of the $[\text{PdCl}_2(\text{COD})]$ was produced and isolated the new palladium compound as an orange solid.

6.3 EXPERIMENTAL SECTION

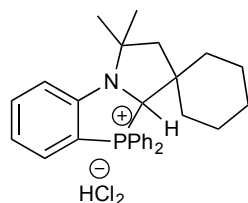
All manipulations were performed under an inert atmosphere of dry argon by using standard Schlenk techniques or glove box. Dry, oxygen-free solvents were employed. NMR spectra were recorded on Bruker avance 300 or Varian Inove 400 spectrometers. Chemical shifts were reported in ppm from

tetramethylsilane (^1H), CCl_3F (^{19}F), or 85% H_3PO_4 (^{31}P), with positive shifts downfield, at ambient probe temperature unless otherwise stated. Unless specified, all compounds were used from commercial sources and used without further purification. The compounds *N*-(cyclohexylmethylene)-2,6-bis(1-methylethyl)Benzenamine,⁹ 1-(2-methyl-2-propen-1-yl)Cyclohexanecarboxaldehyde¹⁰ and 2-(diphenylphosphino)Benzenamine,¹¹ were prepared as reported in the literature.

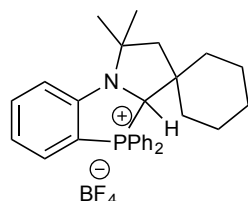
6.3.1 Syntheses of new compounds



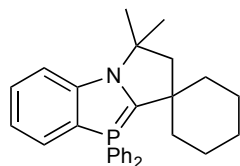
Compound 1. 2-(diphenylphosphino)aniline (3.7 g; 0.013 mol) was dissolved in toluene (50 mL) and 1.3 equivalents of 1-(2-methylallyl)cyclohexanecarbaldehyde (2.88 g, 0.0173 mol) and a few mg of *p*-toluenesulfonic acid were added to the previous solution. The mixture was heated with vigorous stirring, at 155 °C during 24 h, using a Dean Stark system to collect the water formed during the reaction. The reaction mixture was then warmed to room temperature. The toluene was removed under vacuum, and the product was extracted from MeOH as colorless oil. Yield: 85 % ^1H NMR (300 MHz, CDCl_3 , 298 K): δ 7.53–7.30 (m, 5H), δ 7.13–6.78 (m, 10H), δ 4.82 (m, 1H), δ 4.69 (m, 1H), δ 2.25–0.73 (m, 15H). ^{31}P (300 MHz, CDCl_3 , 298 K): δ –14.67 ppm (s).



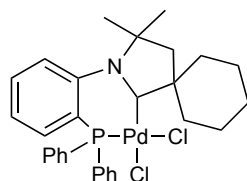
Compound 2. The compound 1 (5.7 g; 0.0134 mol) was dissolved in dry, degassed Et₂O (30 mL) and, under Ar was cooled to -78 °C. 2 equivalents of a solution of HCl 2 M in dry Et₂O (13.4 mL) were added and the solution was warmed up while reached room temperature. Then, the mixture was stirred during 4 hours the solvent was removed through a cannula filtration to get the desired compound as a white solid that was finally dried under vacuum. Yield: 60 %. ¹H NMR (300 MHz, CDCl₃, 298 K): δ 8.30–6.75 (m, 14H), δ 5.59 (s, 1H), δ 2.60–0.50 (m, 18H). ³¹P (300 MHz, CDCl₃, 298 K): δ -17.82 ppm (s).



Compound 3. Two equivalents of NaBF₄ were added to the compound 2 (4.0 g; 0.0080 mol) dissolved in dry acetonitrile (40 mL) and the mixture was stirred at room temperature overnight. The solvent was removed under vacuum and the product was extracted in DCM (40 ml) and filtered a cannula. Finally, the DCM was removed under vacuum, washed the residue with 20 mL of Et₂O and dried under vacuum. Yield: 83 %. ¹H NMR (300 MHz, CDCl₃, 298 K): δ 8.15–8.00 (m, 2H), δ 7.94–7.40 (m, 10H), δ 7.12–6.90 (m, 2H), δ 5.25 (s, 1H), δ 2.55–0.50 (m, 18H). ³¹P (300 MHz, CDCl₃, 298 K): δ -17.79 ppm (s).



Compound 4. One equivalent of the compound three (0.30 g, 0.584 mol) and one equivalent of KHMDS (Potassium bis(trimethylsilyl)amide) (0.116 g, 0.584 mol) were added in a Schlenk under Ar and dissolved it in dry Et₂O at -78 °C. The mixture was stirred overnight at this temperature (purple solution) and the formed solution was used to the next reaction.



Compound 5. A cannula transfer of the ylide solution to another flask with a solution of [PdCl₂(COD)] (0.150 g, 0.526 mol) in THF, was done. After 4 hours stirring at room temperature, the solvent was completely removed, washed the resulting product with Et₂O and dried under vacuum to obtain the desired product as an orange solid. Yield: 78 %. ¹H NMR (300 MHz, CDCl₃, 298 K): δ 7.90–7.76 (m, 1H), δ 7.73–7.12 (m, 12H), δ 6.90–6.83 (m, 1H), δ 2.70–0.70 (m, 18H). ³¹P (300 MHz, CDCl₃, 298 K): δ -26.10 ppm (s).

-
- ¹ Shen, Q. and Hartwig, J. F. *J. Am. Chem. Soc.* **2006**, *128*, 10028–10029.
- ² Vo, G. D. and Hartwig, J. F. *J. Am. Chem. Soc.* **2009**, *131*, 11049–11061.
- ³ Green, R. A. and Hartwig, J. F. *Org. Lett.* **2014**, *16*, 4388–4391.
- ⁴ Green, R. A. and Hartwig, J. F. *Angew. Chem. Int. Ed.* **2015**, *54*, 3768–3772.
- ⁵ Klinkenberg, J. L. and Hartwig, J. F. *J. Am. Chem. Soc.* **2010**, *132*, 11830–11833.
- ⁶ Brusoe, A. T. and Hartwig, J. F. *J. Am. Chem. Soc.* **2015**, *137*, 8460–8468.
- ⁷ Dumrath, A.; Lubbe, C.; Neumann, H.; Jackstell, R. and Beller, M. *Chem. Eur. J.* **2011**, *17*, 9599–9604.
- ⁸ a) Melaimi, M.; Soleilhavoup, M. and Bertrand, G. *Angew. Chem. Int. Ed.* **2010**, *49*, 8810–8849; b) Martin, D.; Melaimi, M.; Soleilhavoup, M. and Bertrand, G. *Organometallics.* **2011**, *30*, 5304–5313; c) Soleilhavoup, M. and Bertrand, G. *Acc. Chem. Res.* **2015**, *48*, 256–266.
- ⁹ Lavallo, V.; Canac, Y. and Bertrand, G. *PCT. Int. Appl.* **2006**, WO 2006138166 A2 20061228.
- ¹⁰ Hirner, J. J.; Roth, K. E.; Shi, Y. and Blum, S. A. *Organometallics*, **2012**, *31*(19), 6843–6850.
- ¹¹ Xue, M.; Li, J.; Peng, J.; Bai, Y.; Zhang, G.; Xiao, W. and Lai, G. *Appl. Organomet. Chem.* **2014**, *28*(2), 120–126.

RESUMEN EN ESPAÑOL

1 INTRODUCCIÓN

Las reacciones de acoplamiento cruzado son reacciones que se producen entre un electrófilo orgánico y un nucleófilo organometálico para lo que es necesario el empleo de un catalizador, habitualmente de paladio. El mecanismo de éste tipo de reacciones consta de las siguientes etapas: adición oxidante, transmetalación y eliminación reductora. Las etapas de adición oxidante y eliminación reductora son independientes del nucleófilo empleado y son comunes a todas las variantes de los procesos catalizados por paladio, mientras que la etapa de transmetalación depende del nucleófilo escogido. La elección de un tipo de nucleófilo u otro limita las posibles condiciones de reacción y la tolerancia a grupos funcionales de la síntesis y el mecanismo por el cual transcurre la etapa de transmetalación es muy diferente en función del nucleófilo empleado. Es muy importante conocer en profundidad la etapa de transmetalación de éste tipo de reacciones ya que nos va a permitir un mejor diseño de los sistemas.

El propósito fundamental de esta tesis doctoral ha sido comprender y mejorar la etapa de transmetalación en las reacciones de acoplamiento cruzado catalizadas por paladio. Nos hemos centrado en el estudio de sistemas Au/Sn, Au/Pd y Zn/Pd.

2 METODOLOGÍA

En el capítulo I se ha realizado el estudio de la termodinámica de la transmetalación Sn/Au para diferentes compuestos de oro y estaño. Los datos obtenidos han permitido planificar racionalmente reacciones catalíticas de acoplamiento cruzado en las que el sistema multimetálico Sn/Au/Pd se ha utilizado para el acoplamiento de arilos voluminosos que son inertes en las condiciones clásicas de la reacción de Stille, en una tesis realizada en paralelo a ésta. Se trata de un proceso muy eficiente sin precedente en la bibliografía, en condiciones de reacción suaves y con compuestos fácilmente accesibles.

El segundo capítulo contiene estudios cinéticos y termodinámicos de las reacciones de intercambio Ph/X entre complejos [AuPhL] (L: PPh₃, PMe₃, PCy₃) y SnBu₃X (X = Cl, OTf and vinilo). Éste trabajo se ha completado con estudios DFT en colaboración con Max García-Melchor, mostrando un cambio drástico en el mecanismo de la reacción. Cuando X = Cl o OTf la reacción se produce a través de un mecanismo clásico concertado, mientras que cuando X = vinilo se produce un mecanismo inesperado a través de una adición oxidante/eliminación reductora y de la formación de un intermedio de oro(III).

En el tercer capítulo se realiza el estudio de la otra parte del sistema bimetálico Sn/Au/Pd, se estudia la interacción entre compuestos de oro(I) y complejos de paladio(II). Concretamente se han estudiado reacciones de intercambio entre grupos arilo y metilo entre los complejos *trans*-[PdRfClL₂] con [AuMeL] (Rf = C₆Cl₂F₃, L = PPh₃). También se han realizado estudios cinéticos para esta reacción de intercambio, mediante RMN de ³¹P y ¹⁹F, haciendo finalmente una propuesta mecanística.

Durante el desarrollo de ésta tesis doctoral, hemos encontrado similitudes entre las transmetalaciones en las que están implicados compuestos de oro con reacciones de transmetalación entre organozíncicos y compuestos de paladio. Por éste motivo se ha realizado un estudio comparando la reactividad entre [AuMeL] y ZnMe₂ con dímeros de paladio del tipo *trans*-[Pd₂(μ-Cl)₂Rf₂L₂] (L = PPh₃, PCy₃ y PMe₃) en el capítulo IV. Mayoritariamente se produce una reacción de intercambio entre los grupos Me y Rf en éste sistema. También se han realizado estudios mecanísticos para ésta reacción.

En el capítulo V se estudia la etapa de transmetalación Zn/Pd en la reacción de Negishi. Se ha realizado el estudio mecanístico para las reacciones de transmetalación y retrotransmetalación de los sistemas formados por *trans* y *cis*-[PdRfMe(PPh₃)₂] con ZnCl₂. También se han estudiado las reacciones entre *trans*-[PdRfCl(PPh₃)₂] con ZnMeCl y los zincatos [ZnMeCl₂]⁻ y [ZnMeCl₃]²⁻.

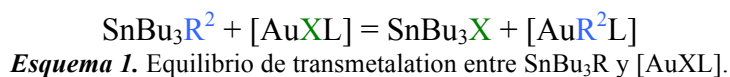
El objetivo del capítulo VI ha sido el desarrollo de nuevos catalizadores de paladio para la aminación de haluros de arilo utilizando amoniaco. Éste trabajo se desarrolló durante la estancia de tres meses en UCSD (University of California, San Diego, USA), bajo la supervisión del profesor Guy Bertrand como se requiere para la mención de doctor internacional.

3 RESUMEN DE LOS RESULTADOS

3.1 Capítulo I: Estudio termodinámico del equilibrio de transmetalación Au/Sn y consecuencias para la reacción de Stille cocatalizada con oro

La reacción de Stille ha sido ampliamente estudiada en nuestro grupo de investigación y presenta una gran aplicabilidad para la síntesis de principios activos como fármacos, cosméticos y otros productos de alto valor añadido, debido a su alta tolerancia de grupos funcionales, su selectividad y su buen rendimiento.

Intentando reproducir el efecto de la adición de cobre a la reacción clásica de Stille, en nuestro grupo de investigación se decidió intentar desarrollar una reacción de Stille cocatalizada por oro. El primer paso para el desarrollo de ésta reacción fue el estudio de la termodinámica del sistema. Se nos encomendó el estudio del equilibrio de transmetalación Au/Sn (Esquema 1) para diferentes organoestannanos y derivados de oro, permitiéndonos establecer las mejores condiciones para el éxito de la reacción de transmetalación para la formación de complejos organometálicos de oro.

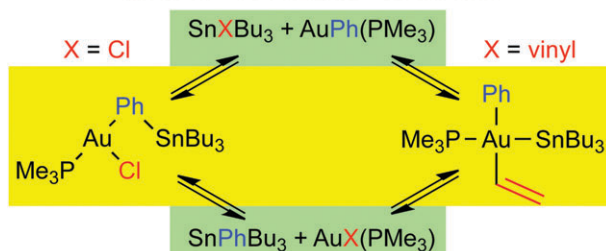


Los datos obtenidos sugirieron la conveniencia de que el haluro X implicado en la transmetalación fuera Cl, que es el que más favorece la termodinámica de la transmetalación. Puesto que el reactivo ArX en la catálisis es un yoduro de arilo, conseguir la condición referida supone trabajar en exceso de LiCl para

mantener el catalizador L-Au-X como cloro derivado y favorecer el intercambio a lo largo del proceso. En tales condiciones la reacción bimetálica funciona muy eficazmente.

3.2 Capítulo II: Estudio mecanístico del intercambio de grupos entre Sn/Au^I

En éste capítulo se describen los estudios cinéticos y termodinámicos realizados para las reacciones de intercambio Ph/X (X = Cl, OTf, vinilo; L: PPh₃, PMe₃, PCy₃), entre los complejos [AuXL] y SnBu₃Ph. El trabajo se ha completado con estudios DFT que muestran que el mecanismo de intercambio Ph/X para reacciones que envuelven compuestos SnBu₃Ph y [AuXL] (X = Cl, OTf y vinilo) cambia drásticamente del mecanismo concertado que envuelve puentes Ar/X, cuando X= Cl y OTf, a un mecanismo inesperado de adición oxidante/eliminación reductora a través de un intermedio de oro(III) cuando X = vinilo.



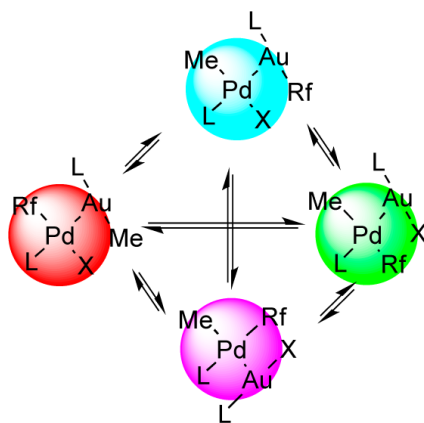
Esquema 3. Esquema para las reacciones de intercambio Ph/X en los complejos [AuCl(PMe₃)] y SnBu₃X.

En éste trabajo finalmente se concluye que el mecanismo de transmetalación Au/Sn está muy influenciado por la acidez del centro de estaño y la metalobasicidad del centro metálico de oro.

3.3 Capítulo III: Heteroacoplamiento alquilo-arilo vs. homoacoplamiento arilo-arilo en reacciones catalizadas por Pd

En éste capítulo se realiza el estudio de reacciones de acoplamiento cruzado catalizadas por paladio, de $[\text{AuMe}(\text{PPh}_3)]$ con distintos yoduros de arilo, mostrando que el homoacoplamiento es el principal producto de la reacción.

Se describe el estudio de reacciones de intercambio de grupos arilo y metilo entre los complejos $\text{trans-}[\text{PdClRfL}_2]$ ($\text{Rf} = \text{C}_6\text{Cl}_2\text{F}_3$, $\text{L} = \text{PPh}_3$) y $[\text{AuMeL}]$. También se describen los estudios cinéticos realizados mediante RMN de ^{31}P y ^{19}F para ésta reacción, encontrando una propuesta mecanística basada en dichos estudios (esquema 4).



Esquema 4. Propuesta mecanística para la reacción entre $\text{trans-}[\text{PdRfCl}(\text{PPh}_3)_3]$ y $[\text{AuMe}(\text{PPh}_3)]$.

3.4 Capítulo IV: Similitudes entre oro y cinc en la reacción de intercambio arilo por alquilo con dímeros de paladio

Se han encontrado ciertas similitudes entre la reacción de isomerización cis/trans $[\text{PdArMeL}_2]$ catalizada por ZnMe_2 y la reacción de trasmetalación Au/Pd entre $\text{cis-}[\text{PdRf}_2(\text{AsPh}_3)_2]$ and $[\text{AuCl}(\text{AsPh}_3)]$, ambas estudiadas previamente en nuestro grupo de investigación y en las que se produce una interacción fuerte Pd-Au y Pd-Zn en los intermedios y en los

estados de transición. Otra similitud encontrada en las reacciones de transmetalación con oro y cinc es su capacidad para producir intercambios C/C. Éste tipo de reacciones son las responsables de la formación de productos de homoacoplamiento indeseados en la reacción de Negishi.

Por éstas similitudes se decidió realizar un estudio comparando la reactividad entre los complejos $[AuMeL]$ y $ZnMe_2$ con dímeros de paladio del tipo $trans-[Pd_2(\mu-X)_2Rf_2L_2]$, encontrando que en ambos casos la reacción mayoritaria es el intercambio del grupo metilo del compuesto de cinc o del compuesto de oro por el grupo Rf del compuesto de paladio. La reacción de intercambio es más rápida con el organocíncico que con el compuesto de oro y se produce a través de un mecanismo de reacción asociativo con la ruptura de uno de los puentes halógeno del dímero de paladio en cada reacción de intercambio, siendo la reacción más rápida con puentes cloro que con puentes iodo. En el caso del $ZnMe_2$ los productos mayoritarios de la reacción son $ZnRfMe$ y $cis-[PdRfL(thf)]$, mientras que para el $[AuMeL]$ se obtienen $[AuRfL]$ y $trans-[Pd_2(\mu-Cl)_2Rf_2(L)_2]$.

3.5 Capítulo V: Estudio de la transmetalación Zn/Pd en la reacción de acoplamiento cruzado de Negishi

El acoplamiento de grupos alquilo tiene una gran importancia en la química de síntesis, pues estos grupos son los más habituales en moléculas con todo tipo de aplicaciones; sin embargo, su síntesis presenta dificultades con nucleófilos poco reactivos como ácidos borónicos o estannanos. La reacción de Negishi es ampliamente utilizada para éste propósito, debido a que los organocíncicos empleados como nucleófilos en la reacción de Negishi son agentes transmetalantes muy activos. La termodinámica de la transmetalación no siempre es muy favorable, dando lugar en algunos casos a productos de retrotransmetalación que forman productos de homoacoplamiento. Algunos estudios sugieren que los organozincatos son las especies que participan en las

reacciones de transmetalación, sin embargo pocos estudios mecanísticos se han hecho a éste respecto.

En este apartado, hemos llevado a cabo el estudio de la reacción de retrotransmetalación entre complejos de paladio del tipo $[\text{PdRfMe}(\text{PR}_3)_2]$ y ZnCl_2 por medio de medidas cinéticas. Los productos que se obtienen de ésta reacción son ZnRfCl (y después $[\text{PdMe}_2(\text{PPh}_3)_2]$ observado mediante RMN de ^{31}P) y pequeñas cantidades *trans*- $[\text{PdRfCl}(\text{PPh}_3)_2]$ y del producto de eliminación reductora RfMe . Las reacciones no se retardan por la adición de PPh_3 libre.

También se han estudiado las reacciones entre *trans*- $[\text{PdRfCl}(\text{PPh}_3)_2]$, con ZnMeCl y los zincatos $[\text{ZnMeCl}_2]^-$ y $[\text{ZnMeCl}_3]^{2-}$, para conocer sus diferencias mecanísticas. En éste caso se producen mayoritariamente *cis*- $[\text{PdRfMe}(\text{PPh}_3)_2]$, ZnRfCl y *trans*- $[\text{PdMeCl}(\text{PPh}_3)_2]$ que reaccionará para producir $[\text{PdMe}_2(\text{PPh}_3)_2]$ (y sus análogos en las reacciones con los zincatos). Las reacciones están fuertemente retardadas por la adición de fosfina libre. Se ha visto que las reacciones son mas rápidas con los zincatos, como era esperable debido a su mayor nucleofilia.

3.6 Capítulo VI: Desarrollo de nuevos catalizadores de paladio para la aminación de haluros arilo con amoniaco

El grupo de investigación del profesor Guy Bertrand está enfocado en el desarrollo de nuevos catalizadores de paladio para la aminación de haluros de arilo usando amoníaco. Su idea es el desarrollo de un ligando carbeno bidentado cíclico alquilo-amino y el correspondiente compuesto de paladio con éste ligando, para utilizarlo en reacciones catalíticas.

Durante mi estancia en su grupo de investigación, mi trabajo consistió en la preparación del catalizador de paladio desde el principio, realizando para ello reacciones de condensación para la síntesis de iminas, reacciones de litación, hidrólisis, síntesis de aminas, formación de la sal de fosfonio y

finalmente la síntesis del catalizador de paladio deseado. No hubo tiempo de probar el catalizador desarrollado en reacciones de catálisis. La continuación está actualmente en desarrollo en aquel grupo.

CONCLUSIONES GENERALES

Aunque la temática abordada en esta Tesis Doctoral es diversa, los estudios realizados en ella se han centrado en la comprensión y mejora de la etapa de transmetalación en reacciones de acoplamiento catalizadas por paladio. Los resultados obtenidos permiten concluir:

- El oro es capaz de transmetalalar grupos con un gran impedimento estérico a compuestos de paladio más rápidamente que los derivados correspondientes de tributilestano empleados en las condiciones clásicas de la reacción de Stille. En condiciones catalíticas, puesto que el reactivo ArX que se utiliza es un yoduro de arilo, se genera [AuIL]. Conseguir un exceso de [AuCIL] es crucial para tener un mayor éxito de la catálisis. Ésto se puede favorecer termodinámicamente utilizando inicialmente un cloro-complejo de Au, y una sal con cloruro (LiCl) que reemplace al yoduro cuando, en el transcurso del proceso se genere [AuIL].
- El mecanismo de intercambio entre grupos Ph/X (X = Cl, OTf y vinilo; L: PPh₃, PMe₃), para las reacciones entre los complejos [AuXL] y SnBu₃Ph cambia drásticamente al pasar de utilizar X = Cl, OTf a utilizar X = vinilo. Para el intercambio Ph/X cuando X = Cl y OTf la reacción se produce a través de un mecanismo concertado pero cuando X = vinilo, la reacción se produce a través de un mecanismo de adición oxidante/eliminación reductora a través de un intermedio de Au^{III}.
- En el estudio de las reacciones de acoplamiento cruzado catalizadas por paladio entre [AuMe(PPh₃)] con distintos yoduros de arilo, se observa que grupos mas electronegativos son mas lentos hacia el homoacoplamiento (el caso extremo es Rf, para el que el producto de homoacoplamiento Rf-Rf no se observa) y también son mas lentas hacia la transmetalación. Ambos efectos, pero especialmente el primero, ayudan a hacer la reacción de homoacoplamiento indeseada menos competitiva para grupos mas electronegativos.

- Se han estudiado las reacciones entre complejos del tipo $[AuMeL]$ y $ZnMe_2$ con dímeros de paladio $trans-[Pd_2(\mu-Cl)_2Rf_2L_2]$, viéndose que la reacción mayoritaria es el intercambio del grupo metilo del compuesto de cinc o del compuesto de oro por el grupo Rf del compuesto de paladio. La reacción de intercambio es mas rápida con el compuesto de cinc que con el de oro (debido a la mayor nucleofilia del $ZnMe_2$ con respecto a $[AuMeL]$) y se produce a través de un mecanismo asociativo con la ruptura de los puentes halógeno del dímero de paladio, siendo mas rápida con el dímero que tiene puentes cloro que con el que tiene puentes iodo. Para el caso de $[AuMeL]$, la reacción se detiene en el dímero, siendo los productos mayoritarios de la misma $[AuRfL]$ y $trans-[Pd_2(\mu-Cl)_2Rf_2(L)_2]$. Sin embargo cuando se utiliza $ZnMe_2$, los productos mayoritarios de la reacción son $ZnRfMe$ y $cis-[PdRfL(thf)]$.

- La reacción de retrotransmetalación entre complejos de paladio del tipo $[PdRfMe(PPh_3)_2]$ y $ZnCl_2$ se ha estudiado por medio de medidas cinéticas. Se trata de una reacción reversible en la que los productos que se obtienen son $ZnRfCl$ (y después $[PdMe_2(PPh_3)_2]$ observado mediante RMN de ^{31}P) y pequeñas cantidades $trans-[PdRfCl(PPh_3)_2]$ y del producto de eliminación reductora $RfMe$. Éstas reacciones no están retardadas por la adición de PPh_3 libre. Otra de las conclusiones obtenidas de éste estudio es que la isomerización de cis - a $trans$ - $[PdRfMe(PPh_3)_2]$ está catalizada por la adición de $ZnCl_2$.

Para el caso de las reacciones entre $trans-[PdRfCl(PPh_3)_2]$ con $ZnMeCl$ y los zincatos $[ZnMeCl_2]^-$ y $[ZnMeCl_3]^{2-}$, se producen mayoritariamente los productos $cis-[PdRfMe(PPh_3)_2]$, $ZnRfCl$ y $trans-[PdMeCl(PPh_3)_2]$ que reaccionará para producir $[PdMe_2(PPh_3)_2]$ (y sus análogos en las reacciones con los zincatos). Para una misma concentración de PPh_3 , las reacciones con los zincatos $[ZnMeCl_2]^-$ y $[ZnMeCl_3]^{2-}$ son un orden de magnitud mas rápidas que la reacción con $ZnMeCl$, como era de esperar debido a su mayor nucleofilia. Lo mismo ocurre con la selectividad respecto a la reacción con $ZnMeCl$. Los mecanismos para las reacciones entre $trans-[PdRfCl(PPh_3)_2]$ con $ZnMeCl$, $[ZnMeCl_2]^-$ y $[ZnMeCl_3]^{2-}$ son similares.

- El capítulo seis, al margen de la línea principal de trabajo, ha sido realizado en el grupo de Guy Bertrand (Universidad de California San Diego, Estados Unidos) como parte de la actividad de tesis doctoral en la modalidad de Doctorado con Mención Internacional.

CONTENIDOS	PÁGINA
PRESENTACIÓN	17
INTRODUCCIÓN GENERAL	23
CAPÍTULO I: Estudio termodinámico del equilibrio de transmetalación Sn/Au y consecuencias para el acoplamiento de Stille cocatalizado con oro	43
1.1 INTRODUCCIÓN	45
1.2 RESULTADOS Y DISCUSIÓN	45
1.2.1 Termodinámica del equilibrio de transmetalación Au/Sn	45
1.2.2 Consecuencias en la realización catalítica del proceso	48
1.3 PARTE EXPERIMENTAL	49
CHAPTER II: Estudio mecanístico del intercambio de grupos Sn/Au^I	57
2.1 INTRODUCCIÓN	59
2.2 RESULTADOS Y DISCUSIÓN	59
2.2.1 Termodinámica de la reacción de transmetalación	59
2.2.2 Cinética de la reacción	60
2.2.3 Discusión de resultados	66
2.3 PARTE EXPERIMENTAL	70

CHAPTER III: <i>Acoplamiento cruzado alquilo-arilo vs. homoacoplamiento arilo-arilo en reacciones catalizadas por Pd</i>	83
3.1 INTRODUCCIÓN	85
3.2 RESULTADOS Y DISCUSIÓN	86
3.2.1 <i>Mecanismo de la reacción</i>	87
3.2.2 <i>Análisis de los datos cinéticos</i>	94
3.3 PARTE EXPERIMENTAL	98
CHAPTER IV: <i>Similitudes entre oro y zinc en la reacción de intercambio de arilo por alquilo con dímeros de paladio</i>	111
4.1 INTRODUCCIÓN	113
4.2 RESULTADOS Y DISCUSIÓN	116
4.2.1 <i>Reacciones entre $trans-[Pd_2(\mu-X)_2Rf_2L_2]$ y $[AuMeL]$</i>	116
4.2.2 <i>Reacciones entre $trans-[Pd_2(\mu-X)_2Rf_2L_2]$ y $ZnMe_2$</i>	127
4.3 PARTE EXPERIMENTAL	133
CHAPTER V: <i>Estudio de la transmetalación Zn-Pd en la reacción de acoplamiento cruzado de Negishi</i>	149
5.1 INTRODUCCIÓN	151
5.2 RESULTADOS Y DISCUSIÓN	157
5.2.1 <i>Cinética de la reacción de transmetalación entre $trans-[PdRfCl(PPh_3)_2]$ y $ZnMeCl$</i>	157

5.2.2	<i>Cinética de la reacción de transmetalación entre trans-[PdRfCl(PPh₃)₂] con [ZnMeCl₂]⁻ y [ZnMeCl₃]²⁻</i>	166
5.3	PARTE EXPERIMENTAL	170
CHAPTER VI:	<i>Desarrollo de nuevos catalizadores de paladio para la aminación de haluros de arilo con amoniaco</i>	185
6.1	INTRODUCCIÓN	187
6.2	RESULTADOS Y DISCUSIÓN	192
6.2.1	<i>Reacción de condensación para la síntesis de la imina</i>	193
6.2.2	<i>Reacción de litiación e hidrólisis</i>	194
6.2.3	<i>Síntesis de la amina</i>	194
6.2.4	<i>Reacción de condensación para generar la nueva imina</i>	194
6.2.5	<i>Formación de la sal de fosfonio</i>	195
6.2.6	<i>Síntesis del complejo de paladio</i>	195
6.3	PARTE EXPERIMENTAL	195
	RESUMEN	201
	CONCLUSIONES GENERALES	211
	ÍNDICE	217

